The Co-evolution of black holes and galaxies

A DISSERTATION SUBMITTED TO THE GRADUATE DIVISION OF THE UNIVERSITY OF HAWAI'I AT MĀNOA IN PARTIAL FULFILLMENT OF THE REQUIREMENTS FOR THE DEGREE OF

DOCTOR OF PHILOSOPHY

IN

ASTRONOMY

August 2017

By
Hyewon Suh

Dissertation Committee:

Günther Hasinger, Chairperson
Francesca Civano
Patrick Henry
Esther Hu
David Sanders
Kimberly Binsted

Acknowledgements

First of all, I especially thank to my advisor, Günther Hasinger for guiding me during the past years of my dissertation work. This work would not have been possible without his support. Thank you for working with me, I had pleasure to work with you. Thanks to Dr. Francesca Civano at CfA, who helped a lot and kept an eye on my work. Her guidance and support is indispensable for my research. I hope we keep working together! I also thank to my Ph.D. committee members for giving valuable comments and providing useful feedbacks. I would also like to express my thanks to collaborators I have had the pleasure of working with.

Thanks to my old and current officemates Thomas Dixon, Marco Micheli, Po-Feng Wu, and Li-Yen Hsu. I also thank to colleagues in IfA, especially Yanxia Li. I had a great time and pleasure to study with you guys! I would like to express special thank to Amy Miyashiro across the corridor, who have brought positive energy into the small, windowless office. Thanks for everyday coffee and being my lunch mate!

I thank to my best friends, ZH, Yumi, JH, MH, A.H., and Jin, who do not have any clue about my work, but still providing moral support and entertainment.

The last, I am indebted to my family, who always provide unconditional support and encouragement.

Abstract

The growth of black holes appears to be closely connected with galaxy evolution, and yet how nuclear activity affects the growth of their host galaxies remains unclear. The main focus of this dissertation research is to systematically study the influence of nuclear activity on the growth of galaxies by examining the possible connection between AGN activity and star formation. By combining multi-wavelength photometry and spectroscopy, I characterize the properties of one of the largest samples of X-ray AGNs and their host galaxies up to $z \sim 3$. To quantify the growth rate of black holes, I determine black hole masses ($M_{\rm BH}$) and Eddington ratios via the virial method using optical and near-IR spectroscopic observations. To derive AGN host galaxy properties, I develop a multi-component SED fitting technique which allows to disentangle the nuclear emission from the stellar light, and derive reliable physical properties, such as stellar masses ($M_{\rm stellar}$) and star formation rates (SFRs).

AGN host galaxies have, on average, SFRs that are consistent with those expected from normal star-forming galaxies with similar $M_{\rm stellar}$ and redshift ranges, suggesting no clear evidence for enhanced or suppressed star formation. Furthermore, the $M_{\rm BH} - M_{\rm stellar}$ distribution for the majority of AGN host galaxies beyond the local universe is broadly consistent with the correlation that we observe today, indicating no significant evolution in the $M_{\rm BH} - M_{\rm stellar}$ relation. These results are in agreement with the observed lack of correlation between SFRs and AGN accretion, which can be explained by the AGN variability along with the broadly distributed Eddington ratios. I conclude that secular evolution may play an important role in growing both black holes and galaxies hosting moderate-luminosity AGNs at later cosmic time ($z < 3$).

Table of Contents

List of Tables

List of Figures

Chapter 1

Introduction

One of the outstanding issues for understanding the formation and evolution of galaxies is how the presence of a supermassive black hole (SMBH) affects its host galaxy. Observations have shown that the growth of SMBHs is tightly linked with their host galaxies, as revealed by correlations between the black hole mass and the bulge stellar mass, i.e., the $M_{\rm BH} - M_{\rm stellar}$ relation (Kormendy & Richstone 1995; Magorrian et al. 1998; Gültekin et al. 2009; Schulze & Gebhardt 2011; McConnell & Ma 2013) and the velocity dispersion, i.e., the $M_{\rm BH} - \sigma$ relation (Ferrarese & Merritt 2000; Gebhardt et al. 2000; Merritt & Ferrarese 2001; Tremaine et al. 2002; Gültekin et al. 2009; Graham et al. 2011; McConnell & Ma 2013; Woo et al. 2013). Furthermore, it has been widely accepted that the growth of active galactic nuclei (AGN) and the star-formation history undergo a very similar evolutionary behavior through cosmic time, where the peak space density of most luminous AGNs and powerful star-forming galaxies occur at a similar cosmic epoch ($z = 2 - 3$) with a dramatic decline towards low redshift, while the moderate-luminosity AGNs and the bulk of star-forming galaxies peak at lower redshift ($z \lesssim 1$; see e.g., Madau et al. 1996; Giacconi et al. 2002; Cowie et al. 2003; Steffen et al. 2003; Ueda et al. 2003; Barger et al. 2005; Hasinger et al. 2005; Hopkins et al. 2007; Aird et al. 2015). The existence of these correlations seems to support that there is a broad connection between nuclear activity and star formation. However, our current understanding of the effects that AGN can have on the star formation processes is

still under debate (see Alexander & Hickox 2012; Kormendy & Ho 2013; Heckman & Best 2014 for recent reviews).

Understanding the origin and evolution of the observed scaling relations (i.e., the $M_{\rm BH} - M_{\rm stellar}$ and the $M_{\rm BH} - \sigma$ relations) is a major challenge for cosmological models, and is a key issue for studying the connection between the evolution of black holes and galaxies. Many studies have investigated the cosmic evolution in the locally observed scaling relations to find the physical link between the growth of galaxies and black holes (e.g., Shields et al. 2003; Peng et al. 2006; Salviander et al. 2007; Treu et al. 2007; Shen et al. 2008; Woo et al. 2008; Decarli et al. 2010; Merloni et al. 2010; Bennert et al. 2011). Several observational studies have found that SMBHs beyond the local universe are over-massive at a given host stellar mass compared with at the present time, suggesting black holes were able to gather mass more efficiently than the stellar populations in their host galaxies (e.g., Treu et al. 2007; Woo et al. 2008; Merloni et al. 2010; Decarli et al. 2010; Bennert et al. 2011; Trakhtenbrot et al. 2015). On the other hand, some other studies found that the relationship between SMBHs and stellar masses matches the correlation that we observe today, suggesting no evolution in the scaling relation (e.g., Shields et al. 2003; Salviander et al. 2007; Shen et al. 2008; Cisternas et al. 2011a). However, small number statistics, large uncertainties, and selection biases could affect the interpretation of the results on the black hole and host galaxy relations. Moreover, probing the $M_{\rm BH} - M_{\rm stellar}$ relation at high redshift is extremely challenging. Measurement of black hole masses at earlier epoch can only be obtained for small samples of extremely luminous objects, with consequent loss of accurate determination of their host stellar masses, with the nuclear light overwhelming the host galaxy emission. Besides, these luminous active galaxies may not represent the general galaxy population, as they are rare subset of all accreting black holes. Thus, to date, the evolution of scaling relations remains uncertain and still a matter of debate.

In the most popular scenario of galaxy formation and evolution, AGN activity can suppress or quench star formation either by heating or removing the cold gas in their host galaxies, known as 'AGN feedback' (e.g., Silk & Rees 1998; Di Matteo et al. 2005; Springel

et al. 2005; Hopkins et al. 2008). The AGN fueling mechanism is important for a better understanding of the feedback that may be related to both AGNs and star-forming activities. Recent theoretical models suggest different mechanisms of the AGN fueling (e.g., Hopkins & Hernquist 2006; Fanidakis et al. 2012). In the hierarchical formation paradigm, the black hole growth is governed by mergers or by gas accretion via secular evolution. Black holes are assumed to undergo several episodes of significant gas accretion with complex hydrodynamic and magnetic processes, along with relativistic effects during which this accretion powers AGNs (e.g., Springel et al. 2005; Choi et al. 2012). The most luminous AGNs are interpreted as results of major mergers. A substantial starburst occurs as a result of major mergers, and some of the gas eventually reaches the black hole at the center of a galaxy, triggering the AGN activity (see e.g., Kauffmann & Haehnelt 2000; Di Matteo et al. 2005). On the other hand, moderate-luminosity AGNs are suggested to be products of modest accretion, in which case the gas accretion via secular processes trigger the AGN activity (e.g., Hopkins et al. 2007; Hasinger 2008; Fanidakis et al. 2012). A slower but significant gas inflow can be driven by internal dynamical processes in the galactic disk. Kormendy & Kennicutt (2004) further point out that this secular evolution creates a pseudo-bulge in the inner region of a galaxy, where significant on-going star formation occurs.

Studying AGN host galaxies can offer insight into the role of AGN activity in galaxy evolution. The morphologies and colors of galaxies may contain a record of their growth history. Observational studies have shown that most AGN host galaxies are likely to be structurally disk-dominated galaxies (e.g., Gabor et al. 2009; Cisternas et al. 2011b; Schawinski et al. 2011; Kocevski et al. 2012; Mullaney et al. 2012; Rosario et al. 2015), and the star formation rates (SFRs) correspond to those expected from typical star-forming populations (e.g., Silverman et al. 2011; Suh et al. 2017), implying that the nuclear activity and star formation seem to co-exist, fueling black hole accretion and star formation simultaneously (e.g., Springel et al. 2005; Netzer 2009; Mullaney et al. 2012; Rosario et al. 2013; Vito et al. 2014). Moreover, Fan et al. (2014) found that the majority of AGN host galaxies show a lack of significant merger features up to $z \sim 2$, suggesting that most AGN

activity does not seem to be triggered by major mergers since $z \sim 2$ (see also Mainieri et al. 2011; Kocevski et al. 2012; Schawinski et al. 2012; Schramm & Silverman 2013; Villforth et al. 2014).

Several studies have addressed that the majority of AGN host galaxies in the local universe are preferentially in the "green valley" on the color-magnitude diagram, between actively star-forming galaxies in the blue cloud and passively evolving galaxies on the red sequence (e.g., Kauffmann et al. 2007; Schawinski et al. 2007; Schiminovich et al. 2007). In addition, some studies found that broad-line AGN (Type 1) host galaxies are likely to be associated with galaxies belonging to the green valley, while narrow-line AGN (Type 2) host galaxies tend to be redder than overall galaxy population (e.g., Nandra et al. 2007). The simplest interpretation for the galaxy evolution is that AGN feedback is mostly responsible for the suppressing of star formation and the migration of galaxies from the blue cloud to the red sequence. The observed red colors of Type 2 AGNs might either be due to dust extinction in dusty star-forming galaxies (Brusa et al. 2009), or linked with passive galaxies (Schawinski et al. 2009). However, the conclusive observational evidence that AGN activity is able to regulate the star formation in galaxies is lacking, and the extent to which AGN activity affects the star-formation process is still a matter of debate.

The main goal of this dissertation research is to investigate the connection between AGN activity and star formation history in their host galaxies to have an accurate understanding on the co-evolution of galaxies and black holes. The majority of the growth of black holes and star formation in galaxies occur during redshift of roughly $z = 1-3$. Therefore, studying this redshift range is quite interesting. My approach is to combine multi-wavelength photometry and spectroscopy to characterize the AGN and their host galaxy properties, examining black hole accretion and star formation in AGN host galaxies at redshift up to $z \sim 3$ to explore the growth of black holes and galaxies.

1.1 Growth of Black holes

The assembly of SMBHs appears to follow a "downsizing" or "anti-hierarchical" trend; i.e., the AGN luminosity function and its evolution show that the co-moving number density of luminous AGNs peaks at higher redshift ($z \sim 2$) than moderate-luminosity AGNs, which peak at $z < 1$ (e.g., Giacconi et al. 2002; Cowie et al. 2003; Steffen et al. 2003; Ueda et al. 2003; Barger et al. 2005; Hasinger et al. 2005; La Franca et al. 2005; Hopkins et al. 2007; Silverman et al. 2008; Aird et al. 2015). This AGN cosmic downsizing trend is seen across a wide range of the electromagnetic spectrum in X-ray, optical, infrared, and radio wavebands (Bongiorno et al. 2007; Cirasuolo et al. 2007). If AGN luminosity would strictly correlate with black hole mass, this finding would imply that more massive black holes formed before lower-mass black holes, which is in apparent contradiction to the currently favored hierarchical structure formation paradigm based on the standard cold dark matter model. In the hierarchical framework, more massive halos grow over time hierarchically via subsequent merging and smooth accretion among low mass halos. The AGN cosmic downsizing, however, is observed in luminosity, and thus the downsizing phenomenon can also be interpreted assuming a relationship between the AGN luminosity and the black hole mass as a function of redshift.

The Eddington ratio, the ratio of the AGN bolometric luminosity and the Eddington luminosity ($L_{\rm bol}/L_{\rm Edd}$), is a key parameter for understanding the accretion history on to the black hole. An AGN with black hole mass of $M_{\rm BH}$ can produce the maximum luminosity via the Eddington limit ($L_{\rm Edd}$) at which the radiation pressure by the accretion of the infalling matter balances the gravitational attraction of the black hole for spherically symmetric time-invariant accretion. Estimating the Eddington ratios provides an observational constraint on the efficiency of gas accretion during the active phases of black holes over cosmic time. One might have expected a correlation between black hole masses and AGN bolometric luminosities, but if there is a range in accretion rates and/or efficiencies, the relation will be weaker. Thus, in order to investigate the observed downsizing trend in black hole growth, it

is particularly interesting to explore the efficiency of gas accretion during the active phases of black holes. Thus, to quantify a growth rate requires the independent measurement of AGN bolometric luminosity and black hole mass in understanding the evolutionary picture for AGNs.

1.2 Growth of AGN host galaxies

The star formation and AGN activity may be closely connected because both processes are predominantly dependent on a cold gas supply. Therefore, it is necessary to understand the star formation history of AGN host galaxies and the connection between black hole accretion and ongoing star formation in order to study the role of AGN activity in the evolution of galaxies. There has been a general consensus that the majority of star-forming galaxies show a tight correlation between the SFR and their stellar mass, commonly referred to as the main sequence (MS) of star formation (e.g., Daddi et al. 2007; Elbaz et al. 2007; Noeske et al. 2007; Rodighiero et al. 2011, 2014; Whitaker et al. 2012). Speagle et al. (2014) present the calibrated relationship between stellar mass and SFR out to $z \sim 6$ using a compilation of 25 star-forming MS studies in a variety of fields, reporting that the MS galaxies have a $\sim$0.2 dex scatter in the slope of their $M_{\rm stellar}$-SFR relation and remains constant over cosmic time. The existence and tightness of this star formation sequence can be interpreted assuming that the growth of the majority of star-forming galaxies have been regulated more by internal secular processes rather than by merger process (e.g., Elbaz et al. 2011; Rodighiero et al. 2011; Wuyts et al. 2011).

Originally the star-forming MS studies concluded that the SFR increases with stellar mass as a single power law, while the log SFR–log $M_{\rm stellar}$ slope and the normalization vary based on the redshifts, sample selection, choice of stellar IMF, and SFR indicators (for a summary, see Speagle et al. 2014). Recent studies have suggested that the SFR–$M_{\rm stellar}$ relation flattens toward the high-mass end (Whitaker et al. 2014; Lee et al. 2015; Tomczak et al. 2016). For example, Lee et al. (2015) examine the star-forming MS, of

which the total SFRs are determined by combination of the obscured SFRs using *Herschel* far-IR photometry and the unobscured SFRs from UV observations, using a large sample of ∼62,000 star-forming galaxies in the COSMOS field. They find that the slope of the MS is dependent on stellar mass, such that it is steeper at low stellar masses and appears to flatten at stellar masses above $M_{\rm stellar} \sim 10^{10.3} M_{\odot}$, suggesting a curvature of the star-forming MS with a flat slope at the high-mass end (see also Whitaker et al. 2014). Furthermore, Tomczak et al. (2016) present similar measurements of the star-forming MS up to $z \sim 4$ using far-IR photometry from the *Spitzer* and *Herschel* observatories. They also suggest that the slope of star-forming MS becomes shallower above a turnover mass that is in the range from $10^{9.5} - 10^{10.8} M_{\odot}$. This "flattening" in the star-forming MS at high masses might be interpreted as a consequence of quenching the star formation in massive galaxies.

Controversial results were found for AGN host galaxies: some studies have indicated similar or enhanced star formation compared to normal star-forming galaxies (e.g., Silverman et al. 2009; Mullaney et al. 2012; Rosario et al. 2012; Santini et al. 2012; Juneau et al. 2013), whereas some others have shown that AGN host galaxies lie below the MS of star-forming galaxies, suggesting that AGN accretion might suppress and eventually quench star formation via a process of feedback (e.g., Barger et al. 2015; Mullaney et al. 2015; Riguccini et al. 2015; Shimizu et al. 2015). Furthermore, there has been a significant disagreement in the correlation between AGN accretion and SFR, which can give a crucial hint of whether AGN activity can significantly enhance or quench star formation in galaxies. Some studies have shown that the SFR increases at high AGN luminosity (i.e., positive relationship; e.g., Lutz et al. 2010; Rovilos et al. 2012; Santini et al. 2012), in agreement with the concept that AGN and star formation activity are connected due to their mutual dependence on the cold gas supply in the galaxy. Other studies have addressed that the SFR decreases with AGN luminosity (i.e., negative relationship; e.g., Page et al. 2012; Barger et al. 2015), suggesting that AGN may suppress or even quench star formation via feedback. On the other hand, there are also studies presenting that the SFR remains constant with respect to AGN luminosity (i.e., flat relationship; e.g., Harrison et al. 2012; Rosario et al. 2012;

Azadi et al. 2015), extending to moderate luminosity AGNs (e.g., Lutz et al. 2010; Shao et al. 2010; Harrison et al. 2012; Mullaney et al. 2012; Rovilos et al. 2012). The difference in the conclusion of such studies also could be attributed to the low source statistics and selection biases. Therefore, the question of whether AGN activity can significantly enhance or quench star formation in galaxies is still unsettled.

Different results can be produced by either physical properties of the sources, or observational biases, or both. The sample selection including completeness and biases due to a specific selection method (X-ray versus infrared selected AGNs, for example), as well as the use of different SFR indicators could introduce systematics since the contribution of AGN emission may significantly hamper the precise determination of SFRs of AGN host galaxies. The *Herschel Space Observatory* (Pilbratt et al. 2010; Poglitsch et al. 2010; Griffin et al. 2010) covers the FIR emission from dust including the characteristic FIR bump typically seen in star-forming galaxies, allowing us for more precise measurements of the total IR luminosity, especially for dusty galaxies and AGN host galaxies, since many of the often used SFR indicators (e.g., Hα, UV continuum) can be substantially contaminated by AGN-related emission (e.g., Dale et al. 2007; Schweitzer et al. 2007; Netzer et al. 2007; Lutz et al. 2016).

The analysis of the spectral energy distribution (SED) of a galaxy can shed light on the star formation history over cosmic time. Its stellar populations are the combination of all the episodes of star formation that a galaxy and its progenitors have undergone. To measure reliable physical properties of AGN host galaxies, it is crucial to constrain the emission associated with stellar populations by removing any contribution from AGN emission (see e.g., Lusso et al. 2011; Bongiorno et al. 2012; Suh et al. 2017). By decomposing the SED of AGN host galaxies into stellar light and nuclear emission, one can estimate reliable host galaxy properties such as galaxy mass and SFR in order to examine the growth history of AGN host galaxies.

1.3 Overview of this Dissertation

This dissertation research is designed to systematically study the influence of AGN on the growth of galaxies by examining the possible connection between AGN activity and star formation in galaxies. This study focuses on the X-ray selected AGNs from several large surveys, which greatly improve upon the statistics of previous works, as it contains one of the largest samples of X-ray AGNs. The deep, large-area survey with the high-quality spectroscopy is particularly important to characterize both AGN and host galaxy properties. Chapter 2 outlines the X-ray selected AGN sample, along with the corresponding optical and NIR spectroscopy. In Chapter 3, I investigate the growth of black holes by examining the AGN accretion rates in the key redshift interval $z = 1 - 2$. Using high-quality optical and NIR spectroscopic observations, I determine black hole masses and Eddington ratios via spectral line fitting. In Chapter 4, I investigate the effect of AGN activity on the star formation in their host galaxies. To derive the physical properties of AGN host galaxies, I develop a multi-component SED fitting technique which allows to disentangle the nuclear emission from the stellar light, and derive host galaxy properties. I then investigate the connection between star formation and AGN activity by examining the $M_{\rm BH} - M_{\rm stellar}$ scaling relation at higher redshifts, the SFR$-M_{\rm stellar}$ distribution, and the correlation between SFR and black hole mass accretion rates to infer the growth history of galaxies and black holes. Finally, Chapter 5 summarizes the major conclusions and outlines possible future directions of related work.

Throughout this paper we assume a ΛCDM cosmology with $\Omega_m = 0.3,\ \Omega_\Lambda = 0.7$, and $H_0 = 70$ km s^{-1} Mpc^{-1}.

References

Aird, J., Coil, A. L., Georgakakis, A., et al. 2015, MNRAS, 451, 1892

Alexander, D. M. & Hickox, R. C. 2012, NewAR, 56, 93

Azadi, M., Aird, J., Coil, A. L., et al. 2015, ApJ, 806, 187

Barger, A. J., Cowie, L. L., Mushotzky, R. F., et al. 2005, AJ, 129, 578

Barger, A. J., Cowie, L. L., Owen, F. N., et al. 2015, ApJ, 801, 87

Bennert, V. N., Auger, M. W.. Treu, T., Woo, J.-H., Malkan, M. A. 2011, ApJ, 742, 107

Bongiorno, A., Zamorani, G., Gavignaud, I., et al. 2007, A&A, 472, 443

Bongiorno, A., Merloni, A., Brusa, M., et al. 2012, MNRAS, 427, 3103

Brusa, M., Fiore, F., Santini, P., et al. 2009, A&A, 507, 1277

Choi, E., Ostriker, J. P., Nabb, T., et al. 2012, ApJ, 754, 125

Choi, Y., Gibson, R. R., Becker, A., et al. 2014, ApJ, 782, 37

Cirasuolo, M., McLure, R. J., Dunlop, J. S., et al. 2007, MNRAS, 380, 585

Cisternas, M., Jahnke, K., Bongiorno, A., et al. 2011, ApJ, 741L, 11

Cisternas, M., Jahnke, K., Inskip, K. J., et al. 2011, ApJ, 726, 57

Cowie, L. L., Barger, A. J., Bautz, M. W., et al. 2003, ApJ, 584L, 57

Daddi, E., Dickinson, M., Morrison, G., et al. 2007, ApJ, 670, 156

Dale, D. A., Gil de Paz, A., Gordon, K. D., et al. 2007, ApJ, 655, 863

Decarli, R., Falomo, R., Treves, A., et al. 2010, MNRAS, 402, 2453

Di Matteo, T., Springel, V., Hernquist, L. 2005, Nature, 433, 604

Donley, J. L., Rieke, G. H., Perez-Gonzalez, P. G., & Barro, G. 2008, ApJ, 687, 111

Elbaz, D., Daddi, E., Le Borgne, D., et al. 2007, A&A, 468, 33

Elbaz, D., Dickinson, M., Hwang, H. S., et al. 2011, A&A, 533, A119

Fan, L., Fang, G., Chen, Y., et al. 2014, ApJL, 784, L9

Fanidakis, N., Baugh, C. M., Benson, A. J., et al. 2012, MNRAS, 419, 2797

Ferrarese, L. & Merritt, D. 2000, ApJ, 539, 9

Gabor, J. M., Impey, C. D., Jahnke, K., et al. 2009, ApJ, 691, 705

Gebhardt, K., Bender, R., Bower, G., et al. 2000, ApJ, 539, 13

Giacconi, R., Zirm, A., Wang, J., et al. 2002, ApJS, 139, 369

Graham, A. W., Onken, C. A., Athanassoula, E., et al. 2011, MNRAS, 412, 2211

Griffin, M. J., Abergel, A., Abreu, A., et al. 2010, A&A, 518, 3

Gültekin, K., Richstone, D., Gebhardt, K., et al. 2009, ApJ, 698, 198

Harrison, C. M., Alexander, D. M., Mullaney, J. R., et al. 2012, ApJ, 760, 15

Hasinger, G. 2008, A&A, 490, 905

Hasinger, G., Miyaji, T., Schmidt, M. 2005, A&A, 441, 417

Heckman, T. M. & Best, P. N. 2014, ARA&A, 52, 589

Hopkins, P. F., & Hernquist, L. 2006, ApJS, 166, 1

Hopkins, P. F., Richards, G. T., Hernquist, L. 2007, ApJ, 654, 731

Hopkins, P. F., Cox, T. J., Keres, D., Hernquist, L. 2008, ApJS, 175, 390

Juneau, S., Dickinson, M., Bournaud, F., et al. 2013, ApJ, 764, 176

Kauffmann, G. & Haehnelt, M. 2000, MNRAS, 311, 576

Kauffmann, G., Heckman, T. M., Budavari, T., et al. 2007, ApJS, 173, 357

Kocevski, D. D., Faber, S. M., Mozena, M., et al. 2012, ApJ, 744, 148

Kormendy, J. & Ho, Luis, C. 2013, ARA&A, 51, 511

Kormendy, J. & Kennicutt, R. C. Jr. 2004, ARA&A, 42, 603

Kormendy, J., & Richstone, D. 1995, ARA&A, 33, 581

La Franca, F., Fiore, F., Comastri, A., et al. 2005, ApJ, 635, 864

Lee, N., Sanders, D. B., Casey, C. M., et al. 2015, ApJ, 801, 80

Lehmer, B. D., Xue, Y. Q., Brandt, W. N., et al. 2012, ApJ, 752, 46

Lusso, E., Comastri, A., Vignali, C., et al. 2011, A&A, 534, A110

Lutz, D., Mainieri, V., Rafferty, D., et al. 2010, ApJ, 712, 1287

Lutz, D., Berta, S., Contursi, A., et al. 2016, A&A, 591, 136

Madau, P., Ferguson, H. C., Dickinson, M. E., et al. 1996, MNRAS, 283, 1388

Magorrian, J., Tremaine, S., Richstone, D., et al. 1998, AJ, 115, 2285

Mainieri, V., Bongiorno, A., & Merloni, A. 2011, A&A, 535, A80

McConnell, N. J., & Ma, C.-P. 2013, ApJ, 764, 184

Merloni, A., Bongiorno, A., Bolzonella, M., et al. 2010, ApJ, 708, 137

Merritt, D., & Ferrarese, L. 2001, ApJ, 547, 140

Mullaney, J. R., Pannella, M., Daddi, E.. et al. 2012, MNRAS, 419, 95

Mullaney, J. R., Alexander, D. M., Aird, J., et al. 2015, MNRAS, 453, L83

Nandra, K., Georgakakis, A., Willmer, C. N. A., et al. 2007, ApJ, 660, 11

Netzer, H., Lutz, D., Schweitzer, M., et al., 2007, ApJ, 666, 806

Netzer 2009, MNRAS, 399, 1907

Noeske, K. G., Weiner, B. J., Faber, S. M., et al. 2007, ApJL, 660, L43

Page, M. J., Symeonidis, M., Vieira, J. D., et al. 2012, Natur, 485, 213

Peng, C. Y., Impey, C. D., Rix, H.-W., et al. 2006, ApJ, 649, 616

Pilbratt, G. L., Riedinger, J. R., Passvogel, T., et al. 2010, A&A, 518, 1

Poglitsch, A., Waelkens, C., Geis, N., et al. 2010, A&A, 518, 2

Riguccini, L., Le Floc'h, E., Mullaney, J. R., et al. 2015, MNRAS, 452, 470

Rodighiero, G., Daddi, E., Baronchelli, I., et al. 2011, ApJL, 739, L40

Rodighiero, G., Renzini, A., Daddi, E., et al. 2014, MNRAS, 443, 19

Rosario, D. J., Santini, P., Lutz, D., et al. 2012, A&A, 545, A45

Rosario, D. J., Mozena, M., Wuyts, S., et al. 2013. ApJ, 763, 59

Rosario, D. J., McIntosh, D. H., van der Wel, A., et al. 2015, A&A, 573, 85

Rovilos, E., Comastri, A., Gilli, R., et al. 2012, A&A, 546, 58

Salviander, S., Shields, G. A., Gebhardt, K., Bonning, E. W. 2007, ApJ, 662, 131

Santini, P., Rosario, D. J., Shao, L., et al. 2012, A&A, 540, A109

Schramm, M. & Silverman, J. D. 2013, ApJ, 767, 13

Schawinski, K., Thomas, D., Sarzi, M., et al. 2007, MNRAS, 382, 1415

Schawinski, K., Virani, S., Simmons, B., et al. 2009, ApJ, 692, 19

Schawinski, K., Treister, E., Urry, C. M., et al. 2011, ApJL, 727, L31

Schawinski, K., Simmons, B. D., Urry, C. M., et al. 2012, MNRAS, 425, L61

Schiminovich, D., Wyder, T. K., Martin, D. C., et al. 2007, ApJS, 173, 315

Schulze, A., & Gebhardt, K. 2011, ApJ, 729, 21

Schweitzer, M., Lutz, D., Sturm, E., et al. 2006, ApJ, 649, 79

Shao, L., Lutz, D., Nordon, R., et al. 2010, A&A, 518, 26

Shen, J., Vanden Berk, D. E., Schneider, D. P., Hall, P. B. 2008, AJ, 135, 928

Shields, G. A., Gebhardt, K., Salviander, S., et al. 2003, ApJ, 583, 124

Shimizu, T. T., Mushotzky, R. F., Meléndez, M., et al. 2015, MNRAS, 452, 1841

Silk, J., & Rees, M. J. 1998, A&A, 331, 1

Silverman, J. D., Mainieri, V., Lehmer B. D., et al. 2008, ApJ, 675, 1025

Silverman, J. D., Lamareille, F., Maier, C., et al. 2009, ApJ, 696, 296

Silverman, J. D., Kampczyk, P., Jahnke, K., et al. 2011, ApJ, 743, 2

Speagle, J. S., Steinhardt, C. L., Capak, P. L., Silverman, J. D. 2014, ApJS, 214, 15

Springel, V., di Matteo, T., & Hernquist, L. 2005, MNRAS, 361, 776

Steffen, A. T., Barger, A. J., Cowie, L. L., et al. 2003, ApJ, 596L, 23

Stern, D., Assef, R. J., Benford, D. J., et al. 2012, ApJ, 753, 30

Suh, H., Hasinger, G., Steinhardt, C., Silverman, J. D., & Schramm, M. 2015, ApJ, 815, 129

Suh, H., Civano, F., Hasinger, G., et al. 2017, ApJ, 841, 102

Tomczak, A. R., Quadri, R. F., Tran K., et al. 2016, ApJ, 817, 118

Trakhtenbrot, B., Urry, C. M., Civano, F., et al. 2015, Sci, 349, 168

Tremaine, S., Gebhardt, K., Bender, R., et al. 2002, ApJ, 574, 740

Treu, T., Woo, J.-H., Malkan, M. A., and Blandford, R. D. 2007, ApJ, 667, 117

Trump, J. R., Hsu, A. D., Fang, J. J., et al. 2013, ApJ, 763, 133

Ueda, Y., Akiyama, M., Ohta, K., et al. 2003, ApJ, 598, 886

Villforth, C., Hamann, F., Rosario, D. J., et al. 2014, MNRAS, 439, 3342

Vito, F., Maiolino, R., Santini, P., et al. 2014, MNRAS, 441, 1059

Whitaker, K. E., van Dokkum, P. G., Brammer, G., Franx, M. 2012, ApJL, 754, L29

Whitaker, K. E., Franx, M., Leja, J., et al. 2014, ApJ, 795, 104

Woo, J.-H., Treu, T., Malkan, M. A., and Blandford, R. D. 2008, ApJ, 681, 925

Woo, J., Schulze, A., Park, D. et al. 2013, ApJ, 772, 49

Wuyts, S., Förster Schreiber, N. M., van der Wel, A., et al. 2011, ApJ, 742, 96

Chapter 2

Data

2.1 X-ray-selected AGN Sample

X-ray surveys are efficient for selecting AGNs because the X-ray emission is a relatively clean signal from the nuclear component. They are less affected by obscuration, and also the contamination from non-nuclear emission, mainly due to star-formation processes, is far less significant than in optical and infrared surveys (Donley et al. 2008, 2012; Lehmer et al. 2012; Stern et al. 2012). Therefore, X-ray surveys are practically the most efficient way for selecting AGNs over a wide range of luminosities and redshifts.

Deep, large-area X-ray observations with *Chandra* (i.e., *Chandra*-COSMOS Survey; Elvis et al. 2009, *Chandra*-COSMOS Legacy Survey; Civano et al. 2016, *Chandra* Deep Field-North and South ; Brandt & Hasinger 2005; Brandt & Alexander 2010) and *XMM-Newton* (i.e., Lockman Hole; see Hasinger et al. 2001; Rovilos et al. 2011) open up a new regime for studying a large sample of the AGN population over a broad range of luminosities ($41 < \log\ L_{0.5-10\ \mathrm{keV}}\ \mathrm{erg\ s^{-1}} < 45$) out to $z \sim 5$, providing a unique opportunity to study AGN evolution. The *Chandra*-COSMOS Legacy Survey (CCLS; Civano et al. 2016) has significantly extended the AGN sample, which has a sufficient volume to probe the AGN population over cosmic time. Furthermore, these fields are the best windows for the deepest and cleanest images at a variety of wavelengths because of the remarkably low Galactic line-

of-sight HI column density (i.e., $N_H = 8.8 \times 10^{19}$ cm^{-2} for *Chandra* Deep Field-South; Stark et al. 1992, $N_H = 5.7 \times 10^{19}$ cm^{-2} for Lockman Hole; Lockman et al. 1986).

A sample of AGNs is selected based on comprehensive catalogs of X-ray sources observed in the *Chandra*-COSMOS Legacy Survey (CCLS), *Chandra* Deep Field-South (CDF-S), and *XMM-Newton*-Lockman Hole (*XMM*-LH) fields, described below.

2.1.1 The *Chandra* COSMOS Legacy Survey

The *Chandra* COSMOS-Legacy Survey (CCLS; Civano et al. 2016) is a large area, medium-depth X-ray survey covering ∼2 deg^2 of the COSMOS field (Cosmic Evolution Survey; Scoville et al. 2007) obtained by combining the 1.8 Ms *Chandra* COSMOS survey (C-COSMOS; Elvis et al. 2009) with 2.8 Ms of new *Chandra* ACIS-I observations. The CCLS is wide enough to have one of the largest samples of X-ray AGNs selected from a single

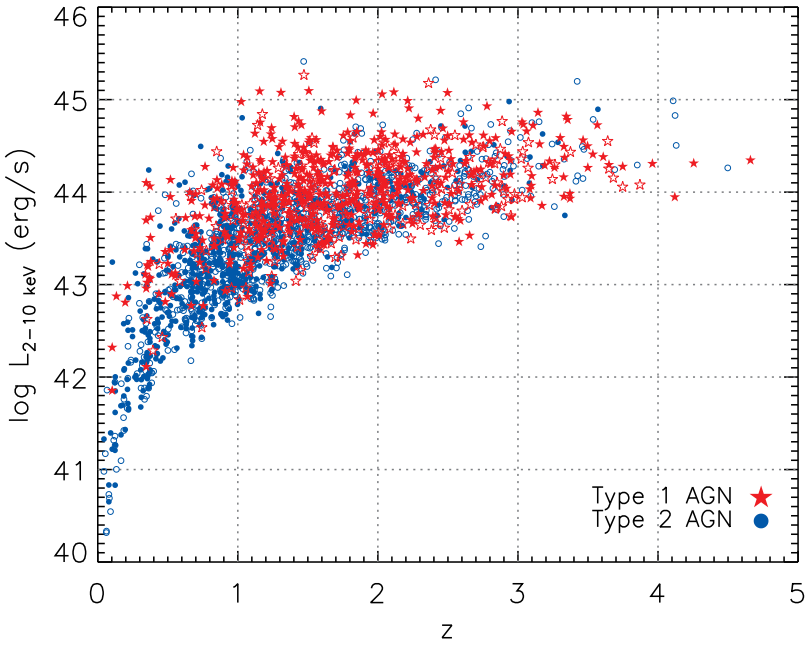

Figure 2.1 The absorption-corrected X-ray ($L_{2-10\ \mathrm{keV}}$) luminosity versus spectroscopic (filled) and/or photometric (open) redshift for a sample of Type 1 (red stars) and Type 2 (blue circles) AGNs from CCLS.

contiguous survey region, containing 4016 X-ray point sources, and also deep enough to find faint sources down to limiting fluxes of 2.2×10^{-16} erg cm^{-2} s^{-1}, 1.5×10^{-15} erg cm^{-2} s^{-1}, 8.9×10^{-16} erg cm^{-2} s^{-1} in the soft ($0.5-2$ keV), hard ($2-10$ keV), and full ($0.5-10$ keV) bands. Moreover, CCLS sources are bright enough so that 97% of these were identified in the optical and infrared bands and therefore photometric redshifts were computed. Thanks to the intense spectroscopic campaigns in the COSMOS field, ∼54% of the X-ray sources have been spectroscopically identified and classified. With these large, uniform X-ray depth and coherent observations, one can minimize the systematic selection effects (e.g., Lauer et al. 2007; Rosario et al. 2013; Caplar et al. 2015). Furthermore, the already existing extensive compilation of multi-wavelength data in the COSMOS field (Capak et al. 2007; Koekemoer et al. 2007; Lilly et al. 2007; Schinnerer et al. 2007; Sanders et al. 2007; Taniguchi et al. 2007; Trump et al. 2007; Zamojski et al. 2007) allows one to investigate AGN host galaxies to have a better understanding of nuclear activity and its connection to the host galaxy. The full catalog of CCLS has been presented by Civano et al. (2016) and Marchesi et al. (2016), including X-ray and optical/infrared photometric and spectroscopic properties.

I select a sample of AGNs from the CCLS catalog (Marchesi et al. 2016), which comprises 3701 X-ray sources with a reliable optical counterpart and the spectroscopic and/or photometric redshift. The spectroscopic information is available for ∼45% (1665) of the sources, while ∼55% (2036) of the sources, only photometric redshifts are available. From the catalog, 985 sources are classified as broad-line and/or unobscured AGN (hereafter, "Type1" AGN) on the basis of broad emission lines in their spectra or the photometric type which are fitted with an unobscured AGN template. 2716 sources are classified as non-broad-line and/or obscured AGN (hereafter, "Type 2" AGN) using the spectroscopic type (sources which show only narrow emission line and/or absorption line features in their spectra), or the photometric type (sources which are fitted either with an obscured AGN template or with a galaxy template).

The absorption-corrected X-ray luminosity is computed using the absorption-correction factor from Marchesi et al. (2016) which is obtained assuming an X-ray spectral index

Γ=1.8. Figure 2.1 shows the absorption-corrected X-ray luminosity ($L_{2-10\ \mathrm{keV}}$) of Type 1 (red stars) and Type 2 (blue circles) AGNs as a function of redshift (spectroscopic or photometric). For sources which are not detected in the hard band but detected in the full band, $L_{2-10\ \mathrm{keV}}$ values are estimated using upper limits. 2826 sources have been detected in the full band (2423 and 2264 in the soft and hard band). Sources with photometric and spectroscopic redshifts are indicated with open and solid symbols, respectively. A sample of X-ray selected AGNs in the CCLS covers a broad range of X-ray luminosities ($L_{2-10\ \mathrm{keV}} = 10^{42-45}$ erg s^{-1}) over the redshift range $z = 0 - 5$.

2.1.2 The *Chandra* Deep Field-South

The 4 Ms *Chandra* Deep Field-South (CDF-S) is the deepest *Chandra* survey covering an area of 464.5 arcmin^2. The catalog for the 4 Ms CDF-S contains 740 X-ray point sources,

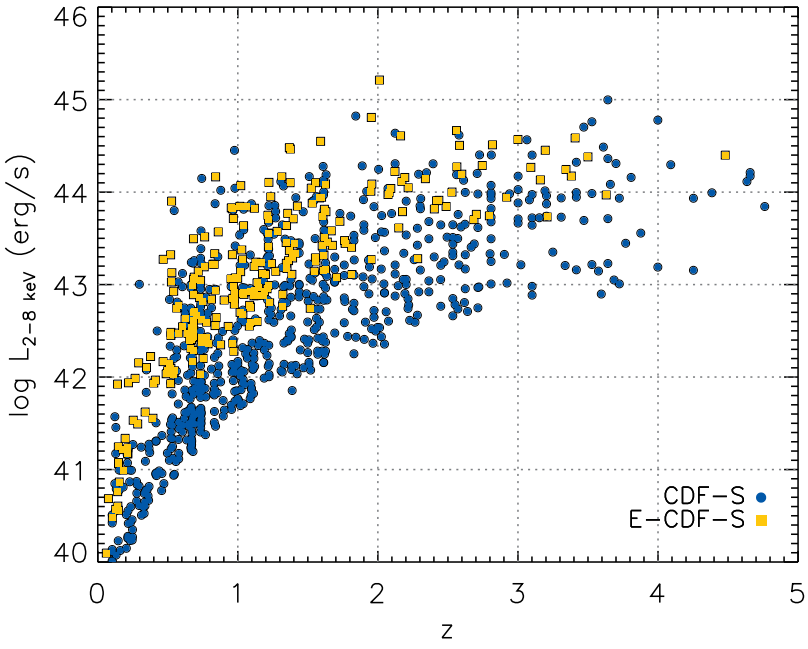

Figure 2.2 The absorption-corrected X-ray ($L_{2-8\ \mathrm{keV}}$) luminosity versus spectroscopic and/or photometric redshift for a sample of AGNs from CDF-S (blue circles) and E-CDF-S (yellow squares).

providing the most sensitive $0.5-8$ keV view of the distant universe (Xue et al. 2011). The survey reaches flux limits of 3.2×10^{-17}, 9.1×10^{-18}, and 5.5×10^{-17} erg cm^{-2} s^{-1} for the full ($0.5-8$ keV), soft ($0.5-2$ keV), and hard ($2-8$ keV) bands, respectively. 674 out of the 740 main catalog sources have either spectroscopic or photometric redshifts, yielding an overall redshift completeness of $\sim$91%. Recently, deeper *Chandra* observations have been covered down to 7 Ms, but not very much more spectroscopic work is available in the new dataset. Therefore, I base this analysis on the 4 Ms sample.

In addition to the 4 Ms CDF-S point source catalog, the Extended *Chandra* Deep Field-South (E-CDF-S) observations have been analyzed and cataloged by Lehmer et al. (2005) and Silverman et al. (2010), providing a sample of 762 distinct X-ray point sources with either spectroscopic or photometric redshifts. Of the 762 E-CDF-S main catalog sources, 523 sources were used since 239 sources were also present in the 4 Ms CDF-S catalog. The sample has an excellent redshift completeness of $\sim$95% (498/523). This survey reaches sensitivity limits of 1.1×10^{-16} and 6.7×10^{-16} ergs cm^{-2} s^{-1} for the soft ($0.5-2.0$ keV) and hard ($2-8$ keV) bands, respectively. A total of 922 X-ray AGNs are generated that have reliable spectroscopic or photometric redshift identifications from the combined catalog of 4 Ms CDF-S and E-CDF-S.

The absorption-corrected intrinsic X-ray luminosity is computed following Xue et al. (2011). As a first step, I assume the intrinsic X-ray spectrum of AGNs modeled by a power-law component with both intrinsic and Galactic absorption (i.e., *zpow* $\times$ *zwabs* $\times$ *wabs* in XSPEC) to estimate the intrinsic column density. A power-law photon index of $\Gamma = 1.8$, which is typical for intrinsic AGN spectra, is assumed and the redshifts of the *zpow* and *zwabs* components are fixed to that of the source. The Galactic column density is fixed to $N_H = 6.0 \times 10^{19}$ cm^{-2}. I then derive the intrinsic column density that reproduces observed hard ($2-8$ keV) and soft ($0.5-2$ keV) band hardness ratios using XSPEC. The intrinsic X-ray luminosity is derived from the equation $L_X = 4\pi d_L^2 \, f_{X,int} \, (1+z)^{\Gamma-2}$ by correcting both intrinsic and Galactic absorption. $f_{X,int}$ is the absorption-corrected X-ray flux and the d_L is luminosity distance. The absorption-corrected $2-8$ *keV* X-ray luminosity of AGNs as a

function of redshift (spectroscopic or photometric) is shown in Figure 2.2. The deep 4 Ms CDF-S survey improves the AGN sample at low luminosities to $L_{2-8\ keV} = 10^{41.5}$erg s^{-1} at $z \sim 1$, while the E-CDF-S, of shallower depth but of wider area, effectively supplies the more luminous AGNs.

2.1.3 The *XMM-Newton* Lockman Hole

The Lockman Hole is on an area of the sky in which the lowest Galactic hydrogen column density ($N_H = 5.7 \times 10^{19}$ cm^{-2}; Lockman et al. 1986) is observed, providing the opportunity to perform extragalactic observations without significant absorption of the radiation in the soft X-rays and the ultraviolet. The catalog of the 409 *XMM-Newton* Lockman Hole (*XMM*-LH) X-ray sources is presented in Brunner et al. (2008), with sensitivity limits of 1.9×10^{-16}, 9×10^{-16}, and 1.8×10^{-15} erg cm^{-2} s^{-1} in the soft ($0.5-2$ keV), hard ($2-10$ keV), and very hard ($5-10$ keV) bands, respectively. Fotopoulou et al. (2012) provide

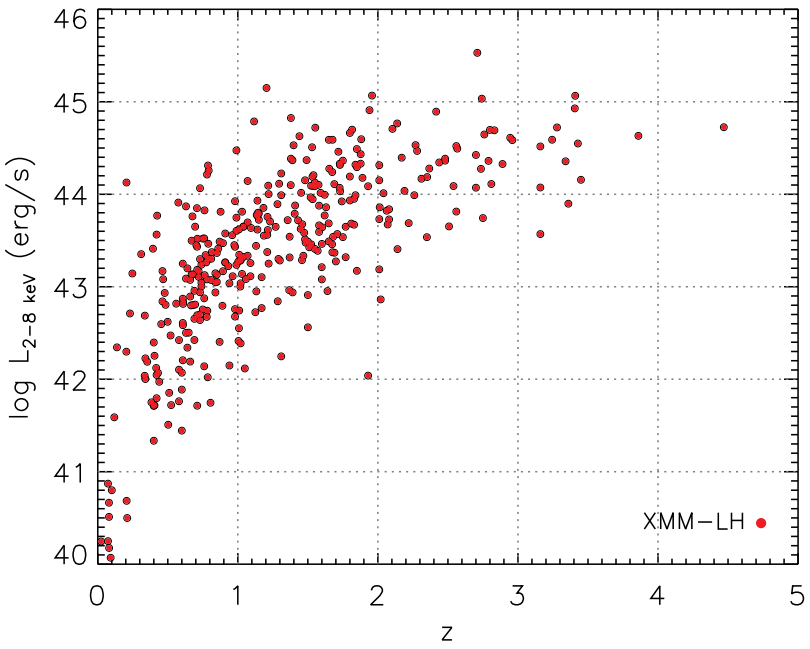

Figure 2.3 The absorption-corrected X-ray ($L_{2-8\ \mathrm{keV}}$) luminosity versus spectroscopic and/or photometric redshift for a sample of AGNs in the *XMM*-LH.

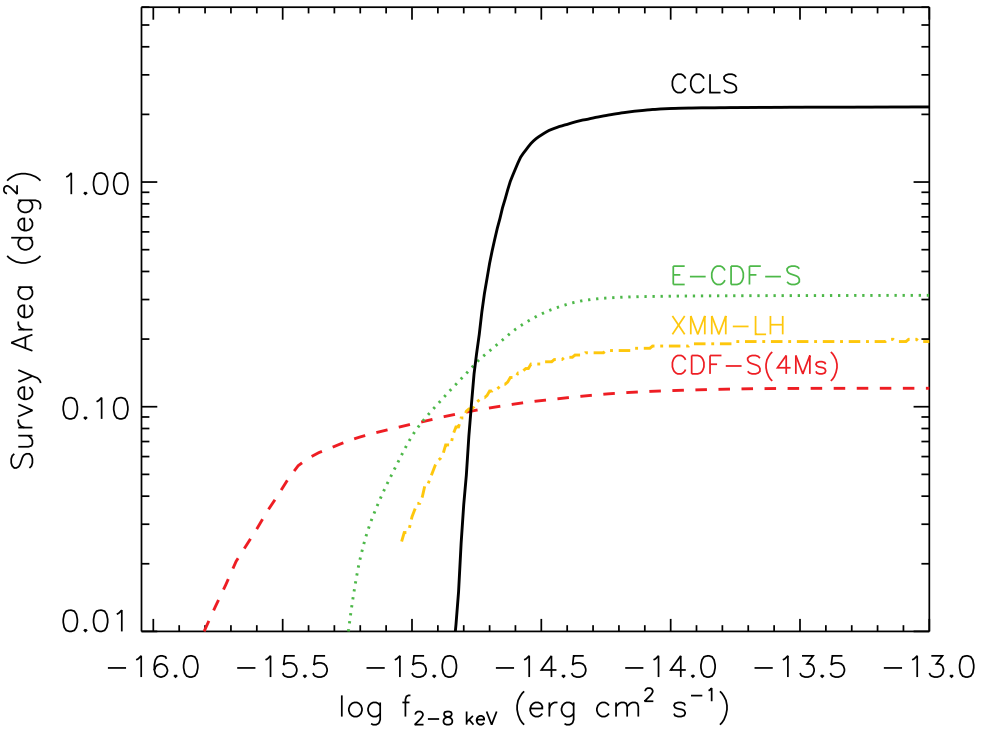

Figure 2.4 Survey area coverage as a function of X-ray flux, color-coded by different X-ray surveys.

spectroscopic or photometric redshifts for the *XMM*-LH X-ray sources. The survey shows a reasonably high redshift completeness with 92% (376 out of 409). Although the sensitivity limit of the *XMM*-LH survey is much higher than that of the 4 Ms CDF-S, the larger field of view of *XMM*-LH (25×25 arcmin^2) offers a significant sample of bright AGNs while the 4 Ms CDF-S observation provides the fainter tail of AGNs. The absorption-corrected intrinsic X-ray luminosity is derived in the same way as used for the CDF-S. Figure 2.3 shows the absorption-corrected $2-8$ keV X-ray luminosity of AGNs as a function of redshift (spectroscopic or photometric) in the *XMM*-LH.

Finally, the sky coverages for the individual surveys (CCLS, black solid; CDF-S, red dashed; E-CDF-S, green dotted; XMM-LH, yellow dash-dotted) are shown in Figure 2.4.

2.2 Spectroscopic Observations

2.2.1 Keck/DEIMOS Optical Spectroscopy

The spectroscopic follow-up campaign in the CCLS (PI: Hasinger) was conducted with the medium-resolution spectrograph Deep Imaging Multi-Object Spectrograph (DEIMOS; Faber et al. 2003) on the Keck II telescope (Hasinger, Suh et al. in preparation). The Field of View (FOV) of DEIMOS is 9×16 arcmin^2. The observations was concentrated on the square annulus of the new *Chandra*-COSMOS Legacy Field around the original *Chandra*-COSMOS area over the three years during 2014–2016. The 600ZD grating at the central wavelength of 7000Å with a GG455 blue blocking filter, and a slit width of $1''$ were used, yielding a wavelength coverage of ∼5500–9800Å with a dispersion of 0.65Å/pixel and a spectral resolution of R∼2000. This is sufficient to distinguish the [O II] λ 3727Å doublet structure and provides secure redshifts. Each mask was observed with a total integration time of 1 hour split into 4 exposures of 900 seconds with an ABBA dither pattern, reaching magnitudes of $I_{AB} < 23.3$. With roughly 48 exposures, the ~ 1 deg^2 deepest area can be almost completely covered with one mask of DEIMOS spectrograph.

The raw data was reduced using a modified version of the DEEP2 data reduction pipeline. The original DEEP2 pipeline (spec2d; Cooper et al. 2012; Newman et al. 2013) consists of the bias removal, flat-fielding, slit-tilt correction, cosmic ray rejection, sky subtraction, and wavelength calibration, and the modified version accounts for dithering, removes the ghosting on the grating data, and corrects for variable slit losses and errors in the alignment introduced by the dithering. The flux calibration was then applied by using the existing multi-wavelength photometry available on the COSMOS field. In addition to Keck/DEIMOS observations, the existing spectroscopy in the original *Chandra*-COSMOS field was also used.

Optical spectroscopy has been obtained in the CDF-S, E-CDF-S, and *XMM*-LH fields (Lehmann et al. 2000, 2001; Szokoly et al. 2004; Silverman et al. 2010; Barger et al. 2014, priv. comm.), providing spectroscopic redshifts for X-ray sources. Szokoly et al. (2004)

present the results of spectroscopic follow-up for the CDF-S, which were observed at the VLT with the FORS1/FORS2 spectrographs for *Chandra* sources. Furthermore, Silverman et al. (2010) provide high-quality optical spectra in the E-CDF-S. 283 *Chandra* sources are observed with deep exposures (2-9 hr per pointing) using multi-slit facilities on both VLT/VIMOS and Keck/DEIMOS. Lehmann et al. (2000, 2001) offer spectroscopy of the ROSAT Deep Surveys in the Lockman Hole using low-resolution Keck spectra. Finally, I compile the existing optical observations of X-ray AGNs from these deep spectroscopic surveys.

2.2.2 Subaru/FMOS Near-infrared Spectroscopy

The NIR spectroscopic observations for the X-ray sources were performed with the FMOS (Kimura et al. 2010) high-resolution spectrographs on the Subaru telescope. FMOS provides up to 400 $1.2''$ diameter fibers in the circular $30'$ diameter field of view. In the high resolution mode, the FMOS spectral coverage is divided into four bands, which are J-short ($0.92 - 1.12$ μm), J-long ($1.11 - 1.35$ μm), H-short ($1.40 - 1.60$ μm), and H-long ($1.60 - 1.80$ μm) with a spectral resolution of R$= \lambda/\Delta\lambda \sim 2200$. The Cross-Beam Switching (CBS) mode, in which two fibers are allocated to each target, was used for optimal sky subtraction of faint sources. The fibers in each pair are separated by 60 arcseconds, alternating between one for the target and the other one simultaneously placed on the sky, so that sky subtraction is not affected by time variation of sky brightness.

The primary targets are X-ray selected AGNs in the CCLS, CDF-S, E-CDF-S, and *XMM*-LH surveys with either spectroscopic or photometric redshifts in the range $1.0 < z < 2.2$, and J magnitudes brighter than 22.5 mag. The FMOS J-band and H-band observations cover the Hα and/or Hβ lines in the redshift range $z = 0.7 - 2.7$. The data was obtained during 2012–2013, shown in Table 2.1. The total integration time is $3.5-4$ hours while accumulating 28-30 frames with an exposure time of 900 seconds per frame. The weather conditions were acceptable, with seeing typically in the range of $0.''6$ to $1.''2$.

Table 2.1. SUBARU FMOS Spectroscopic Observations

Date	**Field**	**Spectrograph**
2012 Mar 13-17	COSMOS	H-long
2012 Mar 25-26	XMM-LH	J-long, H-long
2012 Dec 28	CDF-S, COSMOS	J-long
2012 Dec 29-30	CDF-S, XMM-LH	H-short, H-long
2013 Jan 19	CDF-S	H-long
2013 Jan 20	CDF-S, COSMOS	J-long
2013 Jan 21	CDF-S	J-long
2013 Feb 24	XMM-LH	H-short
2013 Oct 23-24	CDF-S	J-long, H-long
2014 Feb 7-10	COSMOS	J-long, H-long
2014 Mar 6	COSMOS	J-long
2014 Dec 2	COSMOS	H-long
2015 Feb 6-7	COSMOS	H-short-prime
2015 Feb 8	COSMOS	H-long
2015 Feb 11-12	COSMOS	H-long
2015 Apr 10-11	COSMOS	H-long
2016 Jan 15-20	COSMOS	J-long, H-long
2016 Mar 24-30	COSMOS	J-long, H-long
2016 Apr 19-23	COSMOS	J-long

The data was reduced using the publicly available software FIBRE-pac (FMOS Image-Based REduction package; Iwamuro et al. 2012), which is an IRAF-based reduction tool for FMOS. This procedure includes background subtraction, corrections of detector cross talk, bias difference, bad pixels, the spectral distortion, and the removal of residual airglow lines. Individual frames were combined into an ensemble image, and wavelength and flux calibration were carried out. For the absolute flux calibration, the bright (J_{AB}=15-18 mag) stars in each frame were used as a spectral reference. The flux of the reference star was estimated and compared with the photometric data in the catalog. All the spectra were divided by the reference spectrum, and then multiplied by the expected spectrum of the reference star. Apart from the calibration of slit losses through the spectroscopic reference star I do not apply further calibration corrections for a sample of AGNs, since the reference star corrects most of the slit losses for the point-like sources. While systematic effects like weather conditions, position accuracy still may cause differential flux losses across the field of view, the effect of these systematic errors on black hole masses should be small, since the black hole mass is a function of the square root of the luminosity. Finally, the one-dimensional spectrum of each object was extracted from the calibrated image, together with the associated noise spectra.

2.2.3 Spectroscopic Identification

With the fully reduced 1- and 2-dimensional spectra, the redshift was determined through the identification of prominent emission line features. Each spectrum was visually inspected by Suh and Hasinger individually using the SpecPro (Masters & Capak 2011) environment, which is an IDL-based interactive program for viewing and analyzing spectra. We assigned a quality flag to each redshift to indicate the reliability of the redshift determination. All the spectra obtained for X-ray sources in the CCLS contains 1078 Keck/DEIMOS and 897 Subaru/FMOS spectra. Altogether 825 X-ray sources were observed with Subaru/FMOS in the combined CDF-S, E-CDF-S, and *XMM*-LH fields, of which 262 sources are spectroscopically identified.

References

Barger, A. J., et al. 2014, priv. comm.

Brandt, W. N. & Hasinger, G. 2005, ARA&A, 43, 827

Brandt, W. N. & Alexander, D. M. 2010, PNAS, 107, 7184

Brunner, H., Cappelluti, N., Hasinger, G., et al. 2008, A&A, 479, 283

Capak, P., Aussel, H., Ajiki, M., et al. 2007, ApJS, 172, 99

Caplar, Lilly & Trakhtenbrot 2015

Civano, F., Marchesi, S., Comastri, A., et al. 2016, ApJ, 819, 62

Cooper, M. C., Newman, J. A., Davis, M., Finkbeiner, D. P., Gerke, B. F. 2012, spec2d: DEEP2 DEIMOS Spectral Pipeline, astrophysics Source Code Library, ascl:1203.003

Donley, J. L., Rieke, G. H., Pérez-González, P. G., Barro, G. 2008, ApJ, 687, 111

Donley, J. L., Koekemoer, A. M., Brusa, M., et al. 2012, ApJ, 748, 142

Elvis, M., Civano, F., Vignali, C., et al. 2009, ApJS, 184, 158

Faber, S. M., Phillips, A. C., Kibrick, R. I., et al. 2003, SPIE, 4841, 1657

Fotopoulou, S., Salvato, M., Hasinger, G., et al. 2012, ApJS, 198, 1

Hasinger, G., ltieri, B., Arnaud, M., et al. 2001, A&A, 365L, 45

Iwamuro, F., Moritani, Y., Yabe, K., et al. 2012, PASJ, 64, 59

Kimura, M., et al. 2010, PASJ, 62, 1135

Koekemoer, A. M., Aussel, H., Calzetti, D., et al. 2007, ApJS, 172, 196

Lauer, T. R., Tremaine, S., Richstone, D., and Faber, S. M. 2007, ApJ, 670, 249

Lehmann, I., Hasinger, G., Schmidt, M., et al. 2000, A&A, 354, 34

Lehmann, I., Hasinger, G., Schmidt, M., et al. 2001, A&A, 371, 833

Lehmer, B. D., Brandt, W. N., Alexander, D. M., et al. 2005, ApJS, 161, 21

Lehmer, B. D., Xue, Y. Q., Brandt, W. N., et al. 2012, ApJ, 752, 46

Lilly, S. J., Le Fevre, O., Renzini, A., et al. 2007, ApJS, 172, 70

Lockman, F. J., Jahoda, K., & McCammon, D. 1986, ApJ, 302, 432

Marchesi, S., Civano, F., Elvis, M., et al. 2016, ApJ, 817, 34

Masters, D., & Capak, P. 2011, PASP, 123, 638

Newman, J. A., Cooper, M. C., Davis, M., et al. 2013, ApJS, 208, 5

Rosario, D. J., Mozena, M., Wuyts, S., et al. 2013. ApJ, 763, 59

Rovilos, E., Fotopoulou, S., Salvato, M., et al. 2011, A&A, 529, 135

Sanders, D. B., Salvato, M., Aussel, H., et al. 2007, ApJS, 172, 86

Schinnerer, E., Smolcic, V., Carillli, C. L., et al. 2007, ApJS, 172, 46

Scoville, N., Aussel, H., Brusa, M., et al. 2007, ApJS, 172, 1

Silverman, J. D., Mainieri, V., Salvato, M., et al. 2010, ApJS, 191, 124

Stark, A. A., Gammie, C. F., Wilson, R. W., et al. 1992, ApJS, 79, 77

Stern, D., Assef, R. J., Benford, D. J., et al. 2012, ApJ, 753, 30

Suh, H., Hasinger, G., Steinhardt, C., Silverman, J. D., Schramm, M. 2015, ApJ, 815, 129

Szokoly, G. P., Bergeron, J., Hasinger, G., et al. 2004, ApJS, 155, 271

Taniguchi, Y., Scoville, N., Murayama, T., et al. 2007, ApJS, 172, 9

Trump, J. R., Impey, C. D., McCarthy, P. J., et al. 2007, ApJS, 172, 383

Xue, Y. Q., Luo, B., Brandt, W. N., et al. 2011, ApJS, 195, 10

Zamojski, M. A., Schiminovich, D., Rich, R. M., et al. 2007, ApJS, 172, 468

Chapter 3

Black Hole Growth and AGN Accretion

3.1 Introduction

The mass accretion onto the black hole is an important issue for a better understanding the AGN evolution. The Eddington ratio ($L_{\rm bol}/L_{\rm Edd}$) provides insight into the black hole accretion because the bolometric luminosity reflects the mass accretion rate. Therefore, the black hole mass and the AGN bolometric luminosity are the key parameters in understanding the evolutionary picture for AGNs.

Large, modern photometric and spectroscopic surveys open up a new regime for studying a large sample of AGNs (e.g., Sloan Digital Sky Survey (SDSS), Schneider et al. 2010; Shen et al. 2011). Many efforts have been made to describe the properties of thousands of AGNs (e.g., McLure & Dunlop 2004; Vestergaard & Osmer 2009; Steinhardt & Elvis 2010; Choi et al. 2014). In previous studies, the Eddington ratio has been assumed to be close to the Eddington limit regardless of redshift and luminosities. Marconi et al. (2004) suggest that the Eddington ratios of local black holes are in the range between 0.1 and 1.7, suggesting that black hole growth takes place during luminous accretion phases close to the Eddington limit at high redshift. Kollmeier et al. (2006) present that the AGN population is dominated by narrowly distributed near-Eddington accretion rate objects, with a median of 0.1 and a dispersion of 0.3 dex, also suggesting that SMBHs gain most of their mass while radiating close to the Eddington limit. However, it is difficult to draw any conclusions about the

underlying distribution of the Eddington ratio because the shallowness of the large wide area surveys imposes severe restrictions on the combinations of AGN luminosities and black hole masses that are observable, especially at $z > 1$. Recent studies have shown that there is a wide spread in the range of the Eddington ratios (e.g., Babić et al. 2007; Fabian et al. 2008; Kelly et al. 2010; Schulze & Wisotzki 2010; Suh et al. 2015). Lusso et al. (2012) find that the Eddington ratio increases with redshift for AGNs at any given black hole masses. They also show that the Eddington ratio increases with AGN bolometric luminosity, while no clear evolution with redshift is seen. A wide range of Eddington ratios indicates that their luminosity is not directly related to the black hole mass. Therefore, it is necessary to consider a wide range of Eddington ratios with respect to the AGN luminosity and the black hole mass in order to understand the accretion growth history of the black holes. This could give a hint for the AGN downsizing interpretation that might be explained by such massive black holes with low accretion rates, which are relatively fainter than less massive black holes with efficient accretion.

Unfortunately, detailed follow-up study in the redshift interval $z = 1 - 2$, where the AGN downsizing appears, has been difficult because of the lack of emission-line diagnostics in the optical wavelength range, which is often referred to as the redshift desert. The strong Balmer emission lines, Hα and Hβ, are redshifted to 13,126Å and 9722Å at $z = 1$, respectively. The advent of the sensitive NIR spectrograph FMOS on the Subaru telescope finally enables us to determine the black hole mass in the key redshift interval $z = 1 - 2$ using the Balmer lines that are the same lines for which the black hole masses are calibrated at low redshift. This redshift range is of particular interest because it is the epoch in which a significant part of the accretion growth of black holes takes place, where the AGN density peaks and where optical spectroscopy cannot easily determine the redshifts and properties of many of the AGNs.

In this Chapter, I investigate the Eddington ratios for X-ray selected broad-line AGNs in the CCLS, CDF-S, E-CDF-S, and *XMM*-LH fields. Absorption-corrected X-ray luminosities together with bolometric corrections will allow an estimate of bolometric luminosities of

AGNs. The advantage of using X-ray luminosities to derive AGN bolometric luminosities is that they are relatively less affected by the presence of obscuration and contamination effects from the host galaxy. I determine black hole masses using Keck/DEIMOS optical and Subaru/FMOS NIR spectroscopic observations, as well as available optical spectroscopy from the literature. I also investigate the possible biases that are due to systematics and selection effects on the observed data.

3.2 Broad-line AGN sample

The sample of broad-line (Type 1) AGNs is selected for which one or more broad emission lines have been identified in the spectrum. From the optical/NIR spectra, broad Hα, Hβ, and Mg II lines are detected for 77, 11, and 121, respectively, by broad-line widths larger than 2000 km s^{-1} of FWHM with the high S/N. For 19 AGNs, broad lines are detected in the both Hα and Mg II lines (see below Figure 3.3). While all AGNs with detection of broad Hα lines are also detected in the broad Mg II line, five AGNs with a broad Mg II line show no broad Hα line, mainly due to the low S/N NIR spectra. It is noted that there are quite a number of clear, broad Hα lines with practically absent Hβ lines, indicating a large Balmer decrement. The final sample of broad-line AGNs in the CCLS, CDF-S, E-CDF-S, and *XMM*-LH fields consists of 183 objects.

3.3 AGN Bolometric Luminosity

The bolometric luminosity of AGNs can be estimated from the X-ray luminosity by applying a suitable bolometric correction. In order to estimate an accurate total intrinsic luminosity radiated by the AGN accretion disc, it is necessary to constrain the absorption-corrected intrinsic X-ray luminosity because it is often obscured and also includes reprocessed radiation. I thus derive the absorption corrected rest-frame X-ray luminosity and determine the bolometric luminosity with the bolometric correction. To account for the dependence of the optical-to-X-ray flux ratio $\alpha_{\rm ox}$ on luminosity, the luminosity-dependent bolometric

correction factor is used (see e.g., Vignali et al. 2003; Marconi et al. 2004; Hopkins et al. 2007; Lusso et al. 2012). Despite some difference between the luminosity-dependent bolometric correction factor among different studies (e.g., Lusso et al. (2012) predicted lower bolometric correction at high bolometric luminosity with respect to that predicted by Marconi et al. (2004) and Hopkins et al. (2007)), the same trend of increasing bolometric correction at increasing bolometric luminosity is observed within the scatter.

The bolometric luminosity of AGNs is derived from the absorption-corrected rest-frame intrinsic X-ray luminosity (see Chapter 2) with the luminosity-dependent bolometric correction factor described in Marconi et al. (2004). Marconi et al. (2004) derived the bolometric corrections from an AGN template spectrum of optical, ultraviolet, and X-ray luminosities radiated by the accretion disc and hot corona. They considered only the AGN-accretion-powered luminosity, neglecting the luminosity reprocessed by the dust, which is therefore representative of the AGN accretion power. The scatter is given by ~ 0.1 for X-ray luminosities.

3.4 Black Hole Mass Estimation

The black hole mass can be estimated using the broad-line width and the continuum (or line) luminosity from their single-epoch spectra as proxies for the characteristic velocity and the size of the broad-line region (e.g., Kaspi et al. 2000; Vestergaard 2002; Woo & Urry 2002; McLure & Jarvis 2002; McLure & Dunlop 2004; Greene & Ho 2005; Kollmeier et al. 2006; Vestergaard & Peterson 2006; Shen et al. 2008, 2011). Depending on the redshift, single-epoch virial black hole masses have been estimated from different broad emission lines, such as Mg II (McLure & Jarvis 2002; McLure & Dunlop 2004; McGill et al. 2008; Vestergaard & Osmer 2009; Wang et al. 2009; Shen et al. 2011; Rafiee & Hall 2011), Hβ (Greene & Ho 2005; Vestergaard & Peterson 2006), and Hα (Greene & Ho 2005; Matsuoka et al. 2013) lines. The virial black hole masses are calibrated against the black hole mass estimated by the reverberation mapping or that from the single-epoch broad-line width of Hβ emission

line in the local universe. Although there are several systematic uncertainties in these single-epoch virial black hole mass estimators, a number of studies have shown that there is consistency in black hole masses from various estimators. Shen & Liu (2012) point out that there is essentially no difference in black hole mass estimates using Mg II and the Balmer lines for high redshift luminous AGNs. Matsuoka et al. (2013) also show that virial black hole masses based on Hα and Mg II emission lines are very similar over a wide range in black hole mass. They suggest that local scaling relations, using Hα or Mg II emission lines, are applicable for moderate-luminosity AGNs up to $z \sim 2$.

I measure the properties of broad emission lines (Hα, Hβ, and Mg II) present in optical and NIR spectra to derive single-epoch virial black hole mass of broad-line AGNs. The Hα λ6563Å and the Hβ λ4861Å lines are redshifted to the NIR range, and the Mg II λ2798Å line is present in optical spectra in the redshift range $0.5 < z < 2.5$.

3.4.1 Spectral Line Fitting

The fit to the emission lines is performed using the mpfit routine, which adopts a Levenberg-Marquardt least-squares minimization algorithm to derive the best-fit parameters and a measure of the goodness of the overall fit. I specifically measure the width and the luminosity of emission lines in the case of Hα and Hβ lines and the width and the monochromatic continuum luminosity at 3000Å in the case of the Mg II line. There might be a non-negligible host-galaxy contribution at the 3000Å continuum luminosity, but I do not correct for any contamination by the host galaxy and extinction due to dust. While one should be aware of this issue, the impact of these on black hole masses should be small because the black hole mass scales with the square root of the luminosity (see Chapter 3.5.1).

Broad-line AGN spectra in the wavelength region of interest are usually characterized by a power-law continuum, $f_\lambda \propto \lambda^{-\alpha}$, and broad (or narrow) emission-line components. I begin by fitting a power-law continuum with a slope of the continuum as a free parameter. In the case of the Mg II line, it is crucial to consider a complex of Fe II emission lines because in this wavelength range the lines are strongly blended with the broad Fe II emission features (e.g.,

Vestergaard & Wilkes 2001; Matsuoka et al. 2007; Harris et al. 2013). I simultaneously fit the combination of the power-law continuum and Fe II emission components. An empirical Fe II emission template is adopted from Vestergaard & Wilkes (2001) and convolved with Gaussian profiles of various widths. I left the width, normalization, and offset from the line center as free parameters during the fit. From the best-fit power-law continuum, I derive an estimate of monochromatic luminosity at 3000Å. Finally, I subtract the best-fit power-law continuum (and/or the Fe II emission components) from the spectra.

I further consider individual components to determine the pure broad-line components that enable an accurate determination of the virial black hole masses. The line profile is described by a combination of multiple Gaussian components to best characterize the line shape in the sense that broad emission lines in AGNs can have a complex shape (e.g., Collin et al. 2006). The multiple Gaussian components provide non-Gaussian, asymmetric profiles reproducing the observed broad-line profile smoothly, but I am not concerned with the physical significance of the individual components. I fit the Hα λ6563Å (Hβ λ4861Å) line with a narrow and one or two broad Gaussian components, and the [N II] λ6548,6583Å ([O III] λ4959,5007Å) lines with a pair of Gaussians. The line ratios of the [N II] λ6548,6583Å and the [O III] λ4959,5007Å lines are fixed to the laboratory values of 2.96 and 2.98, respectively. The narrow widths of the [N II] and the [O III] lines are fixed to match the narrow components of Hα and Hβ, respectively. I left the FWHM of the narrow-line components as free parameters but limited to 900 km s^{-1}. For the Mg II line, I fit with one or two broad Gaussian components. I do not consider the doublet component of the Mg II line because the line separation is small and does not affect the broad-line width.

As a consistency check, I compare the fit of the Mg II line with Fe II emission components to that of the Hα line because the Hα line is not affected by Fe II emission. Figure 3.1 shows an example fit of the Hα line and that of the Mg II line with and without the Fe II broad emission component for the same AGN source "*XMM*-LH 270" at $z = 1.576$. The observed spectrum (gray) with the best fit (black) of the Hα line (top panel) and the Mg II line (bottom panel) are shown. The different components are also indicated as red Gaussian

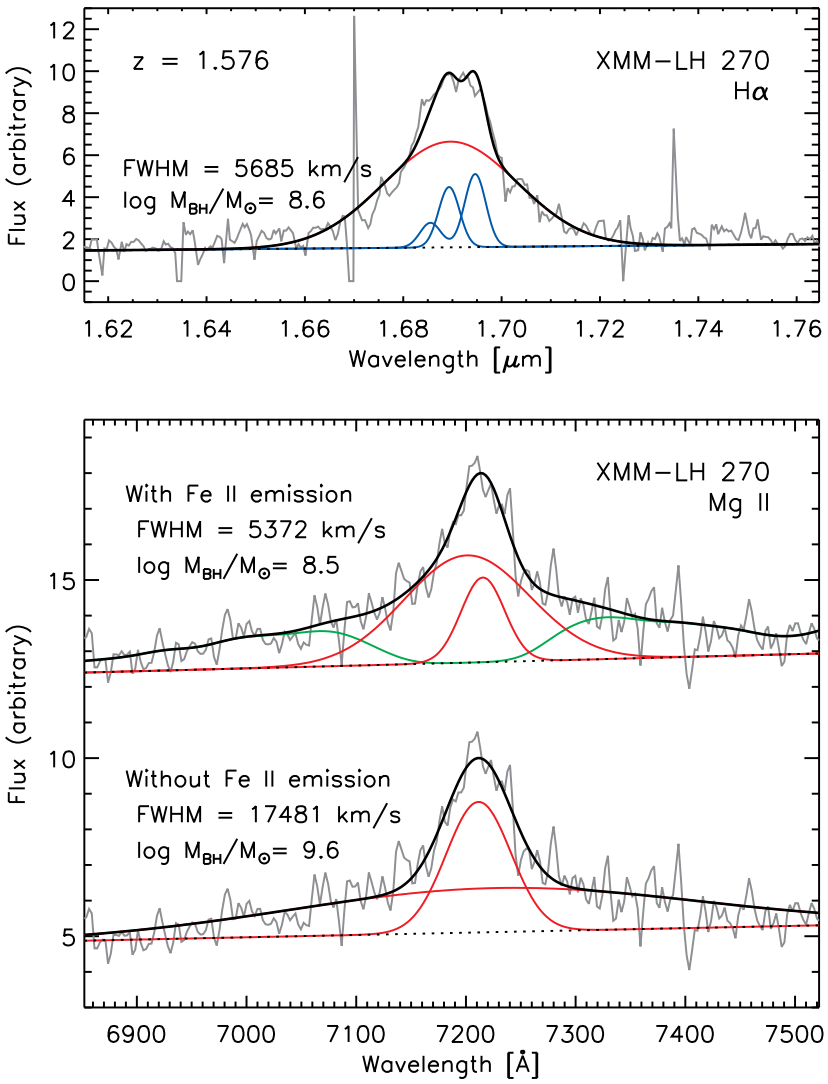

Figure 3.1 Comparison of the broad-line fit for the Hα line (top panel) with that of the Mg II line (bottom panel) with and without an Fe II broad emission component for the same AGN source "*XMM*-LH 270" at $z = 1.576$. The observed spectrum (gray) is shown with the best fit (black). In the top panel, the different components are shown as dotted lines (continuum), red curves (broad-line components), and blue curves (narrow-line components of Hα and a pair of [N II] lines). In the bottom panel, the fits of the Mg II line with Fe II emission (upper) and without Fe II emission (lower) are shown. The different components are indicated as red curves (individual broad-line components) and a green curve (Fe II emission component).

curves (broad-line components), blue curves (narrow-line components of Hα and a pair of [N II] lines), and a green curve (Fe II emission). While it is uncertain whether the Mg II line is blended with Fe II emission or really has a very broad-component in the bottom panel, I confirm that the Mg II line fit with Fe II emission is likely to show a result similar to the Hα line fit in the upper panel.

In order to guarantee a reliable fit, I compare the fit with only narrow-line components, that with narrow-line and one broad Gaussian components, and that with narrow-line and two broad Gaussian components. I perform an F-test to decide whether an additional broad component is needed. I then subtract the narrow-line components from the spectra, obtaining a spectrum that contains only broad-line components. Finally, I inspect all fits by eye to check the cases where a broad component is unclear due to the low signal-to-noise ratio (S/N). I only consider spectra having S/N greater than 10 per pixel.

The broad-line width and the line luminosity are determined from the sum of the broad-line components. From the best fit, the FWHMs of the broad Hα, Hβ, and Mg II lines are computed and corrected for the effect of instrumental resolution to obtain an intrinsic velocity width. I select the broad-line AGNs with broad emission line widths larger than 2000 km s^{-1} of FWHM, a secure threshold for truly broadened lines, as compared to the spectral resolution. Additionally, I take into account the uncertainty in the derived FWHM and luminosity. I perform a Monte Carlo simulation comprising 100 realizations adding noise to each spectrum and iterate the whole procedure to find the best-fit model and the errors compatible with the observations, in order to assess the accuracy of the black hole mass measured. Since the best-fit model could have either one or two broad-line components during different Monte Carlo realizations for each spectrum, this could introduce a larger scatter.

Figure 3.2 shows examples of broad-line fits for Hα (top), Hβ (middle), and Mg II (bottom) emission lines at $z = 1.62,\ 2.13,$ and 1.88, respectively. The upper plot of each panel shows the observed spectrum (gray) with the best-fit model (black). The power-law continuum (black dotted), narrow-line components (blue), and Fe II emission

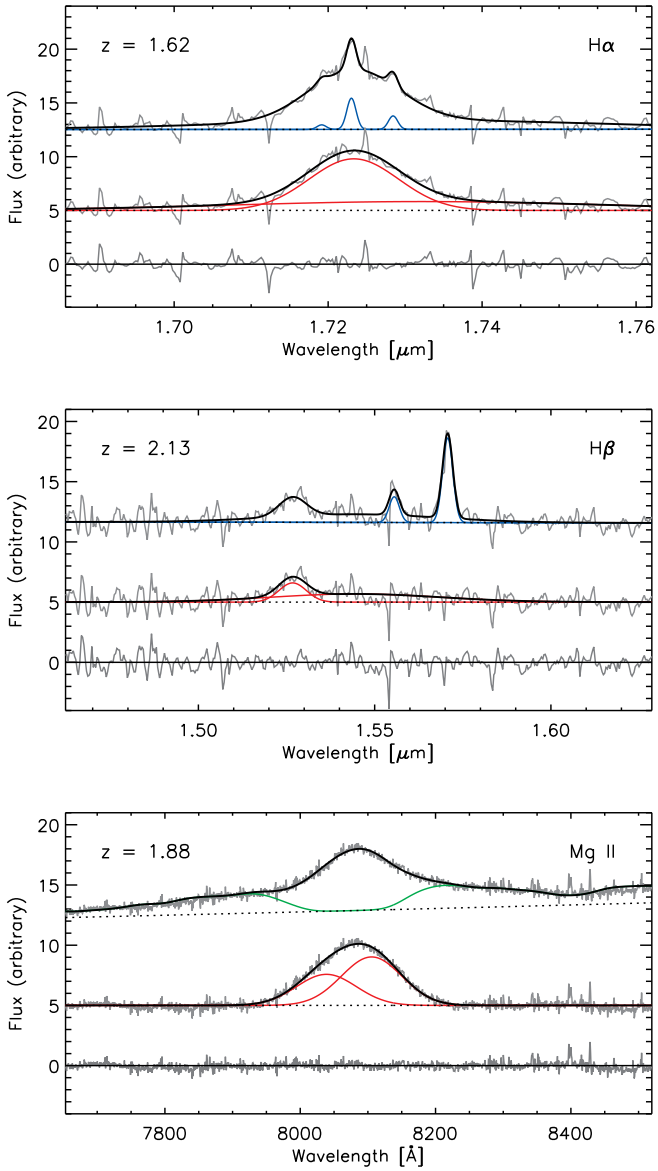

Figure 3.2 Examples of the broad-line fits for Hα (top), Hβ (middle), and Mg II (bottom) emission lines at $z = 1.62,\ 2.13,$ and 1.88, respectively. The upper plot of each panel shows the observed spectrum (gray) with the best-fit model (black). The power-law continuum (dotted), narrow-line components (blue), and Fe II emission component (green) are also indicated. The middle plot of each panel shows the only broad-line components after subtraction of the best-fit model of continuum, narrow components and Fe II emission. The best-fit broad-line model is shown with the black curve. Each Gaussian broad-line component is also shown with red curves. The residual is shown in the lower plot of each panel.

component (green) are also indicated. The middle plot of each panel shows the broad-line-only components after subtraction of the best-fit model of continuum, narrow-line components and Fe II emission. The best-fit broad-line model is shown with the black curve. Each Gaussian broad-line component is also shown with red curves. The residual is shown in the lower plot of each panel.

3.5 Results

3.5.1 Black Hole Mass

Black hole masses are calculated from the FWHM and the luminosity of the sum of the broad-line components. In the case of Hα and Hβ I use the recipes provided by Greene & Ho (2005). In addition, I specifically estimate the black hole mass based on the FWHM of the broad Mg II line and the monochromatic continuum luminosity at 3000Å using the calibration derived by the McLure & Dunlop (2004). The black hole mass can be expressed in the forms:

$$\mathrm{M_{BH}} = 10^{6.301}(\frac{\mathrm{L_{H\alpha}}}{10^{42}\ \mathrm{ergs\ s^{-1}}})^{0.55}(\frac{\mathrm{FWHM_{H\alpha}}}{10^{3}\ \mathrm{km\ s^{-1}}})^{2.06}\ \mathrm{M_{\odot}} \quad (3.1)$$

$$\mathrm{M_{BH}} = 10^{6.556}(\frac{\mathrm{L_{H\beta}}}{10^{42}\ \mathrm{ergs\ s^{-1}}})^{0.56}(\frac{\mathrm{FWHM_{H\beta}}}{10^{3}\ \mathrm{km\ s^{-1}}})^{2.0}\ \mathrm{M_{\odot}} \quad (3.2)$$

$$\mathrm{M_{BH}} = 10^{0.505}(\frac{\lambda \mathrm{L_{\lambda 3000}}}{10^{44}\ \mathrm{ergs\ s^{-1}}})^{0.62}(\frac{\mathrm{FWHM_{MgII}}}{\mathrm{km\ s^{-1}}})^{2.0}\ \mathrm{M_{\odot}} \quad (3.3)$$

where FWHM is the FWHM of the line in units of 1000 km s^{-1}, and $\mathrm{L_{\lambda 3000}}$ is the continuum luminosity at 3000Å.

The comparison of black hole masses estimated using the Hα line with that using the Hβ (red square), or Mg II (red circles) lines is shown in Figure 3.3. I also show the

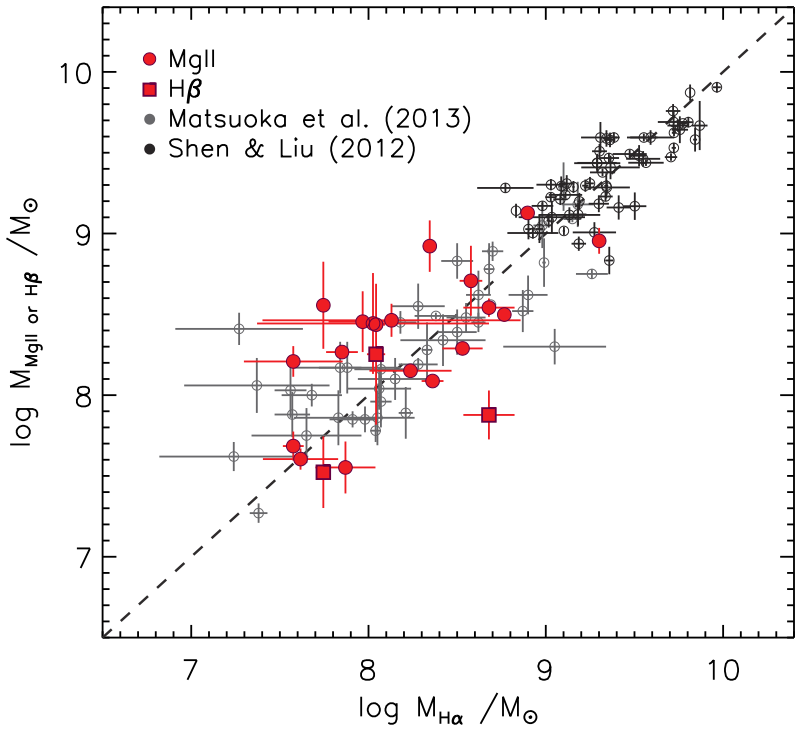

Figure 3.3 Comparison of black hole masses estimated using the Hα line with that using the Mg II line (red circles) or the Hβ line (red squares). The sample of AGNs are shown in red, and the observations from Matsuoka et al. (2013) and Shen & Liu (2012) are also shown as gray and black symbols, respectively. The black dashed line denotes a one-to-one relation.

observations from Matsuoka et al. (2013) and Shen & Liu (2012) as gray and black open circles for comparison, respectively. The black dashed line denotes a one-to-one relation. The sample of broad-line AGNs spans a range of $7.0 < \log M_{\rm BH}/M_{\odot} < 9.5$, which is consistent with the previous studies of moderate-luminosity AGNs at $z \sim 1-2$ (e.g., Merloni et al. 2010; Trump et al. 2011; Matsuoka et al. 2013). The ratios of the mean black hole mass are log $(M_{\rm Mg\,II})$/ log $(M_{\rm H\alpha})$=0.15 and log $(M_{\rm H\beta})$/ log $(M_{\rm H\alpha})$ = -0.27, respectively. The median uncertainty of the black hole mass is ~ 0.1 dex. While there are offsets between the different black hole mass estimations, it is worth noting that the black hole mass estimated with different calibrations carries a scatter of ~ 0.3 dex (McGill et al. 2008). I also note that determination of black hole mass from the Hβ emission line are

known to be affected by significant systematic uncertainties due to the Balmer decrement. If there are multiple lines measured, I use the lines in order of Hα, Mg II, and Hβ for the determination of the black hole mass. There are ten objects in our sample for which black hole masses are determined with the Hβ line.

3.5.2 Eddington Ratio Distribution

To study the accretion rate of black holes, I show AGN bolometric luminosity versus black hole mass for a sample of broad-line AGNs in the different redshift bins in the left panel of Figure 3.4. The different X-ray surveys are shown with different symbols as labeled. The dotted reference lines indicate constant Eddington ratios of 1, 0.1, 0.01, and 0.001. The sample of broad-line AGNs covers the black hole mass range $7.0 < \log M_{\rm BH}/M_{\odot} < 9.5$ and the AGN bolometric luminosity range $43 < \log L_{\rm bol}$ erg s$^{-1} < 47$ with a wide dispersion in the Eddington ratio distribution. For comparison, I show published observations in the same redshift range from the literature in the right panel of Figure 3.4 (Gavignaud et al. 2008; Merloni et al. 2010; Shen et al. 2011; Nobuta et al. 2012; Matsuoka et al. 2013). The SDSS quasar sample (gray points; Shen et al. 2011) is limited to the high-mass and high-luminosity regime because the SDSS detection limit corresponds to a luminosity of $\log L_{\rm bol}$ erg s$^{-1} \sim 46$ at $z \sim 1$. Compared to the SDSS quasar sample, the sample of broad-line AGNs used in this work show a wider dispersion in the black hole mass, AGN bolometric luminosity, and Eddington ratio distribution, consistent with previous studies on deep AGN sample (Gavignaud et al. 2008; Merloni et al. 2010; Nobuta et al. 2012; Matsuoka et al. 2013), which fill in the low-mass and low-luminosity region. The figure shows contours at the 1σ level, together with the literature data, except the SDSS quasar sample. The figure also reveals that only a small number of AGNs exceeds the Eddington limit by a small amount. AGNs with similar black hole masses show a broad range of bolometric luminosities spanning about two orders of magnitude, indicating that the accretion rate of black holes is widely distributed. This suggests that the AGN cosmic downsizing phenomenon could be explained by some more massive black holes with low accretion rates, which are relatively fainter than

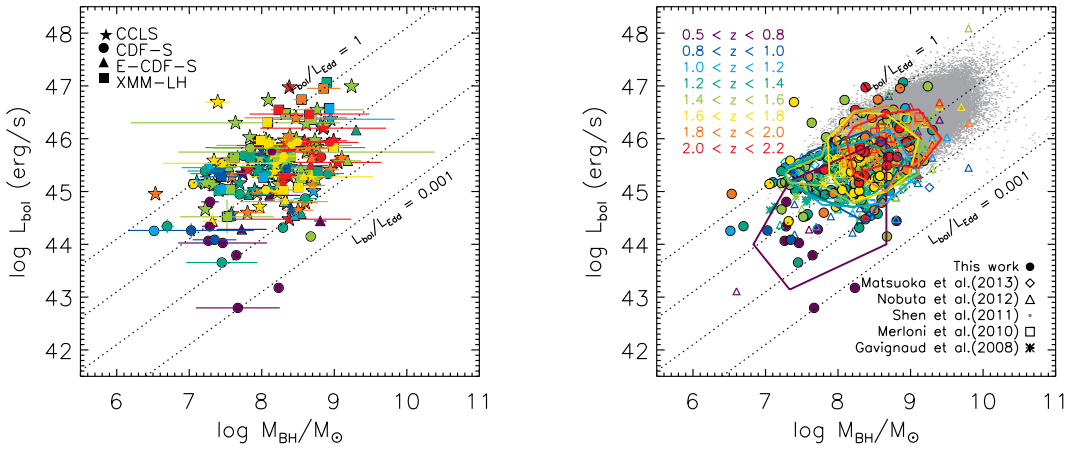

Figure 3.4 AGN bolometric luminosity versus black hole mass for our sample of broad-line AGNs in the different redshift bins (left). In the right panel, contours at the 1σ level are shown in the different redshift bins, together with the published observations from the literature as labeled. As a reference, lines of constant Eddington ratio ($L_{\rm bol}/L_{\rm Edd}$) equals to 1, 0.1, 0.01, and 0.001 are plotted as dotted lines.

less-massive black holes with efficient accretion. Lusso et al. (2012) suggest that AGNs show higher Eddington ratios at higher redshift at any given $M_{\rm BH}$, and the Eddington ratio increases with bolometric luminosity. I confirm that there is a tendency for low-luminosity AGNs (log $L_{\rm bol} \lesssim 45.5$) with less-massive black holes (log $M_{\rm BH}/M_{\odot} \lesssim 8$) to have lower Eddington ratios than high-luminosity AGNs (log $L_{\rm bol} \gtrsim 45.5$) with massive black holes (log $M_{\rm BH}/M_{\odot} \gtrsim 8$), consistent with Lusso et al. (2012). It is important to note that, when comparing with results in the literature, one should take into account the different methods of spectral line fitting and correction for bolometric luminosities. Nevertheless, they show similar distributions of the accretion rate of black holes over a wide range, consistent with previous studies.

Several studies have found a correlation between the X-ray bolometric correction and the Eddington ratio (e.g., Vasudevan & Fabian 2007; Lusso et al. 2012), which may introduce biases into this diagram. Lusso et al. (2012) found that there is a trend for higher bolometric corrections at higher bolometric luminosities. Vasudevan & Fabian (2007) suggest that there appears to be a distinct step change in bolometric correction at an Eddington

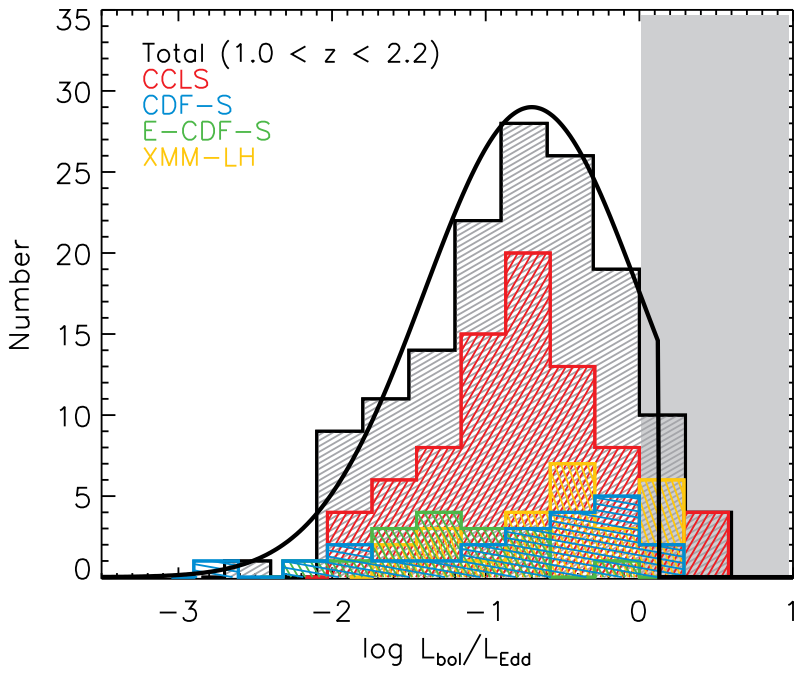

Figure 3.5 Eddington ratio distribution of broad-line AGNs at $1.0 < z < 2.2$. The different X-ray surveys are shown in different color histograms, and the black histogram represents the combined distribution of all surveys. The gray shade indicates the Eddington limit. The red solid line indicates a log-normal fit with a peak of $\log L_{\rm bol}/L_{\rm Edd} = -0.7$ and a dispersion of 0.8 dex.

ratio of ~ 0.1, below which lower bolometric corrections apply and above which higher bolometric corrections apply. If one includes this correlation, the trend between bolometric luminosities and black hole masses in Figure 3.4, in which low-luminosity AGNs have lower accretion rates while high-luminosity AGNs show higher accretion rates, would even be more pronounced. However, I note the possibility that there could be the spurious correlations because $L_{\rm bol}$ is present on both axes when plotting the bolometric correction against the Eddington ratio.

I show the Eddington ratio distribution of the sample of broad-line AGNs in the redshift range $1.0 < z < 2.2$ in Figure 3.5. The different X-ray surveys are shown in different color histograms, and the black histogram represents the combined distribution of all surveys. The distribution of Eddington ratios peaks at $\log {\rm L_{bol}/L_{Edd}} \sim -1$ with an extended tail

towards low Eddington ratios, down to $\log \mathrm{L_{bol}/L_{Edd}} \sim -3$. A log-normal fit with a peak of $\log \mathrm{L_{bol}/L_{Edd}} = -0.7$ and a dispersion of 0.8 dex is shown as black solid line. In previous studies, Kollmeier et al. (2006) suggest that the Eddington ratios are quite narrowly distributed independent of luminosity ($L_{\rm bol} = 10^{45} - 10^{47}$ erg s^{-1}) and redshift ($0.3 < z < 4.0$), with a dispersion of 0.3 dex (see also Steinhardt & Elvis 2010). Lusso et al. (2012) also suggest that the distribution of Eddington ratios are nearly Gaussian especially at high redshift and at high $L_{\rm bol}/M_{\rm BH}$, with a dispersion of $\sim$0.35 dex, while the low redshift and low $L_{\rm bol}/M_{\rm BH}$ are more affected by incompleteness.

It should be emphasized here that the systematic selection effects could certainly be playing a role in determining the distribution of AGN bolometric luminosities and black hole masses. The Eddington ratio distribution, thus, could be a result of the selection bias, mainly the limited X-ray luminosity but also to the broad line width, i.e., the black hole mass. The X-ray luminosity is limited by the X-ray flux limit, depending on redshift and on the limited volume. The detectability of the broad emission line gives rise to a bias against the black hole mass. Also, the black hole mass could be biased by observational limitations in detecting the corresponding very broad lines and low signal-to-noise spectra. This is bound to introduce selection biases, which could mimic artificial correlations in the data. Hence, I will further discuss the possible selection effects in the next section.

3.6 Discussion

3.6.1 Analysis of Selection Biases

I investigate the possible bias due to systematics and selection effects on the observed AGN bolometric luminosity and the black hole mass. To explore the effect of these selection biases, I construct Monte Carlo simulations to make artificial data sets, which are affected by the same selection effects. I start from the bolometric luminosity function of AGNs (Hopkins et al. 2007) in the different redshift bins with an assumption for the Eddington ratio distribution, which has a peak of $\log L_{\rm bol}/L_{\rm Edd} = -0.7$ and a dispersion of 0.8 dex,

bounded by $L_{\rm Edd}$, taken from the observed distribution (see black curve in Figure 3.5). To account for the observed selection biases, I apply the same selection effects based on our combined X-ray surveys. The X-ray flux limit corresponds to a bolometric luminosity of $\log L_{\rm bol} \sim 43$ at $z \sim 1$. I use the survey area of the total combined X-ray surveys. Since it is known that there is a much larger fraction of obscured AGN at lower luminosities (Ueda et al. 2003; Steffen et al. 2003; Simpson 2005; Hasinger 2008), I apply the fraction of broad-line AGNs as a function of AGN luminosity from Hasinger (2008), in which the same bolometric correction (Marconi et al. 2004) was applied to the X-ray luminosity. The black hole mass is biased by the detectability of the broad emission line and the signal-to-noise of spectra. I thus apply a "fudge" factor, which is the exponentially decaying function at low-mass ($6.5 < \log M_{\rm BH} < 7.5$) and high-mass ($8.5 < \log M_{\rm BH} < 9.5$). The "fudge" factor brings down the numbers of low-mass ($6.5 < \log M_{\rm BH} < 7.5$) and high-mass ($8.5 < \log M_{\rm BH} < 9.5$) AGNs and takes into account the spectroscopic incompleteness. For each data set of the different redshift bins, I calculate black hole masses from the AGN bolometric luminosity and the Eddington ratio. The Eddington ratio distribution is assumed to be same regardless of AGN luminosity or redshift, which is a valid assumption for the high-luminosity AGNs (Kollmeier et al. 2006). Steinhardt & Elvis (2010) report that the Eddington ratio distributions are all similar for SDSS quasar populations over a wide range of mass and redshift.

In Figure 3.6, the Monte Carlo-simulated data sets (left panel), and those that are affected by the same observed selection effects (right panel) are shown with gray symbols and contours at the 1σ level in the different redshift bins. The black solid line in the right panel of Figure 3.6 indicates the assumed peak of Eddington ratio, $\log L_{\rm bol}/L_{\rm Edd} = -0.7$. The AGN downsizing trend is seen in the sense that the characteristic AGN luminosity and black hole mass decrease with redshift. This is primarily due to the strong evolution of the comoving number density at the bright end of the AGN luminosity function at $0.5 < z < 2.0$, together with the corresponding selection biases. I compare the simulated data with the observed AGNs in the different redshift bins in Figure 3.7. The simulated

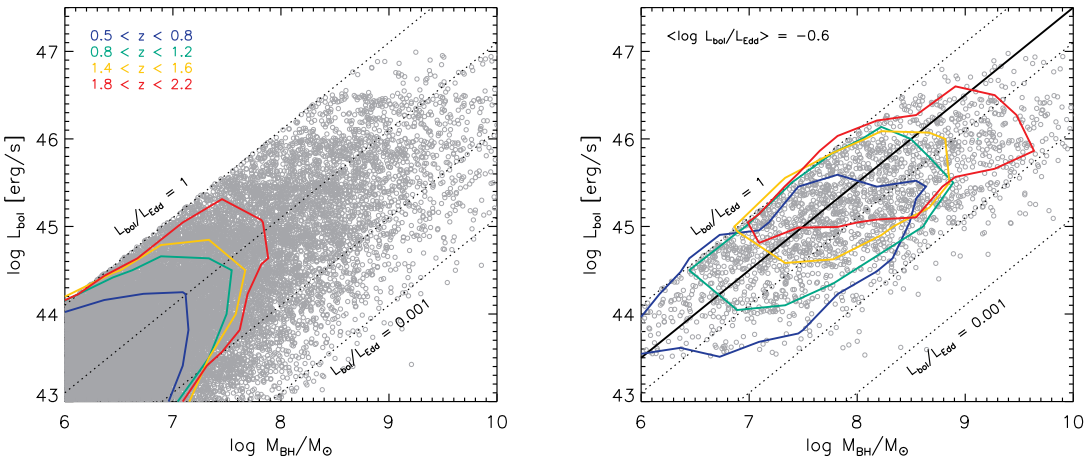

Figure 3.6 Monte Carlo-simulated data sets from the AGN bolometric luminosity function (Hopkins et al. 2007) in the different redshift bins with an assumption for the Eddington ratio distribution, which has a peak of log $L_{bol}/L_{Edd} = -0.7$ and a dispersion of 0.8 dex (black curve in Figure 3.5) regardless of AGN luminosity or redshift. The simulated data sets (left) and those that are affected by the same observed selection effects (right) are shown in gray. As a reference, lines of constant Eddington ratio (L_{bol}/L_{Edd}) equals to 1, 0.1, 0.01, 0.001 are plotted as dotted lines. Contours at the 1σ level are shown in the different redshift bins. The black solid line indicates the assumed peak of Eddington ratio.

data sets are shown in gray with the contour at the 1σ level, and the observed AGNs are shown in colored symbols for each redshift bin in the top panels. For each redshift bin, I group the data into four sets using a constant Eddington ratio of $L_{bol}/L_{Edd} = 0.1$ and a line perpendicular to the Eddington ratio as separation. In the bottom panels, the number of detected (observed) sources over the number of expected (simulated) sources is given in parentheses, as well as the Poisson likelihood calculated from this combination. In bins of high-luminosity AGNs with high Eddington ratio as well as low-luminosity AGNs with low Eddington ratio, the detected number of objects agrees with the prediction from the Monte Carlo simulation within the statistical errors. However, for low-luminosity AGNs with high Eddington ratios, especially at high redshift ($1.8 < z < 2.2$) and low redshift ($0.5 < z < 0.8$) bins, the simulations systematically predict a larger number of objects, than those observed. Taking all Poisson likelihoods together, there is a difference between the observed and the predicted distributions. I therefore suggest that there is a dependence

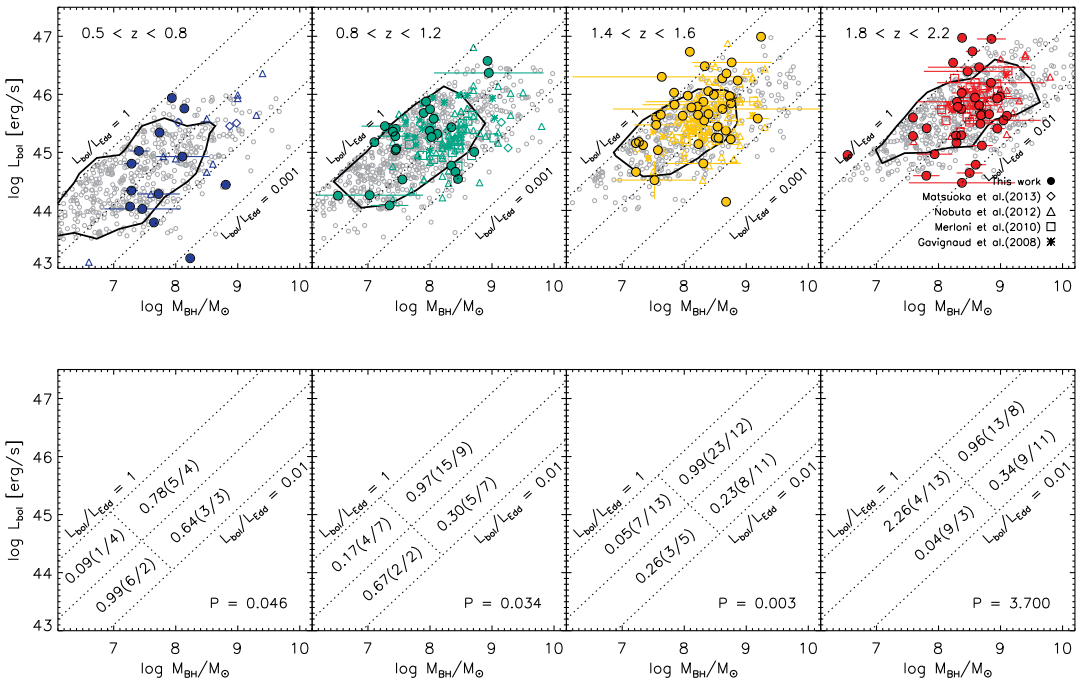

Figure 3.7 Comparison of the Monte Carlo-simulated data sets with the observed AGNs in the different redshift bins. In the top panels, the simulated data sets are shown in gray with the 1σ contour, and the observed AGNs are shown as purple ($0.5 < z < 0.8$), green ($0.8 < z < 1.2$), yellow ($1.4 < z < 1.6$), and red ($1.8 < z < 2.2$) symbols. In the bottom panels, the Poisson likelihood is shown in each bin, which is perpendicular to the Eddington ratio plane. The numbers in parentheses refer to detected (observed) sources over expected (simulated) sources. Reference lines of constant Eddington ratios are plotted as dotted lines.

of AGN luminosities on the Eddington ratios in the sense that luminous AGNs appear to have systematically higher Eddington ratios than low-luminosity AGNs. However, this result is of marginal significance because of the relatively small number of objects in each bin. I note that this sample of high-luminosity X-ray-selected AGNs overlaps with the less luminous quasars from the SDSS sample at the highest Eddington ratios (see gray points in the right panel of Figure 3.4), while the most-luminous, most-massive SDSS quasars lie further away from their Eddington luminosity (Steinhardt & Elvis 2010).

3.6.2 AGN Downsizing Interpretation

I now discuss the observed AGN downsizing phenomenon and possible explanations for the black hole growth over cosmic time. The decrease of the characteristic luminosity of AGNs with redshift has been described as AGN downsizing, implying that the AGN activity at earlier epochs was much more intense. I show that AGNs with similar black hole masses show a broad range of bolometric luminosities, which means the accretion rate of black holes is widely distributed. The average accretion rate of two different AGN fueling mechanisms can play a crucial role for the downsizing interpretation. AGN activity triggered by major mergers is thought to have a higher accretion rate than activity triggered by secular evolution effects. Therefore the luminosity of an AGN with a certain black hole mass may differ widely, depending on the accretion mechanisms.

Several studies have found that the majority of AGN host galaxies show a lack of significant merger features up to $z \sim 2$ (e.g., Fan et al. 2014; Mainieri et al. 2011; Kocevski et al. 2012; Schawinski et al. 2012; Schramm & Silverman 2013; Villforth et al. 2014). It is likely that merger features are visible only for a few gigayears after major mergers (e.g. Lotz et al. 2008; Ji et al. 2014), suggesting that most AGN activity does not seem to be triggered by major mergers. Allevato et al. (2011) further point out that moderate-luminosity AGNs at $z = 0 - 2$ live in relatively massive dark matter halos ($10^{13.5} M_{\odot}$), which corresponds to rich groups of galaxies, independent of redshift. The rich group environment may provide a kind of "goldilocks" zone for AGNs in the sense that on one hand the density is high enough to cause frequent gravitational disturbances bringing cold gas to the center, and on the other hand the gas density in the group is not high enough to remove the cold gas from the galaxies due to ram pressure stripping. This also indicates that major mergers cannot be the main driver of the late evolution of AGNs. This raises interesting questions regarding different fueling mechanisms for the growth of black holes and galaxies at different epochs during cosmic time.

Given these intriguing findings, a possible interpretation for explaining the cosmic downsizing, as well as morphologies and colors of AGN host galaxies, is that there are

two different modes of AGN feedback at different epochs (see Hasinger 2008). In an active AGN phase at high redshift, black holes have experienced vigorous growth by major mergers while radiating close to the Eddington limit (see e.g., Di Matteo et al. 2005). When they reach a critical mass, at which the AGN is sufficient to blow out the surrounding gas, the feedback of the black hole suppresses further star formation and creates a red bulge-dominated remnant (e.g., Fabian 1999; Springel et al. 2005). It is likely that only a small fraction of the transient population can be found in between the blue cloud and the red sequence, due to a rather short merger timescale ($\sim 10^8$ years). The relatively massive galaxies, which have already experienced substantial growth by previous mergers, grow slowly through episodic star formation via secular evolution, leading to a disc surrounding the bulge. The modest AGN activity can be triggered by the gas accretion over cosmic time via internal, secular processes, such as gravitational instabilities in the disc. This secular growth is slow enough, and thus, the presence of AGN host galaxies in the green valley on the color-magnitude diagram could be interpreted as evidence for on-going star formation in the inner region of low-luminosity AGN host galaxies at lower redshift, coming down from the red sequence. This is also compatible to the weak link between merger features and AGN activity, as well as the moderate-luminosity AGNs in the relatively massive dark matter halos at $z \lesssim 2$, where the number density of most luminous AGNs starts to decline. Finally, the late feedback from AGNs suppresses the late cooling flows of hot gas, keeping the galaxy quiescent. This seems to be consistent with dormant SMBHs in dynamically hot systems (e.g., massive early-type galaxies) that contain little cold gas and correspondingly little star-formation. All of these seem to be consistent with the hierarchical growth scenario.

3.7 Summary

I present the Eddington ratio distribution of X-ray selected broad-line AGNs in the CCLS, CDF-S, E-CDF-S, and the *XMM*-LH surveys. I calculate AGN bolometric luminosities from absorption-corrected X-ray luminosities and estimate black hole masses of broad-line

AGNs using the keck/DEIMOS optical and Subaru/FMOS NIR spectroscopy. The sample of broad-line AGNs spans the AGN bolometric luminosity range $L_{\rm bol} \sim 10^{43.5-47}$ erg s^{-1}, and the black hole mass range $M_{\rm BH} \sim 10^{6.5-9.5}$ $M_{\odot}$ with a broad range of Eddington ratios $L_{\rm bol}/L_{\rm Edd} \sim 0.001 - 1$.

I explore the systematics and selection biases, because in general observed distributions are dependent on the X-ray flux limit and the detectability of the broad emission lines. Based on the analysis on these effects, I find that the observed downsizing trend could be simply explained by the strong evolution of the comoving number density at the bright end of the AGN luminosity function at $0.5 < z < 2.0$, together with the corresponding selection effects. However, in order to explain the relatively small fraction of low-luminosity AGNs with high accretion rates, we might need to consider a correlation between the AGN luminosity and the accretion rate of black holes that luminous AGNs have higher Eddington ratios than low-luminosity AGNs. I suggest that the AGN downsizing trend can be interpreted as the fraction of AGNs radiating close to the Eddington limit decrease after their peak activity phases, suggesting that the fueling mechanism of growth of black holes might change through the cosmic time.

References

Allevato, V., Finoguenov, A., Cappelluti, N., et al. 2011, ApJ, 736, 99

Babić, A., Miller, L., Jarvis, M. J., et al. 2007, A&A, 474, 755

Choi, Y., Gibson, R. R., Becker, A., et al. 2014, ApJ, 782, 37

Collin, S., Kawaguchi, T., Peterson, B. M., Vestergaard, M. 2006, A&A, 456, 75

Di Matteo, T., Springel, V., Hernquist, L. 2005, Nature, 433, 604

Fabian, A. C. 1999, MNRAS, 308, 39

Fabian, A. C., Vasudevan, R. V., Gandhi, P. 2008, MNRAS, 385, 43

Fan, L., Fang, G., Chen, Y., et al. 2014, ApJ Letters, 784, L9

Gavignaud, I., Wisotzki, L., Bongiorno, A., et al. 2008, A&A, 492, 637

Greene, J. E., & Ho, L. C. 2005, ApJ, 630, 122

Harris, K. A., Williger, G. M., Haberzettl, L., et al. 2013, MNRAS, 435, 3125

Hasinger, G. 2008, A&A, 490, 905

Hopkins, P. F., Richards, G. T., Hernquist, L. 2007, ApJ, 654, 731

Ji, I., Peirani, S., Yi, S. K. 2014, arXiv:1405.1807v1

Kaspi, S., Smith, P. S., Netzer, H., et al. 2000, ApJ, 533, 631

Kelly, B. C., Vestergaard, M., Fan, X., et al. 2010, ApJ, 719, 1315

Kocevski, D. D., Faber, S. M., Mozena, M. et al. 2012, ApJ, 744, 148

Kollmeier, J. A., Onken, C. A., Kochanek, C. S., et al. 2006, ApJ, 648, 128

Lotz, J. M., Jonsson, P., Cox, T. J., & Primack, J. R. 2008, MNRAS, 391, 1137

Lusso, E., Comastri, B. D., Simmons, M. M., et al. 2012, MNRAS, 425, 623

Mainieri, V., Bongiorno, A., Merloni, A. 2011, A&A, 535, A80

Marconi, A., Risaliti, G., Gilli, R., et al. 2004, MNRAS, 351, 169

Matsuoka, Y., Oyabu, S., Tsuzuki, Y., Kawara, K. 2007, ApJ, 663, 781

Matsuoka, K., Silverman, J. D., Schramm, M., et al. 2013, ApJ, 771, 64

Merloni, A., Bongiorno, A., Bolzonella, M., et al. 2010, ApJ, 708, 137

McGill, K. L., Woo, J., Treu, T., Malkan, M. A. 2008, ApJ, 673, 703

McLure, R. J, & Jarvis, M. J. 2002, MNRAS, 337, 109

McLure, R. J., & Dunlop, J. S. 2004, MNRAS, 352, 1390

Nobuta, K., Akiyama, M., Ueda, Y. et al. 2012, ApJ, 761, 143

Rafiee, A., & Hall, P. B. 2011, ApJS, 194, 42

Schawinski, K., Simmons, B. D., Urry, C. M., et al. 2012, MNRAS, 425, L61

Schneider, D. P., Richards, G. T., Hall, P. B., et al. 2010, AJ, 139, 2360

Schramm, M., and Silverman, J. D. 2013, ApJ, 767, 13

Schulze, A., & Wisotzki, L. 2010, A&A, 516, 87

Shen, Y., Greene, J. E., Strauss, M. A., et al. 2008, ApJ, 680, 169

Shen, Y., Richards, G. T., Strauss, M. A., et al. 2011, ApJS, 194, 45

Shen, Y., & Liu, X. 2012, ApJ, 753, 125

Simpson, C. 2005, MNRAS, 360, 565

Springel, V., Di Matteo, T., & Hernquist, L. 2005, MNRAS, 361, 776

Steffen, A. T., Barger, A. J., Cowie, L. L., et al. 2003, ApJ, 596L, 23

Steinhardt, C. L., & Elvis, M. 2010, MNRAS, 402, 2637

Suh, H., Hasinger, G., Steinhardt, C., Silverman, J. D., Schramm, M. 2015, ApJ, 815, 129

Trump, J. R., Impey, C. D., Kelly, B. C., et al. 2011, ApJ, 733, 60

Ueda, Y., Akiyama, M., Ohta, K., et al. 2003, ApJ, 598, 886

Vasudevan, R. V., and Fabian, A. C. 2007, MNRAS, 381, 1235

Vestergaard, M. 2002, ApJ, 571, 733

Vestergaard, M., & Osmer, P. S. 2009, ApJ, 699, 800

Vestergaard, M., & Peterson, B. M. 2006, ApJ, 641, 689

Vestergaard, M., & Wilkes, B. J. 2001, ApJS, 134, 1

Vignali C., Brandt W. N., Schneider D. P., 2003, AJ, 125, 433

Villforth, C., Hamann, F., Rosario, D. J., et al. 2014, MNRAS, 439, 3342

Wang, J., Dong, X., Wang, T. et al. 2009, ApJ, 707, 1334

Woo, J., & Urry, C. M. 2002, ApJ, 579, 530

Chapter 4

AGN Activity and Growth of Galaxies

4.1 Introduction

A number of efforts have been made to understand the connection between nuclear activity and star formation in AGN host galaxies (e.g., Lutz et al. 2010; Shao et al. 2010; Mainieri et al. 2011; Harrison et al. 2012; Mullaney et al. 2012; Rovilos et al. 2012; Santini et al. 2012; Rosario et al. 2013; Lanzuisi et al. 2015; Suh et al. 2017). Many theoretical models have suggested that SMBHs may regulate the star formation in their host galaxies through feedback from AGN (e.g., Silk & Rees 1998; Di Matteo et al. 2005; Hopkins & Hernquist 2006), while in the alternative view, the galaxy may set the mass of the SMBH by regulating the amount of gas that trickles to the black hole. The relative importance of various modes of AGN feedback likely changes dramatically through cosmic time, it is important to trace the growth of black holes and their contribution to galaxy evolution.

In this Chapter, I investigate the properties of AGN host galaxies in the CCLS to overcome the limitations (see Chapter 1.2) by exploiting a large sample of X-ray-selected moderate-luminosity AGNs to have a better understanding of nuclear activity and its connection with the star formation. Thanks to the large, uniform X-ray depth and the excellent extensive multi-wavelength data in the COSMOS field, I estimate both AGNs and their host galaxy properties in a wide range of redshifts, for the largest data set adopted so far in this kind of studies. The moderate-luminosity AGNs allow us to

determine the host galaxy properties with relatively smaller systematic uncertainties. To derive the physical properties of AGN host galaxies, I utilize multi-wavelength data from near-ultraviolet (NUV) to far-infrared (FIR) wavelengths of a large sample of AGN host galaxies. Specifically, I develop a multi-component SED fitting technique to decompose the entire SED into separate components with nuclear AGN emission, the host galaxy's stellar populations, and a starburst contribution in the FIR, and derive AGN host galaxy properties such as stellar mass and SFR. Finally, I discuss the effects of the nuclear activity on the star formation in AGN host galaxies. In this analysis, I consider 3701 X-ray selected AGNs (985 Type 1 and 2716 Type 2 AGNs) in the CCLS, which has the already existing extensive compilation of multi-wavelength data (see Chapter 2.1.1).

4.2 AGN Host galaxy Properties

I develop a four-component SED fitting technique that allows one to disentangle the nuclear emission from the stellar light over the NUV to FIR wavelength coverage. The emission from the nuclear accretion disk peaks in the UV, and is partly absorbed by the dust and re-emitted in the IR wavelength range. The observed SEDs of AGN, thus, often peak in the X-ray-to-UV and mid-infrared (MIR) regimes (e.g., Elvis et al. 1994; Richards et al. 2006). For Type 2 (obscured) AGN host galaxies, I decompose the entire SED into a nuclear AGN dusty obscuring structure (e.g., a torus), a host galaxy with stellar populations, and a starburst component, which is crucial for estimating reliable physical properties of host galaxies such as galaxy mass and SFR. For Type 1 (unobscured) AGN host galaxies, I add an additional fourth component in the fit that represents the AGN emission in the optical-UV from "big-blue bump", which is thought to be representative of the accretion disk emission around the SMBH (BBB; Sanders et al. 1989; Elvis et al. 1994, 2012; Richards et al. 2006; Shang et al. 2011; Krawczyk et al. 2013). The method used here is similar to the one applied by Lusso et al. (2011) and Bongiorno et al. (2012) on the XMM-COSMOS

dataset, with significant improvements, including the Bayesian method described in the following sections.

4.2.1 Multi-wavelength Dataset

I compile the SEDs of a sample of AGNs from NUV (2300Å) to FIR (500μm) wavelengths using the multi-wavelength photometric data available in the COSMOS field. Specifically, I use the most recent photometric catalog from Laigle et al. (2016) including the *GALEX* NUV band, CFHT U band, five Subaru Suprime-Cam bands (B, V, r, i, z^+), four UltraVista bands (*Y, H, J, Ks*), and four *Spitzer*/IRAC bands (3.6, 4.5, 5.8, and 8.0μm). The detection fraction for each photometry band is presented in Table 4.1. In addition, I use the 24μm and 70μm Multiband Imaging Photometer for *Spitzer* (MIPS) bands (Sanders et al. 2007; Le Floc'h et al. 2009) with ∼63% (2317/3701) of the sources detected in the 24μm band, which is particularly important for identifying the AGN dusty obscuring structure. I also constrain the SEDs in the FIR wavelength range for ∼27% (1011/3701) of the sources that have been detected by the *Herschel Space Observatory* (PACS 100μm (∼15%; 543/3701), 160μm (∼12%; 457/3701) and SPIRE 250μm (∼22%; 798/3701), 350μm (∼11%; 409/3701), 500μm (∼3%; 112/3701); Pilbratt et al. 2010; Poglitsch et al. 2010; Griffin et al. 2010). I limit the work to only those objects with at least ten detected photometric data points (∼91%; 3355/3701), to guarantee a reliable measurement of the SED fits.

4.2.2 Model templates

In order to examine the SEDs for AGN host galaxies, I use model SEDs, which are made by combining a stellar population, optical-UV emission from AGN BBB, hot dust emission from AGN torus, and IR starburst templates to match the broadband photometry SEDs of AGN sample. The nuclear emission contributes significantly to the UV-to-optical parts of the spectra of unobscured (Type 1) AGNs (e.g. Elvis et al. 2012; Hao et al. 2013), while in obscured (Type 2) AGNs, the nuclear emission dominates the SED only in the X-ray band and at other wavelengths, the light is mainly due to the galaxy emission combined with

Table 4.1. Detection Fraction for Each Photometry Band

Photometry Band	**Detection fraction**
GALEX NUV	13%(466/3701)
CFHT U	68%(2519/3701)
Subaru B	76%(2819/3701)
Subaru V	77%(2845/3701)
Subaru r	84%(3104/3701)
Subaru i	85%(3137/3701)
Subaru z^+	87%(3213/3701)
UltraVista Y	73%(2720/3701)
UltraVista J	75%(2783/3701)
UltraVista H	78%(2878/3701)
UltraVista Ks	80%(2944/3701)
Spitzer 3.6μm	92%(3390/3701)
Spitzer 4.5μm	92%(3391/3701)
Spitzer 5.8μm	86%(3169/3701)
Spitzer 8.0μm	78%(2888/3701)

reprocessed nuclear emission in the NIR and MIR. While nuclear emission, reprocessed by dust, could significantly contribute to the MIR luminosity, the FIR luminosity is known to be dominated by galaxy emission produced by star-formation activity (e.g., Kirkpatrick et al. 2012). Although a recent study by Symeonidis (2017) pointed out that the most powerful unobscured quasars could dominate the FIR luminosity, I only consider the far-IR luminosity produced by starburst activity for this sample of moderate-luminosity AGNs.

The optical SED of a galaxy represents the integrated light of the stellar populations. I have generated a set of synthetic spectra from the stellar population synthesis models of Bruzual & Charlot (2003). The solar metallicity and the Chabrier (2003) initial mass function (IMF) have been used. I have built 10 exponentially decaying star-formation histories (SFH), where the optical star-formation rate is defined as SFR $\propto$ $e^{t/\tau}$, with characteristic times ranging from τ = 0.1 to 30 Gyr, and a model with constant star formation. For each SFH, the SEDs are generated by models with 15 grids of ages ($t_{\rm age}$) ranging from 0.1 to 10 Gyr, with the additional constraint on each component that the age should be smaller than the age of the universe at the redshift of the source. The library

of stellar population models is composed of 165 templates. Since the stellar light can be affected by dust extinction, I take into account the reddening effect using the Calzetti et al. (2000) law. I have considered $E(B-V)$ values in the range between 0 and 0.5 with steps of 0.05, and the range between 0.5 and 1 with a step of 0.1. I show some examples of stellar population templates with various combinations of τ=[0.1, 1, 3], and t_{age}=[50 Myr, 2 Gyr] with $E(B-V)$=[0.0, 0.3] in Figure 4.1 (green curves).

The UV-to-optical part of the SED of unobscured (Type 1) AGN is dominated by the nuclear emission from the BBB. The BBB template is taken from Richards et al. (2006). This template is reddened according to the Prevot et al. (1984) reddening law for the Small Magellanic Clouds (SMC, which seems to be appropriate for Type 1 AGNs; Hopkins et al. 2004; Salvato et al. 2009). The $E(B-V)_{\rm AGN}$ values range between 0 and 1 with a variable step ($\Delta E(B-V)_{\rm AGN} = 0.01$ for $E(B-V)_{\rm AGN}$ between 0 and 0.1, and $\Delta E(B-V)_{\rm AGN} = 0.05$ for $E(B-V)_{\rm AGN}$ between 0.1 and 1) for a total of 29 templates. A subsample of BBB templates with different reddening levels $E(B-V)$=[0.00, 0.03, 0.10, 0.50, 0.90] is presented in Figure 4.1 (blue curves).

In general, the SED of an obscured (Type 2) AGN is characterized by the NIR bump that is a result of the absorption of intrinsic nuclear radiation by dust clouds in the proximity of the central region (so-called torus) on parsec scales, which subsequently re-radiate at infrared frequencies (Barvainis 1987). The dust torus SED templates are taken from Silva et al. (2004), as constructed from the study of a large sample of Seyfert galaxies for which clear signatures of non-stellar nuclear emission were detected in the NIR and MIR, and also using the radiative transfer code GRASIL (Silva et al. 1998). There are four different templates depending on the amount of nuclear obscuration in terms of hydrogen column density, $N_H < 10^{22}$ cm^{-2} for Seyfert 1, and $10^{22} < N_H < 10^{23}$ cm^{-2}, $10^{23} < N_H < 10^{24}$ cm^{-2}, and $N_H > 10^{24}$ cm^{-2} for Seyfert 2. The four templates of AGN dust torus are plotted in Figure 4.1 with yellow curves. The larger the column density, the higher is the nuclear contribution to the IR emission. Although the X-ray data for this AGN sample contains

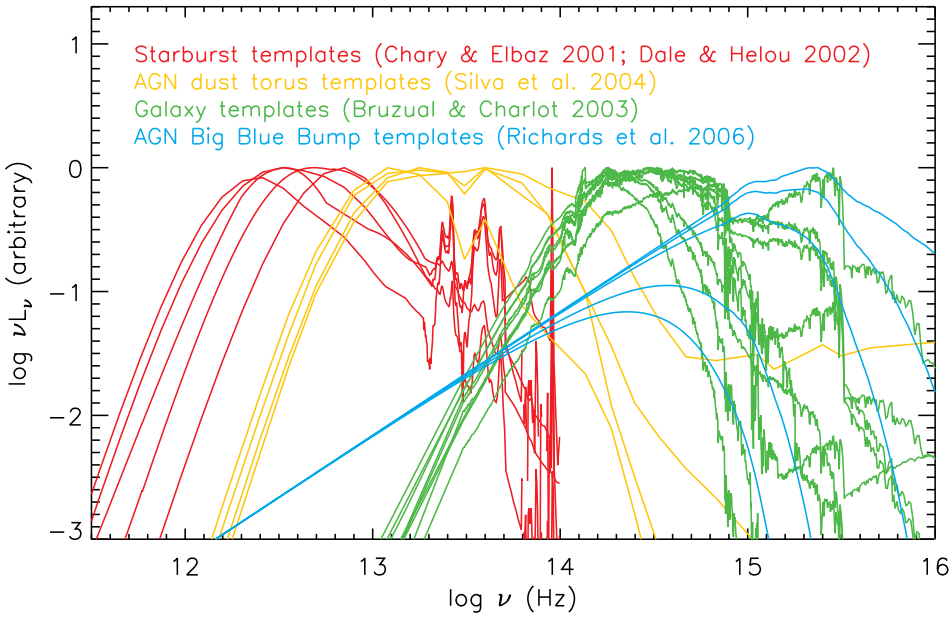

Figure 4.1 Examples of model templates used in the multi-component SED fitting. Blue curves indicate subsamples of BBB templates with different reddening levels $E(B-V)$=[0.00,0.03,0.10,0.50,0.90]. Green curves indicate some examples of host galaxy templates with various combinations of τ=[0.1, 1, 3], and $t_{\rm age}$=[50 Myr, 2 Gyr] with $E(B-V)$=[0.0, 0.3]. Yellow curves correspond to four AGN dust torus templates depending on the hydrogen column density, $N_{\rm H}$. Red curves correspond to the subset of starburst templates.

some information on the N_H toward each source (see Marchesi et al. 2016), I chose to allow N_H to be a free parameter in the SED fitting.

For the starburst component in the far/mid-IR region, I adopted 169 starburst templates (105 from Chary & Elbaz 2001 and 64 from Dale & Helou 2002) for fitting the cold dust emission (i.e. far-IR emission). It has been shown that measuring the FIR luminosity from fitting the FIR region to libraries of SED (Chary & Elbaz 2001; Dale & Helou 2002) gives roughly the same results as the modified blackbody plus power-law model (Casey 2012; U et al. 2012; Lee et al. 2013). The Chary & Elbaz (2001) templates are generated based on the SEDs of four prototypical starburst galaxies (Arp220, ULIRG; NGC 6090, LIRG; M82, starburst; and M51, normal star-forming galaxy). The Dale & Helou (2002) templates are based on 69 normal star-forming galaxies, representing a wide range of SED shapes and IR

luminosities, complementing each other. A small subset of starburst templates are shown in Figure 4.1 as red curves.

4.2.3 Multi-component SED Fitting

I developed a four-component SED fitting procedure in which the observed photometric data is fitted at a fixed redshift of the source with a large grid of models obtained by combining the templates described above. The observed flux can be expressed as the sum of four components as

$$f_{obs} = C_1 f_{\text{stellar population}} + C_2 f_{\text{BBB}} + C_3 f_{\text{torus}} + C_4 f_{\text{starburst}} \tag{4.1}$$

where the C_1, C_2, C_3, and C_4 are coefficients that reproduce the observed data by χ^2 minimization. For the Type 2 AGN host galaxy fits, I set the $C_2 = 0$. The best-fit SED solution for Type 2 AGN host galaxies could be a stellar population with a negligible contribution from AGN/starburst components, or a stellar population with the central AGN component, or a stellar population with starburst component, or a stellar population with both AGN and starburst components. For the Type 1 AGN host galaxy fits, I assume a non-negligible contribution from AGN BBB component ($C_2 \neq 0$), while there could be a negligible contribution from other components. Therefore, there are 11 (8) free parameters in this SED fits for Type 1 (Type 2) AGN host galaxies.

The fit is performed differently for sources detected in the FIR and those that are not. Specifically, for the sources detected at 24μm but not in any FIR *Herschel* wavelength, there are large uncertainties in the estimate of C_3 and C_4, because both could substantially contribute in the observed 24μm band, introducing a degeneracy in the SED fitting. This implies that the fitting can produce two different probable solutions with a similar χ^2. One is a prominent AGN dominating in the IR range with no contribution from the dust emission heated by stars, and the other is a negligible AGN contribution in the 24μm band with the infrared emission dominated by star-forming regions. Therefore, I perform two different

fits for the sources, which are not detected at any FIR wavelength. (1) the best-fit model with a possible star-forming component using *Herschel* upper limits, adopting the same approach as described by Calistro et al. (2016). Specifically, I consider *Herschel* detection limits in each *Herschel* band ($\mathrm{flux_{limit}}$) to make mock data points in the FIR wavelength range, assuming the flux to be $\mathrm{flux_{limit}}/2$ with an uncertainty $\pm\ \mathrm{flux_{limit}}/2$, to fit the possible star-forming component. (2) I assume a negligible contribution from star formation in the IR range, $\mathrm{L_{FIR}}$=0, and a significant contribution from the AGN at 24μm. Thus, I have a range of possible $\mathrm{L_{FIR}}$ values for *Herschel*-undetected sources (i.e., minimum to maximum).

I show examples of the SED fits for the sources that are detected in FIR photometry in the left panels of Figure 4.2 (Type1) and Figure 4.3 (Type 2), and the sources that are undetected in the FIR in the left panels of Figure 4.4 (Type 1) and Figure 4.5 (Type 2). The rest-frame photometric data (black points) and the detection limits (arrows) are shown with the best-fit model (black solid curve). For the FIR faint sources (Figure 4.4 and 4.5), I show two different best-fit models in the IR wavelength range: a possible star-forming component using upper limits (solid curve) and negligible star formation contributions (dashed curve). The galaxy template (green), the AGN BBB template (blue), the AGN dust torus template (yellow), and the starburst component (red) are also indicated. The residuals are also shown in the lower panel of each SED fit.

The χ^2 minimization is used to determine the best fit among all the possible template combinations. However, its absolute value is not a reliable indicator, because systematic uncertainties may dominate the statistical errors. Therefore, I compute a complementary statistic on the quality of fit, which is the variation of the residual from the fit. I remove $\sim$1% of sources that show large variations in their residuals (> 0.5), since this indicates that their high χ^2_{red} is not due to an underestimation of the photometric errors but either caused by the lack of suitable templates or by the bad photometry.

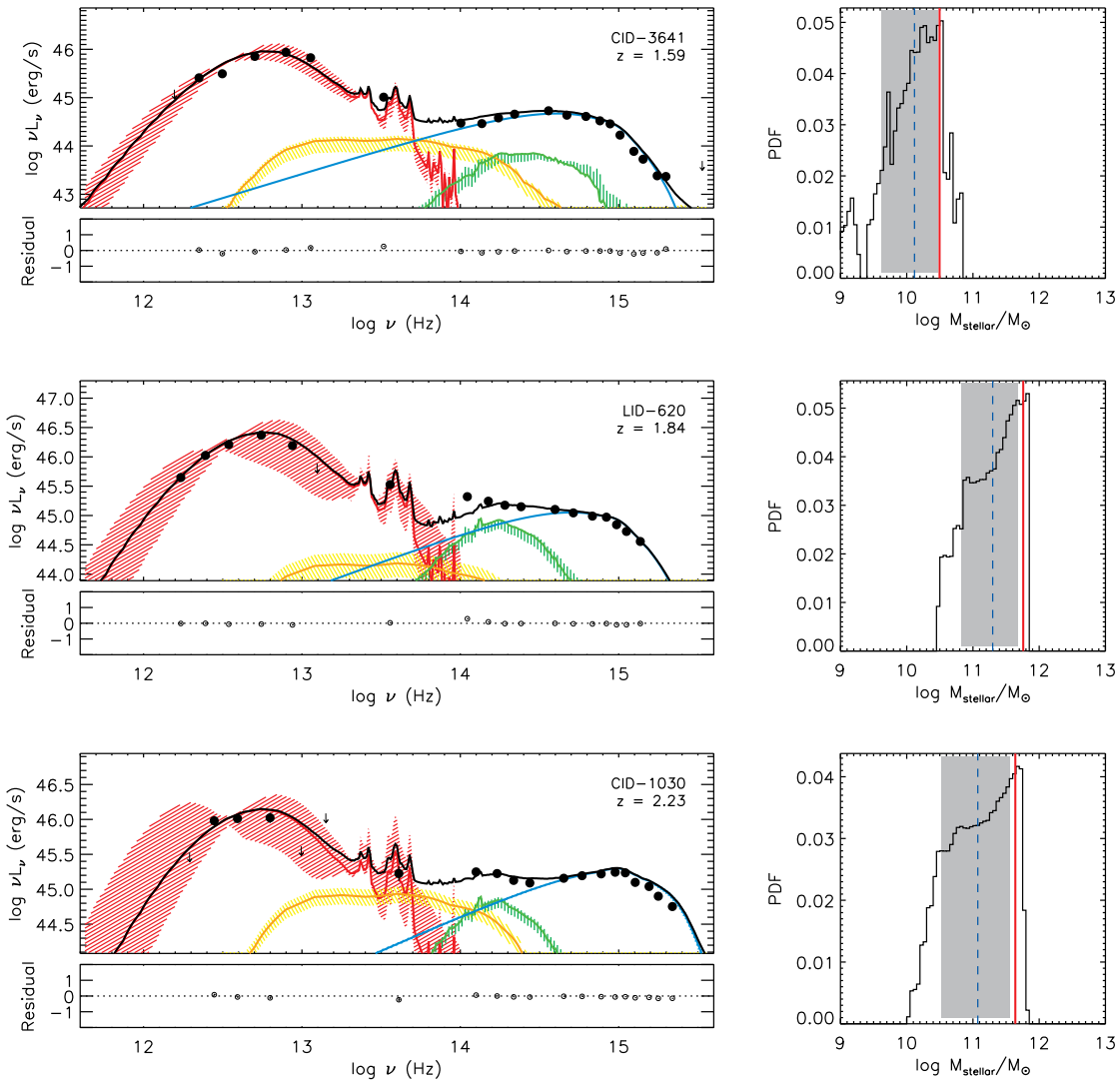

Figure 4.2 Examples of Type 1 SED fits (left panels) for sources that are detected in *Herschel* far-IR photometry. The rest-frame observed photometric data (black points) and the detection limits (arrows) are shown with the best-fit model (black solid curve). The galaxy template (green), the AGN BBB template (blue), the AGN dust torus template (yellow), and the starburst component (red) are also indicated. The residuals are shown in the lower plot of each spectrum. In the right panels, we show the PDFs for the stellar mass of each source. The best-fitting values are shown by the red solid line. The expectation values (blue dashed) and the 16 and 84 percentile intervals (gray shades) are also indicated.

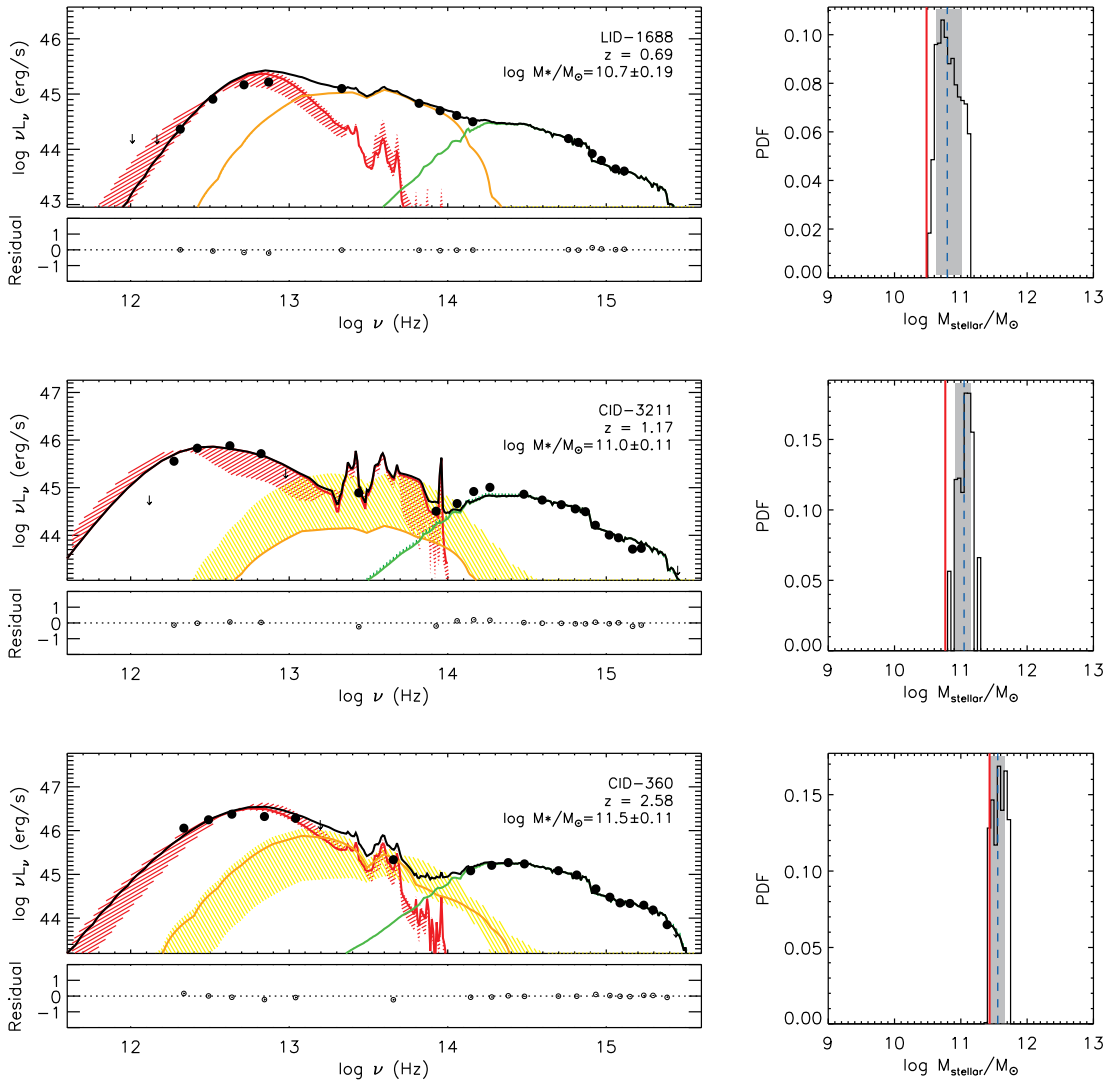

Figure 4.3 Examples of Type 2 SED fits (left panels) for sources that are detected in *Herschel* far-IR photometry. Line types and colors are as in Figure 4.2

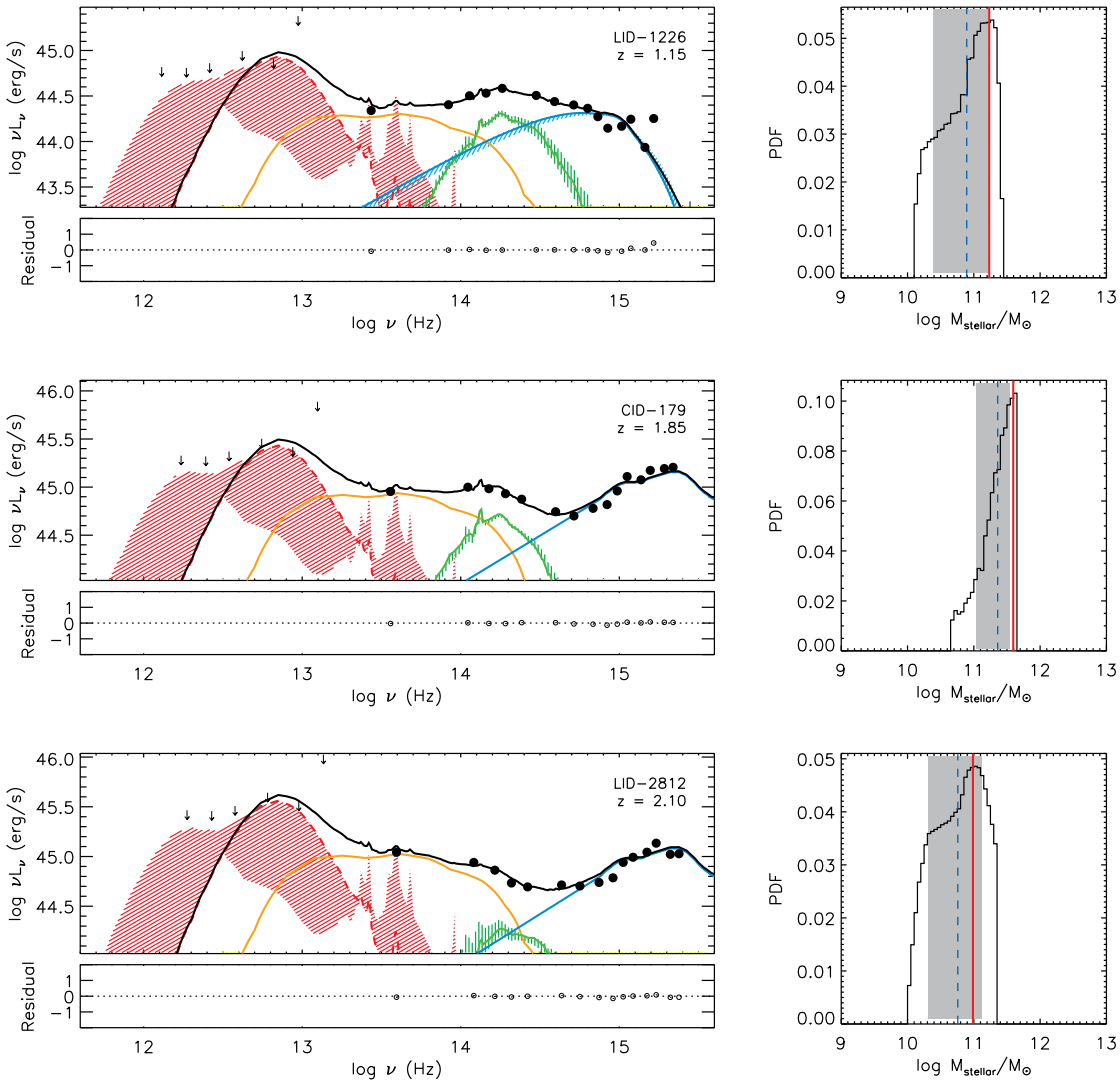

Figure 4.4 Examples of Type 1 SED fits (left panels) for sources that are detected in 24μm MIPS photometry but faint in the far-IR. We show two different best fit models (solid and dashed curves). Line types and colors are as in Figure 4.2.

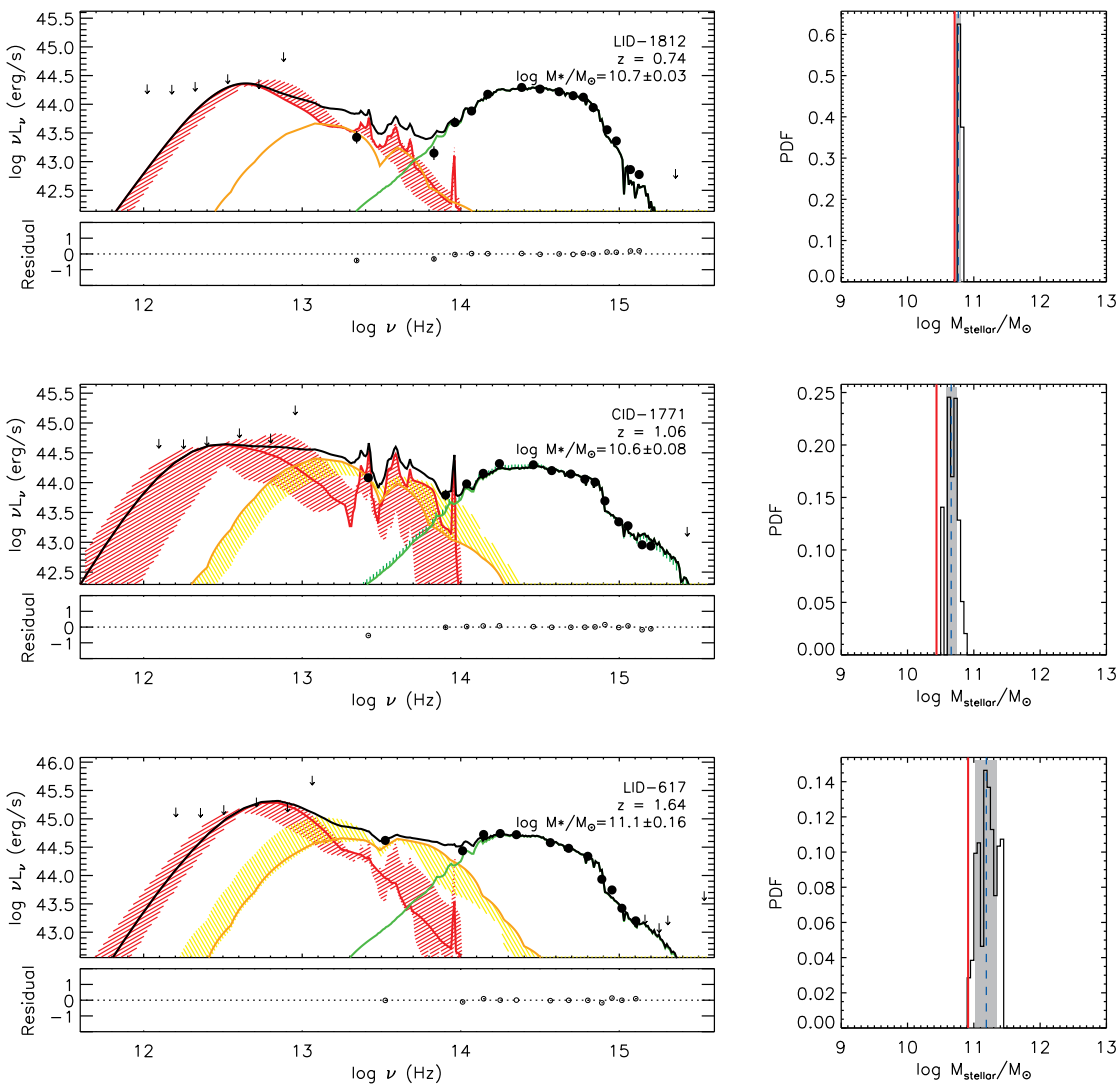

Figure 4.5 Examples of Type 2 SED fits (left panels) for sources which are detected in 24μm MIPS photometry but faint in the far-IR. We show two different best fit models (solid and dashed curves). Line types and colors are as in Figure 4.2.

4.3 Estimation of Physical Properties

Based on the best-fitting solution, I estimate the rest-frame intrinsic luminosity of AGNs and their host galaxies. I derive the monochromatic luminosity of the AGN component at rest-frame 6μm ($L_{6\mu m}$), which can be used as a reliable estimator of the AGN luminosity. I also derive the rest-frame absorption-corrected luminosity of the galaxy component at 5100Å ($L_{5100\mathring{A}}$). The total rest-frame star-forming IR luminosity is calculated by integrating the starburst component between 8 and 1000μm (L_{IR}).

While the use of the χ^2 minimization technique can give an indication of the overall quality of the fitting, the best-fit value could not be a good estimate of representative of physical parameter values in a multi-dimensional parameter space with degeneracies. I, therefore, use Bayesian statistics to derive the most representative value for each parameter of galaxy physical properties, and to evaluate the robust uncertainties since it accounts for the degeneracies inherent in the SED templates.

The parameter space describing the galaxy component is four-dimensional, which includes the physical parameters (e.g., age, τ, extinction) and the galaxy normalization coefficient. For a set of observational data d, and a model M with parameter θ, the Bayesian approach in SED-fitting represents the posterior probability of the parameters P($\theta|$ d, M) that constitute the model M, given by

$$P(\theta|d, M) = \frac{P(d|\theta, M)P(\theta|M)}{P(d|M)} \tag{4.2}$$

P(d $|\theta$, M) is the probability (i.e., likelihood) of d given the model M and its parameter θ. P($\theta|$ M) is the prior, which describes knowledge about the parameters independent of the data. P(d $|$ M) is a normalization constant which is independent of the parameter θ.

4.3.1 Stellar Mass

I explore any possible combination of SED parameters, which includes the age since the onset of star formation, the e-folding time τ for exponential SFH models, and the dust

reddening. I take into account the possible range for each parameter (i.e., for galaxy mass, $7 < \log(M_{\rm stellar}/M_{\odot}) < 13$), and find all the models that produce a value for the parameter. I then build a probability distribution function (PDF) for the stellar mass with the likelihood, $\exp(-0.5\ \chi^2)$, associated with that model for a given source. I estimate expectation values and uncertainties as the width of the parameter values corresponding to the 16 and 84 percentiles of the cumulative PDF. In the right panels of Figure 4.2, 4.3, 4.4, and 4.5, I show PDFs for the stellar mass for each of the example sources. In each case, the best-fitting values are shown as red solid lines. I also show the expectation values (blue dashed) and the 16 and 84 percentile intervals (gray shades) derived from the cumulated PDFs. I note that the expectation and the best-fitting values are usually very close to each other. In the case of Type 1 AGNs, the SMBH-powered emission contributes significantly to the UV-to-optical parts of the spectra (e.g., Elvis et al. 2012; Hao et al. 2013) as shown in Figure 4.2 and 4.4. Therefore, it is extremely difficult to determine reliable stellar mass for Type 1 AGNs (e.g., Maiolino et al. 2010). Thus, I do not take into consideration the stellar mass of Type 1 AGNs in the further discussion.

In Figure 4.6, I show the stellar mass distribution for a sample of Type 2 AGN host galaxies, normalized to the total area (left panel). For comparison, the stellar mass distributions of all galaxies in the COSMOS field (Laigle et al. 2016) are shown in the gray shaded histogram. The distributions of Type 2 AGNs in the *XMM*-COSMOS field from Bongiorno et al. (2012) and Lusso et al. (2011) are also indicated with blue and yellow histograms, respectively. The stellar mass of our sample ranges from $\sim 10^9$ to $\sim 10^{12}$ $M_{\odot}$, peaking at higher masses ($\sim 5 \times 10^{10}$ $M_{\odot}$) compared to normal galaxies, consistent with results from Bongiorno et al. (2012) and Lusso et al. (2011). In the right panel, I show the comparison of the stellar masses for Type 2 AGN host galaxies obtained from our SED fitting with the results from Lusso et al. (2011; blue circles) and Bongiorno et al. (2012; red squares) based on their SED fitting, and Le Phare pipeline products (Laigle et al. 2016; black open circles). While the sample used in this study explores a broader range of redshifts and luminosities, I find good agreements on the stellar masses of matched sources, mainly

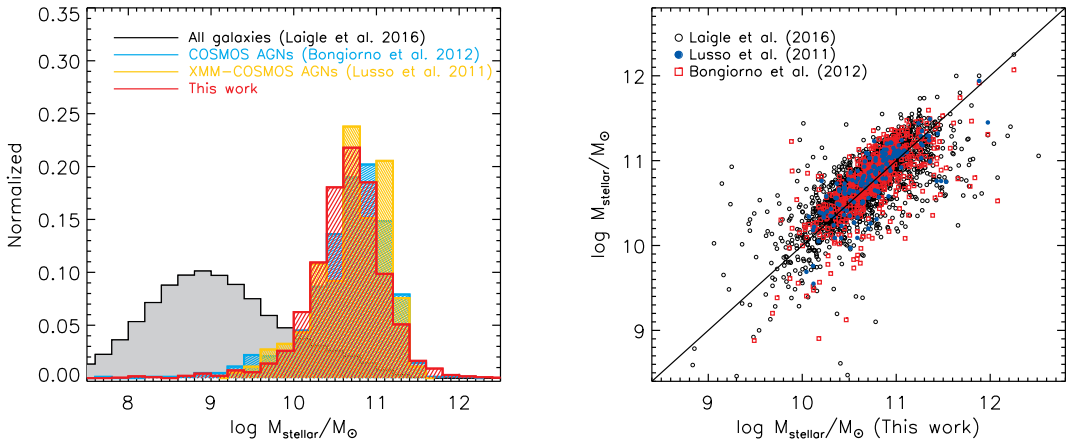

Figure 4.6 Left: Stellar mass distribution of our sample of Type 2 AGN host galaxies, normalized to the total area. The stellar mass distribution of our sample is shown in thick red histograms. The distribution of all galaxies from the COSMOS catalog (Laigle et al. 2016) is also shown in gray shaded histogram for comparison. We also show the distribution of Type 2 AGNs in the COSMOS field from Bongiorno et al. (2012; blue) and Lusso et al. (2011; yellow). Right: Comparison between stellar masses derived from our SED fitting and that from Lusso et al. (2011; blue circles), Bongiorno et al. (2012; red squares), and Laigle et al. (2016, Le Phare; black open circles). The black line denotes a one-to-one relation.

bright AGNs. The 1σ dispersions between the stellar mass derived in this work and other works are 0.27 dex (Lusso et al. 2011) and 0.30 dex (Bongiorno et al. 2012), respectively.

I show the redshift evolution of stellar masses for my sample of Type 2 AGN host galaxies in Figure 4.7. Individual sources are indicated with gray filled stars (*Herschel*-detected; which are detected at least in one *Herschel* band) and circles (*Herschel*-undetected). Black squares represent the mean and the standard deviation. The typical uncertainty for the stellar masses ($\sim$0.19 dex) is shown in the bottom right corner. There is a lack of significant evolution of stellar masses of Type 2 AGN host galaxies with redshift, which are relatively massive since $z \sim 3$, indicating that they might have already experienced substantial growth at higher redshift ($z > 3$).

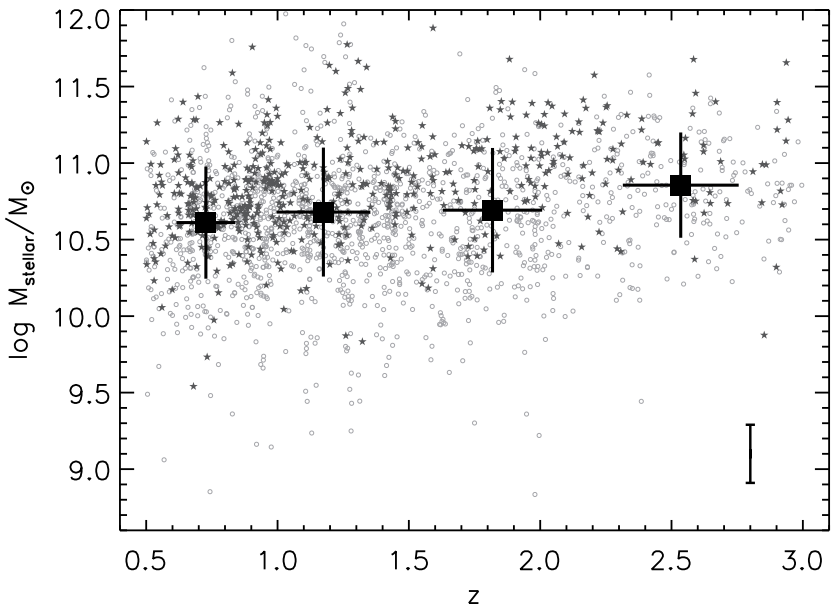

Figure 4.7 Stellar mass distribution of our sample of Type 2 AGN host galaxies. The individual sources are indicated with filled stars (*Herschel*-detected) and open circles (*Herschel*-undetected) as a function of redshift. We also show the typical uncertainties in bottom right corner.

4.3.2 Star Formation Rate

The SFR can be estimated by combining the contributions from UV and IR luminosity, which can estimate reliable total SFR since dust in the galaxy is heated by UV emission produced by young massive stars, and then re-emitted in the mid-to-far infrared regime (see e.g., Draine 2003). I derive the total SFR conversion using the relation from Arnouts et al. (2013), which is similar to that proposed by Bell et al. (2005) and adjusted for a Chabrier (2003) IMF,

$$\mathrm{SFR_{total}}\ (\mathrm{M_\odot/yr}) = (8.6 \times 10^{-11}) \times (L_{\mathrm{IR}}/L_\odot + 2.3 \times \nu L_\nu(2300\mathring{A})) \qquad (4.3)$$

where L_{IR} is the total rest-frame star-forming IR luminosity, which is integrated between 8 and 1000μm from the starburst template, and L_ν(2300Å) represents the rest-frame intrinsic absorption-corrected near-UV luminosity at 2300Å in units of $\mathrm{L_\odot}$. To account for *Herschel*-

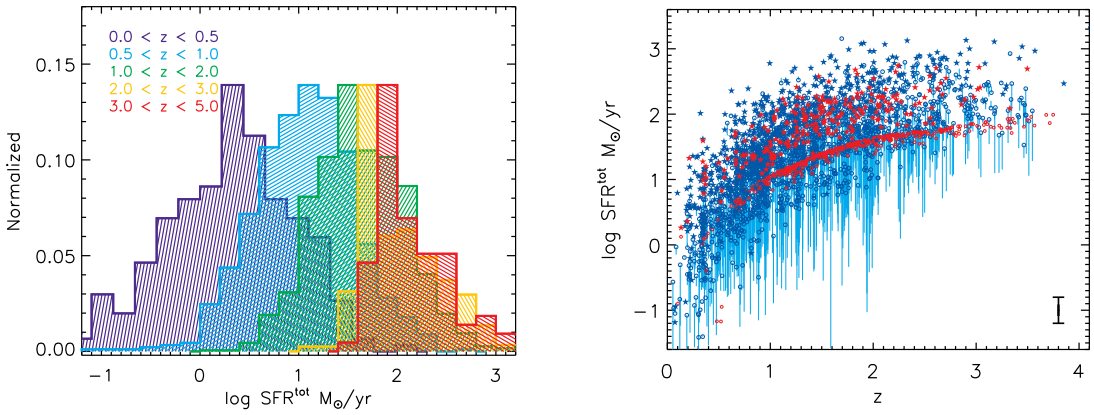

Figure 4.8 Left: SFR distribution of our sample of AGN host galaxies, normalized to the total area. We show the histograms of SFRs, split into five redshift bins. Right: SFR versus redshift. The individual sources are indicated with filled stars (*Herschel*-detected) and open circles (*Herschel*-undetected) as a function of redshift. Red and blue symbols indicate Type 1 and Type 2 AGN host galaxies, respectively. The range of SFRs for *Herschel*-undetected Type 2 sources are indicated with blue error bars. I also show the typical uncertainties in the bottom right corner.

undetected sources, I derive upper limits on their SFRs by assuming possible star-forming IR luminosity from the best-fit using *Herschel* detection limits. In addition, I also derive the minimum SFRs using only UV luminosity, assuming $L_{\rm IR} = 0$. Therefore, There is a range of possible values for SFRs for *Herschel*-undetected sources (i.e., from minimum to the maximum SFRs).

In the case of Type 1 (unobscured) AGNs, on the other hand, it is extremely difficult to estimate the reliable star-forming UV contribution because the accretion disk emission strongly contributes in the UV range, introducing a degeneracy in the SED fitting between the UV emission from star formation and from the central AGN. Therefore, I infer SFRs of Type 1 AGN host galaxies using only IR luminosities assuming $\rm SFR_{total}$ ($\rm M_\odot$/yr) = $10^{-11} \times L_{\rm IR}/L_\odot$ (Kennicutt 1988) for a Chabrier (2003) IMF.

In Figure 4.8, I show the total SFR distribution (left) for my sample of AGN host galaxies, normalized to the total area, split into five redshift bins. I also show the redshift evolution of SFRs in the right panel of Figure 4.8. Individual sources are indicated with

filled stars (*Herschel*-detected; which are detected at least in one *Herschel* band) and circles (*Herschel*-undetected). Red and blue symbols indicate Type 1 and Type 2 AGN host galaxies, respectively. The range of SFRs for *Herschel*-undetected Type 2 sources are also indicated with blue lines. The typical uncertainties for the SFRs (for the *Herschel*-detected sources; ∼0.20 dex) are shown in the bottom right corner. The sample of AGN host galaxies spans a wide range of SFRs, peaking at higher values toward higher redshifts. I note that the measurement of the SFR has considerably larger uncertainties than that of stellar mass, because it depends on the *Herschel* detections, SFRs could be inherently biased towards higher values, while a significant fraction (∼73%) of our sample are faint in the far-IR photometry, which could have lower SFRs.

In the appendix Table B.1 and B.2, I present AGN host galaxy properties derived from the SED fitting.

4.4 Results

4.4.1 The X-ray to MIR relation

X-ray ($L_{\rm X}$) and MIR ($L_{\rm MIR}$) luminosity both have been used as robust indicators of an intrinsic AGN power. Since the MIR emission originates from re-processed UV emission, it is crucial to study the correlation between the MIR and the X-ray luminosity for understanding the structure of the hot dust surrounding the central SMBH as well as the AGN accretion physics. Several studies have investigated the $L_{\rm X} - L_{\rm MIR}$ relation and found a strong correlation between X-ray and MIR luminosity (e.g., Lutz et al. 2004; Gandhi et al. 2009; Fiore et al. 2009; Lanzuisi et al. 2009; Lusso et al. 2011; Asmus et al. 2015; Stern 2015). The linear $L_{\rm X} - L_{\rm MIR}$ correlation has been investigated for local Seyfert galaxies by Lutz et al. (2004) using low angular resolution MIR data, and later by Gandhi et al. (2009) using the spatially resolved high resolution data. Gandhi et al. (2009) found that even the obscured AGNs follow the same correlation as the unobscured AGNs without large offsets or scatter. Using *Spitzer*, this correlation has been extended towards higher luminosities for luminous

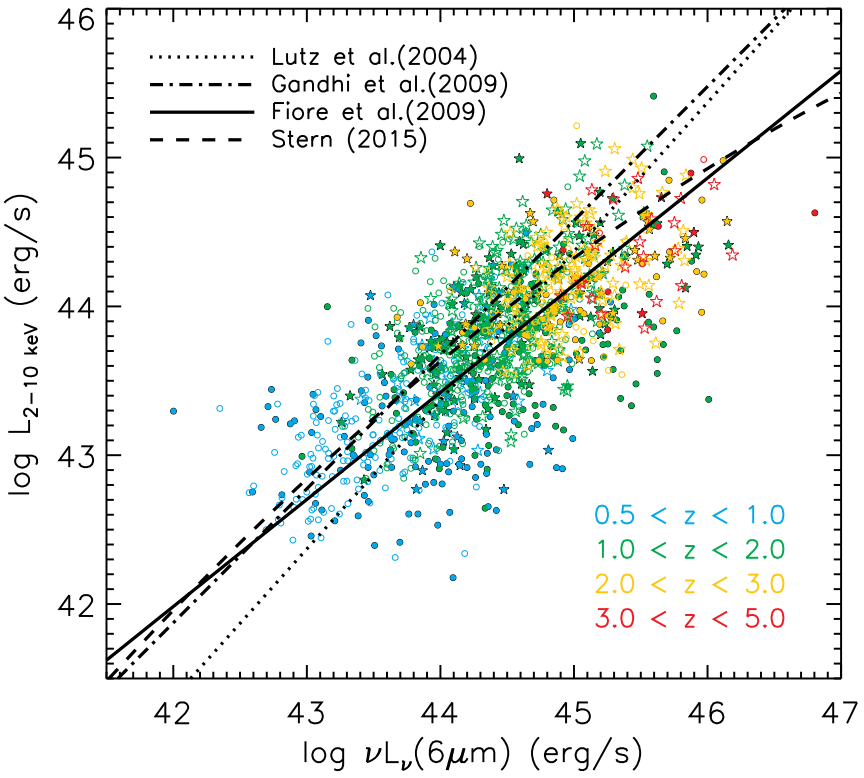

Figure 4.9 Relation of the intrinsic X-ray ($L_{2-10\ keV}$) and the 6μm ($L_{6\mu m}$) luminosities for our sample of AGNs. Stars and circles are Type 1 and Type 2 AGN, respectively. Filled symbols mark *Herschel*-detected sources while empty symbols are *Herschel*-undetected ones.

quasars (e.g., Fiore et al. 2009; Lanzuisi et al. 2009; Stern 2015), and shown to be valid even for radio-loud AGNs (e.g., Hardcastle, Evans & Croston 2009). Recently, Stern (2015) have demonstrated a luminosity-dependent $L_{\rm X} - L_{\rm MIR}$ relation for luminous quasars, reporting the $L_{\rm X} - L_{\rm MIR}$ fit bends at higher luminosities to lower $L_{\rm X}$-to-$L_{\rm MIR}$ ratios.

I investigate the correlation between the X-ray emission and AGN MIR luminosity over a wide dynamic range in luminosities and redshifts using both Type 1 and Type 2 AGNs in the CCLS. In Figure 4.9, I show the intrinsic 2–10 keV X-ray luminosity ($L_{2-10\ \rm keV}$) against the uncontaminated MIR ($L_{6\mu m}$) luminosity derived from the best-fitting AGN component of the sample of AGNs. Stars and circles represent Type 1 and Type 2 AGNs, respectively. Filled and empty symbols indicate the *Herschel*-detected and *Herschel*-undetected sources.

For comparison, I also show the $L_{\rm X} - L_{6\mu m}$ relation from Lutz et al. (2004; dotted line), Gandhi et al. (2009; dash-dotted line), Fiore et al. (2009; solid line) and Stern et al. (2015; dashed curve). Lutz et al. (2004) and Gandhi et al. (2009) presented this relation for local Seyfert galaxies, establishing the correlation at low luminosities, while Fiore et al. (2009) and Stern (2015) investigated this relation for the most luminous quasars, presenting the relation from the Seyfert to the powerful quasar regime. I convert the monochromatic luminosity measured at different wavelengths for these comparison samples (e.g., 5.8μm and 12μm) to $\rm L_{6\mu m}$ using the AGN template. The $L_{\rm X} - L_{6\mu m}$ distribution of moderate-luminosity AGNs is in broad agreement with previous studies (e.g., Lutz et al. 2004; Gandhi et al. 2009; Fiore et al. 2009; Stern 2015).

Some of the observed scatter can be attributed to the fact that this study is extending the previous relation, which was derived for a sample of local Seyfert galaxies, to a sample spanning a much wider range of luminosity and redshift. It is also plausible that in a fraction of these sources, the SED-fitting procedure over- or under-estimates the nuclear contribution, which results in a MIR luminosity. However, how much of this uncertainty is inherently a result of the physical conditions of the AGN and torus cloud, as compared to observational selection effects, remains an important unresolved issue, which is beyond the scope of this work. Nevertheless, the comparison points out that, on average, the MIR luminosity derived from the SED-fitting is a reasonably good measure of the AGN luminosity. Indeed, the assumption that the MIR emission is dominated by the AGN emission because of accretion on to the central black hole rather than star-formation from the host galaxy is plausible for most of the sources. This made the X-ray-to-MIR correlation the tightest among the other multiple wavelength correlations found for AGN and especially intriguing because of its applicability to all different AGN types.

I also show the ratio of the X-ray-to-MIR luminosity with respect to X-ray luminosities in Figure 4.10. Gray filled symbols indicate the individual sources which are detected in *Herschel* photometry, and gray open symbols represent the *Herschel*-undetected sources. Black squares indicate mean values in the X-ray luminosity bins for the total sample. Red

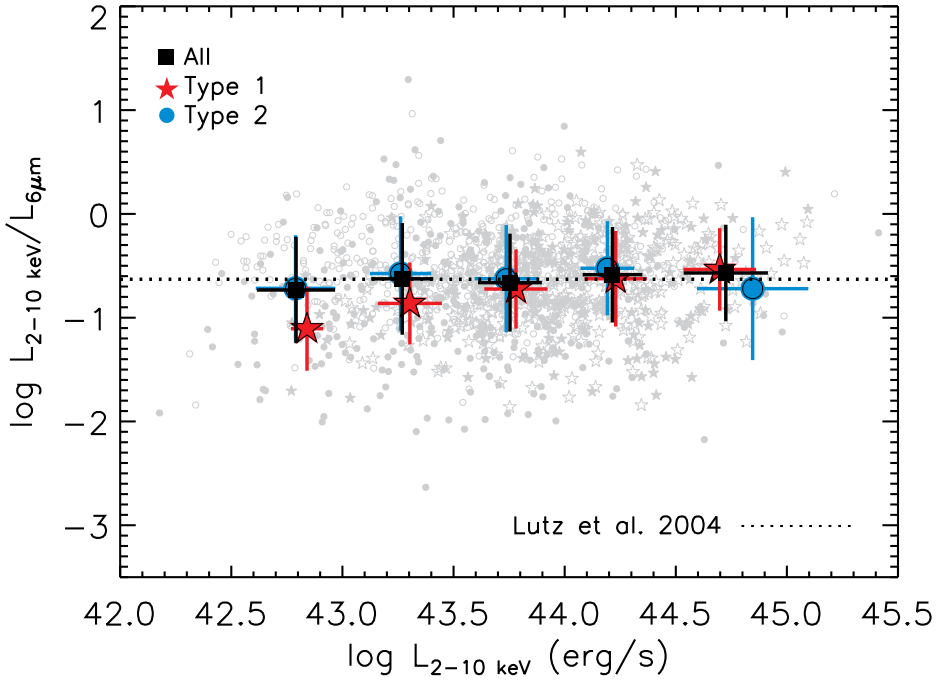

Figure 4.10 The ratio between the X-ray and the 6μm luminosities for our sample of AGNs. Gray filled symbols indicate the individual sources which are detected in *Herschel* photometry, and gray open symbols represent the *Herschel*-undetected sources. Black squares indicate mean values in the X-ray luminosity bins. Red stars and blue circles represent the Type 1 and Type 2 AGN, respectively. The horizontal dotted line marks the average $L_X - L6\mu m$ ratio of local Seyferts from Lutz et al. (2004).

stars and blue circles represent mean values for the Type 1 and Type 2 AGN, respectively. The horizontal dotted line marks the average $L_{\rm X} - L_{6\mu{\rm m}}$ ratio of local Seyfert galaxies from Lutz et al. (2004). This figure indicates that both Type 1 and Type 2 AGNs closely follow the same correlation, indicating good agreement with the Lutz et al. (2004) relation. Gandhi et al. (2009) also have reported that the obscured and unobscured AGN follow the same correlation. It is interesting because the relation might depend on the structure of obscuring dust torus in the sense that the unobscured (Type 1) AGNs should have higher MIR luminosities compared to the obscured (Type 2) AGNs at the same intrinsic power. This suggests that the observed MIR emission is important for determining the AGN bolometric accretion energetic for both obscured and unobscured AGNs.

One advantage of adopting the rest-frame MIR luminosity as an AGN power estimator is that, contrary to the X-ray luminosity, this quantity was measured homogeneously for all the sources, regardless of obscuration of AGNs. Hence, it can be used to derive the AGN bolometric luminosity for the entire AGN population, for example, optically- and infrared-selected AGNs, including the objects with no X-ray emission. Therefore, I derive the MIR bolometric corrections using the bolometric luminosity of AGNs derived from the intrinsic X-ray luminosity with the luminosity-dependent bolometric correction described in Marconi et al. (2004). The MIR bolometric correction is obtained as follows:

$$log\ L_{bol} = 0.70 \times log\ \nu L_{\nu}(6\mu m) + 14.12 \tag{4.4}$$

Using the MIR bolometric correction, one can derive the AGN bolometric luminosity of Compton-thick AGNs, which might not be detected in the X-ray band because of the high $N_{\rm H}$ absorption.

4.4.2 The $M_{\rm BH} - M_{\rm stellar}$ Scaling Relation

I study the $M_{\rm BH} - M_{\rm stellar}$ distribution for a sample of 96 Type 1 AGNs in the CCLS, which are the moderate-luminosity AGNs and are a more representative subset of the general AGN population. The black hole mass is estimated using the broad Hα, Hβ, and Mg II emission lines via the virial method (see Chapter 3). Due to the large uncertainties in the stellar mass of Type 1 AGNs (see Chapter 4.3.1), I note that the stellar masses of Type 1 AGNs mostly represent upper limit. In Figure 4.11, the $M_{\rm BH} - M_{\rm stellar}$ distribution for Type 1 AGNs is shown in four redshift bins. Bigger symbols represent higher Eddington ratios. As a reference, the local scaling relations from McConnel & Ma (2013; dotted), Graham (2012; dashed), Sani et al. (2011; dash-dotted), and Haring & Rix (2004; dash-dot-dotted) are indicated. The typical uncertainties are shown in the bottom left corner. I also show the published observation of the zCOSMOS bright spectroscopic broad-line AGN sample

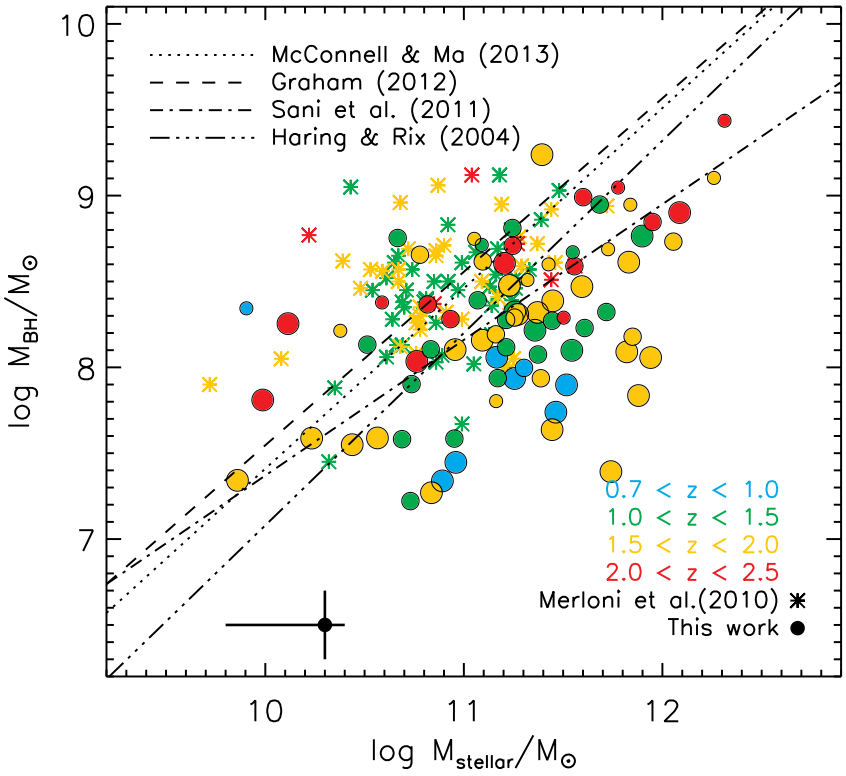

Figure 4.11 The $M_{\rm BH} - M_{\rm stellar}$ Scaling Relation for our sample of Type 1 AGNs (circles) in the redshift range $0.7 < z < 2.5$, together with the published observation from Merloni et al. (2010; asterisk symbols). As a reference, local scaling relations from the literature are plotted as labeled. Bigger symbols represent higher Eddington ratios.

(asterisk) in the same color-coded redshift from Merloni et al. (2010), for which $M_{\rm stellar}$ was derived by SED-fitting and $M_{\rm BH}$ was estimated using the broad Mg II emission line.

The majority of Type 1 AGN host galaxies in this study are broadly scattered around the local scaling relation, slightly offset toward small $M_{\rm BH}/M_{\rm stellar}$ ratios. On the other hand, most of the data of Type 1 AGNs from Merloni et al. (2010) are found above the local relation, which led them to suggest that the average $M_{\rm BH}/M_{\rm stellar}$ ratio at higher redshifts is higher than what was observed in the local universe. Overall, I do not find a significant cosmic evolution of the $M_{\rm BH} - M_{\rm stellar}$ relation that sample of moderate-luminosity AGNs, together with the relatively bright sources from Merloni et al. (2010), does indeed show values broadly consistent with the local scaling relation at all redshifts probed, although

the scatter is large, consistent with the previous results (Shields et al. 2003; Salviander et al. 2007; Shen et al. 2008; Cisternas et al. 2011a). The sample shows that the higher Eddington ratio AGNs (bigger symbol) have smaller black hole masses for a given stellar mass. Shen et al. (2008) pointed out that the difference in Eddington ratio is sufficient to account for the intrinsic scatter of about 0.4 dex in the $M_{\rm BH} - \sigma$ relation, because higher Eddington ratios have smaller black hole masses for a given velocity dispersion, which is consistent with our results.

However, this result is in contrast to the previous studies that black holes predate the formation of their host galaxies (e.g., Treu et al. 2007; Shen et al. 2008; Woo et al. 2008; Merloni et al. 2010; Bennert et al. 2011). It is interesting to note that Jahnke et al. (2009) found no evolution in the $M_{\rm BH} - M_{\rm stellar}$ ratio using 10 of the targets in Merloni's sample when they independently derive host galaxy luminosities using *HST*. They suggest that there are indications that the $M_{\rm BH} - M_{\rm stellar}$ is not evolving, or at least not as rapidly as the relations between black hole mass and spheroid properties.

4.4.3 The SFR$-M_{\rm Stellar}$ Relation

To investigate the effects of AGNs on the star formation in galaxies, I explore the distribution of a sample of Type 2 AGN host galaxies on the SFR–$M_{\rm stellar}$ diagram compared to normal star-forming galaxies. I show SFRs and stellar masses of my sample of Type 2 AGN host galaxies, split into four redshift bins in the upper panels of Figure 4.12. The individual sources are indicated with filled gray stars when the sources are detected in *Herschel* far-IR photometry, while the circles represent the possible maximum SFR for the sources detected only up to 24 μm. The range of SFRs (i.e. from minimum to maximum) for *Herschel*-undetected sources is indicated with gray bars. I indicate the star-forming MS relationships from Tomczak et al. (2016; solid curve) and Speagle et al. (2014; dashed line) for comparison. The relation reported in the Lee et al. (2015) study is also indicated with dotted curves at the low redshift bins. I show mean values of the combination of the SFR of *Herschel* detected sources (filled gray stars) and the maximum SFRs of the *Herschel*-

undetected sources (open gray circles) in the stellar mass bins (black stars). Black circles mark the mean values of the combination of SFR of *Herschel* detected sources (filled gray stars) and the minimum SFRs of the *Herschel*-undetected sources. The thick black error bars represent the range of mean SFRs, which account for the maximum and minimum SFRs for the *Herschel*-undetected sources. I also display the mean SFRs for the sources at each X-ray luminosity bin in the stellar mass bins (colored stars).

In the lower panels of Figure 4.12, I show the SFR offset (ΔSFR) for the AGN host galaxies relative to the star-forming MS of Tomczak et al. (2016). The gray shades mark the intrinsic scatter ($\sim$0.2 dex) of the star-forming MS. Most previous studies have found no clear evidence for a correlation between the X-ray luminosity and the SFR of the AGN host galaxy (Lutz et al. 2010; Shao et al. 2010; Harrison et al. 2012; Mullaney et al. 2012; Rosario et al. 2012; Rovilos et al. 2012; Stanley et al. 2015). These results indicate that there is no significant difference in the SFRs with respect to X-ray luminosity. Interestingly, it seems that there is a tendency for luminous ($10^{43.5} < L_{2-10\ keV}(\mathrm{erg/s}) < 10^{44.0}$) AGN host galaxies to deviate from the star-forming MS relation in the range of $0.5 < z < 0.9$. In this redshift range, AGN host galaxies with $\mathrm{M_{stellar}}/M_{\odot} < 10^{10.5}$ show higher SFRs than star-forming MS galaxies, while massive AGN host galaxies ($\mathrm{M_{stellar}}/M_{\odot} > 10^{11}$) seem to have SFRs that lie below the star-forming MS relation.

Type 2 AGN host galaxies, on average, seem to have SFRs that lie on the star-forming MS at all redshifts, consistent with previous studies (e.g., Xue et al. 2010; Mainieri et al. 2011; Mullaney et al. 2012; Rosario et al. 2013), but with much broader dispersions. Mullaney et al. (2015) found that AGN host galaxies with $\log \mathrm{M_{stellar}}/\mathrm{M_{\odot}} \gtrsim 10.3$ show significantly broader SFR distributions compared to the star-forming MS galaxies, compared to normal galaxies (see also Shimizu et al. 2015). However, Type 2 AGN host galaxies at high-mass bins remain on the star-forming MS, when taking into account the dependence of the slope of the star-forming MS on stellar mass (Whitaker et al. 2014; Lee et al. 2015; Tomczak et al. 2016). The selection effects and observational biases can be important since a significant fraction ($\sim$75%) of our sample are not detected in far-IR photometry, which

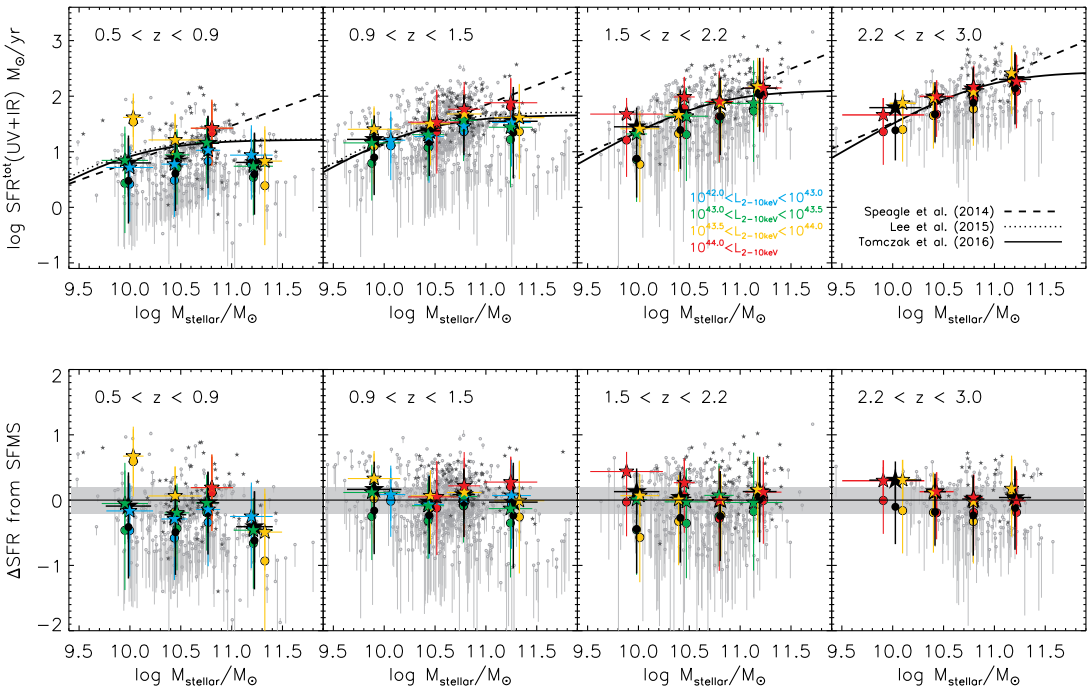

Figure 4.12 Top: SFR versus stellar mass of our sample of Type 2 AGN host galaxies in the four redshift bins. Gray filled stars indicate the individual sources which are detected in the far-IR *Herschel* photometry, and gray open circles represent the possible maximum SFR for the sources which are not detected in any *Herschel* bands. The range of SFRs (i.e. from minimum to maximum) for *Herschel*-undetected sources is indicated with gray error bars. I indicate the star-forming MS relationships from Speagle et al. (2014) (dashed line), Tomczak et al. (2016) (solid curve), and Lee et al. (2015) (dotted curve) for comparison. Black stars indicate mean values of SFRs of *Herschel*-detected sources combined with possible maximum SFR of *Herschel*-undetected sources, while black circles represent that of SFRs of *Herschel*-detected sources combined with minimum SFR of *Herschel*-undetected sources. Black thick error bars represent the range of mean SFRs which account for the maximum and minimum SFRs of the *Herschel*-undetected sources. We also display the mean SFRs for the sources at each X-ray luminosity bin (colored stars). Bottom: SFR offsets (ΔSFR) relative to the star-forming MS of Tomczak et al. (2016). The gray shades mark the ΔSFR$\pm$0.2 dex.

is crucial for precise measurements of the SFRs. The SFR distribution, therefore, is much broader than that of star-forming MS galaxies, when taking into account the fact that the SFRs of the *Herschel*-undetected sources could ultimately be much lower (i.e., minimum SFRs). Overall, Type 2 AGN host galaxies remain on the star-forming MS over a broad

redshift range, indicating no sign of strong SFR enhancements in the redshift range of $0.5 < z < 3.0$.

4.4.4 Star Formation and AGN activity

I explore the relationship between star formation and AGN activity for a sample of AGNs in the CCLS. To investigate the star-forming properties with an AGN power, I present the results of the total star-forming IR luminosities ($L_{\rm IR}$) derived from the best-fitting starburst component against the X-ray luminosities ($L_{2-10\ keV}$) in the left panel of Figure 4.13. I divide our sample into four redshift ranges, $z = 0.5 - 1.0,\ z = 1.0 - 2.0,\ z = 2.0 - 3.0$, and $z = 3.0 - 5.0$. Small open symbols show the individual sources of *Herschel*-detected Type 1 (open stars) and Type 2 (open circles) AGN host galaxies. Arrows mark the possible maximum $L_{\rm IR}$(SF) luminosity for the sources that are not detected in any *Herschel* bands. For each redshift range, I calculate the average $L_{\rm IR}$ in each bin of $L_{2-10\ \rm keV}$. Filled stars represent the mean $L_{\rm IR}$ luminosity for the *Herschel*-detected sources. While the *Herschel*-detected sources could be the most dusty star-forming galaxies with high SFRs, the majority of the AGN sample is not detected by *Herschel*. For those *Herschel*-undetected sources I calculate the possible maximum $L_{\rm IR}$ luminosity as estimated from the *Herschel*-detection limits (arrows). Solid circles indicate mean values of $L_{\rm IR}$ luminosity of *Herschel*-detected sources with inclusion of possible maximum $L_{\rm IR}$ luminosity of *Herschel*-undetected sources.

I find that the IR luminosity for this sample of AGN host galaxies increases toward higher redshift, in agreement with the observed evolution found for previous studies (e.g., Elbaz et al. 2011; Mullaney et al. 2012; Rosario et al. 2012; Rovilos et al. 2012). To take into account the contribution of the *Herschel*-undetected sources, I find that mean $L_{\rm IR}$ drops by $\sim$0.3 dex from that for only *Herschel*-detected sources. Across all redshift bins, I do not find a strong correlation between $L_{\rm IR}$ and $L_{2-10\ \rm keV}$ luminosities, broadly consistent with the flat relationship suggested by previous studies for moderate-luminosity ($L_{\rm X} < 10^{44}$ erg/s) AGNs (Lutz et al. 2010; Shao et al. 2010; Harrison et al. 2012; Mullaney et al. 2012; Rovilos et al. 2012; Stanley et al. 2015). I note that the observed flat relationship is still

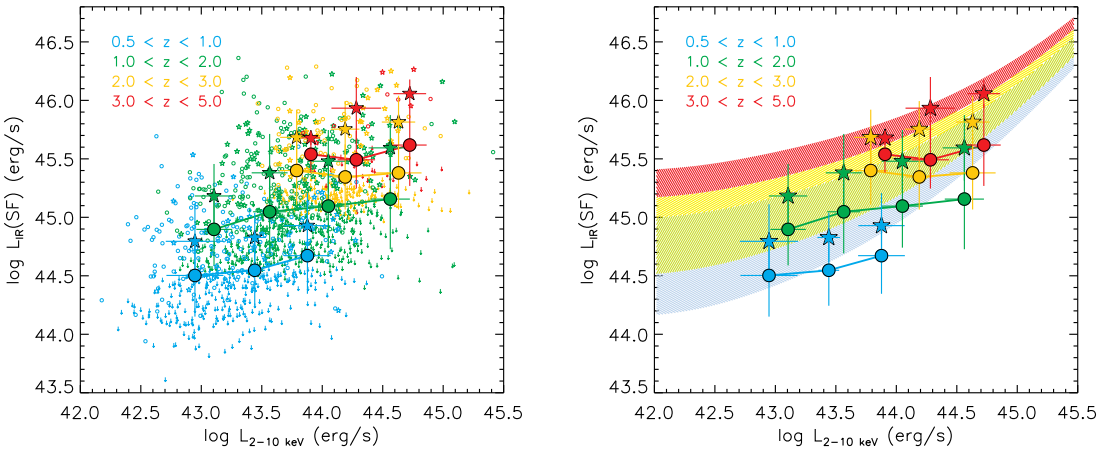

Figure 4.13 Left: Total IR luminosity due to star formation (L_{IR}) versus X-ray luminosity ($L_{2-10\ keV}$) for our sample of AGN host galaxies in the four redshift ranges. Small open symbols indicate the individual Type 1 (open stars) and Type 2 (open circles) AGN host galaxies that are detected in the far-IR *Herschel* photometry. Arrows mark the possible maximum L_{IR}(SF) luminosity for the sources that are not detected in any *Herschel* bands. Solid circles indicate mean values of L_{IR} luminosity of *Herschel*-detected sources combined with possible maximum L_{IR} luminosity of *Herschel*-undetected sources, while solid stars represent that of L_{IR} luminosity for only *Herschel*-detected sources. Right: Mean L_{IR}(SF) vs. Mean $L_{2-10keV}$ in four redshift ranges compared to model tracks from Hickox et al. (2014) (shades).

shown with an extreme scenario where all the *Herschel*-undetected sources are assumed to correspond to upper limits, although the true value may have some offsets. This result seems in disagreement with that reported by some other studies which found a correlation between the average $L_{\rm agn}$ and SFRs of AGN host galaxies (Rafferty et al. 2011; Mullaney et al. 2012; Chen et al. 2013; Delvecchio et al. 2014; Rodighiero et al. 2015). However, it has been suggested that the shorter variability timescale of AGN than that of star formation could lead to flat correlation between the SFR and the AGN luminosity when taking the average over the most variable quantity (e.g., Hickox et al. 2014; Volonteri et al. 2015). Those studies which found a correlation calculate the average AGN luminosity over bins of SFR, while we take the average L_{IR}(SF) in bins of AGN luminosity.

In order to investigate if indeed AGN variability is the driver of the flat relationship that we observe, I compare this result with the predictions from the empirical model by

Hickox et al. (2014) in the right panel of Figure 4.13. The mean values are color-coded by redshift, same as the left panel. The empirical models presented in Hickox et al. (2014) are shown with shades as color-coded by same four redshift ranges. In this model, the individual AGN are allowed to vary on short timescales on the basis of an assumed $L_{\rm agn}$ distribution, providing the average SFR as a function of AGN luminosity of a large population of simulated AGNs. It seems that the model reproduces a trend of the $L_{\rm IR}$ with redshift, and is in good agreement with that of the *Herschel*-detected sources (stars). However, it fails to reproduce the observed trend when including the *Herschel*-undetected sources (circles), especially at high redshift ranges. At the high redshift bin ($z > 2.0$), there is no significant difference in $L_{\rm IR}$ with respect to $L_{\rm X}$ bins when taking account for the *Herschel*-undetected sources. In particular, the model trend of $L_{\rm IR}$ with L_X is much steeper than our observed results. I also find that the $L_{\rm IR}$ values of the most luminous AGN bin for all of the redshift ranges are systematically below the predicted model. This could be caused by the lack of an explicit Eddington ratio distributions in the model since the observed Eddington ratio is widely distributed (see Chapter 3). Recently, Stanley et al. (2015) showed that the different assumed Eddington ratio distributions could make a significant difference in the predicted $L_{\rm IR} - L_{\rm X}$ trend (i.e., the use of a broken power-law Eddington ratio distribution describes the observed trend much better than with a narrow Eddington ratio distributions). Therefore, I suggest that our results of a flat relationship between $L_{\rm IR}$ and $L_{\rm X}$ are likely to be a consequence of AGN variability with widely distributed Eddington ratios.

To acquire a more direct relationship between the rate at which AGN host galaxies accrete in relation with their black hole accretion, I derive the specific SFR (sSFR=SFR/$\rm M_{stellar}$) of the host galaxy and Eddington ratio of AGNs ($L_{\rm bol}/L_{\rm Edd}$) for the subsample of Type 1 AGN host galaxies that have a reliable black hole mass measurement. In Figure 4.14, I show the distribution of sSFR with respect to Eddington ratios. Star symbols indicate the *Herschel*-detected sources, while the downward triangle represents the upper limit of SFR for the *Herschel*-undetected sources. The vertical dotted line marks the Eddington limit. I do not find a clear correlation between sSFR and Eddington ratios,

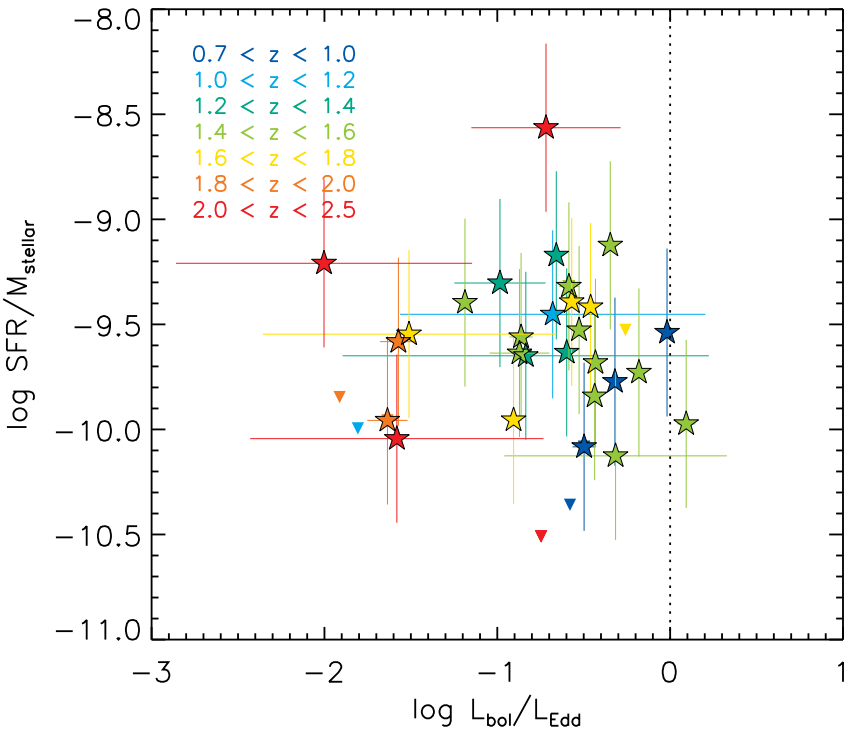

Figure 4.14 The specific SFR (sSFR=SFR/$M_{stellar}$) versus Eddington ratio for the subsample of Type 1 AGN host galaxies that have a reliable black hole mass measurement. Star symbols indicate the *Herschel*-detected sources, while the downward triangle represents the upper limit of SFR for the *Herschel*-undetected sources. Vertical dotted line marks the Eddington limit.

supporting that the flat relationship between $L_{\rm IR}$ and $L_{\rm X}$ with widely distributed Eddington ratios.

Finally, I explore whether Type 1 AGN host galaxies have SFR that are consistent with those for normal star-forming galaxy population with respect to the Eddington ratios. I calculate the offsets from the expected SFR for star-forming MS galaxies using Tomczak et al. (2016) (see Chapter 4.4.3). In Figure 4.15, I show the SFR offsets (ΔSFR) relative to the star-forming MS of Tomczak et al. (2016) of Type 1 AGN host galaxies with respect to the Eddington ratio. Downward triangles correspond to the cases for which having only an upper limit on the SFR while filled stars to the objects with Herschel detections.

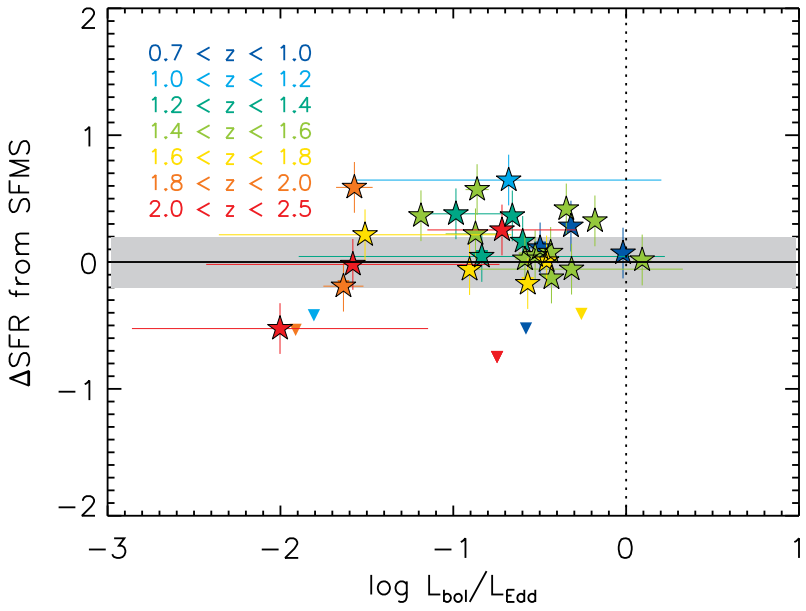

Figure 4.15 SFR offsets (ΔSFR) relative to the star-forming MS of Tomczak et al. (2016) versus the Eddington ratio for the subsample of Type 1 AGN host galaxies that have a reliable black hole mass measurement. The gray shade regions correspond to the expected range in SFR for the normal star-forming galaxy population (ΔSFR±0.2 dex) as defined by Tomczak et al. (2016).

I find that, for the most of Type 1 AGN host galaxies, SFRs in all redshift ranges are consistent with that of star-forming MS galaxies of the same mass. No clear trend is visible between the SFRs and the Eddington ratios. This results agrees with the the previous studies (e.g., Bongiorno et al. 2012; Harrison et al. 2012; Mullaney et al. 2012; Lanzuisi et al. 2015; Suh et al. 2017).

4.5 Discussion

One of the largest samples of X-ray AGNs combining with the extensive multi-wavelength data in the COSMOS field has been analyzed to study the growth of black holes and galaxies over cosmic time. There has been a disagreement in studies on the evolution of black hole mass and host stellar mass, which are described by the $M_{\rm BH} - M_{\rm stellar}$ relation, with large

uncertainties. In Chapter 4.4.2, the majority of moderate-luminosity AGNs slightly tend to lie below the local $M_{\rm BH} - M_{\rm stellar}$ relation. However, combined with the relatively bright sources of the zCOSMOS AGNs from Merloni et al. (2010) which are found above the local relation, the distribution of $M_{\rm BH} - M_{\rm stellar}$ shows a broadly consistent with the local scaling relation, suggesting no significant evolution in the $M_{\rm BH} - M_{\rm stellar}$ relation with redshift up to $z \sim 2.5$. The $M_{\rm BH} - M_{\rm stellar}$ relation appears to depend on the Eddington ratio in the sense that the AGNs with higher Eddington ratio have smaller black hole masses for a given stellar mass, lying below the local $M_{\rm BH} - M_{\rm stellar}$ relation. However, it is important to keep in mind that selection effects have to be taken into account when trying to infer the intrinsic scaling relations from the observed data.

In Chapter 4.4.3 the majority of AGN host galaxies seem to reside along the star-forming MS, consistent with previous studies (e.g., Mainieri et al. 2011; Mullaney et al. 2012; Rosario et al. 2013). While the "flattening" in the star-forming MS at high masses could be interpreted as a consequence of quenching the star formation in massive galaxies (e.g., Whitaker et al. 2014; Lee et al. 2015; Schreiber et al. 2015), the SFRs of AGN host galaxies are consistent with those expected from normal star-forming galaxies in most stellar mass bins up to $z \sim 3$, indicating no clear signature for enhanced or suppressed SFRs compared to normal star-forming galaxies. This can be interpreted by internal secular processes, which might be responsible for driving both star formation and nuclear activity in AGN host galaxies. These results are consistent with the weak link between merger features and the modest AGN activity. From previous works in the literature (e.g. Cisternas et al. 2011b; Mainieri et al. 2011; Schawinski et al. 2012; Fan et al. 2014; Villforth et al. 2014), the majority of AGN host galaxies do not show significant merger features, indicating that mergers do not dominate the triggering of AGN activity, at least for moderate-luminosity AGNs. Allevato et al. (2011, 2012, 2016) further point out that moderate-luminosity AGNs inhabit group-sized halos ($10^{13-13.5}$ $M_{\odot}$), almost independent of redshift up to $z \sim 5$. This also implies that major mergers cannot be the main driver of the evolution of AGNs.

However, these results could be also interpreted by the different timescales and the spatial scales associated with the star formation and nuclear activity (e.g., Hickox et al. 2014) in the sense that most AGN vary on a timescale much shorter ($\sim 10^5$yr) than that of star formation ($\sim$ 100Myr) (e.g., Hickox et al. 2009; Aird et al. 2012; Bongiorno et al. 2012). According to this scenario, all episodes of star formation and AGN activity could be intimately connected at any time. In Chapter 4.4.4, it seems that there is no strong correlation between $L_{\rm IR}$ due to star formation and $L_{2-10\ \rm keV}$ luminosities, broadly consistent with the flat relationship, which can be explained by the AGN variability along with the broad Eddington ratio distribution. Furthermore, it is important to point out that these could be driven by the selection biases, mainly due to the interplay between the limited X-ray luminosity, Eddington ratio, SFRs and stellar masses of AGN host galaxies (e.g., Lauer et al. 2007; Xue et al. 2010). While AGNs preferentially reside in massive galaxies, when considering in the same stellar mass bins, SFRs of AGN host galaxies indicate no significant difference compared to normal star-forming galaxies. Xue et al. (2010) also found that for mass-matched samples, the SFRs of AGN host galaxies are similar to those of non-AGN galaxies at $z \sim 1-3$, consistent with our results. I further consider different X-ray luminosities to minimize potential luminosity-dependent effects. Within each stellar mass bin, I subdivide our sample into bins of the X-ray luminosity. With luminosity-selection effects taken into account, I find that there is no clear signature for a correlation between the AGN luminosity and the SFRs of AGN host galaxies. The Eddington ratio could be a factor that creates a bias against low-luminosity AGNs accreting at the lowest Eddington ratios at high redshift. The X-ray AGN sample used in this study may also bias against the heavily obscured, Compton-thick sources, which might be missed by X-ray selection (e.g., Treister et al. 2004; Kocevski et al. 2015). However, at least for the sample of moderate-luminosity X-ray selected AGNs, it seems that there is no significant difference between AGN hosts and normal star-forming galaxies.

From the perspective of the investigation on the star-formation and AGN activity for the moderate-luminosity AGN host galaxies, I propose that the relatively massive galaxies have

already experienced substantial growth by major mergers, which are capable of triggering both a significant starburst and high accretion AGN activity at higher redshift ($z > 3$), and grow slowly through secular fueling processes hosting moderate luminosity AGNs. Major merger-triggering mechanism may hold only for the most luminous quasars at earlier epoch. The black holes and galaxies both have grown predominantly at high redshift ($z > 3$) possibly by major mergers, and all necessary stellar mass may already exists in galaxies at $z \sim 3$. Jahnke et al. (2009) found some evidence of substantial disk components from their *HST* data, suggesting that if the objects were purely bulge-dominated, $M_{\rm BH} - M_{\rm stellar}$ relation has not evolved since $z \sim 2$. In the later stage of AGN evolution, the moderate-luminosity AGNs with relatively high Eddington ratios, which found below the local scaling relation, will presumably move up to the $M_{\rm BH} - M_{\rm stellar}$ plane induced by secular processes, becoming eventually inactive galaxies harboring SMBHs. The secular process may not change the overall $M_{\rm BH} - M_{\rm stellar}$ ratio by adding feeding both black hole and stellar masses. To explain the tight relationship between the final black hole and spheroid bulge mass, a re-distribution of stellar masses is required from disk to the bulge, also induced by secular processes such as disk instabilities. This could be also supported by the fact that the $M_{\rm BH} - M_{\rm stellar}$ relation is not as tight for late-type galaxies. Combined with almost no evolution in stellar masses of AGN host galaxies (see Chapter 4.3.1), these results indicate that secular evolution may play an important role in growing SMBHs and the bulge formation in massive galaxies.

Aird et al. (2012) present that AGN Eddington ratios are independent of stellar masses of their hosts at $z < 1$, suggesting that the same physical processes regulate AGN activity in galaxies at stellar masses $9.5 \lesssim \log {\rm M_{stellar}/M_\odot} \lesssim 12.0$. Suh et al. (2015) further point out that a substantial fraction of massive black holes accreting significantly below the Eddington limit at $z < 2$, suggesting that modest AGN activity can be triggered via internal, secular processes in massive galaxies. This is also compatible with the lack of significant evolution of stellar masses of AGN host galaxies. These results suggest that the majority of AGN

host galaxies at $z < 3$ might be driven more by internal secular processes, implying that they have substantially grown at much earlier epoch.

4.6 Summary

I analyze the host galaxy properties of a large sample of ∼3700 X-ray-selected AGNs out to $z \sim 3$ in the CCLS in order to examine whether AGN activity can significantly enhance or quench star formation in galaxies. The large number statistics, together with the extensive multi-wavelength photometry and spectroscopy available in the COSMOS field, allow us to explore one of the largest samples of AGN host galaxies and to study the relationship between AGN and galaxy properties. To derive the physical properties of AGN host galaxies, I develop a multi-component SED-fitting technique to disentangle the nuclear emission from the stellar light, and derive host galaxy properties. Specifically, I use multi-band photometry (from NUV through the FIR) to decompose the entire SED into separate components with nuclear AGN emission, the host galaxy's stellar populations, and a starburst contribution in the FIR. I derive stellar masses of AGNs in the range $9 < \log M_{\rm stellar}/M_{\odot} < 12$ with uncertainties of ∼0.19 dex. The SFR is estimated by combining the contributions from UV and IR luminosity. Our sample of Type 2 AGN host galaxies span a wide range of SFRs ($-1 < \log {\rm SFR}\ (M_{\odot}/{\rm yr}) < 3$) with uncertainties of ∼0.20 dex.

The main conclusions are as follows.

1. In combination with black hole mass estimated via the virial method using Hα, Hβ, Mg II emission lines (see Chapter 3), I study the evolution of the $M_{\rm BH}-M_{\rm stellar}$ scaling relation out to $z \sim 2.5$. The majority of the moderate-luminosity AGNs are broadly scattered around the local scaling relation, suggesting that there is no significant evolution in the $M_{\rm BH} - M_{\rm stellar}$ relation.

2. I explore the distribution of AGN host galaxies on the SFR-stellar mass diagram compared to the normal star-forming galaxies. Overall, AGN host galaxies seem to have SFRs that lie on the star-forming MS up to $z \sim 3$, independent of X-

ray luminosities. These results indicate that AGN host galaxies do not show clear signature for enhanced or suppressed SFRs compared to normal star-forming galaxies.

3. There is not a strong correlation between $L_{\rm IR}$ due to star formation and $L_{\rm X}$ luminosities, broadly consistent with the flat relationship for the moderate-luminosity AGNs. This result could be explained by AGN variability and the broad range of Eddington ratios.

References

Aird, J., Coil, A. L., Moustakas, J., et al. 2012, ApJ, 746, 90

Allevato, V., Finoguenov, A., Cappelluti, N., et al. 2011, ApJ, 736, 99

Allevato, V., Finoguenov, A., Hasinger, G., et al. 2012, ApJ, 758, 47

Allevato, V., Civano, F., Finoguenov, A., et al. 2016, ApJ, 832, 70

Asmus, D., Gandhi, P., Hoñig, S. F., Smette, A., Duschl, W. J. 2015, MNRAS, 454, 766

Arnouts, S., Le Floc'h, E., Chevallard, J., et al. 2013, A&A, 558, A67

Azadi, M., Aird, J., Coil, A. L., et al. 2015, ApJ, 806, 187

Barger, A. J., Cowie, L. L., Owen, F. N., et al. 2015, ApJ, 801, 87

Barvainis, R. 1987, ApJ, 320, 537

Bell, E. F., Papovich, C., Wolf, C., et al. 2005, ApJ, 625, 23

Bennert, V. N., Auger, M. W.. Treu, T., Woo, J.-H., Malkan, M. A. 2011, ApJ, 742, 107

Bongiorno, A., Merloni, A., Brusa, M., et al. 2012, MNRAS, 427, 3103

Bruzual, G. and Charlot, S. 2003, MNRAS, 344, 1000

Calistro, R. G., Lusso, E., Hennawi, J. F., Hogg, D. W. ApJ, 2016, 833, 98

Casey, C. M. 2012, MNRAS, 425, 3094

Calzetti, D., Armus, L., Bohlin, R. C., et al. 2000, ApJ, 533, 682

Chabrier, G. 2003, ApJ, 586L, 133

Chary, R., & Elbaz, D. 2001, ApJ, 556, 562

Chen, C.-T. J., Hickox, R. C., Stacey, A., et al. 2013, ApJ, 773, 3

Cisternas, M., Jahnke, K., Bongiorno, A., et al. 2011, ApJ, 741L, 11

Cisternas, M., Jahnke, K., Inskip, K. J., et al. 2011, ApJ, 726, 57

Dale, D. A., & Helou, G. 2002, ApJ, 576, 159

Dale, D. A., Gil de Paz, A., Gordon, K. D., et al. 2007, ApJ, 655, 863

Decarli, R., Falomo, R., Treves, A., et al. 2010, MNRAS, 402, 2453

Delvecchio, I., Cruppioni, C., Pozzi, F., et al. 2014, MNRAS, 439, 2736

Di Matteo, T., Springel, V., Hernquist, L. 2005, Nature, 433, 604

Draine, B. T. 2003, ARA&A, 41, 241

Elbaz, D., Dickinson, M., Hwang, H. S., et al. 2011, A&A, 533, A119

Elvis, M., Wilkes, B. J., McDowell, J. C., et al. 1994, ApJS, 95, 1

Elvis, M., Hao, H., Civano, F., et al. 2012, ApJ, 759, 6

Fan, L., Fang, G., Chen, Y., et al. 2014, ApJL, 784, L9

Ferrarese, L., & Merritt, D. 2000, ApJ, 539, 9

Fiore, F., Puccetti, S., Brusa, M., et al. 2009, ApJ, 693, 447

Gandhi, P., Horst, H., Smette, A., et al. 2009, A&A, 502, 457

Gebhardt, K., Bender, R., Bower, G., et al. 2000, ApJ, 539, 13

Graham, A. W., Onken, C. A., Athanassoula, E., et al. 2011, MNRAS, 412, 2211

Griffin, M. J., Abergel, A., Abreu, A., et al. 2010, A&A, 518, 3

Gültekin, K., Richstone, D., Gebhardt, K., et al. 2009, ApJ, 698, 198

Hao, H., Elvis, M., Bongiorno, A., eg al. 2013, MNRAS, 434, 3104

Hardcastle, M. J., Evans, D. A., Croston, J. H. 2009, MNRAS, 396, 1929

Haïring, N. and Rix, H.-W. 2004, ApJ, 604, 89

Harrison, C. M., Alexander, D. M., Mullaney, J. R., et al. 2012, ApJ, 760, 15

Hickox, R. C., Jones, C., Forman, W. R., et al. 2009, ApJ, 696, 891

Hickox, R. C., Mullaney, J. R., Alexander, D. M. et al., 2014, ApJ, 782, 9

Hopkins, P. F., & Hernquist, L. 2006, ApJS, 166, 1

Hopkins, P. F., Strauss, M. A., Hall, P. B., et al. 2004, AJ, 128, 1112

Jahnke, K., Bongiorno, A., Brusa, M., et al. 2009, ApJ, 706, L215

Kennicutt, R. C. 1998, ApJ, 498, 541

Kirkpatrick, A., Pope, A., Alexander, D. M., et al. 2012, ApJ, 759, 139

Kocevski, D. D., Brightman, M., Nandra, K., et al. 2015, ApJ, 814, 104

Kormendy, J., & Richstone, D. 1995, ARA&A, 33, 581

Krawczyk, C. M., Richards, G. T., Mehta, S. S., et al. 2013, ApJS, 206, 4

Laigle, C., McCracken, H. J., Ilbert, O., et al. 2016, ApJS, 224, 24

Lanzuisi, G., Piconcelli, E., Fiore, F., et al. 2009, A&A, 498, 67

Lauer, T. R., Tremaine, S., Richstone, D., and Faber, S. M. 2007, ApJ, 670, 249

Lanzuisi, G., Ranalli, P., Georgantopoulos, I., et al. A&A, 573, A137

Le Floc'h, E., Aussel, H., Ilbert, O., et al. 2009, ApJ, 703, 222

Lee, N., Sanders, D. B., Casey, C. M., et al. 2013, ApJ, 778, 131

Lee, N., Sanders, D. B., Casey, C. M., et al. 2015, ApJ, 801, 80

Lusso, E., Comastri, A., Vignali, C., et al. 2011, A&A, 534, A110

Lutz, D., Maiolino, R., Spoon, H. W. W., Moorwood, A. F. M. 2004, A&A, 418, 465

Lutz, D., Mainieri, V., Rafferty, D., et al. 2010, ApJ, 712, 1287

Lutz, D., Berta, S., Contursi, A., et al. 2016, A&A, 591, 136

Mainieri, V., Bongiorno, A., & Merloni, A. 2011, A&A, 535, A80

Magorrian, J., Tremaine, S., Richstone, D., et al. 1998, AJ, 115, 2285

Maiolino, R., Risaliti, G., Salvati, M., et al., 2010, A&A, 517, 47

Marchesi, S., Civano, F., Elvis, M., et al. 2016, ApJ, 817, 34

Marconi, A., Risaliti, G., Gilli, R., et al. 2004, MNRAS, 351, 169

Merloni, A., Bongiorno, A., Bolzonella, M., et al. 2010, ApJ, 708, 137

Merritt, D., & Ferrarese, L. 2001, ApJ, 547, 140

McConnell, N. J., & Ma, C.-P. 2013, ApJ, 764, 184

Mullaney, J. R., Pannella, M., Daddi, E.. et al. 2012, MNRAS, 419, 95

Mullaney, J. R., Alexander, D. M., Aird, J., et al. 2015, MNRAS, 453, L83

Netzer, H., Lutz, D., Schweitzer, M., et al., 2007, ApJ, 666, 806

Page, M. J., Symeonidis, M., Vieira, J. D., et al. 2012, Natur, 485, 213

Peng, C. Y., Impey, C. D., Rix, H.-W., et al. 2006, ApJ, 649, 616

Pilbratt, G. L., Riedinger, J. R., Passvogel, T., et al. 2010, A&A, 518, 1

Poglitsch, A., Waelkens, C., Geis, N., et al. 2010, A&A, 518, 2

Prevot, M. L., Lequeux, J., Prevot, L., Maurice, E., Rocca-Volmerange, B. 1984, A&A, 132, 389

Rafferty, D. A., Brandt, W. N., Alexander, D. M, et al. 2011, ApJ, 742, 3

Richards, G. T., Lacy, M., Storrie-Lombardi, L. J., et al. 2006, ApJS, 166, 470

Rodighiero, G., Brusa, M., Daddi, E., et al. 2015, ApJ, 800, 10

Rosario, D. J., Santini, P., Lutz, D., et al. 2012, A&A, 545, A45

Rosario, D. J., Mozena, M., Wuyts, S., et al. 2013, ApJ, 763, 59

Rovilos, E., Comastri, A., Gilli, R., et al. 2012, A&A, 546, 58

Salvato, M., Hasinger, G., Ilbert, O., et al. 2009, ApJ, 690, 1250

Salviander, S., Shields, G. A., Gebhardt, K., Bonning, E. W. 2007, ApJ, 662, 131

Sanders, D. B., Phinney, E. S., Neugebauer, G., Soifer, B. T., Matthews, K. 1989, ApJ, 347, 29

Sanders, D. B., Salvato, M., Aussel, H., et al. 2007, ApJS, 172, 86

Santini, P., Rosario, D. J., Shao, L., et al. 2012, A&A, 540, A109

Schawinski, K., Simmons, B. D., Urry, C. M., et al. 2012, MNRAS, 425, L61

Schreiber, C., Pannella, M., Elbaz, D., et al. 2015, A&A, 575, 74

Schulze, A., & Gebhardt, K. 2011, ApJ, 729, 21

Schweitzer, M., Lutz, D., Sturm, E., et al. 2006, ApJ, 649, 79

Shang, Z., Brotherton, M. S., Wills, B. J., et al. 2011, ApJS, 196, 2

Shao, L., Lutz, D., Nordon, R., et al. 2010, A&A, 518, 26

Shen, J., Vanden Berk, D. E., Schneider, D. P., Hall, P. B. 2008, AJ, 135, 928

Shields, G. A., Gebhardt, K., Salviander, S., et al. 2003, ApJ, 583, 124

Shimizu, T. T., Mushotzky, R. F., Meléndez, M., et al. 2015, MNRAS, 452, 1841

Silk, J., & Rees, M. J. 1998, A&A, 331, 1

Silva, L., Granato, G. L., Bressan, A., Danese, L. 1998, ApJ, 509, 103

Silva, L., Maiolino, R. and Granato, G. L. 2004, MNRAS, 355, 973

Speagle, J. S., Steinhardt, C. L., Capak, P. L., Silverman, J. D. 2014, ApJS, 214, 15

Stenley, F., Harrison, C. M., Alexander, D. M., et al. 2015, MNRAS, 453, 591

Stern, D. 2015, ApJ, 807, 129

Suh, H., Hasinger, G., Steinhardt, C., Silverman, J. D., Schramm, M. 2015, ApJ, 815, 129

Suh, H., Civano, F., Hasinger, G., et al. 2017, ApJ, 841, 102

Symeonidis, M. 2017, MNRAS, 2017, 465, 1401

Tomczak, A. R., Quadri, R. F., Tran K., et al. 2016, ApJ, 817, 118

Trakhtenbrot, B., Urry, C. M., Civano, F., et al. 2015, Sci, 349, 168

Treister, E., Urry, C. M., Chatzichristou, E., et al. 2004, ApJ, 616, 123

Tremaine, S., Gebhardt, K., Bender, R., et al. 2002, ApJ, 574, 740

Treu, T., Woo, J.-H., Malkan, M. A., and Blandford, R. D. 2007, ApJ, 667, 117

U, V., Sanders, D. B., Mazzarella, J. M., et al. 2012, ApJS, 203, 9

Villforth, C., Hamann, F., Rosario, D. J., et al. 2014, MNRAS, 439, 3342

Volonteri, M., Capelo, P. R., Netzer, H., et al. 2015, MNRAS, 452, 6

Whitaker, K. E., Franx, M., Leja, J., et al. 2014, ApJ, 795, 104

Woo, J.-H., Treu, T., Malkan, M. A., and Blandford, R. D. 2008, ApJ, 681, 925

Woo, J.-H., Schulze, A., Park, D. et al. 2013, ApJ, 772, 49

Xue, Y. Q., Grandt, W. N., Luo, B., et al. 2010, ApJ, 720, 368

Chapter 5

Summary and Future Outlook

5.1 Dissertation Summary

One of the major outstanding questions in galaxy evolution concerns the interplay between star formation and AGN activity. Many theoretical models have proposed that AGN feedback is responsible for regulation of star formation, either by heating or removing the cold gas in their host galaxies (e.g., Silk & Rees 1998; Di Matteo et al. 2005; Springel et al. 2005; Hopkins et al. 2008). In this picture, galaxy mergers are thought to be a possible fueling mechanism for AGN activity wherein black holes grow rapidly close to the Eddington limit, until the AGN feedback is sufficient to blow out the surrounding gas, suppressing star formation. On the other hand, stochastic low-luminosity AGNs, triggered by secular processes, maintain a hot gas halo to prevent further star formation in galaxies (e.g., Bower et al. 2006; Croton et al. 2006). However, the observational evidence for the existence and nature of this feedback is highly incomplete, and the extent to which AGN activity affects the star formation process is still a matter of debate.

The main focus of this dissertation research is to systematically study the influence of AGN on the growth of galaxies by examining the possible connection between AGN activity and star formation in galaxies. The primary targets are selected in the X-ray, which is the most efficient way to select AGN over a wide range of luminosities and redshifts because these galaxies are less affected by obscuration, and the contamination from non-nuclear

emission (mainly due to star-formation) is far less significant than in optical- or infrared-selected samples (e.g., Donley et al. 2008; Lehmer et al. 2012; Stern et al. 2012). My approach is to combine multi-wavelength photometry and spectroscopy to characterize the AGN and their host galaxy properties, examining (1) black hole accretion at $z \sim 1-2$, when SMBH growth is at its peak, to explore the growth of black holes, and (2) the AGN activity and its connection with star formation in AGN host galaxies. Below I highlight key results from this dissertation research.

5.1.1 AGN accretion and Growth of Black Holes

The assembly of galaxies and SMBHs appears to follow a "downsizing" trend; i.e. the AGN luminosity function and the SFRs show a violent phase with the most luminous AGNs and powerful star-forming galaxies at $z \sim 2-3$, and more moderate activity at later cosmic times ($z < 1$; see e.g., Hasinger et al. 2005). The Eddington ratio, the ratio of the AGN bolometric and the Eddington luminosity, is particularly interesting because it provides an observational constraint on the efficiency of gas accretion during the active phases of a black hole's life. Thus, to quantify a growth rate requires the independent measurement of AGN bolometric luminosity and black hole mass. Unfortunately, the detailed study in the redshift interval $z \sim 1-2$, where the downsizing appears and where a significant part of the accretion growth of black holes takes place, has been difficult because of the lack of emission line diagnostics in the optical wavelength range, which is why the range $z \sim 1-2$ is often referred to as the redshift desert.

Using high-quality optical and near-infrared spectroscopy from Keck/DEIMOS and Subaru/FMOS observations, I determine black hole masses and Eddington ratios via spectral-line fitting in the key redshift interval $z = 1-2$ using the Balmer lines that are the same lines for which the black hole masses are calibrated at low redshift. AGNs with similar black hole masses show a broad range of bolometric luminosities, which are calculated from X-ray luminosities, indicating that the accretion rate of black holes is distributed over a wide range. This suggests that the "AGN cosmic downsizing" phenomenon can be explained

by a substantial fraction of massive black holes accreting significantly below the Eddington limit at $z < 2$, in contrast to what is generally found for luminous AGNs at high redshift. This can be interpreted as the fraction of AGNs radiating close to the Eddington limit is decreasing after their peak activity phases ($z \sim 2-3$), suggesting that the dominant fueling mechanism for the growth of black holes might change through the cosmic time (Suh et al. 2015).

5.1.2 AGN activity and Star Formation in AGN host galaxies

To examine whether AGN activity can significantly enhance or quench star formation in galaxies, I focused on the X-ray selected AGNs in the Chandra COSMOS Legacy Survey (CCLS; Civano et al. 2016). This study greatly improves upon the statistics of previous works, as it contains one of the largest samples of X-ray selected AGNs (4016 sources). In order to derive the physical properties of AGN host galaxies, I develop a multi-component SED fitting technique which allows one to disentangle the nuclear emission from the stellar light, and derived host galaxy properties using the Bayesian statistics. Specifically, I decompose the entire SED into separate components with nuclear AGN emission, the host galaxy's stellar populations, and a starburst contribution in the FIR using the existing multi-wavelength photometric data (from NUV through the FIR) available in the COSMOS field. This technique of SED decomposition is crucial for estimating reliable physical properties of the host galaxies, such as stellar mass and star formation rate (SFR).

Combining with black hole masses estimated via virial method, I investigate the evolution of $M_{\rm BH} - M_{\rm stellar}$ relation up to $z \sim 2.5$. The $M_{\rm BH} - M_{\rm stellar}$ distribution for the moderate-luminosity AGNs shows a broadly consistent with the local scaling relation, suggesting that there is no significant evolution with redshift. The $M_{\rm BH} - M_{\rm stellar}$ ratios seem to depend on the Eddington ratio in the sense that AGNs with higher Eddington ratio have smaller black hole masses for a given stellar mass, lying below the local $M_{\rm BH} - M_{\rm stellar}$ relation. I also explore the distribution of AGN host galaxies on the SFR$-M_{\rm stellar}$ diagram compared to the normal star-forming galaxies, which show a tight correlation between

the SFR and their stellar mass, commonly referred to as the main sequence (MS) of star formation (e.g., Noeske et al. 2007; Daddi et al. 2007; Elbaz et al. 2007). Overall, AGN host galaxies seem to have SFRs that lie on the star-forming MS, but with much broader dispersions. While the "flattening" in the star-forming MS at high masses could be interpreted as a consequence of quenching the star formation, the SFRs of AGN host galaxies are consistent with those expected from normal star-forming galaxies in most stellar mass bins up to $z \sim 3$, indicating no clear signature for enhanced or suppressed SFRs compared to normal star-forming galaxies (Suh et al. 2017). The correlation between $L_{\rm IR}$ due to star formation and X-ray luminosities show broadly consistent with being flat relationship, which can be explained by the AGN variability along with the broad Eddington ratio distribution.

All of these results imply that nuclear activity and star formation seem to co-exist fueling black hole accretion and star formation simultaneously. There seems to be a lack of significant evolution in the stellar masses of X-ray selected AGN host galaxies, which are typically massive ($> 10^{10}$ $M_{\odot}$) since z$\sim$3, indicating that they might have already experienced substantial growth at higher redshift. This could be suggests that the secular evolution may play an important role in growing SMBHs and the bulge formation in massive galaxies for the majority of AGN host galaxies at later cosmic time ($z < 3$).

5.2 Future Prospect

While the deepest X-ray surveys (e.g., *ROSAT, XMM-Newton, Chandra*) have provided the most complete sample of AGN with a broad range of luminosities out to $z \sim 5$, heavily obscured Compton-thick AGNs are not well sampled by the X-ray (e.g., Treister et al. 2004; Kocevski et al. 2015). The highly obscured AGNs are particularly interesting, because they might represent a hidden phase of obscured SMBH growth, during which they accrete the bulk of their mass and produce most of their feedback into their host galaxies. Furthermore, while the majority of X-ray selected AGNs show a lack of significant merger features, there is an increased fraction of disturbances among luminous IR-selected AGNs, suggesting a

more significant role of mergers for this population (e.g., Kocevski et al. 2012). Thus, these heavily obscured AGNs would provide a valuable observational constraint on a missing-link phase in the early Universe.

The heavily obscured AGNs missed by X-ray surveys might be the key epoch in which to study these feeding and feedback processes in both black holes and galaxies. If heavily obscured AGNs are triggered by major mergers (e.g., Kocevski et al. 2015), the black hole may radiate close to the Eddington limit, in contrast to X-ray selected moderate-luminosity AGNs, which are thought to evolve through secular processes. It would be interesting to see differences in the SFRs and black hole accretion rates for these populations. Therefore, in order to make the complete and unbiased sample of AGNs, the IR selection for identifying heavily obscured Compton-thick AGN in addition to the X-ray selected AGNs is crucial.

References

Bower, R. G., Benson, A. J., Malbon, R., et al. 2006, MNRAS, 370, 645

Civano, F., Marchesi, S., Comastri, A., et al. 2016, ApJ, 819, 62

Croton, D. J., Springel, V., White, S. D. M., et al. 2006, MNRAS, 365, 11

Daddi, E., Dickinson, M., Morrison, G., et al. 2007, ApJ, 670, 156

Di Matteo, T., Springel, V., Hernquist, L. 2005, Nature, 433, 604

Donley, J. L., Rieke, G. H., Pérez-González, P. G., Barro, G. 2008, ApJ, 687, 111

Elbaz, D., Daddi, E., Le Borgne, D., et al. 2007, A&A, 468, 33

Fan, L., Fang, G., Chen, Y., et al. 2014, ApJL, 784, L9

Hasinger, G., Miyaji, T., Schmidt, M. 2005, A&A, 441, 417

Hopkins, P. F., Hernquist, L., Cox, T. J., Keres, D. 2008, ApJS, 175, 356

Kocevski, D. D., Faber, S. M., Mozena, M., et al. 2012, ApJ, 744, 148

Kocevski, D. D., Brightman, M., Nandra, K., et al. 2015, ApJ, 814, 104

Lehmer, B. D., Xue, Y. Q., Brandt, W. N., et al. 2012, ApJ, 752, 46

Noeske, K. G., Weiner, B. J., Faber, S. M., et al. 2007, ApJL, 660, L43

Silk, J., & Rees, M. J. 1998, A&A, 331, 1

Springel, V., di Matteo, T., & Hernquist, L. 2005, MNRAS, 361, 776

Stern, D., Assef, R. J., Benford, D. J., et al. 2012, ApJ, 753, 30

Suh, H., Hasinger, G., Steinhardt, C., Silverman, J. D., Schramm, M. 2015, ApJ, 815, 129

Suh, H., Civano, F., Hasinger, G., et al. 2017, ApJ, 841, 102

Treister, E., Urry, C. M., Chatzichristou, E., et al. 2004, ApJ, 616, 123

Appendix A
Emission line properties of broad-line AGNs

In Table A.1, I list the sample of broad-line AGNs, which includes AGN bolometric luminosities, black hole masses, and measurements of emission line properties. The X-ray source ID is from the published catalog of CCLS (Civano et al. 2016), CDF-S (Xue et al. 2011), E-CDF-S (Lehmer et al. 2005), and *XMM*-LH (Brunner et al. 2008).

Table A.1: Emission line properties of Broad-line AGNs

ID	z	log L_{bol} (erg s^{-1})	log M_{BH} ($M_\odot$)	log FWHM (km s^{-1})			log L (erg s^{-1})		
				Hα	Hβ	MgII	Hα	Hβ	3000Å
CID-36	1.826	45.63	9.10±0.11	···	···	3.80±0.05	···	···	45.61±0.00
CID-61	1.478	45.38	8.67±0.13	···	···	3.77±0.06	···	···	45.02±0.00
CID-69	0.980	45.68	7.90±0.00	···	···	3.63±0.33	···	···	44.21±0.00
CID-70	1.648	45.28	8.69±0.85	···	···	3.75±0.24	···	···	45.10±0.00
CID-87	1.607	46.69	7.39±0.17	3.44±0.05	···	···	42.34±0.12	···	···
CID-98	1.520	45.59	7.55±0.00	···	···	3.57±0.50	···	···	43.83±0.00
CID-102	1.847	45.81	8.66±0.30	···	···	3.88±0.13	···	···	44.64±0.00
CID-103	1.432	45.63	7.98±0.00	···	···	3.78±0.36	···	···	43.87±0.00
CID-110	0.729	45.02	7.41±0.15	3.60±0.04	···	···	41.77±0.10	···	···
CID-112	1.320	46.25	8.81±0.00	···	···	3.87±0.87	···	···	44.91±0.00
CID-120	1.003	45.18	7.10±0.05	3.32±0.02	···	···	42.25±0.04	···	···
CID-134	1.849	44.96	6.53±0.00	···	···	3.39±2.15	···	···	42.79±0.00
CID-157	1.333	45.46	8.39±0.37	···	···	3.70±0.15	···	···	44.78±0.00
CID-162	2.459	46.10	8.25±0.00	···	3.51±0.33	···	···	43.22±0.08	···
CID-175	1.627	45.51	8.19±0.00	···	···	3.74±0.39	···	···	44.33±0.00
CID-179	1.850	46.40	8.47±0.71	···	···	3.70±0.22	···	···	44.91±0.00
CID-307	2.051	45.94	8.59±0.30	···	···	3.83±0.12	···	···	44.68±0.00
CID-340	2.187	45.66	8.71±0.00	···	···	4.05±0.44	···	···	44.17±0.00
CID-346	2.213	45.96	9.44±0.85	···	···	3.87±0.24	···	···	45.93±0.00
CID-369	1.171	45.32	8.12±0.00	···	···	3.71±0.33	···	···	44.33±0.00
CID-389	1.537	45.23	8.75±0.02	3.88±0.00	···	···	43.17±0.02	···	···
CID-399	2.177	45.96	8.99±0.19	···	···	3.78±0.08	···	···	45.48±0.04
CID-434	1.530	46.30	7.64±1.44	3.44±0.28	···	···	42.77±0.20	···	···
CID-438	1.662	45.96	8.32±0.00	···	···	3.89±0.59	···	···	44.06±0.00
CID-445	1.259	45.52	8.13±0.07	3.67±0.02	···	···	42.81±0.04	···	···
CID-452	1.407	45.79	8.22±0.00	···	···	3.72±0.51	···	···	44.43±0.00
CID-454	1.486	45.55	8.32±0.17	···	···	3.61±0.08	···	···	44.98±0.00

TableA.1 – continued

ID	z	log L_{bol} (erg s^{-1})	log M_{BH} ($M_\odot$)	log FWHM (km s^{-1}) Hα	Hβ	MgII	log L (erg s^{-1}) Hα	Hβ	3000Å
CID-467	2.285	46.59	8.90±0.00	···	···	3.72±0.33	···	···	45.54±0.00
CID-492	0.967	45.87	7.93±0.00	3.62±0.36	···	···	42.65±0.15	···	···
CID-495	2.015	45.55	9.05±0.60	···	···	3.77±0.20	···	···	45.63±0.00
CID-512	1.517	45.98	8.06±0.00	3.53±0.40	···	···	43.20±0.08	···	···
CID-513	1.122	46.37	8.95±0.88	···	···	4.03±0.25	···	···	44.62±0.00
CID-517	2.097	45.17	8.29±0.00	···	···	3.66±0.63	···	···	44.76±0.00
CID-536	0.881	45.40	7.45±0.00	3.36±0.41	···	···	42.73±0.06	···	···
CID-543	1.298	45.03	7.90±0.55	···	···	3.44±0.19	···	···	44.83±0.00
CID-548	1.642	45.74	8.29±0.00	···	···	3.79±0.44	···	···	44.33±0.00
CID-553	0.829	44.77	8.34±0.00	···	···	4.00±0.60	···	···	43.74±0.00
CID-556	1.596	45.75	8.62±1.77	···	···	3.98±0.29	···	···	44.24±0.00
CID-566	1.459	45.84	8.75±0.00	···	···	3.99±0.48	···	···	44.42±0.00
CID-599	1.081	45.01	8.71±0.00	···	···	3.99±0.53	···	···	44.43±0.00
CID-604	1.340	45.60	8.10±0.00	···	···	3.67±0.46	···	···	44.42±0.00
CID-632	0.825	45.42	7.34±0.04	3.42±0.01	···	···	42.33±0.03	···	···
CID-642	1.368	45.39	8.27±0.26	···	···	3.72±0.11	···	···	44.54±0.00
CID-644	0.986	45.37	8.00±0.07	3.71±0.02	···	···	42.42±0.05	···	···
CID-925	1.817	45.41	8.95±0.12	···	···	3.75±0.05	···	···	45.52±0.00
CID-933	2.491	45.74	8.03±0.14	···	3.50±0.04	···	···	42.84±0.09	···
CID-958	1.869	45.28	7.59±0.00	···	···	3.53±0.36	···	···	44.03±0.00
CID-1031	1.359	45.05	8.10±0.00	···	···	3.78±0.55	···	···	44.06±0.00
CID-1044	1.560	46.28	8.61±0.02	3.75±0.01	···	···	43.86±0.01	···	···
CID-1086	2.233	45.43	7.41±0.00	···	···	3.37±0.00	···	···	44.27±0.00
CID-1109	1.827	45.60	7.59±0.00	···	···	3.58±0.74	···	···	43.89±0.00
CID-1141	1.660	44.97	8.21±0.00	3.69±0.35	···	···	42.90±0.14	···	···
CID-1167	1.856	44.65	8.50±0.21	···	···	3.74±0.09	···	···	44.84±0.00
CID-1170	1.821	44.97	7.94±0.29	···	···	3.56±0.12	···	···	44.51±0.00
CID-1281	1.444	45.16	7.22±0.00	···	···	3.37±0.00	···	···	43.96±0.00

TableA.1 – continued

ID	z	log L_{bol} (erg s^{-1})	log M_{BH} ($M_\odot$)	log FWHM (km s^{-1}) Hα	Hβ	MgII	log L (erg s^{-1}) Hα	Hβ	3000Å
CID-1305	2.177	44.48	8.38±0.86	···	···	3.89±0.24	···	···	44.15±0.00
CID-1489	1.952	44.60	7.80±0.21	···	···	3.41±0.09	···	···	44.76±0.00
CID-1551	1.948	45.12	8.70±0.17	···	···	3.74±0.08	···	···	45.16±0.25
CID-1913	2.089	45.75	8.37±0.43	···	···	3.77±0.16	···	···	44.52±0.00
CID-1930	1.567	45.97	8.73±0.07	3.86±0.02	···	···	43.21±0.05	···	···
CID-2252	1.964	44.79	8.60±0.17	···	···	3.75±0.08	···	···	44.97±0.00
CID-2564	2.011	45.29	8.28±0.00	···	···	3.79±0.30	···	···	44.30±0.00
CID-2728	1.506	45.18	7.27±0.00	3.57±0.06	···	3.37±0.00	42.52±0.21	···	44.04±0.00
CID-3021	1.755	45.58	7.34±0.00	···	···	3.42±0.57	···	···	43.99±0.00
CID-3242	1.530	45.25	8.51±0.04	3.76±0.40	···	3.70±0.01	45.20±0.00	···	43.38±0.02
CID-3270	1.309	45.05	7.59±0.00	···	···	3.64±1.07	···	···	43.68±0.00
LID-286	1.206	44.57	7.58±0.00	···	···	3.52±0.86	···	···	44.06±0.00
LID-291	0.851	45.58	8.06±0.00	···	···	3.65±0.49	···	···	44.41±0.00
LID-338	1.209	45.83	8.32±1.10	···	···	3.73±0.27	···	···	44.57±0.00
LID-381	0.767	45.34	7.74±0.07	3.54±0.02	···	···	42.60±0.05	···	···
LID-395	1.610	45.94	8.10±0.08	3.57±0.02	···	···	43.14±0.05	···	···
LID-405	1.433	46.55	8.76±0.64	···	···	3.75±0.21	···	···	45.24±0.00
LID-414	1.381	45.16	7.69±0.00	···	···	3.66±0.82	···	···	43.77±0.00
LID-430	2.114	46.97	8.38±0.06	···	3.47±0.02	···	···	43.57±0.04	···
LID-437	1.260	45.59	8.28±0.00	···	···	3.78±0.56	···	···	44.33±0.00
LID-485	2.034	45.42	7.81±0.00	···	···	3.55±0.63	···	···	44.33±0.00
LID-491	2.543	46.34	8.61±0.04	···	3.54±0.01	···	···	43.74±0.02	···
LID-579	2.079	45.87	8.30±0.64	···	···	3.67±0.21	···	···	44.74±0.00
LID-592	1.561	46.06	8.39±0.00	···	···	3.65±0.39	···	···	44.95±0.00
LID-638	1.421	45.13	7.34±0.00	···	···	3.52±0.76	···	···	43.65±0.00
LID-673	1.452	44.66	7.22±0.00	···	···	3.45±0.87	···	···	43.70±0.00
LID-685	2.030	46.20	8.85±0.87	···	···	3.65±0.25	···	···	45.67±0.00
LID-736	1.264	45.45	7.95±0.00	···	···	3.53±0.37	···	···	44.63±0.00

TableA.1 – continued

ID	z	log L_{bol} (erg s^{-1})	log M_{BH} ($M_\odot$)	log FWHM (km s^{-1})			log L (erg s^{-1})		
				Hα	Hβ	MgII	Hα	Hβ	3000Å
LID-738	1.477	45.14	8.23±0.00	···	···	3.69±0.75	···	···	44.56±0.00
LID-961	1.507	46.99	9.24±0.02	3.97±0.01	···	···	43.72±0.01	···	···
LID-1273	1.622	45.37	8.18±0.03	3.55±0.01	···	···	43.35±0.02	···	···
LID-1305	1.247	45.38	7.94±0.00	···	···	3.62±0.40	···	···	44.31±0.00
LID-1476	1.263	45.34	8.07±1.06	···	···	3.67±0.26	···	···	44.38±0.00
LID-1502	1.539	45.87	8.31±0.93	···	···	3.68±0.25	···	···	44.71±0.00
LID-1538	1.523	46.03	7.84±0.05	3.49±0.02	···	···	42.95±0.03	···	···
LID-1565	1.593	46.73	8.09±0.05	3.54±0.02	···	···	43.22±0.03	···	···
LID-1590	1.596	45.99	8.48±0.06	3.73±0.02	···	···	43.22±0.04	···	···
LID-1607	1.509	46.24	8.86±0.01	3.71±0.00	···	···	43.99±0.01	···	···
LID-1802	2.084	45.29	8.37±0.10	···	···	3.57±0.05	···	···	45.16±0.00
LID-1878	1.607	45.69	8.16±0.00	3.40±0.37	···	···	43.89±0.02	···	···
CDF-S-1	1.630	45.89	8.41±0.08	3.74±0.02	···	···	43.08±0.06	···	···
CDF-S-4	1.270	45.39	7.22±0.24	3.40±0.05	···	···	42.16±0.12	···	···
CDF-S-11	1.888	46.02	8.37±0.16	···	···	3.61±0.02	···	···	45.52±0.00
CDF-S-14	1.370	44.32	8.29±0.05	···	···	3.68±0.13	···	···	45.19±0.01
CDF-S-15	1.065	44.25	6.52±0.07	···	···	3.36±0.33	···	···	43.34±0.03
CDF-S-25	1.336	44.34	6.69±0.09	···	···	3.32±0.04	···	···	43.51±0.02
CDF-S-66	0.575	42.80	7.67±0.58	···	3.39±0.60	···	···	41.65±0.00	···
CDF-S-76	1.042	45.06	7.45±0.07	3.63±0.08	···	3.68±0.02	42.04±0.17		43.81±0.00
CDF-S-87	1.437	44.15	8.67±0.06	···	···	4.41±0.17	···	···	43.43±0.02
CDF-S-88	1.613	45.14	7.05±0.02	···	···	3.67±0.01	···	···	43.22±0.01
CDF-S-101	0.966	45.36	7.40±0.16	3.70±0.05	···	3.73±0.02	42.23±0.11	···	43.57±0.00
CDF-S-166	1.608	45.67	8.30±0.19	3.64±0.07	···	3.84±0.16	42.64±0.19	···	44.68±0.00
CDF-S-229	1.326	45.68	7.75±0.02	3.35±0.33	3.37±0.05	3.71±0.14	43.30±0.00	41.93±0.14	45.26±0.01
CDF-S-241	0.566	44.07	7.26±0.06	···	···	3.67±0.14	···	···	43.55±0.01
CDF-S-329	0.954	44.26	7.03±0.86	3.39±0.09	···	···	41.86±0.27	···	···
CDF-S-344	1.615	45.03	8.06±0.09	3.35±0.23	···	3.89±0.01	43.02±0.16	···	44.13±0.02

TableA.1 – continued

ID	z	log L_{bol} (erg s^{-1})	log M_{BH} ($M_\odot$)	log FWHM (km s^{-1})			log L (erg s^{-1})		
				Hα	Hβ	MgII	Hα	Hβ	3000Å
CDF-S-367	1.041	45.45	7.27±0.38	···	···	3.39±0.02	···	···	44.46±0.00
CDF-S-369	1.612	45.53	7.46±0.82	3.47±0.16	···	···	42.35±0.15	···	···
CDF-S-375	0.742	45.76	8.14±0.02	3.78±0.24	···	3.81±0.01	43.12±0.03	···	44.51±0.01
CDF-S-417	1.222	45.33	8.91±0.14	4.03±0.15	···	···	42.90±0.12	···	···
CDF-S-420	0.960	44.09	7.35±0.30	3.38±0.65	···	···	42.47±0.00	···	···
CDF-S-473	1.557	45.82	7.84±0.52	3.50±0.59	···	···	42.92±0.00	···	···
CDF-S-514	0.664	44.03	7.46±0.61	···		3.85±0.27	···	···	43.27±0.00
CDF-S-523	0.838	45.43	8.35±0.03	3.69±0.40	···	4.11±0.29	43.14±0.00	···	44.56±0.03
CDF-S-537	1.216	44.87	8.60±0.16	···	···	3.96±0.17	···	···	44.76±0.02
CDF-S-614	0.664	43.18	8.23±0.03	···	···	4.14±0.02	···	···	43.58±0.02
CDF-S-627	0.736	44.80	7.29±0.12	···	···	3.72±0.02	···	···	43.43±0.02
CDF-S-656	1.367	43.66	7.45±0.49	3.36±0.49	···	···	42.72±0.00	···	···
CDF-S-681	0.733	44.34	7.28±0.11	···	···	3.65±0.11	···	···	43.65±0.00
CDF-S-691	2.005	45.93	8.95±0.39	···	···	3.81±0.15	···	···	45.82±0.01
CDF-S-695	0.622	43.79	7.65±0.05	···	···	3.87±0.04	···	···	43.51±0.02
CDF-S-720	1.609	45.94	8.50±0.12	3.85±0.04	···	···	42.81±0.08	···	···
CDF-S-723	2.072	45.66	8.82±0.02	···	···	3.82±0.01	···	···	45.55±0.02
CDF-S-724	1.337	44.95	7.69±0.16	3.52±0.30	···	···	42.81±0.00	···	···
E-CDF-S-7	1.368	46.16	9.30±0.04	4.12±0.02	···	3.90±0.00	43.27±0.04	···	45.29±0.02
E-CDF-S-53	1.524	45.58	9.18±0.19	···	···	4.03±0.18	···	···	45.48±0.02
E-CDF-S-68	1.362	44.58	8.55±0.06	···	···	3.77±0.03	···	···	45.30±0.02
E-CDF-S-89	1.613	44.44	7.32±0.14	3.44±0.08	···	···	42.22±0.17	···	···
E-CDF-S-100	1.957	45.64	8.69±0.12	···	···	3.73±0.13	···	···	45.65±0.01
E-CDF-S-158	0.717	44.44	8.81±0.08	···	3.89±0.02	···	···	41.88±0.03	···
E-CDF-S-166	1.408	44.81	8.31±0.61	3.70±0.42	···	···	43.02±0.00	···	···
E-CDF-S-358	1.626	45.64	8.29±0.02	3.42±0.43	3.73±0.09	3.61±0.00	43.59±0.00	41.95±0.21	45.38±0.01
E-CDF-S-381	0.526	44.28	7.72±0.34	···	3.63±0.17	···	···	40.87±0.19	···
E-CDF-S-517	1.345	44.94	7.82±0.30	3.64±0.08	···	···	42.37±0.23	···	···

TableA.1 – continued

ID	z	log L_{bol} (erg s^{-1})	log M_{BH} ($M_\odot$)	log FWHM (km s^{-1}) Hα	Hβ	MgII	log L (erg s^{-1}) Hα	Hβ	3000Å
E-CDF-S-601	1.598	45.47	7.55±0.35	3.41±0.59	···	···	42.74±0.00	···	···
E-CDF-S-631	2.072	45.49	8.67±0.24	···	···	3.79±0.06	···	···	45.42±0.05
E-CDF-S-678	1.629	45.30	8.58±0.06	3.77±0.18	···	3.73±0.21	43.25±0.07	···	45.43±0.01
E-CDF-S-681	0.834	44.66	8.41±0.06	3.88±0.02	···	···	42.53±0.04	···	···
E-CDF-S-700	2.171	45.78	8.31±0.24	···	···	3.91±0.19	···	···	44.45±0.02
E-CDF-S-712	0.841	45.74	8.00±0.02	3.76±0.34	···	3.73±0.01	42.66±0.00	···	44.55±0.07
E-CDF-S-716	0.763	44.93	8.11±0.43	3.70±0.33	···	···	42.65±0.00	···	···
E-CDF-S-725	1.314	45.74	8.31±0.10	3.59±0.23	···	3.71±0.01	43.11±0.13	···	45.12±0.02
E-CDF-S-728	1.583	45.44	8.54±0.19	3.81±0.03	···	···	43.02±0.05	···	···
E-CDF-S-742	1.762	44.85	8.33±0.18	···	···	3.60±0.03	···	···	45.48±0.01
XMM-LH-5	2.138	46.55	8.24±0.08	···	3.35±0.54	···	···	42.77±0.00	···
XMM-LH-25	1.599	44.52	7.52±0.65	3.50±0.07	···	···	42.36±0.17	···	···
XMM-LH-41	1.653	45.89	8.09±0.20	···	···	3.71±0.15	···	···	44.75±0.02
XMM-LH-85	1.144	45.26	8.03±0.02	···	···	3.75±0.18	···	···	44.52±0.02
XMM-LH-119	1.406	45.25	8.55±0.08	3.83±0.02	···	···	42.97±0.03	···	···
XMM-LH-120	1.523	45.65	7.62±0.16	3.54±0.09	···	···	42.39±0.25	···	···
XMM-LH-148	1.116	46.58	8.93±0.06	···	···	3.74±0.13	···	···	46.02±0.01
XMM-LH-168	1.958	46.95	8.85±0.23	···	3.74±0.06	···	···	42.49±0.14	···
XMM-LH-176	1.533	45.77	8.12±0.04	3.43±0.01	···	3.55±0.01	43.19±0.02	···	45.30±0.01
XMM-LH-191	0.787	45.94	7.94±0.02	3.86±0.01	···	3.82±0.18	42.53±0.02	···	44.16±0.02
XMM-LH-261	3.406	46.77	7.58±0.05	···	···	3.37±0.00	···	···	45.02±0.02
XMM-LH-270	1.576	45.66	8.39±0.06	3.75±0.01	3.55±0.05	3.73±0.14	43.50±0.02	41.93±0.11	45.17±0.01
XMM-LH-321	1.008	45.04	7.44±0.03	···	···	3.55±0.01	···	···	44.24±0.00
XMM-LH-332	1.676	46.31	8.08±0.02	···	···	3.74±0.02	···	···	44.64±0.01
XMM-LH-354	3.409	46.95	8.93±0.17	···	···	3.76±0.16	···	···	45.93±0.02
XMM-LH-364	0.932	44.53	7.55±0.09	···	···	3.65±0.04	···	···	44.09±0.02
XMM-LH-387	1.449	45.04	7.58±0.06	3.38±0.02	···	3.47±0.01	42.90±0.03	···	44.61±0.02
XMM-LH-406	1.283	45.39	8.77±0.02	3.92±0.01	···	3.80±0.03	43.03±0.01	···	44.86±0.01

TableA.1 – continued

ID	z	log L_{bol} (erg s^{-1})	log M_{BH} ($M_\odot$)	log FWHM (km s^{-1}) Hα	Hβ	MgII	log L (erg s^{-1}) Hα	Hβ	3000Å
XMM-LH-430	1.553	46.48	8.33±0.17	···	···	3.90±0.17	···	···	44.54±0.02
XMM-LH-453	1.214	45.02	7.41±0.04	···	···	3.52±0.02	···	···	44.26±0.02
XMM-LH-456	0.877	45.28	7.44±0.30	3.62±0.06	···	···	41.76±0.15	···	···
XMM-LH-475	1.205	47.07	8.90±0.00	3.69±0.00	···	3.87±0.14	44.13±0.00	···	45.66±0.01
XMM-LH-523	1.217	45.65	7.84±0.08	3.60±0.03	···	···	42.57±0.08	···	···
XMM-LH-529	1.940	46.74	8.55±0.11	···	3.68±0.09	···	···	42.16±0.20	···
XMM-LH-532	1.675	45.01	8.29±0.31	3.60±0.03	···	3.73±0.02	42.91±0.06	···	45.01±0.01
XMM-LH-553	1.440	46.36	8.68±0.03	3.76±0.01	···	···	43.49±0.02	···	···
XMM-LH-555	1.674	45.84	8.99±0.13	4.01±0.04	···	···	43.11±0.07	···	···
XMM-LH-591	1.535	45.65	8.22±0.08	3.62±0.32	···	···	43.18±0.00	···	···
XMM-LH-595	1.602	45.08	8.50±0.29	3.78±0.27	···	···	43.09±0.07	···	···
XMM-LH-604	2.104	46.47	8.66±0.83	···	3.54±0.62	···	···	42.86±0.00	···
XMM-LH-2020	1.728	45.96	7.98±0.10	3.55±0.01	···	···	42.99±0.02	···	···

Appendix B
AGN Host galaxy properties derived from the SED fitting

In Table B.1 and Table B.1, I present Type 1 and Type 2 AGN host galaxy properties derived from the SED fitting, including host stellar mass, host galaxy SFR, and luminosity of AGN and host galaxy.

Table B.1: Type 1 AGN Host galaxy properties derived from the SED fitting

ID	log $M_{stellar}$ ($M_\odot$)	log SFR^{IR} ($M_\odot$ yr^{-1})	log $L_{2-10\ keV}$ (erg s^{-1})	log L_{bol} (erg s^{-1})	log L_{2500} (erg s^{-1})	log $L_{6\mu m}$ (erg s^{-1})	log L_{IR} (erg s^{-1})
CID-20	$11.07^{+0.01}_{-0.94}$	1.15	43.62	45.03	44.19	44.49	-44.70
CID-21	$10.98^{+0.00}_{-1.07}$	1.54	44.38	46.03	45.16	44.80	-45.09
CID-26	$11.60^{+0.19}_{-0.09}$	1.80	43.74	45.19	45.08	44.17	45.35
CID-29	$10.11^{+0.18}_{-0.31}$	1.07	43.14	44.42	43.71	44.53	-44.61
CID-31	$11.79^{+0.00}_{-0.37}$	1.63	44.76	46.53	45.70	45.49	-45.17
CID-32	$11.15^{+0.02}_{-0.83}$	2.02	43.30	44.62	44.24	44.04	45.56
CID-35	$11.26^{+0.16}_{-0.03}$	1.14	43.10	44.36	44.27	44.03	44.69
CID-36	$12.26^{+0.00}_{-0.00}$	2.68	44.08	45.63	45.48	45.04	46.22
CID-40	$11.57^{+0.17}_{-0.22}$	1.34	43.99	45.51	44.95	44.87	-44.89
CID-42	$10.80^{+0.02}_{-0.12}$	1.10	43.19	44.49	44.06	43.98	44.64
CID-43	$11.52^{+0.06}_{-1.03}$	1.82	-44.71	46.48	45.07	45.26	-45.37
CID-47	$12.02^{+0.20}_{-0.06}$	1.61	44.14	45.71	45.95	45.56	-45.16
CID-50	$7.68^{+0.84}_{-0.35}$	0.96	44.63	46.36	45.51	45.52	-44.51
CID-54	$11.13^{+0.24}_{-0.03}$	1.44	44.09	45.65	44.37	44.44	44.98
CID-59	$11.46^{+0.04}_{-0.76}$	1.51	43.88	45.37	44.67	44.74	-45.06
CID-60	$11.25^{+0.29}_{-0.19}$	0.86	43.57	44.97	44.84	44.80	-44.41
CID-61	$11.55^{+0.03}_{-2.16}$	1.39	-43.88	45.38	45.28	44.42	-44.94
CID-62	$11.71^{+0.05}_{-0.37}$	1.52	44.45	46.13	45.29	45.10	-45.07
CID-66	$11.25^{+0.06}_{-0.77}$	1.38	44.18	45.77	44.43	44.58	-44.93
CID-68	$10.32^{+0.17}_{-0.45}$	0.60	43.38	44.72	43.79	43.70	-44.14
CID-69	$11.52^{+0.10}_{-0.04}$	1.75	44.12	45.68	44.56	44.23	45.29
CID-70	$11.73^{+0.09}_{-0.04}$	2.18	43.81	45.28	45.21	45.20	45.73
CID-71	$11.38^{+0.04}_{-0.09}$	1.19	43.74	45.19	44.30	44.04	44.74
CID-72	$8.87^{+0.28}_{-0.12}$	1.71	44.56	46.27	45.27	45.09	-45.25
CID-74	$10.78^{+0.15}_{-0.32}$	0.67	43.50	44.88	44.19	44.18	-44.21
CID-75	$11.87^{+0.16}_{-0.32}$	2.72	44.76	46.53	44.54	44.80	46.26
CID-83	$11.12^{+0.16}_{-2.24}$	1.84	44.54	46.24	45.03	45.09	-45.38
CID-84	$11.58^{+0.04}_{-0.10}$	2.27	43.95	45.46	44.81	44.43	45.81
CID-87	$11.74^{+0.08}_{-0.06}$	1.37	44.88	46.69	44.42	45.04	-44.91
CID-90	$11.86^{+0.10}_{-0.38}$	1.60	44.43	46.09	45.07	44.68	-45.14
CID-93	$9.56^{+0.18}_{-0.33}$	0.12	43.06	44.32	43.36	43.46	-43.66
CID-94	$12.50^{+0.00}_{-0.00}$	2.24	44.56	46.26	45.90	45.62	45.79
CID-97	$10.27^{+0.00}_{-2.51}$	1.67	44.42	46.08	43.83	44.77	-45.22
CID-98	$10.44^{+0.00}_{-2.65}$	1.40	44.05	45.59	43.53	44.41	-44.95
CID-102	$10.78^{+0.09}_{-1.22}$	1.54	44.22	45.81	44.75	44.86	-45.08
CID-104	$6.93^{+0.56}_{-0.19}$	0.83	42.90	44.12	42.39	43.87	44.38
CID-108	$11.80^{+0.22}_{-0.08}$	2.13	44.05	45.59	45.08	44.71	45.68

Table B.1 – continued

ID	log $M_{stellar}$ ($M_\odot$)	log SFR^{IR} ($M_\odot$ yr^{-1})	log $L_{2-10\ keV}$ (erg s^{-1})	log L_{bol} (erg s^{-1})	log L_{2500} (erg s^{-1})	log $L_{6\mu m}$ (erg s^{-1})	log L_{IR} (erg s^{-1})
CID-109	$9.08^{+0.29}_{-0.81}$	1.07	43.44	44.80	43.08	44.92	-44.62
CID-112	$11.24^{+0.00}_{-0.00}$	2.08	44.55	46.25	45.66	45.60	45.62
CID-113	$11.86^{+0.16}_{-0.02}$	1.79	44.37	46.02	46.17	45.76	-45.34
CID-119	$10.49^{+0.31}_{-0.79}$	1.35	43.95	45.46	44.99	44.76	-44.90
CID-126	$10.94^{+0.04}_{-0.23}$	1.42	43.22	44.52	43.88	43.77	44.97
CID-128	$11.43^{+0.16}_{-0.11}$	2.00	44.36	46.01	45.41	45.29	45.54
CID-134	$10.98^{+0.00}_{-2.17}$	1.57	-43.56	44.96	44.22	44.46	-45.12
CID-136	$11.76^{+0.17}_{-0.46}$	2.15	43.97	45.48	45.44	44.85	45.69
CID-139	$9.69^{+0.44}_{-1.34}$	1.36	44.00	45.53	44.38	44.30	-44.90
CID-140	$11.01^{+0.00}_{-1.33}$	1.74	44.62	46.35	45.46	44.91	-45.28
CID-142	$11.26^{+0.16}_{-0.03}$	0.55	43.98	45.50	45.10	44.98	-44.10
CID-144	$11.72^{+0.16}_{-0.26}$	1.52	44.28	45.89	44.99	45.35	-45.07
CID-147	$10.55^{+0.15}_{-1.38}$	1.19	43.68	45.11	44.10	44.13	-44.73
CID-149	$11.85^{+0.19}_{-0.73}$	1.85	44.65	46.40	45.72	44.88	-45.40
CID-150	$11.55^{+0.17}_{-0.36}$	1.57	44.36	46.01	44.67	44.41	-45.12
CID-153	$11.20^{+0.07}_{-0.84}$	1.43	43.87	45.35	44.63	44.57	-44.98
CID-155	$10.90^{+0.06}_{-1.14}$	1.55	44.11	45.68	44.49	44.59	-45.10
CID-157	$11.07^{+0.25}_{-0.33}$	1.25	43.95	45.46	44.78	44.64	-44.79
CID-161	$10.17^{+0.22}_{-0.09}$	1.91	43.65	45.06	45.03	45.04	45.46
CID-162	$10.11^{+0.43}_{-0.45}$	1.65	44.44	46.10	45.04	45.39	-45.19
CID-166	$12.92^{+0.00}_{-0.00}$	1.55	44.88	46.70	46.36	45.84	-45.09
CID-171	$11.29^{+0.10}_{-0.17}$	1.05	43.55	44.94	44.16	43.97	44.60
CID-174	$10.30^{+0.39}_{-1.44}$	1.72	44.32	45.94	45.52	45.38	-45.26
CID-175	$11.16^{+0.20}_{-0.06}$	1.46	43.99	45.51	44.60	44.48	-45.01
CID-178	$11.66^{+0.13}_{-0.13}$	1.82	43.99	45.51	45.45	45.19	45.37
CID-179	$11.60^{+0.00}_{-0.54}$	1.52	44.65	46.40	45.04	44.94	-45.07
CID-181	$11.26^{+0.07}_{-0.54}$	2.01	43.57	44.97	44.20	43.78	45.56
CID-192	$11.12^{+0.10}_{-0.04}$	2.04	43.94	45.45	44.82	44.97	45.58
CID-193	$11.31^{+0.05}_{-0.66}$	1.50	44.65	46.39	45.51	44.84	-45.05
CID-199	$11.39^{+0.00}_{-2.65}$	2.17	44.37	46.01	43.97	44.11	45.72
CID-201	$11.89^{+0.00}_{-0.00}$	2.01	44.19	45.78	44.30	45.13	45.56
CID-202	$10.93^{+0.17}_{-1.56}$	1.73	44.22	45.82	44.96	44.90	-45.27
CID-203	$10.70^{+0.09}_{-0.75}$	1.31	44.05	45.60	44.22	43.93	-44.86
CID-206	$10.91^{+0.37}_{-0.25}$	1.34	44.00	45.52	45.05	44.78	-44.88
CID-208	$11.19^{+0.00}_{-0.00}$	1.52	44.69	46.45	45.79	45.75	45.06
CID-210	$11.43^{+0.16}_{-0.11}$	1.56	43.86	45.35	44.59	43.85	45.11
CID-211	$11.04^{+0.10}_{-0.44}$	1.16	43.38	44.72	44.56	44.38	-44.70
CID-216	$11.36^{+0.17}_{-0.37}$	1.42	43.70	45.13	44.50	44.53	-44.97
CID-220	$10.92^{+0.38}_{-0.11}$	1.37	43.76	45.21	44.52	44.05	44.92
CID-222	$11.54^{+0.08}_{-0.05}$	1.97	44.09	45.65	45.00	44.36	45.51

Table B.1 – continued

ID	log $M_{stellar}$ ($M_\odot$)	log SFR^{IR} ($M_\odot$ yr^{-1})	log $L_{2-10\ keV}$ (erg s^{-1})	log L_{bol} (erg s^{-1})	log L_{2500} (erg s^{-1})	log $L_{6\mu m}$ (erg s^{-1})	log L_{IR} (erg s^{-1})
CID-228	$10.75^{+0.15}_{-1.85}$	1.70	44.16	45.74	44.88	44.81	-45.25
CID-231	$11.30^{+0.16}_{-0.65}$	2.14	43.88	45.37	44.87	44.19	45.69
CID-237	$12.07^{+0.14}_{-0.10}$	2.24	44.09	45.65	45.40	45.04	45.78
CID-238	$10.65^{+0.19}_{-0.28}$	0.88	43.04	44.30	44.53	43.95	-44.43
CID-239	$11.20^{+0.14}_{-0.36}$	1.51	44.07	45.62	45.22	44.92	-45.05
CID-247	$10.61^{+0.07}_{-1.22}$	1.73	44.26	45.87	45.02	44.79	-45.27
CID-255	$11.26^{+0.18}_{-0.13}$	1.38	44.09	45.65	45.60	45.14	-44.92
CID-258	$10.45^{+0.10}_{-1.13}$	1.36	-43.96	45.47	44.24	44.26	-44.90
CID-259	$11.24^{+0.05}_{-0.88}$	1.48	44.49	46.18	45.15	44.64	-45.02
CID-260	$11.50^{+0.09}_{-0.19}$	1.32	43.50	44.88	44.64	44.20	44.86
CID-266	$11.42^{+0.17}_{-0.10}$	1.56	-43.36	44.69	44.43	44.03	45.10
CID-273	$12.01^{+0.18}_{-0.09}$	2.08	43.86	45.34	44.87	44.72	45.62
CID-275	$11.35^{+0.19}_{-0.27}$	1.12	43.73	45.18	44.87	44.59	-44.66
CID-277	$10.93^{+0.10}_{-0.95}$	1.49	43.65	45.07	44.42	44.49	-45.03
CID-282	$11.41^{+0.12}_{-0.49}$	1.59	44.15	45.73	45.40	45.00	-45.14
CID-290	$11.12^{+0.08}_{-0.41}$	1.12	43.53	44.92	44.38	44.61	-44.67
CID-291	$11.80^{+0.18}_{-0.09}$	1.57	44.65	46.39	45.68	45.11	-45.12
CID-292	$9.40^{+0.08}_{-1.75}$	1.24	-43.11	44.38	43.46	43.97	-44.79
CID-296	$10.79^{+0.00}_{-1.51}$	0.97	43.76	45.22	44.04	43.94	-44.52
CID-305	$10.46^{+0.19}_{-0.33}$	1.26	44.22	45.82	45.30	45.22	-44.81
CID-307	$11.56^{+0.16}_{-0.41}$	1.61	44.32	45.94	44.83	44.99	-45.15
CID-313	$10.85^{+0.00}_{-0.00}$	0.79	43.21	44.51	43.66	43.81	44.33
CID-320	$11.88^{+0.31}_{-0.03}$	1.07	45.09	46.99	45.24	45.17	-44.62
CID-322	$11.42^{+0.14}_{-0.30}$	1.10	44.22	45.81	45.01	44.83	-44.64
CID-329	$10.68^{+0.11}_{-0.17}$	0.84	44.98	46.83	44.91	45.08	-44.39
CID-330	$11.70^{+0.11}_{-0.02}$	1.37	44.61	46.34	45.79	45.33	-44.91
CID-335	$11.02^{+0.12}_{-0.46}$	1.62	43.76	45.21	43.84	44.10	45.16
CID-338	$10.47^{+0.21}_{-1.00}$	1.65	44.12	45.69	44.58	44.36	-45.19
CID-340	$11.25^{+0.07}_{-0.88}$	1.68	44.10	45.66	45.13	44.65	-45.23
CID-342	$11.07^{+0.00}_{-0.93}$	1.59	44.30	45.93	44.95	44.60	-45.14
CID-343	$11.90^{+0.07}_{-0.38}$	1.67	44.31	45.93	46.00	45.83	-45.21
CID-344	$10.52^{+0.32}_{-0.62}$	1.58	43.22	44.52	43.99	43.26	45.13
CID-346	$12.31^{+0.00}_{-0.00}$	2.27	44.33	45.96	46.01	45.72	45.82
CID-347	$9.58^{+0.16}_{-0.36}$	0.08	43.02	44.27	43.18	43.29	-43.63
CID-348	$10.82^{+0.11}_{-1.36}$	1.68	43.94	45.45	44.42	44.83	-45.23
CID-349	$11.05^{+0.22}_{-1.72}$	1.91	44.26	45.87	45.39	45.38	-45.46
CID-351	$10.22^{+0.42}_{-1.69}$	1.58	44.60	46.32	44.57	45.05	-45.13
CID-352	$11.43^{+0.16}_{-0.11}$	2.26	44.61	46.33	46.07	45.52	45.81
CID-354	$11.80^{+0.08}_{-0.84}$	1.57	44.62	46.35	45.92	45.54	-45.12
CID-356	$10.73^{+0.10}_{-0.87}$	1.08	43.69	45.12	44.07	44.13	-44.62

Table B.1 – continued

ID	log $M_{stellar}$ ($M_\odot$)	log SFR^{IR} ($M_\odot$ yr^{-1})	log $L_{2-10\ keV}$ (erg s^{-1})	log L_{bol} (erg s^{-1})	log L_{2500} (erg s^{-1})	log $L_{6\mu m}$ (erg s^{-1})	log L_{IR} (erg s^{-1})
CID-357	$9.96^{+0.68}_{-0.61}$	1.64	44.10	45.66	44.68	44.90	-45.19
CID-358	$8.05^{+0.00}_{-0.00}$	****	44.06	45.61	44.67	44.33	-43.15
CID-361	$11.34^{+0.37}_{-0.03}$	1.50	44.14	45.71	44.89	44.14	45.05
CID-363	$12.01^{+0.20}_{-0.07}$	2.11	44.28	45.90	45.46	45.70	45.65
CID-365	$11.70^{+0.03}_{-0.75}$	2.30	44.54	46.24	45.61	45.11	45.85
CID-369	$11.21^{+0.05}_{-0.88}$	1.17	43.84	45.32	44.45	44.28	-44.72
CID-376	$10.68^{+0.00}_{-1.17}$	1.39	44.43	46.09	44.24	44.29	-44.94
CID-377	$11.20^{+0.19}_{-0.09}$	1.70	44.31	45.93	44.83	44.90	-45.24
CID-378	$10.28^{+0.06}_{-0.45}$	****	43.11	44.38	44.03	43.84	-42.60
CID-379	$11.42^{+0.10}_{-0.65}$	2.08	-43.22	44.51	44.36	43.89	45.62
CID-380	$10.78^{+0.00}_{-2.17}$	1.32	43.66	45.09	43.78	44.16	-44.87
CID-385	$10.38^{+0.00}_{-1.78}$	1.32	44.01	45.54	43.61	44.20	-44.87
CID-389	$11.05^{+0.26}_{-0.39}$	1.39	43.77	45.22	45.04	44.69	-44.93
CID-391	$11.12^{+0.20}_{-0.32}$	1.68	44.60	46.32	45.38	44.94	-45.23
CID-393	$8.32^{+0.51}_{-0.17}$	0.18	42.28	43.37	42.70	43.00	-43.72
CID-395	$12.53^{+0.00}_{-0.00}$	2.09	44.57	46.28	46.33	46.15	45.63
CID-399	$11.60^{+0.22}_{-0.08}$	1.61	44.33	45.96	45.42	45.15	-45.15
CID-403	$11.87^{+0.13}_{-0.14}$	2.15	43.83	45.30	45.25	44.56	45.70
CID-404	$11.59^{+0.03}_{-0.11}$	1.54	44.99	46.85	45.52	45.44	-45.08
CID-406	$10.53^{+0.00}_{-2.10}$	1.90	43.75	45.20	44.18	44.88	-45.44
CID-410	$11.17^{+0.00}_{-1.37}$	1.85	-43.69	45.12	44.99	44.90	-45.40
CID-413	$8.59^{+1.68}_{-0.04}$	1.71	44.82	46.62	45.58	46.05	-45.26
CID-416	$11.97^{+0.04}_{-0.19}$	2.05	43.75	45.20	44.88	44.61	45.60
CID-417	$10.15^{+0.06}_{-0.09}$	1.03	43.73	45.17	42.52	43.54	44.58
CID-418	$10.58^{+0.00}_{-0.00}$	0.26	42.87	44.09	43.06	43.51	43.81
CID-420	$10.05^{+0.17}_{-0.02}$	****	43.25	44.56	43.26	44.00	-41.66
CID-422	$10.12^{+0.16}_{-0.41}$	1.06	43.81	45.27	44.30	44.24	-44.61
CID-424	$10.98^{+0.07}_{-1.17}$	1.64	44.20	45.79	44.29	44.50	-45.18
CID-425	$8.91^{+0.53}_{-0.02}$	0.70	43.34	44.67	44.04	44.13	-44.24
CID-433	$10.04^{+0.22}_{-2.04}$	1.19	-43.45	44.81	43.70	44.17	-44.73
CID-434	$11.44^{+0.10}_{-1.78}$	1.36	44.58	46.30	44.45	44.92	-44.90
CID-438	$11.37^{+0.00}_{-0.42}$	1.96	44.33	45.96	44.39	44.37	45.50
CID-440	$10.87^{+0.15}_{-0.01}$	1.60	44.10	45.66	44.17	43.94	45.14
CID-441	$10.92^{+0.13}_{-0.19}$	1.09	43.63	45.05	44.64	44.67	-44.63
CID-443	$11.64^{+0.01}_{-0.90}$	1.77	44.24	45.84	45.19	45.01	-45.31
CID-445	$10.51^{+0.19}_{-1.04}$	1.12	44.00	45.53	44.57	44.90	-44.66
CID-446	$10.61^{+0.15}_{-0.25}$	0.63	43.36	44.70	44.31	44.58	-44.18
CID-452	$11.36^{+0.16}_{-0.45}$	1.83	44.20	45.79	44.55	44.27	45.38
CID-454	$11.72^{+0.25}_{-0.02}$	2.08	44.02	45.55	45.09	44.64	45.63
CID-455	$11.21^{+0.10}_{-0.77}$	1.73	43.86	45.34	44.88	44.14	45.27

Table B.1 – continued

ID	log $M_{stellar}$ ($M_\odot$)	log SFR^{IR} ($M_\odot$ yr^{-1})	log $L_{2-10\ keV}$ (erg s^{-1})	log L_{bol} (erg s^{-1})	log L_{2500} (erg s^{-1})	log $L_{6\mu m}$ (erg s^{-1})	log L_{IR} (erg s^{-1})
CID-458	$9.47^{+0.67}_{-0.09}$	1.56	44.56	46.27	43.96	45.03	-45.11
CID-459	$7.96^{+3.36}_{-0.25}$	1.67	44.77	46.55	43.21	45.66	-45.22
CID-463	$10.79^{+0.05}_{-1.26}$	1.28	43.91	45.40	44.15	44.34	-44.82
CID-466	$9.93^{+0.43}_{-1.41}$	1.65	44.04	45.57	44.53	44.56	-45.19
CID-467	$12.09^{+0.00}_{-0.00}$	1.58	44.80	46.59	46.02	45.44	-45.12
CID-468	$10.88^{+0.30}_{-0.03}$	1.16	44.07	45.62	44.28	43.48	44.70
CID-470	$11.07^{+0.11}_{-0.94}$	1.59	43.76	45.22	44.32	44.69	-45.14
CID-473	$11.00^{+0.00}_{-2.40}$	1.38	43.90	45.40	43.62	44.12	-44.92
CID-474	$11.69^{+0.28}_{-0.01}$	1.73	44.47	46.15	45.60	45.04	45.28
CID-475	$11.47^{+0.31}_{-0.04}$	1.63	43.94	45.44	44.60	44.40	45.17
CID-477	$11.36^{+0.20}_{-0.18}$	1.73	43.77	45.23	44.07	43.99	45.27
CID-481	$11.26^{+0.22}_{-0.19}$	1.67	44.12	45.68	45.08	45.00	-45.22
CID-487	$10.85^{+0.14}_{-0.13}$	0.57	43.91	45.40	44.57	44.37	-44.12
CID-488	$11.39^{+0.12}_{-0.24}$	1.10	44.16	45.74	44.65	44.74	-44.65
CID-490	$11.15^{+0.16}_{-0.06}$	1.82	44.01	45.54	45.39	44.84	45.37
CID-492	$11.26^{+0.13}_{-0.14}$	0.93	44.26	45.87	44.96	44.63	-44.48
CID-495	$11.78^{+0.18}_{-0.22}$	1.40	44.02	45.55	46.31	45.79	-44.94
CID-499	$11.84^{+0.14}_{-0.13}$	1.80	44.73	46.49	45.36	45.29	45.35
CID-501	$10.84^{+0.11}_{-0.35}$	0.93	43.77	45.22	44.60	44.33	-44.48
CID-504	$11.16^{+0.02}_{-0.40}$	1.75	43.90	45.40	45.59	45.25	-45.29
CID-508	$10.71^{+0.05}_{-1.38}$	1.39	43.65	45.07	44.40	44.64	-44.93
CID-509	$11.33^{+0.06}_{-0.21}$	1.24	43.56	44.96	44.22	43.96	44.78
CID-510	$11.76^{+0.06}_{-0.08}$	1.73	44.09	45.65	45.08	44.73	45.27
CID-512	$11.94^{+0.24}_{-0.03}$	2.21	44.34	45.98	45.00	44.89	45.76
CID-513	$11.68^{+0.13}_{-0.00}$	2.23	44.63	46.37	44.95	44.88	45.78
CID-515	$9.18^{+0.41}_{-0.47}$	1.15	43.78	45.24	44.30	44.17	-44.69
CID-517	$11.50^{+0.03}_{-0.61}$	1.63	43.72	45.17	45.08	44.78	-45.17
CID-520	$11.29^{+0.22}_{-0.16}$	1.39	43.74	45.19	44.38	43.96	44.93
CID-531	$10.97^{+0.17}_{-0.26}$	2.32	43.87	45.35	44.41	43.62	45.86
CID-532	$9.77^{+0.60}_{-0.70}$	1.50	44.46	46.13	43.97	44.97	-45.05
CID-535	$7.43^{+0.57}_{-0.01}$	1.24	42.77	43.96	42.10	43.82	44.78
CID-536	$10.96^{+0.38}_{-0.03}$	0.90	43.91	45.40	44.77	44.36	-44.44
CID-539	$11.44^{+0.15}_{-0.12}$	1.40	43.04	44.29	44.03	44.10	44.95
CID-543	$10.74^{+0.33}_{-0.53}$	1.20	43.62	45.03	45.11	44.73	-44.75
CID-548	$11.26^{+0.12}_{-0.20}$	1.48	44.16	45.74	44.57	44.25	-45.02
CID-553	$9.90^{+0.05}_{-0.67}$	0.85	43.42	44.77	44.17	44.24	-44.39
CID-556	$11.10^{+0.10}_{-0.91}$	1.45	44.17	45.75	44.23	44.30	-45.00
CID-560	$11.26^{+0.28}_{-0.19}$	1.75	43.87	45.35	43.77	44.33	45.29
CID-566	$10.67^{+0.09}_{-2.06}$	1.36	44.24	45.84	44.46	44.46	-44.91
CID-570	$11.26^{+0.09}_{-0.52}$	1.77	44.09	45.65	44.49	44.16	45.32

Table B.1 – continued

ID	log $M_{stellar}$ ($M_\odot$)	log SFR^{IR} ($M_\odot$ yr^{-1})	log $L_{2-10\ keV}$ (erg s^{-1})	log L_{bol} (erg s^{-1})	log L_{2500} (erg s^{-1})	log $L_{6\mu m}$ (erg s^{-1})	log L_{IR} (erg s^{-1})
CID-571	$7.71^{+2.38}_{-0.01}$	0.66	43.03	44.28	44.27	44.28	-44.21
CID-574	$11.24^{+0.23}_{-0.45}$	1.64	44.40	46.06	45.19	44.73	-45.19
CID-576	$8.99^{+0.00}_{-0.00}$	1.46	43.40	44.75	43.61	44.54	45.01
CID-577	$10.56^{+0.10}_{-1.65}$	1.68	43.87	45.36	44.45	44.53	-45.22
CID-580	$11.07^{+0.10}_{-0.94}$	1.67	44.49	46.18	44.72	44.52	-45.21
CID-581	$11.56^{+0.00}_{-0.68}$	1.50	44.45	46.12	45.26	44.55	-45.04
CID-583	$11.15^{+0.00}_{-2.23}$	1.64	44.09	45.64	44.49	44.90	-45.19
CID-584	$10.09^{+0.35}_{-2.13}$	1.73	43.81	45.28	44.53	44.91	-45.27
CID-587	$10.63^{+0.08}_{-1.42}$	1.64	-43.93	45.43	44.85	44.38	-45.19
CID-589	$11.28^{+0.22}_{-0.14}$	2.11	44.11	45.68	44.07	44.22	45.65
CID-595	$10.59^{+0.08}_{-0.85}$	1.58	-42.89	44.10	44.34	43.95	45.12
CID-596	$11.36^{+0.03}_{-0.86}$	1.56	44.27	45.88	44.48	44.60	-45.11
CID-597	$11.17^{+0.21}_{-0.06}$	1.63	43.64	45.06	44.78	44.74	45.17
CID-599	$11.09^{+0.07}_{-0.54}$	1.10	43.60	45.01	44.37	44.37	-44.64
CID-603	$11.03^{+0.12}_{-0.84}$	1.63	44.13	45.69	44.74	44.59	-45.18
CID-604	$11.54^{+0.22}_{-0.17}$	1.91	44.06	45.60	44.71	44.92	45.46
CID-605	$9.71^{+0.45}_{-1.16}$	1.58	43.71	45.15	43.93	44.89	-45.12
CID-606	$10.79^{+0.01}_{-1.23}$	1.40	43.83	45.31	44.10	44.08	-44.94
CID-607	$11.20^{+0.31}_{-0.07}$	1.13	44.49	46.17	45.19	44.96	-44.68
CID-608	$11.94^{+0.00}_{-0.00}$	2.11	43.98	45.49	45.50	45.30	45.65
CID-609	$11.40^{+0.15}_{-0.39}$	1.31	44.70	46.46	44.61	44.62	-44.86
CID-614	$11.81^{+0.18}_{-0.09}$	2.19	44.01	45.54	43.69	44.09	45.74
CID-617	$11.65^{+0.06}_{-0.73}$	1.86	43.87	45.36	44.35	44.45	45.41
CID-621	$11.64^{+0.11}_{-0.40}$	1.59	43.98	45.49	45.00	44.82	-45.14
CID-624	$10.91^{+0.17}_{-0.67}$	1.36	44.15	45.73	44.35	44.14	-44.91
CID-627	$11.71^{+0.11}_{-0.03}$	1.95	44.24	45.84	44.94	44.63	45.49
CID-628	$10.51^{+0.17}_{-2.75}$	1.78	44.06	45.60	44.42	44.98	-45.32
CID-629	$11.73^{+0.09}_{-0.05}$	1.46	44.08	45.64	45.62	45.19	-45.01
CID-632	$10.89^{+0.10}_{-0.17}$	1.36	43.92	45.42	44.18	44.78	44.90
CID-636	$11.83^{+0.15}_{-0.12}$	1.54	44.04	45.58	45.47	45.21	-45.09
CID-640	$11.22^{+0.20}_{-0.06}$	1.42	43.59	44.99	44.34	44.01	44.97
CID-642	$11.44^{+0.32}_{-0.05}$	2.14	43.89	45.39	44.77	44.24	45.69
CID-643	$11.92^{+0.00}_{-0.00}$	1.53	45.06	46.94	46.03	45.31	-45.08
CID-644	$11.30^{+0.09}_{-0.19}$	0.94	43.88	45.37	44.85	44.69	-44.48
CID-646	$10.53^{+0.02}_{-0.49}$	1.27	-43.52	44.91	44.28	44.14	-44.81
CID-649	$11.37^{+0.19}_{-0.21}$	1.58	43.57	44.97	43.61	44.23	45.12
CID-650	$11.28^{+0.02}_{-0.78}$	1.81	-44.06	45.60	44.06	43.66	45.35
CID-652	$10.73^{+0.16}_{-2.02}$	1.76	43.87	45.35	44.43	44.81	-45.31
CID-656	$11.16^{+0.04}_{-1.04}$	1.73	-44.45	46.12	45.07	44.85	-45.27
CID-659	$9.41^{+0.66}_{-1.01}$	1.63	44.06	45.61	43.51	44.75	-45.17

Table B.1 – continued

ID	log $M_{stellar}$ ($M_\odot$)	log SFR^{IR} ($M_\odot$ yr^{-1})	log $L_{2-10\ keV}$ (erg s^{-1})	log L_{bol} (erg s^{-1})	log L_{2500} (erg s^{-1})	log $L_{6\mu m}$ (erg s^{-1})	log L_{IR} (erg s^{-1})
CID-678	$10.38^{+0.17}_{-0.85}$	1.64	43.74	45.19	45.06	44.76	-45.19
CID-689	$10.98^{+0.15}_{-2.15}$	1.99	44.15	45.73	44.91	45.06	-45.54
CID-696	$10.73^{+0.02}_{-1.32}$	1.48	43.50	44.88	44.25	44.48	-45.02
CID-697	$10.76^{+0.00}_{-2.61}$	1.46	43.51	44.89	43.67	44.61	-45.01
CID-698	$10.58^{+0.05}_{-1.50}$	1.50	43.72	45.16	44.17	44.53	-45.04
CID-705	$10.58^{+0.00}_{-2.16}$	1.93	44.16	45.74	44.99	45.05	-45.47
CID-709	$12.60^{+0.19}_{-0.09}$	1.77	-44.49	46.17	45.51	44.99	-45.31
CID-718	$11.75^{+0.04}_{-0.32}$	2.22	-43.88	45.37	45.38	45.07	45.76
CID-720	$10.64^{+0.15}_{-1.74}$	2.10	-44.21	45.80	42.34	44.13	45.64
CID-729	$10.21^{+0.10}_{-2.13}$	1.38	43.63	45.05	44.10	44.35	-44.93
CID-740	$11.05^{+0.10}_{-1.22}$	1.80	43.95	45.46	45.03	44.83	-45.34
CID-744	$10.87^{+0.00}_{-2.68}$	1.65	43.60	45.01	43.50	44.65	-45.19
CID-746	$11.22^{+0.18}_{-0.06}$	1.36	43.51	44.89	44.12	44.29	44.90
CID-749	$10.89^{+0.13}_{-0.91}$	1.67	43.66	45.08	44.88	44.92	-45.22
CID-762	$10.40^{+0.27}_{-0.50}$	1.51	43.76	45.22	44.36	44.83	-45.06
CID-769	$10.65^{+0.04}_{-1.82}$	1.65	-43.97	45.49	44.40	44.86	-45.20
CID-781	$12.51^{+0.18}_{-0.50}$	1.93	44.35	45.98	45.60	46.19	-45.47
CID-807	$11.18^{+0.18}_{-0.23}$	1.63	43.65	45.07	44.48	43.86	45.17
CID-818	$9.35^{+0.19}_{-1.74}$	1.14	-43.69	45.12	43.41	43.97	-44.69
CID-824	$11.05^{+0.11}_{-0.32}$	1.49	43.65	45.06	44.61	44.46	-45.03
CID-852	$10.12^{+0.35}_{-0.42}$	1.64	-43.96	45.48	44.22	45.13	-45.19
CID-862	$11.41^{+0.17}_{-0.23}$	2.28	44.31	45.94	45.49	45.48	45.82
CID-890	$11.93^{+0.00}_{-0.81}$	2.38	-44.51	46.20	45.44	44.90	45.93
CID-914	$11.14^{+0.05}_{-1.11}$	1.67	44.03	45.56	44.33	44.53	-45.22
CID-917	$11.74^{+0.12}_{-0.80}$	1.88	43.94	45.44	44.75	44.95	-45.42
CID-918	$10.92^{+0.05}_{-1.16}$	1.55	-43.90	45.39	44.16	44.69	-45.10
CID-920	$11.51^{+0.00}_{-0.96}$	1.67	43.71	45.15	45.47	45.34	-45.22
CID-923	$9.62^{+0.26}_{-1.05}$	1.11	44.14	45.71	43.41	45.01	-44.65
CID-925	$11.84^{+0.18}_{-0.04}$	1.88	43.91	45.41	45.47	44.97	45.43
CID-926	$11.61^{+0.21}_{-0.07}$	2.42	-43.92	45.42	44.90	43.96	45.96
CID-933	$10.76^{+0.12}_{-0.68}$	1.71	44.16	45.74	45.37	45.08	-45.26
CID-947	$11.40^{+0.19}_{-0.08}$	2.09	43.95	45.46	45.83	45.51	45.64
CID-953	$11.19^{+0.39}_{-0.59}$	1.88	44.07	45.62	45.06	44.90	-45.43
CID-954	$11.36^{+0.16}_{-0.18}$	1.53	44.21	45.80	45.32	45.12	-45.08
CID-955	$10.82^{+0.09}_{-1.69}$	1.87	-44.71	46.47	45.65	45.42	-45.41
CID-958	$10.56^{+0.00}_{-1.91}$	1.58	43.81	45.28	44.12	44.36	-45.13
CID-987	$9.89^{+0.37}_{-1.96}$	1.58	-44.13	45.69	43.25	44.37	-45.12
CID-994	$9.98^{+0.10}_{-0.81}$	0.24	42.90	44.12	43.31	43.32	-43.78
CID-997	$11.95^{+0.13}_{-0.06}$	2.31	44.18	45.76	45.04	45.10	45.85
CID-1009	$10.82^{+0.00}_{-2.58}$	2.20	43.40	44.75	43.75	43.32	45.74

Table B.1 – continued

ID	log $M_{stellar}$ ($M_\odot$)	log SFR^{IR} ($M_\odot$ yr^{-1})	log $L_{2-10\ keV}$ (erg s^{-1})	log L_{bol} (erg s^{-1})	log L_{2500} (erg s^{-1})	log $L_{6\mu m}$ (erg s^{-1})	log L_{IR} (erg s^{-1})
CID-1027	$11.05^{+0.01}_{-1.62}$	2.16	-44.24	45.84	44.15	43.83	45.70
CID-1028	$10.94^{+0.08}_{-0.94}$	1.36	44.04	45.58	44.44	44.32	-44.90
CID-1030	$11.64^{+0.00}_{-1.12}$	2.30	44.19	45.78	45.23	45.01	45.84
CID-1031	$10.83^{+0.08}_{-0.85}$	1.30	43.63	45.05	44.12	44.34	-44.84
CID-1039	$8.27^{+2.15}_{-0.07}$	1.00	43.69	45.13	44.11	44.34	-44.54
CID-1044	$11.83^{+0.30}_{-0.06}$	1.99	44.56	46.28	45.49	45.01	45.54
CID-1045	$11.16^{+0.00}_{-0.95}$	2.15	43.95	45.46	45.26	45.29	45.69
CID-1048	$7.84^{+2.39}_{-0.37}$	1.68	-44.38	46.02	43.94	45.03	-45.22
CID-1054	$8.27^{+1.49}_{-0.06}$	1.60	43.95	45.46	44.89	44.96	-45.15
CID-1057	$8.25^{+2.05}_{-0.07}$	1.51	44.15	45.72	44.27	45.49	-45.05
CID-1065	$8.36^{+0.77}_{-0.74}$	1.08	-43.80	45.27	44.46	44.95	-44.63
CID-1066	$11.01^{+0.00}_{-1.34}$	1.75	44.08	45.63	44.90	45.04	-45.29
CID-1074	$10.69^{+0.07}_{-1.51}$	1.68	-43.71	45.15	44.42	44.76	-45.22
CID-1079	$12.74^{+0.00}_{-1.21}$	1.55	44.05	45.59	45.51	45.14	-45.10
CID-1085	$11.32^{+0.21}_{-0.03}$	1.67	44.54	46.24	45.33	44.93	-45.22
CID-1099	$10.82^{+0.17}_{-1.64}$	1.70	44.21	45.80	44.10	45.18	-45.24
CID-1104	$10.71^{+0.00}_{-0.89}$	2.65	-43.73	45.18	44.47	44.28	46.19
CID-1108	$9.78^{+0.36}_{-0.47}$	0.95	-43.51	44.90	43.26	43.93	-44.50
CID-1109	$10.23^{+0.00}_{-2.52}$	1.56	-44.06	45.60	43.95	44.47	-45.10
CID-1111	$11.04^{+0.27}_{-0.17}$	1.14	43.54	44.93	44.55	44.57	-44.68
CID-1129	$10.25^{+0.12}_{-1.05}$	1.25	43.96	45.47	44.30	44.47	-44.80
CID-1140	$11.65^{+0.10}_{-2.95}$	2.19	43.87	45.35	43.58	44.82	45.73
CID-1141	$10.38^{+0.00}_{-2.09}$	1.47	43.57	44.97	44.33	44.61	-45.02
CID-1142	$11.17^{+0.00}_{-2.29}$	1.75	-44.39	46.04	44.97	45.06	-45.29
CID-1143	$10.09^{+0.35}_{-2.36}$	1.72	44.03	45.57	43.83	44.89	-45.27
CID-1168	$11.24^{+0.00}_{-1.64}$	1.82	-44.27	45.88	44.36	44.78	-45.36
CID-1170	$11.39^{+0.10}_{-0.84}$	1.55	43.57	44.97	44.62	44.53	-45.10
CID-1174	$11.41^{+0.12}_{-0.49}$	1.33	-44.04	45.58	45.11	45.02	-44.88
CID-1184	$10.44^{+0.00}_{-1.91}$	1.23	43.25	44.56	43.84	44.17	-44.78
CID-1186	$10.43^{+0.20}_{-0.30}$	1.02	43.81	45.28	44.18	44.38	-44.56
CID-1187	$10.39^{+0.03}_{-0.11}$	0.99	42.11	43.16	43.71	43.58	44.54
CID-1194	$11.61^{+0.14}_{-0.37}$	2.25	43.37	44.71	44.71	44.10	45.80
CID-1196	$11.08^{+0.00}_{-3.03}$	2.15	-44.51	46.20	44.31	44.09	45.69
CID-1202	$10.57^{+0.00}_{-2.82}$	1.73	44.00	45.53	43.60	44.78	-45.27
CID-1210	$7.56^{+2.52}_{-0.11}$	1.59	-43.80	45.26	43.55	44.64	-45.14
CID-1215	$11.49^{+0.21}_{-0.24}$	1.68	44.10	45.65	45.18	45.20	-45.23
CID-1216	$10.76^{+0.12}_{-1.89}$	1.73	44.21	45.80	45.32	45.15	-45.27
CID-1219	$10.32^{+0.22}_{-2.48}$	1.85	44.19	45.78	44.58	44.76	-45.40
CID-1222	$10.00^{+0.27}_{-0.76}$	1.53	-43.80	45.26	44.13	44.52	-45.07
CID-1224	$10.24^{+0.53}_{-0.22}$	1.56	43.75	45.20	44.97	45.61	-45.10

Table B.1 – continued

ID	log $M_{stellar}$ ($M_\odot$)	log SFR^{IR} ($M_\odot$ yr^{-1})	log $L_{2-10\ keV}$ (erg s^{-1})	log L_{bol} (erg s^{-1})	log L_{2500} (erg s^{-1})	log $L_{6\mu m}$ (erg s^{-1})	log L_{IR} (erg s^{-1})
CID-1230	$10.71^{+0.08}_{-0.19}$	1.59	42.77	43.96	44.20	44.47	45.14
CID-1250	$10.78^{+0.10}_{-1.48}$	1.70	43.76	45.22	44.43	44.75	-45.24
CID-1252	$10.99^{+0.09}_{-0.81}$	1.19	43.56	44.95	44.00	44.16	-44.73
CID-1258	$11.04^{+0.00}_{-2.11}$	1.65	-43.92	45.42	43.85	44.01	45.19
CID-1265	$9.56^{+0.45}_{-1.46}$	1.64	-43.89	45.38	44.03	44.94	-45.19
CID-1268	$12.81^{+0.00}_{-0.00}$	1.95	-43.78	45.23	46.12	46.58	45.49
CID-1270	$10.57^{+0.00}_{-1.67}$	1.12	43.36	44.69	43.87	43.97	-44.67
CID-1282	$11.35^{+0.07}_{-0.06}$	1.57	43.99	45.51	45.21	44.91	-45.12
CID-1299	$10.02^{+0.29}_{-1.85}$	1.52	43.88	45.38	44.25	45.31	-45.06
CID-1305	$10.59^{+0.14}_{-0.96}$	1.38	-43.19	44.48	43.71	43.15	44.93
CID-1451	$8.97^{+1.07}_{-1.19}$	1.56	-43.74	45.19	44.52	44.53	-45.10
CID-1489	$11.16^{+0.05}_{-0.96}$	1.60	-43.28	44.60	44.78	44.71	-45.14
CID-1506	$9.26^{+0.88}_{-0.37}$	1.51	-43.61	45.02	44.35	45.14	-45.06
CID-1513	$9.97^{+0.00}_{-1.43}$	1.65	-43.65	45.07	44.07	44.47	-45.19
CID-1547	$10.34^{+0.06}_{-1.06}$	0.71	-43.22	44.51	43.65	43.58	-44.26
CID-1570	$11.07^{+0.00}_{-1.15}$	1.76	44.07	45.62	45.75	45.30	-45.31
CID-1593	$11.34^{+0.18}_{-2.30}$	1.23	44.38	46.02	44.85	44.78	-44.78
CID-1594	$11.29^{+0.27}_{-0.12}$	1.48	44.12	45.69	44.56	44.13	45.03
CID-1596	$11.43^{+0.13}_{-0.27}$	1.13	43.67	45.09	44.32	44.42	-44.67
CID-1605	$11.51^{+0.00}_{-0.00}$	2.19	44.63	46.36	45.40	44.67	45.74
CID-1609	$10.72^{+0.05}_{-0.26}$	1.51	43.48	44.85	44.63	44.61	45.06
CID-1611	$9.80^{+0.15}_{-0.53}$	0.10	42.63	43.78	41.24	43.11	-43.65
CID-1616	$10.01^{+0.38}_{-0.19}$	1.54	-43.40	44.75	44.46	44.88	-45.08
CID-1620	$11.05^{+0.11}_{-0.40}$	1.63	44.38	46.03	45.30	45.08	-45.17
CID-1624	$10.45^{+0.08}_{-0.64}$	1.26	44.28	45.90	44.19	44.66	-44.81
CID-1634	$10.96^{+0.06}_{-0.08}$	1.04	43.12	44.40	43.98	44.13	44.58
CID-1637	$11.23^{+0.11}_{-0.37}$	1.13	43.60	45.00	44.48	44.66	-44.68
CID-1638	$10.65^{+0.04}_{-1.55}$	1.19	44.02	45.56	43.82	44.07	-44.74
CID-1643	$11.35^{+0.20}_{-0.21}$	1.80	43.27	44.58	44.60	43.96	45.35
CID-1649	$11.10^{+0.00}_{-2.18}$	1.57	43.68	45.10	44.13	44.63	-45.12
CID-1654	$10.44^{+0.17}_{-2.19}$	1.99	44.06	45.60	44.35	45.13	-45.54
CID-1661	$11.67^{+0.26}_{-0.28}$	1.78	43.85	45.34	45.17	44.65	45.33
CID-1666	$12.01^{+0.21}_{-0.08}$	2.11	44.57	46.28	45.91	45.55	45.65
CID-1667	$11.25^{+0.12}_{-0.28}$	0.65	43.48	44.85	44.23	44.24	-44.20
CID-1684	$10.18^{+0.00}_{-2.20}$	1.20	43.85	45.33	44.05	44.24	-44.74
CID-1702	$11.43^{+0.16}_{-0.12}$	1.46	44.48	46.17	44.82	44.75	-45.01
CID-1705	$10.86^{+0.00}_{-2.15}$	1.54	-43.73	45.17	44.62	44.92	-45.08
CID-1740	$11.15^{+0.11}_{-1.34}$	1.71	43.69	45.12	44.75	45.04	-45.25
CID-1913	$10.82^{+0.26}_{-1.18}$	2.26	-44.17	45.75	44.72	44.09	45.80
CID-1930	$12.06^{+0.16}_{-0.03}$	2.50	44.34	45.97	45.18	45.38	46.04

Table B.1 – continued

ID	log $M_{stellar}$ ($M_\odot$)	log SFR^{IR} ($M_\odot$ yr^{-1})	log $L_{2-10\ keV}$ (erg s^{-1})	log L_{bol} (erg s^{-1})	log L_{2500} (erg s^{-1})	log $L_{6\mu m}$ (erg s^{-1})	log L_{IR} (erg s^{-1})
CID-2252	$11.43^{+0.05}_{-0.89}$	1.58	43.43	44.79	44.95	44.95	-45.13
CID-2258	$10.19^{+0.01}_{-2.03}$	1.22	43.01	44.26	43.48	43.85	-44.77
CID-2315	$11.83^{+0.18}_{-0.05}$	2.03	-43.69	45.12	44.48	44.81	45.58
CID-2470	$11.38^{+0.02}_{-2.53}$	2.27	-43.81	45.27	44.50	44.47	45.81
CID-2564	$10.93^{+0.11}_{-1.75}$	1.62	43.82	45.29	44.45	44.69	-45.17
CID-3016	$9.26^{+0.57}_{-1.61}$	1.31	-43.37	44.71	43.38	44.04	-44.86
CID-3021	$9.86^{+0.20}_{-2.11}$	1.54	-44.04	45.58	44.10	44.26	-45.08
CID-3121	$9.25^{+0.87}_{-1.28}$	1.57	-43.64	45.06	43.94	44.53	-45.12
CID-3242	$11.32^{+0.11}_{-0.54}$	1.34	-43.79	45.25	45.23	44.97	-44.88
CID-3361	$9.86^{+0.32}_{-1.54}$	1.69	-43.63	45.05	44.47	44.46	-45.23
CID-3385	$10.51^{+0.00}_{-2.46}$	1.56	-43.95	45.46	43.82	44.39	-45.11
CID-3395	$11.90^{+0.00}_{-0.00}$	1.65	44.43	46.10	45.82	45.18	-45.19
CID-3441	$9.65^{+0.16}_{-0.01}$	0.13	-41.01	41.90	43.35	43.65	-43.67
CID-3501	$10.48^{+0.00}_{-1.44}$	1.23	-43.49	44.86	43.77	44.31	-44.78
CID-3555	$9.02^{+0.34}_{-0.69}$	1.23	-43.43	44.79	44.41	44.72	-44.78
CID-3556	$11.19^{+0.13}_{-0.61}$	1.47	43.66	45.09	44.84	44.78	-45.01
CID-3570	$10.95^{+0.00}_{-1.20}$	1.89	-43.38	44.73	43.67	44.26	45.44
CID-3576	$12.34^{+0.05}_{-0.22}$	1.74	44.39	46.04	46.28	45.78	-45.29
CID-3627	$10.89^{+0.00}_{-1.37}$	1.43	-43.38	44.73	43.65	44.26	-44.98
CID-3641	$10.50^{+0.08}_{-0.80}$	2.17	43.39	44.73	44.15	44.41	45.72
CID-3714	$11.63^{+0.13}_{-0.35}$	2.26	43.38	44.73	44.56	44.26	45.81
CID-3803	$10.95^{+0.17}_{-0.50}$	1.65	43.85	45.32	44.62	44.39	-45.20
CID-11754	$10.93^{+0.21}_{-0.26}$	1.69	-43.74	45.19	43.82	43.33	45.24
LID-69	$10.76^{+0.00}_{-1.40}$	1.18	43.50	44.88	43.79	43.95	-44.73
LID-135	$9.55^{+0.00}_{-0.00}$	0.87	44.35	45.99	45.52	45.14	-44.42
LID-137	$11.02^{+0.19}_{-0.08}$	2.16	43.47	44.84	44.58	44.67	45.71
LID-138	$11.31^{+0.24}_{-0.23}$	1.09	44.27	45.88	44.92	44.59	-44.63
LID-143	$10.81^{+0.00}_{-1.41}$	1.14	43.56	44.95	43.99	43.90	-44.69
LID-145	$10.42^{+0.01}_{-1.01}$	0.96	43.49	44.86	43.88	43.68	-44.51
LID-154	$11.23^{+0.14}_{-0.26}$	1.86	43.56	44.96	44.94	45.14	45.41
LID-171	$10.60^{+0.12}_{-1.36}$	1.75	43.15	44.43	44.33	44.05	45.29
LID-190	$11.31^{+0.11}_{-0.03}$	1.53	43.79	45.25	44.58	43.69	45.07
LID-205	$10.90^{+0.21}_{-2.13}$	1.93	44.78	46.57	44.95	45.13	-45.48
LID-213	$10.77^{+0.01}_{-0.26}$	1.25	43.23	44.53	44.05	43.85	44.80
LID-223	$10.26^{+0.04}_{-1.43}$	1.16	-43.24	44.54	44.53	44.15	-44.70
LID-231	$11.77^{+0.05}_{-0.09}$	1.52	44.41	46.07	45.14	45.06	-45.06
LID-233	$10.12^{+0.27}_{-0.63}$	1.74	44.03	45.57	44.81	45.62	-45.29
LID-249	$11.54^{+0.00}_{-0.00}$	2.55	44.46	46.13	45.81	45.83	46.09
LID-250	$9.70^{+0.49}_{-1.00}$	1.53	44.06	45.60	44.09	44.59	-45.08
LID-254	$11.48^{+0.00}_{-0.95}$	1.58	44.33	45.97	44.95	45.01	-45.13

Table B.1 – continued

ID	log $M_{stellar}$ ($M_\odot$)	log SFR^{IR} ($M_\odot$ yr^{-1})	log $L_{2-10\ keV}$ (erg s^{-1})	log L_{bol} (erg s^{-1})	log L_{2500} (erg s^{-1})	log $L_{6\mu m}$ (erg s^{-1})	log L_{IR} (erg s^{-1})
LID-257	$10.88^{+0.02}_{-0.86}$	1.03	43.88	45.37	44.08	44.09	-44.58
LID-263	$11.49^{+0.14}_{-0.44}$	1.97	44.42	46.08	44.49	44.62	45.52
LID-264	$11.26^{+0.04}_{-0.72}$	1.94	43.73	45.18	44.95	44.26	45.49
LID-266	$10.98^{+0.04}_{-0.09}$	1.20	43.51	44.89	43.99	43.98	44.75
LID-277	$10.91^{+0.23}_{-0.34}$	1.12	43.29	44.62	44.22	44.56	-44.66
LID-280	$11.72^{+0.10}_{-0.04}$	1.67	44.00	45.53	45.02	44.35	45.21
LID-283	$9.49^{+0.94}_{-1.73}$	1.81	44.56	46.27	45.06	45.75	-45.35
LID-284	$11.73^{+0.09}_{-0.05}$	1.93	44.37	46.01	45.61	45.10	45.48
LID-286	$10.69^{+0.00}_{-1.39}$	1.19	43.26	44.57	44.28	44.32	-44.73
LID-291	$11.17^{+0.39}_{-0.02}$	0.81	44.04	45.58	44.65	44.58	-44.35
LID-293	$11.96^{+0.15}_{-0.37}$	1.70	44.93	46.77	45.17	45.51	-45.24
LID-294	$10.88^{+0.14}_{-0.00}$	0.66	44.13	45.70	44.15	44.38	44.20
LID-296	$11.12^{+0.12}_{-0.80}$	1.43	43.67	45.10	44.59	44.62	-44.98
LID-304	$11.18^{+0.17}_{-1.08}$	1.67	44.29	45.91	44.73	44.52	-45.22
LID-307	$11.08^{+0.00}_{-0.90}$	1.03	43.51	44.88	44.71	44.41	-44.57
LID-323	$10.95^{+0.06}_{-1.09}$	1.73	43.94	45.44	45.11	44.59	-45.28
LID-324	$10.68^{+0.03}_{-2.39}$	1.41	43.69	45.12	43.67	44.24	-44.96
LID-326	$10.88^{+0.00}_{-2.32}$	1.60	43.85	45.33	44.00	44.68	-45.15
LID-332	$10.98^{+0.17}_{-0.78}$	1.44	44.18	45.77	44.45	44.36	-44.99
LID-333	$11.22^{+0.08}_{-0.71}$	1.59	44.27	45.88	45.44	45.23	-45.14
LID-337	$11.06^{+0.00}_{-2.56}$	1.80	43.92	45.43	44.05	44.31	45.35
LID-338	$11.26^{+0.00}_{-2.66}$	1.18	44.23	45.83	43.92	44.53	-44.72
LID-345	$11.07^{+0.17}_{-0.28}$	1.65	44.15	45.73	45.61	45.29	-45.20
LID-351	$10.46^{+0.04}_{-2.23}$	1.44	43.61	45.02	44.52	44.28	-44.98
LID-352	$11.03^{+0.04}_{-0.96}$	1.91	43.47	44.84	44.38	43.95	45.46
LID-358	$11.30^{+0.05}_{-0.42}$	1.26	44.28	45.89	44.17	44.40	44.80
LID-360	$12.02^{+0.17}_{-0.10}$	2.02	-43.65	45.08	45.53	45.16	45.56
LID-367	$10.49^{+0.31}_{-0.75}$	0.64	43.24	44.54	44.04	43.80	-44.19
LID-368	$11.76^{+0.11}_{-0.76}$	1.70	44.31	45.93	45.05	45.54	-45.25
LID-370	$11.62^{+0.14}_{-0.26}$	1.06	44.40	46.06	44.79	44.39	-44.60
LID-379	$10.10^{+0.05}_{-1.32}$	1.42	44.12	45.68	44.81	44.66	-44.97
LID-381	$11.46^{+0.13}_{-0.14}$	1.38	43.86	45.34	45.06	44.75	44.93
LID-393	$11.14^{+0.05}_{-1.07}$	1.41	43.61	45.01	44.59	44.48	-44.95
LID-395	$10.96^{+0.11}_{-0.66}$	1.43	44.32	45.94	45.04	44.70	-44.98
LID-399	$9.57^{+0.20}_{-0.07}$	2.03	43.95	45.46	45.66	45.21	-45.57
LID-401	$11.60^{+0.15}_{-0.31}$	1.95	43.82	45.29	44.40	44.35	45.49
LID-405	$11.90^{+0.10}_{-0.15}$	1.77	44.77	46.55	45.34	45.20	45.32
LID-410	$12.67^{+0.10}_{-0.26}$	1.74	44.31	45.93	46.01	45.10	-45.28
LID-411	$10.89^{+0.11}_{-0.97}$	1.37	43.90	45.40	44.40	44.33	-44.92
LID-417	$11.61^{+0.11}_{-0.46}$	1.96	44.26	45.87	45.09	44.57	45.51

Table B.1 – continued

ID	log $M_{stellar}$ ($M_\odot$)	log SFR^{IR} ($M_\odot$ yr^{-1})	log $L_{2-10\ keV}$ (erg s^{-1})	log L_{bol} (erg s^{-1})	log L_{2500} (erg s^{-1})	log $L_{6\mu m}$ (erg s^{-1})	log L_{IR} (erg s^{-1})
LID-421	$11.13^{+0.20}_{-0.96}$	2.36	43.73	45.18	45.01	43.99	45.91
LID-426	$11.81^{+0.13}_{-0.41}$	1.75	43.96	45.47	45.24	44.61	45.29
LID-429	$11.15^{+0.16}_{-0.29}$	1.10	43.52	44.91	44.31	44.15	44.64
LID-437	$11.21^{+0.09}_{-0.70}$	1.24	44.05	45.59	44.47	44.09	-44.78
LID-441	$11.50^{+0.07}_{-0.32}$	1.10	44.01	45.54	44.58	44.63	-44.65
LID-444	$11.55^{+0.21}_{-0.18}$	2.27	43.94	45.45	44.63	44.26	45.82
LID-449	$12.32^{+0.15}_{-0.03}$	1.44	43.88	45.36	45.39	44.36	-44.99
LID-451	$11.98^{+0.20}_{-0.07}$	2.38	44.52	46.21	45.80	45.56	45.93
LID-460	$11.45^{+0.20}_{-2.47}$	1.81	44.86	46.67	45.58	45.48	-45.35
LID-462	$11.04^{+0.11}_{-0.39}$	1.25	44.26	45.87	44.28	44.27	-44.80
LID-464	$10.46^{+0.18}_{-0.30}$	0.81	43.72	45.15	44.30	44.17	-44.36
LID-476	$12.20^{+0.16}_{-0.26}$	2.41	44.73	46.50	46.05	45.65	45.95
LID-477	$8.12^{+0.10}_{-0.03}$	1.82	44.08	45.62	44.63	44.69	45.36
LID-478	$11.41^{+0.14}_{-0.36}$	1.66	43.64	45.06	44.83	43.83	45.21
LID-481	$9.22^{+0.23}_{-0.24}$	0.37	42.81	44.00	43.23	43.46	43.91
LID-484	$10.33^{+0.07}_{-0.20}$	1.33	42.99	44.23	43.33	43.94	44.87
LID-485	$9.99^{+0.46}_{-1.90}$	1.63	43.92	45.42	44.50	44.71	-45.17
LID-487	$11.71^{+0.00}_{-0.98}$	1.95	-43.44	44.80	44.69	44.42	45.50
LID-491	$11.20^{+0.12}_{-0.49}$	2.59	44.61	46.34	46.02	45.55	46.13
LID-496	$12.18^{+0.00}_{-0.00}$	2.39	44.34	45.97	45.92	45.61	45.94
LID-499	$10.97^{+0.34}_{-0.44}$	1.79	44.59	46.31	45.53	45.58	-45.34
LID-500	$11.45^{+0.22}_{-0.93}$	1.75	44.51	46.21	45.01	45.15	-45.29
LID-504	$8.95^{+0.45}_{-0.01}$	1.62	44.91	46.74	45.72	45.23	-45.16
LID-512	$11.40^{+0.13}_{-1.06}$	1.82	44.18	45.77	44.83	45.06	-45.36
LID-516	$11.15^{+0.08}_{-0.95}$	1.21	44.16	45.73	45.21	45.13	-44.75
LID-519	$11.33^{+0.24}_{-0.03}$	1.99	43.93	45.43	45.84	45.12	45.54
LID-523	$11.29^{+0.08}_{-0.36}$	2.01	43.46	44.82	44.46	44.07	45.55
LID-538	$11.84^{+0.12}_{-0.32}$	2.20	43.85	45.33	45.52	44.67	45.75
LID-545	$11.96^{+0.06}_{-0.08}$	2.06	44.30	45.92	45.54	45.25	45.60
LID-546	$11.05^{+0.00}_{-0.00}$	1.09	44.39	46.04	45.23	45.38	-44.64
LID-549	$11.35^{+0.07}_{-0.07}$	1.06	45.08	46.97	45.91	45.55	-44.60
LID-586	$9.90^{+0.07}_{-0.40}$	****	42.96	44.19	43.08	43.22	-41.60
LID-589	$10.30^{+0.03}_{-2.49}$	1.80	43.85	45.33	44.82	45.53	-45.34
LID-590	$10.45^{+0.18}_{-0.56}$	1.96	44.41	46.07	45.12	45.16	-45.51
LID-592	$11.45^{+0.00}_{-0.00}$	1.77	44.40	46.06	45.48	45.93	45.31
LID-595	$10.87^{+0.12}_{-0.15}$	1.99	42.93	44.16	44.39	44.15	45.53
LID-596	$11.31^{+0.07}_{-0.23}$	1.57	43.30	44.62	44.38	44.01	45.12
LID-603	$11.30^{+0.34}_{-0.21}$	2.16	-43.85	45.34	44.78	44.59	45.70
LID-612	$12.19^{+0.00}_{-0.00}$	2.25	44.41	46.07	45.56	46.16	45.80
LID-618	$9.87^{+0.11}_{-1.91}$	0.98	43.52	44.90	43.32	44.06	-44.53

Table B.1 – continued

ID	log $M_{stellar}$ ($M_\odot$)	log SFR^{IR} ($M_\odot$ yr^{-1})	log $L_{2-10\ keV}$ (erg s^{-1})	log L_{bol} (erg s^{-1})	log L_{2500} (erg s^{-1})	log $L_{6\mu m}$ (erg s^{-1})	log L_{IR} (erg s^{-1})
LID-620	$11.76^{+0.00}_{-0.94}$	2.62	44.99	46.85	44.74	44.59	46.16
LID-623	$10.82^{+0.00}_{-2.75}$	1.80	-43.91	45.40	44.20	44.80	-45.35
LID-635	$10.40^{+0.03}_{-2.55}$	1.63	43.56	44.96	44.12	44.47	-45.18
LID-657	$10.79^{+0.08}_{-1.06}$	1.83	44.33	45.97	45.43	45.52	-45.37
LID-659	$11.54^{+0.00}_{-0.74}$	1.54	43.97	45.49	45.20	44.82	-45.09
LID-660	$11.53^{+0.17}_{-0.27}$	2.00	44.27	45.88	44.88	44.46	45.55
LID-663	$10.37^{+0.06}_{-2.79}$	0.85	43.42	44.77	44.21	44.30	-44.40
LID-678	$11.59^{+0.24}_{-0.07}$	1.69	44.44	46.10	44.63	44.59	45.23
LID-680	$11.13^{+0.09}_{-0.05}$	1.30	43.72	45.16	44.09	43.92	44.85
LID-681	$11.13^{+0.19}_{-0.29}$	0.97	43.79	45.25	44.69	44.56	-44.52
LID-685	$11.95^{+0.07}_{-0.07}$	1.44	44.51	46.20	46.00	45.82	-44.99
LID-686	$9.56^{+0.47}_{-0.92}$	1.17	43.97	45.49	44.06	44.61	-44.71
LID-703	$11.01^{+0.00}_{-1.41}$	2.07	44.32	45.95	44.71	44.20	45.61
LID-705	$11.61^{+0.20}_{-0.07}$	1.17	44.81	46.61	45.40	45.38	-44.72
LID-708	$11.42^{+0.19}_{-0.06}$	2.33	-44.33	45.97	45.49	46.05	45.87
LID-710	$9.79^{+0.22}_{-0.33}$	0.02	43.11	44.38	43.28	43.42	-43.57
LID-711	$12.17^{+0.00}_{-0.00}$	2.05	44.35	45.98	45.95	45.91	45.59
LID-720	$11.26^{+0.04}_{-0.84}$	1.32	44.52	46.22	44.16	44.57	-44.86
LID-721	$11.10^{+0.21}_{-1.76}$	1.85	44.72	46.49	45.71	45.29	-45.39
LID-727	$11.51^{+0.22}_{-0.56}$	1.72	44.69	46.44	45.64	45.02	-45.27
LID-738	$11.61^{+0.16}_{-0.19}$	2.21	43.71	45.14	44.86	44.03	45.76
LID-747	$11.28^{+0.06}_{-0.51}$	1.13	44.55	46.25	44.87	44.64	-44.67
LID-748	$8.06^{+2.12}_{-0.43}$	1.87	44.43	46.10	44.77	45.49	-45.41
LID-749	$11.64^{+0.00}_{-0.00}$	2.26	44.53	46.24	46.12	46.92	45.81
LID-760	$10.41^{+0.00}_{-1.78}$	1.32	44.08	45.64	44.25	44.71	-44.86
LID-762	$10.73^{+0.20}_{-3.16}$	1.37	43.40	44.74	44.11	44.06	44.91
LID-763	$11.28^{+0.26}_{-1.06}$	1.76	44.18	45.77	45.00	44.88	-45.31
LID-784	$9.95^{+0.39}_{-1.37}$	1.60	44.00	45.53	44.24	44.38	-45.15
LID-786	$11.48^{+0.08}_{-1.20}$	1.80	44.50	46.19	45.03	44.79	-45.34
LID-961	$11.39^{+0.00}_{-0.00}$	2.27	45.10	46.99	45.34	45.05	45.82
LID-970	$11.19^{+0.13}_{-0.56}$	1.68	44.38	46.02	45.03	45.14	-45.22
LID-973	$10.87^{+0.16}_{-0.38}$	1.53	43.63	45.04	44.43	44.34	-45.08
LID-975	$11.34^{+0.14}_{-0.72}$	1.85	44.09	45.64	45.49	45.21	45.40
LID-977	$10.43^{+0.06}_{-0.73}$	1.65	44.25	45.86	45.21	45.00	-45.20
LID-1002	$11.64^{+0.01}_{-1.08}$	2.70	44.57	46.28	44.47	44.69	46.25
LID-1027	$10.33^{+0.13}_{-0.43}$	****	43.38	44.72	43.72	43.40	-42.38
LID-1151	$10.83^{+0.05}_{-0.81}$	0.90	43.63	45.04	44.50	43.95	-44.45
LID-1154	$11.44^{+0.18}_{-0.25}$	1.66	44.41	46.07	45.07	44.75	-45.21
LID-1157	$11.44^{+0.12}_{-0.45}$	1.47	43.97	45.48	44.83	44.84	-45.01
LID-1158	$11.37^{+0.07}_{-0.33}$	1.61	44.36	46.00	45.76	45.13	-45.15

Table B.1 – continued

ID	log $M_{stellar}$ ($M_\odot$)	log SFR^{IR} ($M_\odot$ yr^{-1})	log $L_{2-10\ keV}$ (erg s^{-1})	log L_{bol} (erg s^{-1})	log L_{2500} (erg s^{-1})	log $L_{6\mu m}$ (erg s^{-1})	log L_{IR} (erg s^{-1})
LID-1164	$12.85^{+0.00}_{-0.00}$	2.41	44.85	46.66	46.39	47.21	45.95
LID-1175	$12.19^{+0.00}_{-0.00}$	2.01	44.40	46.06	45.94	45.85	45.55
LID-1179	$11.36^{+0.08}_{-0.86}$	1.95	43.41	44.76	44.46	43.98	45.50
LID-1183	$10.86^{+0.27}_{-0.30}$	1.24	44.29	45.92	45.25	44.77	-44.78
LID-1186	$9.33^{+1.09}_{-1.63}$	1.73	44.27	45.88	43.86	44.79	-45.27
LID-1191	$10.91^{+0.00}_{-0.81}$	2.13	44.41	46.07	44.51	44.00	45.68
LID-1193	$10.83^{+0.28}_{-0.31}$	1.31	42.83	44.04	43.27	43.43	44.86
LID-1207	$9.54^{+0.55}_{-0.91}$	1.36	43.97	45.49	44.47	44.09	-44.91
LID-1212	$11.70^{+0.05}_{-0.48}$	1.43	44.40	46.05	45.17	44.89	-44.98
LID-1213	$11.06^{+0.00}_{-0.93}$	1.37	44.12	45.69	44.59	44.44	-44.91
LID-1224	$7.34^{+0.34}_{-0.01}$	****	43.35	44.69	44.14	44.14	-42.38
LID-1226	$11.23^{+0.10}_{-0.45}$	1.15	44.21	45.80	44.10	44.36	-44.69
LID-1228	$10.53^{+0.16}_{-2.16}$	1.40	43.47	44.83	44.31	44.95	-44.95
LID-1236	$11.19^{+0.12}_{-0.49}$	1.18	43.09	44.36	44.57	44.53	-44.73
LID-1248	$10.59^{+0.14}_{-0.84}$	1.16	43.90	45.40	44.91	45.17	-44.71
LID-1249	$8.77^{+0.88}_{-0.97}$	0.82	43.37	44.71	43.29	43.81	-44.37
LID-1252	$11.14^{+0.40}_{-0.00}$	1.36	44.13	45.70	44.75	44.10	44.90
LID-1267	$11.23^{+0.29}_{-0.15}$	1.92	43.17	44.46	44.42	44.34	45.46
LID-1273	$11.85^{+0.16}_{-0.00}$	1.90	43.88	45.37	45.42	45.23	45.44
LID-1281	$9.90^{+0.36}_{-1.82}$	1.51	44.38	46.02	43.99	44.42	-45.05
LID-1305	$11.17^{+0.18}_{-0.26}$	1.19	43.89	45.38	44.43	44.52	-44.73
LID-1452	$11.74^{+0.20}_{-0.27}$	1.70	43.89	45.38	45.33	44.62	45.24
LID-1476	$11.37^{+0.05}_{-0.09}$	1.73	43.86	45.34	44.67	43.77	45.27
LID-1477	$10.57^{+0.00}_{-2.15}$	1.53	44.34	45.98	44.35	45.27	-45.08
LID-1494	$11.09^{+0.26}_{-0.13}$	1.70	43.70	45.14	45.10	44.54	-45.24
LID-1502	$11.27^{+0.22}_{-0.37}$	1.36	44.26	45.87	44.80	44.90	-44.91
LID-1517	$11.45^{+0.22}_{-0.39}$	1.67	44.62	46.35	44.91	45.12	-45.21
LID-1519	$9.45^{+1.07}_{-0.71}$	1.88	-44.41	46.07	44.99	45.41	-45.42
LID-1520	$10.11^{+0.45}_{-0.88}$	1.41	-42.97	44.20	43.65	44.08	44.95
LID-1521	$11.02^{+0.00}_{-1.34}$	1.60	-43.65	45.07	44.25	44.38	-45.15
LID-1538	$11.88^{+0.12}_{-0.15}$	1.91	44.38	46.03	45.31	44.79	45.45
LID-1550	$12.01^{+0.12}_{-0.98}$	1.34	44.26	45.86	45.11	44.37	-44.89
LID-1560	$11.06^{+0.25}_{-0.23}$	1.23	43.88	45.37	44.48	43.80	44.78
LID-1563	$11.06^{+0.00}_{-0.90}$	1.20	44.15	45.72	44.29	44.37	-44.74
LID-1566	$11.19^{+0.01}_{-0.25}$	0.93	43.08	44.34	43.73	43.47	44.47
LID-1584	$11.35^{+0.00}_{-0.72}$	1.20	44.58	46.29	44.77	44.47	-44.74
LID-1587	$10.28^{+0.41}_{-1.86}$	1.68	-43.60	45.01	44.20	44.71	-45.22
LID-1589	$11.04^{+0.09}_{-3.05}$	0.87	44.08	45.64	44.69	44.40	-44.41
LID-1590	$11.23^{+0.25}_{-0.55}$	1.91	44.35	45.99	44.92	44.53	45.46
LID-1592	$11.42^{+0.20}_{-0.06}$	1.32	43.03	44.29	45.29	44.81	44.87

Table B.1 – continued

ID	log $M_{stellar}$ ($M_\odot$)	log SFR^{IR} ($M_\odot$ yr^{-1})	log $L_{2-10\ keV}$ (erg s^{-1})	log L_{bol} (erg s^{-1})	log L_{2500} (erg s^{-1})	log $L_{6\mu m}$ (erg s^{-1})	log L_{IR} (erg s^{-1})
LID-1596	$11.51^{+0.11}_{-0.03}$	2.04	44.56	46.27	45.35	45.20	45.59
LID-1614	$11.40^{+0.10}_{-0.66}$	1.40	43.84	45.32	44.83	44.84	-44.95
LID-1618	$10.57^{+0.00}_{-2.29}$	1.53	43.63	45.05	44.24	44.88	-45.07
LID-1622	$11.85^{+0.17}_{-0.04}$	1.89	43.94	45.44	45.48	45.04	45.43
LID-1627	$10.40^{+0.10}_{-0.79}$	1.15	43.87	45.35	44.95	44.71	-44.69
LID-1631	$10.63^{+0.16}_{-1.70}$	1.68	44.08	45.62	44.64	44.51	-45.22
LID-1638	$11.88^{+0.01}_{-0.73}$	2.70	44.50	46.19	46.05	45.90	46.24
LID-1639	$12.38^{+0.20}_{-0.07}$	2.58	44.48	46.16	45.24	45.15	46.12
LID-1652	$11.20^{+0.14}_{-0.35}$	1.07	44.06	45.61	44.68	44.65	-44.61
LID-1658	$8.85^{+0.17}_{-0.03}$	****	41.85	42.86	42.13	41.64	-42.65
LID-1666	$11.31^{+0.44}_{-0.03}$	1.37	44.02	45.55	44.66	44.18	44.92
LID-1676	$11.79^{+0.16}_{-0.31}$	1.93	44.20	45.79	45.27	44.59	45.47
LID-1682	$11.52^{+0.18}_{-0.43}$	1.18	44.19	45.77	45.02	44.88	-44.73
LID-1697	$10.97^{+0.00}_{-3.14}$	1.86	43.77	45.22	43.77	43.93	45.40
LID-1710	$12.28^{+0.14}_{-0.84}$	1.83	44.72	46.49	45.63	45.80	-45.37
LID-1713	$10.87^{+0.07}_{-0.70}$	1.22	43.91	45.41	44.73	44.32	-44.77
LID-1714	$10.67^{+0.03}_{-0.85}$	1.03	43.92	45.42	44.41	43.92	-44.58
LID-1722	$11.20^{+0.03}_{-0.91}$	1.35	43.72	45.15	44.42	44.11	-44.89
LID-1723	$11.02^{+0.00}_{-1.20}$	1.42	43.81	45.28	44.65	44.31	-44.96
LID-1724	$10.38^{+0.00}_{-2.07}$	1.27	43.81	45.28	44.69	44.50	-44.81
LID-1729	$11.07^{+0.28}_{-0.51}$	1.34	44.48	46.17	45.07	44.46	-44.88
LID-1730	$10.85^{+0.11}_{-0.85}$	1.41	44.13	45.70	44.74	44.77	-44.96
LID-1733	$6.88^{+3.25}_{-0.75}$	1.64	-43.26	44.57	43.55	44.43	-45.18
LID-1797	$9.45^{+0.28}_{-0.69}$	1.11	43.42	44.77	44.31	44.06	-44.66
LID-1809	$10.43^{+0.28}_{-1.27}$	1.33	43.54	44.93	43.42	43.56	44.87
LID-1820	$11.35^{+0.21}_{-0.17}$	1.28	44.32	45.95	44.99	45.08	-44.83
LID-1822	$11.37^{+0.13}_{-0.63}$	1.50	43.96	45.47	44.83	44.81	-45.04
LID-1825	$10.91^{+0.07}_{-0.95}$	1.17	43.60	45.01	44.11	44.20	-44.72
LID-1828	$11.48^{+0.30}_{-0.03}$	1.87	44.02	45.56	44.28	44.41	45.41
LID-1832	$10.86^{+0.11}_{-1.88}$	1.73	44.46	46.14	44.61	44.72	-45.27
LID-1842	$10.95^{+0.11}_{-1.54}$	1.67	44.20	45.79	44.58	44.57	-45.22
LID-1847	$10.89^{+0.24}_{-0.38}$	1.18	44.33	45.96	44.41	43.85	-44.73
LID-1851	$12.36^{+0.14}_{-0.27}$	2.48	44.38	46.03	45.65	45.46	46.02
LID-1852	$10.16^{+0.36}_{-0.91}$	1.72	-44.24	45.85	44.80	44.87	-45.26
LID-1855	$11.35^{+0.20}_{-0.86}$	1.71	44.31	45.93	44.92	45.10	-45.26
LID-1868	$11.49^{+0.00}_{-0.00}$	1.27	43.70	45.13	44.36	44.23	44.82
LID-1870	$10.43^{+0.01}_{-1.04}$	0.71	43.74	45.18	43.54	43.86	-44.25
LID-1874	$11.14^{+0.02}_{-0.45}$	0.98	44.07	45.62	44.42	44.29	-44.53
LID-1878	$11.09^{+0.00}_{-0.00}$	1.70	44.12	45.69	45.59	45.84	45.25
LID-1886	$10.93^{+0.25}_{-0.65}$	1.79	44.14	45.71	45.27	45.81	-45.34

Table B.1 – continued

ID	log $M_{stellar}$ ($M_\odot$)	log SFR^{IR} ($M_\odot$ yr^{-1})	log $L_{2-10\ keV}$ (erg s^{-1})	log L_{bol} (erg s^{-1})	log L_{2500} (erg s^{-1})	log $L_{6\mu m}$ (erg s^{-1})	log L_{IR} (erg s^{-1})
LID-1965	$10.17^{+0.22}_{-0.96}$	1.22	-43.43	44.78	44.32	44.35	-44.77
LID-1995	$10.85^{+0.12}_{-0.93}$	1.52	-43.85	45.33	44.32	44.57	-45.06
LID-2033	$11.37^{+0.13}_{-0.58}$	1.84	-43.83	45.31	44.93	43.92	45.39
LID-2081	$11.22^{+0.11}_{-0.52}$	1.71	-43.63	45.05	44.32	43.52	45.25
LID-2141	$9.98^{+0.18}_{-0.73}$	1.08	-43.11	44.38	43.63	44.07	-44.62
LID-2164	$11.14^{+0.03}_{-1.03}$	2.22	-43.78	45.24	44.72	44.42	45.77
LID-2219	$7.97^{+0.96}_{-0.06}$	1.40	-43.56	44.96	44.33	44.59	-44.94
LID-2243	$11.14^{+0.00}_{-2.35}$	2.00	-43.96	45.47	44.33	43.79	45.55
LID-2266	$10.39^{+0.00}_{-2.55}$	1.54	-43.85	45.33	43.93	44.45	-45.09
LID-2269	$10.79^{+0.19}_{-0.88}$	1.59	-43.12	44.40	43.93	43.16	45.14
LID-2280	$10.65^{+0.14}_{-0.84}$	1.21	-43.22	44.53	44.33	44.24	-44.76
LID-2301	$11.50^{+0.04}_{-0.63}$	2.41	-43.54	44.93	44.95	44.94	45.96
LID-2346	$11.19^{+0.15}_{-0.76}$	2.20	-42.87	44.08	43.74	44.01	45.74
LID-2409	$9.33^{+0.70}_{-1.12}$	1.47	-44.02	45.56	44.47	44.38	-45.02
LID-2413	$11.49^{+0.09}_{-0.21}$	1.55	-44.36	46.00	44.95	44.52	-45.09
LID-2440	$11.06^{+0.23}_{-0.60}$	1.97	-43.29	44.61	43.89	43.72	45.51
LID-2448	$11.26^{+0.07}_{-0.57}$	2.74	-43.33	44.66	44.71	44.17	46.29
LID-2575	$10.23^{+0.66}_{-0.13}$	1.87	-43.69	45.12	44.78	44.55	45.41
LID-2599	$10.81^{+0.15}_{-0.98}$	1.35	-43.50	44.88	44.02	44.31	-44.89
LID-2620	$10.39^{+0.17}_{-1.30}$	1.47	-43.82	45.28	44.33	44.32	-45.02
LID-2727	$10.37^{+0.18}_{-1.77}$	1.73	-43.94	45.44	44.46	44.63	-45.27
LID-2806	$9.76^{+0.46}_{-1.84}$	1.68	-43.77	45.22	44.50	44.51	-45.22
LID-2812	$10.99^{+0.23}_{-0.64}$	1.62	-43.32	44.65	44.97	45.02	-45.16
LID-2826	$9.04^{+0.37}_{-0.39}$	0.68	-42.51	43.64	43.78	43.73	-44.23
LID-2833	$11.23^{+0.00}_{-2.65}$	1.93	-44.09	45.64	44.65	44.97	-45.47
LID-2848	$10.76^{+0.00}_{-2.53}$	1.77	-43.97	45.48	44.76	44.69	-45.31
LID-2861	$10.77^{+0.00}_{-0.57}$	1.30	-43.04	44.30	43.72	43.37	44.84
LID-2866	$10.39^{+0.17}_{-1.94}$	1.77	-44.25	45.86	45.36	45.06	-45.32
LID-3044	$10.95^{+0.17}_{-0.56}$	1.57	-43.33	44.66	43.36	43.94	45.11
LID-3062	$10.03^{+0.07}_{-0.74}$	0.62	-42.52	43.65	43.50	43.68	-44.17
LID-3072	$11.42^{+0.13}_{-0.38}$	2.23	43.31	44.63	44.53	44.36	45.77
LID-3124	$9.00^{+0.33}_{-0.06}$	0.38	-41.91	42.93	43.66	43.28	-43.92
LID-3192	$9.01^{+0.32}_{-0.40}$	1.06	-43.51	44.90	44.38	43.97	-44.60
LID-3226	$9.37^{+1.09}_{-1.61}$	1.82	43.83	45.31	44.52	44.84	-45.36
LID-3297	$9.82^{+0.38}_{-1.71}$	1.72	-43.61	45.02	44.44	44.71	-45.27
LID-3310	$11.40^{+0.19}_{-0.09}$	0.94	-43.63	45.04	44.78	44.60	-44.49
LID-3350	$10.36^{+0.07}_{-1.00}$	1.37	43.66	45.08	43.76	44.19	44.92
LID-3351	$11.15^{+0.01}_{-1.35}$	1.78	44.21	45.80	44.73	44.86	-45.32
LID-3456	$11.92^{+0.04}_{-0.39}$	2.05	-43.62	45.03	44.82	44.81	45.59
LID-3758	$9.72^{+0.63}_{-1.78}$	1.69	-43.52	44.91	44.21	44.74	-45.23

Table B.1 – continued

ID	log $M_{stellar}$ ($M_\odot$)	log SFR^{IR} ($M_\odot$ yr^{-1})	log $L_{2-10\ keV}$ (erg s^{-1})	log L_{bol} (erg s^{-1})	log L_{2500} (erg s^{-1})	log $L_{6\mu m}$ (erg s^{-1})	log L_{IR} (erg s^{-1})
LID-4509	$11.25^{+0.00}_{-2.38}$	1.68	-44.00	45.53	44.57	45.13	-45.23
LID-4527	$10.34^{+0.10}_{-0.92}$	0.66	-43.06	44.32	44.03	43.82	-44.20
LID-4841	$10.81^{+0.13}_{-2.65}$	1.87	-43.65	45.07	43.52	43.68	45.42
LID-4940	$10.29^{+0.29}_{-0.02}$	1.72	-42.62	43.78	44.20	43.59	45.27
LID-4941	$11.57^{+0.00}_{-1.77}$	2.55	-44.04	45.58	44.73	44.51	46.10
LID-5585	$10.00^{+0.42}_{-2.30}$	2.08	-44.11	45.67	45.40	45.28	-45.62

NOTE: Parameters derived from the SED fitting. The columns are (1) *Chandra* source ID from Civano et al. (2016); (2) host galaxy stellar mass; (3) host galaxy SFR; (4) absorption-corrected X-ray luminosity in 2–10 keV band; (5) AGN bolometric luminosity; (6) rest-frame UV luminosity at 2500Åof the AGN BBB component; (7) rest-frame 6μm luminosity of the AGN component; and (8) IR luminosity, $L_{8-1000\mu m}$, of the starburst component. Negative values represent the maximum IR luminosity of the *Herschel*-undetected sources.

Table B.2: Type 2 AGN Host galaxy properties derived from the SED fitting

ID	log $M_{stellar}$ ($M_\odot$)	log SFR^{tot} ($M_\odot$ yr^{-1})	log $L_{2-10\ keV}$ (erg s^{-1})	log L_{2300} (erg s^{-1})	log L_{5100} (erg s^{-1})	log $L_{6\mu m}$ (erg s^{-1})	log L_{IR} (erg s^{-1})
CID-1	$10.59^{+0.38}_{-0.36}$	$1.72^{+0.00}_{-1.02}$	44.31	44.05	44.17	0.00	-45.19
CID-3	$9.98^{+0.04}_{-0.09}$	$0.48^{+0.05}_{-0.29}$	42.95	43.50	43.75	42.64	-43.99
CID-6	$10.24^{+0.31}_{-0.23}$	$0.52^{+0.11}_{-0.80}$	43.43	42.94	43.75	0.00	-44.12
CID-12	$10.44^{+0.17}_{-0.04}$	$1.29^{+0.04}_{-0.43}$	43.08	44.14	44.04	44.06	-44.48
CID-22	$10.37^{+0.05}_{-0.09}$	$1.08^{+0.06}_{-0.30}$	43.76	44.04	44.12	43.80	-44.46
CID-23	$11.28^{+0.14}_{-0.00}$	$2.42^{+0.02}_{-0.05}$	44.23	44.96	45.39	45.92	45.97
CID-24	$10.79^{+0.03}_{-0.11}$	$1.45^{+0.09}_{-0.00}$	42.98	44.40	44.39	44.16	44.65
CID-25	$11.36^{+0.19}_{-0.26}$	$2.14^{+0.08}_{-0.05}$	43.64	45.08	44.65	44.88	45.28
CID-27	$10.86^{+0.23}_{-0.24}$	$1.35^{+0.08}_{-0.13}$	43.42	44.42	44.24	44.10	-44.87
CID-33	$10.53^{+0.19}_{-0.34}$	$1.91^{+0.01}_{-0.64}$	43.99	44.78	44.58	0.00	-45.30
CID-37	$10.50^{+0.12}_{-0.02}$	$0.53^{+0.14}_{-0.55}$	43.24	43.23	44.05	43.36	-44.43
CID-38	$10.66^{+0.15}_{-0.09}$	$1.41^{+0.02}_{-0.08}$	43.42	44.66	43.93	44.21	-44.41
CID-39	$11.17^{+0.17}_{-0.30}$	$2.34^{+0.19}_{-0.00}$	44.16	45.41	44.58	44.73	45.75
CID-41	$10.30^{+0.42}_{-0.28}$	$1.93^{+0.09}_{-0.20}$	43.79	45.07	44.08	44.26	-45.03
CID-44	$10.51^{+0.11}_{-0.14}$	$1.32^{+0.11}_{-0.66}$	43.49	43.98	44.12	44.04	-44.90
CID-46	$11.41^{+0.17}_{-0.19}$	$2.67^{+0.15}_{-0.00}$	44.20	45.94	45.25	45.62	45.31
CID-51	$10.45^{+0.00}_{-0.00}$	$1.13^{+0.10}_{-0.27}$	42.96	44.14	44.40	44.07	-44.31
CID-52	$10.33^{+0.20}_{-0.24}$	$1.58^{+0.06}_{-0.02}$	43.59	44.83	43.77	0.00	-44.06
CID-53	$11.07^{+0.23}_{-0.28}$	$1.78^{+0.01}_{-0.36}$	44.20	44.68	44.42	0.00	-45.12
CID-55	$10.18^{+0.15}_{-0.21}$	$2.03^{+0.10}_{-0.23}$	44.28	45.20	44.29	44.80	-45.00
CID-56	$11.05^{+0.16}_{-0.03}$	$2.04^{+0.09}_{-0.02}$	43.28	45.35	44.98	43.96	-44.62
CID-63	$11.08^{+0.28}_{-0.15}$	$2.28^{+0.16}_{-0.00}$	44.17	45.53	44.87	45.01	-45.14
CID-67	$10.87^{+0.00}_{-0.00}$	$1.55^{+0.08}_{-0.23}$	43.97	44.64	44.54	44.38	-44.69
CID-76	$10.93^{+0.00}_{-0.00}$	$1.43^{+0.10}_{-0.09}$	43.12	44.61	44.51	43.25	-44.52
CID-77	$10.77^{+0.05}_{-0.09}$	$2.15^{+0.08}_{-0.00}$	43.96	45.28	44.33	44.94	45.22
CID-78	$10.73^{+0.17}_{-0.19}$	$1.73^{+0.11}_{-0.08}$	43.71	44.92	43.85	43.96	-44.48
CID-80	$10.78^{+0.03}_{-0.10}$	$0.67^{+0.07}_{-0.38}$	43.01	43.50	44.14	43.03	-44.18
CID-81	$10.90^{+0.33}_{-0.34}$	$2.71^{+0.02}_{-0.11}$	44.05	45.90	44.06	44.94	-45.13
CID-85	$10.76^{+0.16}_{-0.29}$	$1.42^{+0.11}_{-0.08}$	43.88	44.66	43.93	0.00	-44.20
CID-86	$11.46^{+0.13}_{-0.14}$	$1.73^{+0.10}_{-0.34}$	44.31	44.72	44.83	44.97	-45.00
CID-89	$10.82^{+0.28}_{-0.25}$	$2.11^{+0.14}_{-0.01}$	44.44	45.36	44.48	44.94	-45.25
CID-91	$10.43^{+0.19}_{-0.05}$	$0.06^{+0.00}_{-0.21}$	43.04	43.20	44.02	0.00	-43.11
CID-92	$11.04^{+0.18}_{-0.14}$	$2.87^{+0.17}_{-0.00}$	43.38	46.12	44.65	46.01	46.20
CID-95	$10.52^{+0.11}_{-0.04}$	$2.56^{+0.07}_{-0.02}$	44.11	45.80	44.67	45.36	45.29
CID-96	$10.40^{+0.17}_{-0.14}$	$0.77^{+0.14}_{-0.07}$	43.34	43.98	43.80	0.00	-43.67
CID-99	$10.14^{+0.30}_{-0.25}$	$1.24^{+0.10}_{-0.13}$	43.38	44.38	43.49	43.74	-44.55
CID-101	$10.74^{+0.20}_{-0.28}$	$1.20^{+0.04}_{-0.19}$	43.73	44.35	43.99	0.00	-44.22

Table B.2 – continued

ID	log $M_{stellar}$ ($M_\odot$)	log SFR^{tot} ($M_\odot$ yr^{-1})	log $L_{2-10\ keV}$ (erg s^{-1})	log L_{2300} (erg s^{-1})	log L_{5100} (erg s^{-1})	log $L_{6\mu m}$ (erg s^{-1})	log L_{IR} (erg s^{-1})
CID-105	$10.94^{+0.08}_{-0.06}$	$0.93^{+0.10}_{-0.56}$	43.55	43.67	44.31	43.73	-44.22
CID-106	$10.26^{+0.16}_{-0.03}$	$0.93^{+0.10}_{-0.25}$	43.42	43.97	43.87	43.08	-44.22
CID-107	$10.47^{+0.32}_{-0.15}$	$1.45^{+0.07}_{-0.35}$	44.05	44.53	43.38	45.04	-44.70
CID-114	$10.59^{+0.15}_{-0.09}$	$2.17^{+0.07}_{-0.02}$	44.33	45.38	44.16	45.37	45.13
CID-116	$10.35^{+0.06}_{-0.07}$	$0.30^{+0.04}_{-0.54}$	43.31	43.05	43.87	42.35	-43.97
CID-117	$10.53^{+0.21}_{-0.19}$	$1.57^{+0.06}_{-0.15}$	43.68	44.77	44.15	43.54	-44.56
CID-118	$10.90^{+0.00}_{-0.00}$	$0.84^{+0.09}_{-0.43}$	43.63	43.70	44.43	43.75	-44.48
CID-123	$10.00^{+0.00}_{-0.00}$	$0.40^{+0.04}_{-0.89}$	42.54	42.77	43.76	42.81	-44.12
CID-127	$10.94^{+0.19}_{-0.18}$	$1.82^{+0.05}_{-0.22}$	44.54	44.57	44.65	0.00	-45.26
CID-129	$10.67^{+0.00}_{-0.00}$	$0.67^{+0.16}_{-0.00}$	42.66	43.31	44.12	0.00	-44.26
CID-131	$10.77^{+0.21}_{-0.10}$	$1.26^{+0.17}_{-0.00}$	43.55	44.44	44.52	43.73	-44.62
CID-132	$10.69^{+0.25}_{-0.27}$	$1.67^{+0.06}_{-0.28}$	43.71	44.70	44.15	44.62	-44.90
CID-135	$10.61^{+0.14}_{-0.25}$	$1.03^{+0.10}_{-0.11}$	43.69	44.23	43.87	43.70	-44.57
CID-141	$10.00^{+0.18}_{-0.10}$	$1.07^{+0.07}_{-0.12}$	43.04	44.24	43.70	43.00	-44.25
CID-143	$10.31^{+0.11}_{-0.03}$	$0.14^{+0.09}_{-0.35}$	42.67	43.06	43.79	42.79	-44.14
CID-145	$10.07^{+0.25}_{-0.25}$	$1.31^{+0.18}_{-0.23}$	43.44	44.46	43.79	0.00	-44.29
CID-146	$10.39^{+0.02}_{-0.11}$	$0.98^{+0.15}_{-0.17}$	43.33	44.15	44.23	0.00	-44.14
CID-151	$10.77^{+0.18}_{-0.08}$	$2.04^{+0.01}_{-0.16}$	43.30	45.22	44.44	44.17	-45.00
CID-152	$10.52^{+0.22}_{-0.19}$	$1.89^{+0.14}_{-0.09}$	43.74	45.14	44.01	44.27	-44.68
CID-156	$10.18^{+0.35}_{-0.23}$	$1.57^{+0.28}_{-0.48}$	44.33	44.52	44.41	44.83	-45.26
CID-158	$11.31^{+0.25}_{-0.14}$	$1.79^{+0.14}_{-0.02}$	44.00	44.63	44.57	45.38	45.34
CID-159	$10.40^{+0.45}_{-0.26}$	$2.15^{+0.17}_{-0.08}$	43.99	45.42	43.93	44.55	-45.08
CID-163	$11.02^{+0.00}_{-0.00}$	$1.64^{+0.12}_{-0.00}$	43.33	44.73	44.54	44.00	44.99
CID-164	$10.39^{+0.03}_{-0.11}$	$0.94^{+0.09}_{-0.11}$	43.60	44.09	43.73	43.87	-42.68
CID-167	$10.82^{+0.21}_{-0.29}$	$1.10^{+0.08}_{-1.13}$	43.47	43.23	43.79	0.00	-44.62
CID-169	$10.35^{+0.38}_{-0.59}$	$1.26^{+0.08}_{-0.09}$	43.08	44.46	43.62	0.00	-44.12
CID-170	$10.39^{+0.39}_{-0.43}$	$2.20^{+0.14}_{-0.24}$	44.04	44.35	43.88	0.00	-45.82
CID-172	$10.59^{+0.15}_{-0.10}$	$1.09^{+0.15}_{-0.27}$	43.62	44.15	44.23	0.00	-44.46
CID-173	$10.90^{+0.12}_{-0.02}$	$1.65^{+0.09}_{-0.00}$	44.06	44.68	44.41	45.33	44.90
CID-182	$10.55^{+0.25}_{-0.52}$	$1.96^{+0.16}_{-0.01}$	44.10	44.82	44.04	44.55	45.54
CID-187	$11.12^{+0.22}_{-0.18}$	$2.39^{+0.17}_{-0.00}$	44.72	45.60	44.89	44.85	45.51
CID-188	$10.69^{+0.12}_{-0.11}$	$1.53^{+0.00}_{-0.07}$	42.96	44.31	44.21	42.64	44.72
CID-190	$10.85^{+0.12}_{-0.15}$	$1.98^{+0.05}_{-0.04}$	43.99	45.17	44.30	44.46	45.08
CID-194	$10.96^{+0.06}_{-0.08}$	$2.21^{+0.12}_{-0.00}$	44.15	45.47	44.78	44.68	45.10
CID-195	$11.23^{+0.16}_{-0.11}$	$1.77^{+0.07}_{-0.24}$	44.28	44.84	44.48	44.65	-44.98
CID-196	$11.11^{+0.00}_{-0.00}$	$0.69^{+0.14}_{-0.12}$	43.12	43.85	44.58	43.72	-44.33
CID-197	$10.54^{+0.23}_{-0.19}$	$1.51^{+0.02}_{-0.18}$	44.07	44.60	44.23	44.28	-44.82
CID-198	$10.87^{+0.11}_{-0.16}$	$1.29^{+0.04}_{-0.22}$	43.41	44.47	44.20	0.00	-44.21
CID-200	$10.42^{+0.16}_{-0.20}$	$1.36^{+0.08}_{-0.04}$	42.96	44.60	44.15	0.00	-44.25
CID-204	$10.85^{+0.15}_{-0.12}$	$1.23^{+0.10}_{-0.07}$	43.37	44.43	44.15	43.47	-44.43

Table B.2 – continued

ID	log $M_{stellar}$ ($M_\odot$)	log SFR^{tot} ($M_\odot$ yr^{-1})	log $L_{2-10\ keV}$ (erg s^{-1})	log L_{2300} (erg s^{-1})	log L_{5100} (erg s^{-1})	log $L_{6\mu m}$ (erg s^{-1})	log L_{IR} (erg s^{-1})
CID-205	$10.90^{+0.23}_{-0.23}$	$2.02^{+0.00}_{-0.16}$	44.05	45.14	44.22	0.00	-45.12
CID-207	$10.53^{+0.08}_{-0.15}$	$0.85^{+0.09}_{-0.03}$	43.10	44.13	43.86	44.16	44.74
CID-213	$10.72^{+0.09}_{-0.04}$	$0.76^{+0.07}_{-0.52}$	42.93	43.49	44.13	42.92	-44.11
CID-214	$11.18^{+0.16}_{-0.22}$	$1.83^{+0.01}_{-0.31}$	43.95	44.85	44.43	44.59	-44.94
CID-215	$10.79^{+0.15}_{-0.25}$	$1.77^{+0.06}_{-0.00}$	44.00	45.02	44.22	43.15	45.16
CID-219	$10.45^{+0.14}_{-0.13}$	$-0.03^{+0.07}_{-0.07}$	42.60	43.20	43.93	43.24	-43.92
CID-221	$10.78^{+0.00}_{-0.00}$	$1.35^{+0.09}_{-0.00}$	43.24	44.41	44.49	43.81	44.85
CID-223	$10.86^{+0.32}_{-0.20}$	$2.01^{+0.03}_{-0.04}$	43.44	45.22	43.95	43.65	45.53
CID-224	$10.68^{+0.24}_{-0.43}$	$1.14^{+0.44}_{-1.88}$	44.08	42.52	43.97	0.00	-44.73
CID-226	$10.85^{+0.18}_{-0.25}$	$1.56^{+0.07}_{-0.00}$	43.88	44.49	44.13	44.07	45.07
CID-227	$10.75^{+0.20}_{-0.26}$	$1.89^{+0.07}_{-0.32}$	44.26	44.88	44.33	44.26	-45.09
CID-230	$9.97^{+0.32}_{-0.35}$	$0.98^{+0.54}_{-0.50}$	43.54	43.78	43.88	0.00	-44.49
CID-233	$10.89^{+0.13}_{-0.01}$	$1.48^{+0.06}_{-0.06}$	42.92	44.54	44.36	44.20	44.73
CID-234	$10.43^{+0.14}_{-0.13}$	$1.62^{+0.11}_{-0.10}$	42.84	44.80	44.02	43.44	-44.67
CID-236	$10.13^{+0.42}_{-0.19}$	$2.02^{+0.12}_{-0.13}$	43.39	45.24	43.92	44.37	-44.78
CID-241	$10.59^{+0.03}_{-0.11}$	$0.83^{+0.10}_{-0.00}$	42.60	43.28	44.09	43.83	44.50
CID-242	$10.51^{+0.10}_{-0.06}$	$1.10^{+0.13}_{-0.25}$	42.61	44.15	44.05	43.29	-44.38
CID-243	$10.40^{+0.17}_{-0.10}$	$0.73^{+0.10}_{-0.03}$	43.37	44.04	43.85	43.82	44.64
CID-245	$10.77^{+0.28}_{-0.26}$	$1.54^{+0.06}_{-0.29}$	43.63	44.48	44.03	0.00	-45.01
CID-248	$10.74^{+0.00}_{-0.00}$	$1.43^{+0.11}_{-0.01}$	43.73	44.42	44.41	43.56	44.70
CID-250	$10.88^{+0.11}_{-0.16}$	$2.25^{+0.09}_{-0.05}$	44.23	45.49	44.23	44.49	-44.76
CID-251	$10.92^{+0.00}_{-0.00}$	$1.47^{+0.06}_{-0.10}$	43.08	44.60	44.42	43.91	-44.58
CID-254	$10.45^{+0.14}_{-0.13}$	$1.46^{+0.00}_{-0.10}$	42.92	44.61	44.13	43.81	44.90
CID-256	$9.95^{+0.18}_{-0.22}$	$1.12^{+0.12}_{-0.25}$	43.62	44.17	43.81	44.43	-44.54
CID-257	$11.08^{+0.22}_{-0.15}$	$2.11^{+0.13}_{-0.00}$	44.25	45.38	44.43	45.18	-44.92
CID-261	$10.48^{+0.23}_{-0.14}$	$1.90^{+0.03}_{-0.03}$	43.87	44.92	44.15	44.38	45.22
CID-262	$10.72^{+0.00}_{-0.00}$	$1.71^{+0.02}_{-0.05}$	42.81	44.41	44.22	43.89	45.27
CID-264	$10.23^{+0.14}_{-0.12}$	$0.43^{+0.04}_{-0.79}$	42.76	42.91	43.64	0.00	-44.01
CID-265	$10.55^{+0.07}_{-0.06}$	$1.85^{+0.09}_{-0.02}$	43.44	45.06	44.28	44.05	-44.64
CID-267	$10.50^{+0.09}_{-0.18}$	$1.61^{+0.03}_{-0.18}$	43.32	44.79	44.22	43.73	-44.19
CID-269	$11.35^{+0.05}_{-0.23}$	$2.41^{+0.28}_{-0.00}$	43.35	45.58	44.69	44.99	46.06
CID-271	$10.41^{+0.29}_{-0.17}$	$1.39^{+0.00}_{-0.69}$	43.58	44.11	43.93	0.00	-44.75
CID-272	$11.22^{+0.12}_{-0.28}$	$1.73^{+0.20}_{-0.22}$	43.79	44.78	44.60	44.94	-45.22
CID-274	$10.95^{+0.00}_{-0.00}$	$1.53^{+0.10}_{-0.19}$	44.02	44.65	44.55	44.01	-44.47
CID-276	$10.23^{+0.19}_{-0.05}$	$0.28^{+0.16}_{-0.03}$	42.88	42.88	43.69	0.00	-43.86
CID-278	$9.94^{+0.24}_{-0.19}$	$0.19^{+0.17}_{-0.90}$	43.23	42.60	43.51	0.00	-43.81
CID-279	$10.92^{+0.23}_{-0.17}$	$1.81^{+0.19}_{-0.05}$	43.62	45.07	44.43	0.00	-44.50
CID-281	$10.85^{+0.00}_{-0.00}$	$0.88^{+0.05}_{-0.02}$	44.11	43.60	44.24	44.20	44.22
CID-283	$10.69^{+0.22}_{-0.16}$	$1.52^{+0.12}_{-0.14}$	43.25	44.69	44.23	43.49	-44.63
CID-284	$10.98^{+0.00}_{-0.00}$	$1.31^{+0.13}_{-0.00}$	43.74	43.72	44.79	44.53	44.87

Table B.2 – continued

ID	log $M_{stellar}$ ($M_\odot$)	log SFR^{tot} ($M_\odot$ yr^{-1})	log $L_{2-10\ keV}$ (erg s^{-1})	log L_{2300} (erg s^{-1})	log L_{5100} (erg s^{-1})	log $L_{6\mu m}$ (erg s^{-1})	log L_{IR} (erg s^{-1})
CID-289	$10.70^{+0.00}_{-0.00}$	$1.25^{+0.09}_{-0.00}$	43.04	44.39	44.30	43.63	44.51
CID-294	$10.92^{+0.09}_{-0.07}$	$2.34^{+0.14}_{-0.00}$	43.84	45.47	44.24	45.77	45.31
CID-295	$10.37^{+0.08}_{-0.08}$	$0.98^{+0.06}_{-0.28}$	42.92	44.02	43.84	43.02	-44.12
CID-297	$10.76^{+0.06}_{-0.08}$	$0.62^{+0.11}_{-0.41}$	43.02	43.47	44.20	42.76	-44.16
CID-298	$10.66^{+0.00}_{-0.00}$	$1.46^{+0.08}_{-0.00}$	43.34	44.36	44.35	44.70	44.55
CID-299	$10.59^{+0.24}_{-0.07}$	$0.93^{+0.09}_{-0.86}$	43.34	43.26	44.16	0.00	-44.50
CID-300	$10.94^{+0.21}_{-0.28}$	$1.78^{+0.12}_{-0.78}$	43.95	44.33	44.48	44.39	-45.09
CID-302	$10.70^{+0.09}_{-0.18}$	$1.20^{+0.14}_{-0.22}$	43.28	44.23	44.04	43.91	-44.42
CID-303	$10.41^{+0.16}_{-0.10}$	$1.41^{+0.02}_{-0.23}$	43.76	44.46	44.35	43.96	-44.53
CID-304	$10.84^{+0.18}_{-0.04}$	$1.94^{+0.08}_{-0.06}$	43.56	45.16	44.44	0.00	-44.66
CID-306	$10.73^{+0.18}_{-0.20}$	$2.56^{+0.00}_{-0.09}$	43.73	45.54	44.72	44.50	45.69
CID-309	$11.01^{+0.20}_{-0.40}$	$2.09^{+0.12}_{-0.04}$	44.07	45.27	44.81	0.00	-44.72
CID-311	$10.52^{+0.17}_{-0.20}$	$1.66^{+0.08}_{-0.15}$	43.93	44.76	44.13	44.52	-44.75
CID-312	$10.36^{+0.14}_{-0.23}$	$0.83^{+0.00}_{-0.33}$	43.59	43.84	43.83	0.00	-44.07
CID-314	$11.03^{+0.13}_{-0.17}$	$2.13^{+0.29}_{-0.00}$	44.09	45.37	44.59	44.19	45.70
CID-315	$11.14^{+0.23}_{-0.16}$	$1.81^{+0.08}_{-0.66}$	44.61	44.57	44.63	0.00	-45.30
CID-316	$10.00^{+0.28}_{-0.28}$	$1.12^{+0.11}_{-0.09}$	43.93	44.31	44.03	0.00	-44.33
CID-318	$10.94^{+0.23}_{-0.15}$	$1.63^{+0.10}_{-0.48}$	44.26	44.40	44.47	44.73	-45.24
CID-319	$10.80^{+0.15}_{-0.11}$	$0.94^{+0.47}_{-0.65}$	43.02	43.55	44.19	0.00	-44.47
CID-323	$10.37^{+0.05}_{-0.08}$	$0.88^{+0.05}_{-0.10}$	43.64	44.15	44.14	44.10	-44.52
CID-327	$10.80^{+0.00}_{-0.00}$	$1.47^{+0.07}_{-0.00}$	42.59	44.49	44.31	43.38	44.81
CID-328	$10.62^{+0.15}_{-0.15}$	$1.72^{+0.09}_{-0.08}$	43.89	44.94	43.99	43.85	-44.71
CID-331	$10.57^{+0.06}_{-0.09}$	$1.53^{+0.11}_{-0.03}$	43.10	44.79	44.16	43.92	-44.53
CID-332	$10.97^{+0.13}_{-0.08}$	$2.24^{+0.09}_{-0.06}$	43.39	45.49	44.70	44.32	-44.52
CID-333	$10.90^{+0.10}_{-0.15}$	$1.87^{+0.07}_{-0.06}$	43.83	45.15	44.44	43.86	-44.74
CID-334	$10.71^{+0.23}_{-0.17}$	$1.82^{+0.11}_{-0.00}$	43.65	45.05	44.09	43.92	44.92
CID-336	$10.20^{+0.33}_{-0.22}$	$1.63^{+0.01}_{-0.85}$	43.56	44.14	44.02	0.00	-45.18
CID-337	$11.22^{+0.15}_{-0.15}$	$2.18^{+0.16}_{-0.00}$	44.07	45.43	44.54	44.93	-45.21
CID-341	$10.75^{+0.00}_{-0.00}$	$1.29^{+0.04}_{-0.02}$	43.35	44.45	44.35	43.43	44.92
CID-345	$10.06^{+0.12}_{-0.15}$	$0.65^{+0.16}_{-0.25}$	43.26	43.62	43.60	43.05	-44.14
CID-353	$10.58^{+0.31}_{-0.36}$	$2.19^{+0.04}_{-0.04}$	44.03	45.34	43.96	44.83	-45.06
CID-359	$10.82^{+0.13}_{-0.27}$	$1.72^{+0.07}_{-0.88}$	44.41	44.12	44.53	44.79	-45.27
CID-360	$11.68^{+0.08}_{-0.18}$	$2.82^{+0.17}_{-0.00}$	44.29	45.86	45.03	45.11	46.12
CID-362	$11.17^{+0.19}_{-0.21}$	$2.90^{+0.04}_{-0.06}$	43.86	46.00	44.83	44.61	46.20
CID-368	$10.30^{+0.00}_{-0.00}$	$0.65^{+0.00}_{-0.90}$	42.98	43.05	44.04	43.56	-43.92
CID-370	$11.14^{+0.14}_{-0.31}$	$1.11^{+0.32}_{-0.66}$	44.27	43.78	44.33	0.00	-44.67
CID-372	$10.21^{+0.16}_{-0.10}$	$0.88^{+0.05}_{-0.26}$	43.21	43.88	43.87	0.00	-44.25
CID-373	$11.03^{+0.19}_{-0.05}$	$1.53^{+0.10}_{-0.00}$	44.11	44.81	44.36	44.57	44.88
CID-374	$10.68^{+0.20}_{-0.26}$	$1.83^{+0.12}_{-0.04}$	43.08	45.06	44.14	43.55	-44.75
CID-375	$10.18^{+0.39}_{-0.47}$	$1.92^{+0.01}_{-0.06}$	44.22	45.06	43.58	44.58	45.37

Table B.2 – continued

ID	log $M_{stellar}$ ($M_\odot$)	log SFR^{tot} ($M_\odot$ yr^{-1})	log $L_{2-10\ keV}$ (erg s^{-1})	log L_{2300} (erg s^{-1})	log L_{5100} (erg s^{-1})	log $L_{6\mu m}$ (erg s^{-1})	log L_{IR} (erg s^{-1})
CID-381	$10.78^{+0.00}_{-0.00}$	$2.07^{+0.06}_{-0.00}$	43.92	45.15	44.52	45.00	45.09
CID-387	$10.62^{+0.17}_{-0.11}$	$1.73^{+0.11}_{-0.00}$	43.09	44.94	43.88	43.82	45.23
CID-388	$10.87^{+0.20}_{-0.15}$	$2.10^{+0.04}_{-0.03}$	43.51	45.07	44.53	44.80	45.69
CID-392	$9.85^{+0.16}_{-0.17}$	$1.78^{+0.05}_{-0.06}$	43.58	45.03	43.81	0.00	-44.23
CID-394	$10.74^{+0.08}_{-0.06}$	$1.23^{+0.10}_{-0.09}$	43.53	44.42	44.33	43.71	-44.65
CID-396	$10.76^{+0.06}_{-0.08}$	$1.40^{+0.04}_{-0.12}$	43.71	44.55	44.80	0.00	-44.45
CID-401	$10.87^{+0.00}_{-0.00}$	$1.72^{+0.11}_{-0.16}$	43.56	44.55	44.46	45.11	45.02
CID-402	$10.77^{+0.08}_{-0.08}$	$1.29^{+0.14}_{-0.17}$	43.66	44.41	44.14	44.52	-44.53
CID-405	$10.76^{+0.06}_{-0.08}$	$1.20^{+0.14}_{-0.00}$	43.27	42.72	44.26	0.00	-44.85
CID-408	$10.34^{+0.45}_{-0.20}$	$2.24^{+0.07}_{-0.06}$	43.95	45.45	44.14	0.00	-45.08
CID-409	$11.05^{+0.13}_{-0.14}$	$1.92^{+0.11}_{-0.12}$	43.19	45.10	44.63	44.29	-44.50
CID-411	$11.33^{+0.00}_{-0.00}$	$1.79^{+0.13}_{-0.09}$	44.09	45.01	44.82	43.99	-44.61
CID-412	$10.43^{+0.18}_{-0.12}$	$1.78^{+0.05}_{-0.07}$	43.83	45.01	44.04	44.08	-44.65
CID-414	$11.66^{+0.20}_{-0.14}$	$3.67^{+0.14}_{-0.80}$	44.98	46.98	44.79	46.12	45.69
CID-415	$10.65^{+0.18}_{-0.13}$	$2.48^{+0.05}_{-0.11}$	44.11	45.68	44.43	44.75	-45.19
CID-419	$10.48^{+0.10}_{-0.17}$	$1.16^{+0.07}_{-0.34}$	43.28	44.09	43.99	44.07	-44.70
CID-421	$10.74^{+0.29}_{-0.20}$	$2.48^{+0.06}_{-0.01}$	43.77	45.71	44.45	45.14	-45.08
CID-426	$10.68^{+0.00}_{-0.00}$	$1.14^{+0.10}_{-0.01}$	43.47	44.37	44.27	44.07	-44.44
CID-427	$10.44^{+0.18}_{-0.04}$	$1.07^{+0.05}_{-0.28}$	43.53	44.10	44.09	0.00	-44.27
CID-428	$10.92^{+0.00}_{-0.00}$	$1.58^{+0.07}_{-0.01}$	43.67	44.59	44.15	44.76	44.98
CID-429	$10.41^{+0.30}_{-0.11}$	$1.88^{+0.06}_{-0.03}$	43.28	45.13	44.27	44.04	-44.30
CID-430	$10.99^{+0.00}_{-0.00}$	$1.69^{+0.05}_{-0.04}$	43.55	44.65	44.55	44.25	45.02
CID-431	$10.57^{+0.09}_{-0.08}$	$1.67^{+0.06}_{-0.01}$	43.16	44.90	44.12	0.00	-44.51
CID-432	$10.77^{+0.17}_{-0.07}$	$1.34^{+0.00}_{-0.36}$	43.85	44.37	44.10	0.00	-44.22
CID-435	$10.85^{+0.16}_{-0.03}$	$1.27^{+0.17}_{-0.05}$	43.41	44.49	44.40	43.93	-44.63
CID-436	$10.82^{+0.31}_{-0.19}$	$2.15^{+0.08}_{-0.01}$	43.41	45.28	44.15	44.66	45.54
CID-437	$10.47^{+0.12}_{-0.16}$	$1.87^{+0.06}_{-0.04}$	43.62	45.04	44.34	44.24	44.86
CID-439	$11.10^{+0.20}_{-0.17}$	$2.51^{+0.11}_{-0.19}$	43.83	45.43	44.48	43.81	45.86
CID-442	$10.38^{+0.03}_{-0.10}$	$1.04^{+0.08}_{-0.18}$	43.11	44.09	44.08	0.00	-44.35
CID-447	$10.55^{+0.25}_{-0.20}$	$1.78^{+0.05}_{-0.14}$	43.84	44.95	43.99	44.38	-44.67
CID-448	$10.77^{+0.00}_{-0.00}$	$1.40^{+0.14}_{-0.25}$	43.44	44.45	44.44	44.16	-44.26
CID-450	$10.87^{+0.00}_{-0.00}$	$1.96^{+0.07}_{-0.00}$	43.52	45.22	44.47	43.46	44.85
CID-451	$11.13^{+0.22}_{-0.17}$	$1.90^{+0.09}_{-0.43}$	44.72	44.76	44.75	45.96	45.86
CID-453	$10.81^{+0.18}_{-0.14}$	$2.51^{+0.12}_{-0.00}$	43.82	45.69	44.61	44.79	45.83
CID-456	$10.62^{+0.19}_{-0.06}$	$1.93^{+0.10}_{-0.14}$	44.02	45.08	44.56	44.54	-44.54
CID-465	$10.57^{+0.18}_{-0.28}$	$1.47^{+0.02}_{-1.80}$	43.40	42.97	43.91	0.00	-45.10
CID-469	$10.83^{+0.14}_{-0.12}$	$1.40^{+0.05}_{-0.17}$	43.71	44.44	44.17	0.00	-44.70
CID-471	$10.15^{+0.19}_{-0.18}$	$1.18^{+0.05}_{-0.06}$	43.24	44.42	43.80	0.00	-43.42
CID-476	$10.06^{+0.11}_{-0.16}$	$2.00^{+0.14}_{-0.00}$	43.88	45.21	43.20	44.96	45.12
CID-480	$10.94^{+0.19}_{-0.15}$	$2.78^{+0.06}_{-0.14}$	43.83	45.99	45.08	0.00	-45.63

Table B.2 – continued

ID	log $M_{stellar}$ ($M_\odot$)	log SFR^{tot} ($M_\odot$ yr^{-1})	log $L_{2-10\ keV}$ (erg s^{-1})	log L_{2300} (erg s^{-1})	log L_{5100} (erg s^{-1})	log $L_{6\mu m}$ (erg s^{-1})	log L_{IR} (erg s^{-1})
CID-483	$10.84^{+0.18}_{-0.04}$	$1.76^{+0.08}_{-0.00}$	43.58	45.06	44.26	43.92	44.76
CID-484	$9.67^{+0.00}_{-0.00}$	$0.22^{+0.10}_{-0.13}$	42.30	43.37	43.54	0.00	-43.28
CID-485	$10.55^{+0.20}_{-0.20}$	$1.57^{+0.06}_{-0.08}$	43.85	44.73	43.84	43.77	-44.55
CID-486	$10.59^{+0.17}_{-0.16}$	$1.82^{+0.01}_{-0.07}$	43.53	44.95	44.00	44.64	45.06
CID-491	$11.09^{+0.11}_{-0.14}$	$2.24^{+0.10}_{-0.00}$	43.92	45.53	44.57	44.65	-44.85
CID-493	$10.31^{+0.38}_{-0.04}$	$1.37^{+0.07}_{-1.79}$	43.97	43.06	44.14	44.97	-45.12
CID-494	$10.92^{+0.20}_{-0.28}$	$1.97^{+0.17}_{-0.00}$	44.08	45.18	44.35	0.00	-45.29
CID-496	$10.90^{+0.00}_{-0.00}$	$1.88^{+0.15}_{-0.00}$	43.81	44.56	44.55	44.04	45.37
CID-497	$10.45^{+0.14}_{-0.13}$	$1.25^{+0.09}_{-0.00}$	43.21	44.11	44.10	43.74	44.89
CID-498	$10.73^{+0.28}_{-0.19}$	$2.27^{+0.06}_{-0.06}$	43.92	45.50	44.32	44.57	-44.90
CID-502	$10.67^{+0.15}_{-0.02}$	$1.28^{+0.06}_{-0.20}$	43.13	44.43	44.25	43.60	-44.56
CID-503	$10.65^{+0.14}_{-0.13}$	$1.04^{+0.10}_{-0.00}$	43.58	44.34	44.07	44.03	-44.49
CID-511	$10.59^{+0.14}_{-0.25}$	$1.65^{+0.08}_{-0.07}$	43.96	44.90	44.21	43.96	-44.65
CID-518	$10.35^{+0.07}_{-0.06}$	$1.89^{+0.14}_{-0.00}$	43.23	45.12	44.25	44.55	44.52
CID-519	$10.85^{+0.22}_{-0.12}$	$2.04^{+0.09}_{-0.00}$	43.64	45.16	44.27	45.62	45.24
CID-522	$11.07^{+0.00}_{-0.00}$	$1.70^{+0.03}_{-0.05}$	44.09	44.76	44.66	44.46	44.80
CID-524	$10.66^{+0.16}_{-0.03}$	$0.93^{+0.10}_{-0.10}$	42.67	44.14	44.04	0.00	-43.99
CID-525	$11.03^{+0.24}_{-0.14}$	$2.33^{+0.10}_{-0.02}$	43.47	45.36	44.27	44.23	45.72
CID-526	$10.44^{+0.15}_{-0.12}$	$2.25^{+0.08}_{-0.05}$	43.91	45.45	44.32	45.32	45.40
CID-528	$11.13^{+0.22}_{-0.18}$	$2.13^{+0.10}_{-0.00}$	43.56	45.41	44.41	44.44	44.72
CID-530	$10.51^{+0.10}_{-0.06}$	$1.58^{+0.15}_{-0.00}$	44.28	44.12	44.11	44.53	45.30
CID-533	$10.57^{+0.17}_{-0.07}$	$0.39^{+0.04}_{-0.45}$	43.11	43.22	43.95	0.00	-43.84
CID-534	$10.45^{+0.17}_{-0.03}$	$-0.11^{+0.05}_{-0.07}$	42.76	43.13	43.95	0.00	-42.30
CID-538	$10.86^{+0.00}_{-0.00}$	$1.43^{+0.10}_{-0.00}$	43.51	44.55	44.45	44.38	44.68
CID-540	$10.96^{+0.17}_{-0.06}$	$2.04^{+0.09}_{-0.21}$	43.60	45.24	44.53	44.30	-44.94
CID-542	$10.57^{+0.20}_{-0.20}$	$0.90^{+0.57}_{-0.14}$	43.36	43.90	44.14	0.00	-44.46
CID-545	$10.30^{+0.41}_{-0.14}$	$2.21^{+0.03}_{-0.23}$	44.05	45.37	44.06	0.00	-44.62
CID-549	$10.45^{+0.12}_{-0.19}$	$1.28^{+0.16}_{-0.05}$	43.04	44.60	43.80	43.64	-44.42
CID-550	$10.32^{+0.26}_{-0.16}$	$0.82^{+0.13}_{-0.20}$	43.32	43.93	43.75	0.00	-44.21
CID-551	$10.41^{+0.00}_{-0.00}$	$1.28^{+0.05}_{-0.04}$	42.60	44.08	44.25	43.76	44.83
CID-552	$11.24^{+0.14}_{-0.13}$	$1.70^{+0.13}_{-0.50}$	44.09	44.55	44.58	0.00	-45.22
CID-554	$10.59^{+0.17}_{-0.09}$	$1.79^{+0.15}_{-0.00}$	43.69	44.96	44.01	44.48	44.69
CID-555	$10.40^{+0.18}_{-0.12}$	$0.99^{+0.04}_{-0.29}$	43.25	43.99	43.89	43.69	-44.44
CID-557	$11.13^{+0.20}_{-0.27}$	$1.68^{+0.05}_{-0.13}$	44.15	44.85	44.76	44.37	-44.95
CID-562	$10.26^{+0.16}_{-0.02}$	$0.25^{+0.09}_{-0.57}$	42.81	43.00	43.91	0.00	-43.76
CID-564	$10.67^{+0.15}_{-0.01}$	$1.26^{+0.07}_{-0.19}$	43.48	44.36	44.27	43.75	-44.30
CID-565	$10.55^{+0.07}_{-0.06}$	$1.84^{+0.09}_{-0.17}$	43.00	45.01	44.58	44.26	44.72
CID-567	$10.67^{+0.22}_{-0.21}$	$2.06^{+0.18}_{-0.00}$	43.82	45.35	44.23	44.20	45.17
CID-569	$10.80^{+0.19}_{-0.08}$	$1.35^{+0.08}_{-0.03}$	43.36	44.57	44.26	43.73	-44.29
CID-573	$10.90^{+0.11}_{-0.02}$	$1.41^{+0.02}_{-0.13}$	43.02	44.56	44.29	43.30	-44.52

Table B.2 – continued

ID	log $M_{stellar}$ ($M_\odot$)	log SFR^{tot} ($M_\odot$ yr^{-1})	log $L_{2-10\ keV}$ (erg s^{-1})	log L_{2300} (erg s^{-1})	log L_{5100} (erg s^{-1})	log $L_{6\mu m}$ (erg s^{-1})	log L_{IR} (erg s^{-1})
CID-575	$10.44^{+0.17}_{-0.04}$	$0.47^{+0.06}_{-0.93}$	42.70	42.83	43.83	42.97	-43.63
CID-579	$11.04^{+0.14}_{-0.13}$	$1.78^{+0.02}_{-0.42}$	43.94	44.61	44.51	0.00	-45.23
CID-582	$10.22^{+0.26}_{-0.24}$	$1.39^{+0.04}_{-0.21}$	43.45	44.41	43.70	44.01	-44.46
CID-585	$10.90^{+0.10}_{-0.17}$	$2.18^{+0.06}_{-0.05}$	43.60	45.31	44.19	44.78	44.98
CID-588	$10.89^{+0.29}_{-0.27}$	$2.09^{+0.14}_{-0.07}$	43.55	45.22	44.16	44.45	45.01
CID-591	$10.75^{+0.06}_{-0.07}$	$1.17^{+0.16}_{-0.09}$	43.69	44.40	44.57	0.00	-44.25
CID-592	$10.50^{+0.28}_{-0.15}$	$1.97^{+0.06}_{-0.04}$	43.82	45.20	43.85	43.68	-44.55
CID-593	$10.71^{+0.15}_{-0.15}$	$1.99^{+0.06}_{-0.03}$	43.82	45.09	43.82	45.19	45.08
CID-598	$10.33^{+0.35}_{-0.71}$	$1.67^{+0.01}_{-0.77}$	43.51	44.14	43.83	0.00	-45.19
CID-600	$10.51^{+0.11}_{-0.03}$	$1.60^{+0.03}_{-0.03}$	43.88	44.88	44.26	44.25	-44.41
CID-601	$11.19^{+0.17}_{-0.24}$	$1.85^{+0.10}_{-0.07}$	44.14	45.02	44.70	44.69	-45.02
CID-602	$10.73^{+0.21}_{-0.23}$	$1.77^{+0.06}_{-0.02}$	43.99	44.99	44.27	43.65	-44.90
CID-610	$11.23^{+0.14}_{-0.18}$	$2.43^{+0.01}_{-0.06}$	44.22	45.61	44.92	45.21	-45.22
CID-611	$10.58^{+0.03}_{-0.10}$	$0.43^{+0.10}_{-0.40}$	43.03	43.30	44.12	0.00	-43.83
CID-612	$10.12^{+0.09}_{-0.04}$	$0.28^{+0.02}_{-0.61}$	43.19	42.94	43.75	43.28	-43.87
CID-613	$11.15^{+0.07}_{-0.07}$	$0.62^{+0.12}_{-0.00}$	42.92	43.88	44.52	43.04	-44.15
CID-616	$10.80^{+0.02}_{-0.12}$	$1.29^{+0.04}_{-0.10}$	43.12	44.48	44.39	42.94	-44.12
CID-618	$10.65^{+0.12}_{-0.14}$	$1.26^{+0.08}_{-0.09}$	43.10	44.43	44.05	43.55	-44.09
CID-619	$10.81^{+0.00}_{-0.00}$	$1.47^{+0.06}_{-0.19}$	43.12	44.58	44.48	43.39	-44.58
CID-620	$10.97^{+0.05}_{-0.09}$	$1.69^{+0.05}_{-0.02}$	44.17	44.72	44.62	44.60	44.87
CID-622	$10.17^{+0.05}_{-0.09}$	$0.78^{+0.06}_{-0.29}$	42.90	43.80	43.80	43.55	-43.99
CID-625	$10.91^{+0.21}_{-0.31}$	$2.11^{+0.13}_{-0.00}$	44.16	45.35	44.16	44.99	-45.17
CID-626	$11.32^{+0.25}_{-0.17}$	$2.79^{+0.04}_{-0.11}$	44.22	46.04	44.92	45.03	-45.02
CID-631	$11.19^{+0.00}_{-0.00}$	$2.36^{+0.08}_{-0.00}$	44.10	45.58	44.96	44.37	45.27
CID-635	$10.59^{+0.12}_{-0.10}$	$0.67^{+0.07}_{-0.68}$	43.31	43.23	44.05	0.00	-44.26
CID-638	$10.67^{+0.14}_{-0.01}$	$1.21^{+0.03}_{-0.08}$	42.92	44.35	44.34	43.46	44.99
CID-645	$10.79^{+0.26}_{-0.06}$	$2.88^{+0.00}_{-0.14}$	44.17	45.92	44.48	44.36	45.76
CID-647	$10.21^{+0.47}_{-0.26}$	$1.97^{+0.06}_{-0.01}$	43.58	45.25	43.94	44.04	-44.14
CID-648	$10.88^{+0.12}_{-0.15}$	$2.04^{+0.00}_{-0.07}$	43.62	45.24	44.43	44.23	-44.80
CID-653	$9.94^{+0.39}_{-0.47}$	$1.69^{+0.00}_{-0.33}$	43.45	44.70	43.52	0.00	-44.83
CID-657	$10.73^{+0.11}_{-0.28}$	$1.70^{+0.12}_{-0.84}$	43.91	44.31	44.39	0.00	-45.31
CID-660	$10.60^{+0.18}_{-0.09}$	$1.19^{+0.02}_{-0.21}$	42.99	44.26	44.08	43.20	-44.59
CID-661	$10.55^{+0.21}_{-0.21}$	$1.46^{+0.07}_{-0.00}$	43.21	44.57	43.76	42.88	44.64
CID-662	$10.58^{+0.32}_{-0.40}$	$1.56^{+0.00}_{-0.71}$	43.62	44.02	43.91	0.00	-45.09
CID-667	$10.29^{+0.24}_{-0.40}$	$1.59^{+0.04}_{-0.69}$	43.64	44.16	44.01	44.27	-44.95
CID-668	$11.15^{+0.00}_{-0.00}$	$1.73^{+0.10}_{-0.01}$	42.91	44.44	44.77	44.91	45.33
CID-669	$10.83^{+0.14}_{-0.12}$	$0.66^{+0.08}_{-0.87}$	42.79	43.06	44.00	0.00	-44.24
CID-674	$10.11^{+0.09}_{-0.14}$	$0.72^{+0.11}_{-0.25}$	42.93	43.73	43.55	43.73	-44.00
CID-680	$11.19^{+0.03}_{-0.11}$	$1.69^{+0.04}_{-0.10}$	42.97	44.89	44.71	43.63	-44.57
CID-682	$10.99^{+0.00}_{-0.00}$	$1.41^{+0.12}_{-0.07}$	43.57	44.67	44.48	44.60	-44.14

Table B.2 – continued

ID	log $M_{stellar}$ ($M_\odot$)	log SFR^{tot} ($M_\odot$ yr^{-1})	log $L_{2-10\ keV}$ (erg s^{-1})	log L_{2300} (erg s^{-1})	log L_{5100} (erg s^{-1})	log $L_{6\mu m}$ (erg s^{-1})	log L_{IR} (erg s^{-1})
CID-684	$10.46^{+0.14}_{-0.11}$	$1.01^{+0.03}_{-0.12}$	43.34	44.11	43.92	43.22	-44.55
CID-685	$10.65^{+0.13}_{-0.14}$	$0.08^{+0.05}_{-0.07}$	42.79	43.33	44.05	0.00	0.00
CID-686	$10.69^{+0.10}_{-0.17}$	$1.09^{+0.15}_{-0.05}$	43.60	44.29	44.10	0.00	-44.07
CID-687	$11.03^{+0.28}_{-0.22}$	$2.04^{+0.00}_{-0.34}$	43.78	45.10	44.28	44.67	-45.16
CID-690	$11.25^{+0.00}_{-0.00}$	$0.84^{+0.09}_{-0.09}$	42.84	44.05	44.69	0.00	-43.63
CID-692	$10.25^{+0.25}_{-0.28}$	$1.22^{+0.12}_{-0.10}$	43.09	44.39	43.82	43.20	-44.54
CID-694	$9.36^{+0.31}_{-0.26}$	$0.47^{+0.13}_{-0.71}$	43.08	42.97	43.32	0.00	-44.02
CID-695	$10.73^{+0.08}_{-0.14}$	$1.74^{+0.09}_{-0.08}$	42.83	44.96	44.25	43.30	-44.44
CID-699	$10.62^{+0.26}_{-0.41}$	$2.14^{+0.16}_{-0.04}$	43.78	45.36	43.97	44.94	-45.13
CID-701	$10.62^{+0.19}_{-0.06}$	$1.19^{+0.12}_{-0.15}$	42.64	44.32	44.22	43.05	-44.27
CID-703	$10.57^{+0.05}_{-0.09}$	$0.60^{+0.03}_{-0.57}$	43.24	43.26	43.90	0.00	-44.12
CID-704	$10.48^{+0.22}_{-0.24}$	$1.29^{+0.04}_{-0.18}$	43.42	44.44	43.89	0.00	-44.19
CID-706	$10.88^{+0.34}_{-0.49}$	$2.07^{+0.14}_{-0.10}$	43.93	45.26	44.07	0.00	-45.22
CID-707	$9.44^{+0.60}_{-0.45}$	$1.19^{+0.14}_{-0.70}$	43.20	43.95	42.44	0.00	-44.69
CID-708	$10.99^{+0.37}_{-0.37}$	$1.91^{+0.22}_{-0.14}$	43.96	45.15	44.37	0.00	-45.18
CID-710	$10.59^{+0.19}_{-0.09}$	$1.10^{+0.13}_{-0.25}$	43.73	44.16	44.06	43.88	-44.49
CID-712	$10.93^{+0.32}_{-0.18}$	$2.49^{+0.14}_{-0.00}$	44.28	45.77	44.66	45.25	-45.21
CID-713	$11.09^{+0.23}_{-0.16}$	$2.44^{+0.00}_{-0.07}$	44.21	45.51	44.58	44.85	45.57
CID-715	$10.74^{+0.18}_{-0.32}$	$2.05^{+0.07}_{-0.28}$	99.00	45.02	44.51	0.00	-45.37
CID-717	$10.59^{+0.17}_{-0.19}$	$1.81^{+0.12}_{-0.09}$	43.19	45.01	44.31	44.04	-44.47
CID-721	$11.34^{+0.21}_{-0.26}$	$2.44^{+0.09}_{-0.00}$	44.03	45.64	44.84	45.23	-45.34
CID-723	$10.83^{+0.27}_{-0.25}$	$2.47^{+0.00}_{-0.16}$	43.82	45.58	44.24	44.55	45.38
CID-724	$10.60^{+0.04}_{-0.12}$	$1.04^{+0.10}_{-0.02}$	43.29	44.24	44.15	0.00	-44.06
CID-726	$10.68^{+0.00}_{-0.00}$	$1.25^{+0.08}_{-0.16}$	42.81	44.37	44.28	43.72	-44.45
CID-727	$10.80^{+0.01}_{-0.12}$	$1.33^{+0.10}_{-0.07}$	42.97	44.54	44.44	0.00	-44.14
CID-728	$10.87^{+0.17}_{-0.16}$	$2.72^{+0.11}_{-0.18}$	44.36	45.91	44.60	44.79	45.61
CID-730	$10.56^{+0.05}_{-0.08}$	$1.23^{+0.09}_{-0.20}$	43.31	44.34	44.24	0.00	-44.55
CID-732	$10.49^{+0.13}_{-0.01}$	$1.13^{+0.11}_{-0.21}$	43.32	44.21	44.37	43.90	-44.68
CID-733	$10.39^{+0.56}_{-0.48}$	$1.53^{+0.39}_{-0.14}$	43.53	44.71	43.61	0.00	-44.51
CID-736	$10.65^{+0.17}_{-0.03}$	$1.70^{+0.13}_{-0.06}$	43.21	44.94	44.40	44.26	-44.48
CID-738	$10.39^{+0.25}_{-0.18}$	$1.92^{+0.11}_{-0.03}$	43.58	45.12	44.38	44.26	-45.00
CID-741	$11.47^{+0.22}_{-0.14}$	$2.52^{+0.11}_{-0.14}$	43.87	45.75	44.66	44.89	-45.08
CID-745	$10.17^{+0.31}_{-0.16}$	$1.21^{+0.27}_{-0.00}$	42.94	44.49	43.86	0.00	-44.24
CID-747	$10.76^{+0.25}_{-0.05}$	$2.72^{+0.12}_{-0.12}$	44.44	45.96	44.65	45.38	-45.20
CID-750	$10.59^{+0.03}_{-0.10}$	$0.54^{+0.10}_{-0.48}$	42.88	43.32	44.14	0.00	-44.05
CID-752	$10.81^{+0.29}_{-0.17}$	$2.08^{+0.04}_{-0.20}$	43.63	45.19	44.58	44.48	-45.17
CID-753	$10.70^{+0.10}_{-0.17}$	$1.25^{+0.09}_{-0.20}$	43.23	44.37	43.92	43.30	-44.37
CID-758	$10.64^{+0.16}_{-0.13}$	$1.74^{+0.08}_{-0.17}$	43.68	44.90	44.45	0.00	-44.94
CID-760	$10.72^{+0.10}_{-0.06}$	$1.42^{+0.09}_{-0.24}$	43.65	44.44	44.26	43.86	-44.67
CID-763	$11.01^{+0.20}_{-0.07}$	$1.47^{+0.07}_{-0.01}$	43.26	44.74	44.55	43.29	-44.56

Table B.2 – continued

ID	log $M_{stellar}$ ($M_\odot$)	log SFR^{tot} ($M_\odot$ yr^{-1})	log $L_{2-10\ keV}$ (erg s^{-1})	log L_{2300} (erg s^{-1})	log L_{5100} (erg s^{-1})	log $L_{6\mu m}$ (erg s^{-1})	log L_{IR} (erg s^{-1})
CID-764	$10.94^{+0.08}_{-0.06}$	$2.24^{+0.09}_{-0.04}$	43.58	45.30	44.59	45.29	45.25
CID-765	$10.38^{+0.03}_{-0.10}$	$0.41^{+0.23}_{-0.66}$	42.65	43.12	43.94	42.90	-44.42
CID-768	$10.82^{+0.22}_{-0.20}$	$1.50^{+0.22}_{-0.26}$	43.72	44.49	44.04	44.63	-45.05
CID-774	$10.61^{+0.20}_{-0.07}$	$1.28^{+0.05}_{-0.07}$	42.96	44.34	44.24	43.62	45.11
CID-776	$10.52^{+0.20}_{-0.23}$	$1.10^{+0.23}_{-0.14}$	43.19	44.13	43.77	0.00	-44.50
CID-780	$10.84^{+0.28}_{-0.29}$	$2.27^{+0.31}_{-0.36}$	43.71	45.40	44.35	44.84	-45.09
CID-782	$11.00^{+0.28}_{-0.36}$	$1.50^{+0.09}_{-0.45}$	43.57	44.40	44.11	0.00	-45.05
CID-785	$10.69^{+0.38}_{-0.27}$	$1.89^{+0.15}_{-0.62}$	44.11	44.62	44.63	0.00	-45.25
CID-788	$10.60^{+0.17}_{-0.26}$	$2.06^{+0.07}_{-0.07}$	43.51	45.26	44.26	44.12	-45.04
CID-789	$11.31^{+0.26}_{-0.17}$	$3.12^{+0.02}_{-0.16}$	43.93	46.33	45.11	43.68	45.91
CID-794	$11.02^{+0.15}_{-0.22}$	$1.62^{+0.00}_{-0.45}$	43.68	44.31	44.51	44.61	-45.17
CID-795	$10.60^{+0.01}_{-0.12}$	$1.70^{+0.04}_{-0.04}$	43.00	44.85	44.31	43.75	44.93
CID-797	$10.04^{+0.33}_{-0.68}$	$0.76^{+0.50}_{-1.31}$	43.23	42.79	43.52	0.00	-44.37
CID-799	$10.71^{+0.11}_{-0.03}$	$1.08^{+0.05}_{-0.02}$	43.13	44.37	44.28	42.96	-44.24
CID-800	$10.44^{+0.16}_{-0.13}$	$1.40^{+0.14}_{-0.13}$	43.43	44.65	43.84	43.06	-44.51
CID-802	$10.81^{+0.28}_{-0.18}$	$1.85^{+0.26}_{-0.03}$	43.82	45.09	44.90	0.00	-45.08
CID-804	$10.42^{+0.15}_{-0.12}$	$1.09^{+0.05}_{-0.39}$	43.58	44.05	43.95	43.31	-44.47
CID-806	$10.88^{+0.14}_{-0.01}$	$1.29^{+0.14}_{-0.04}$	43.13	44.48	44.47	43.28	45.11
CID-808	$10.91^{+0.38}_{-0.27}$	$1.79^{+0.30}_{-0.00}$	43.82	45.07	44.26	0.00	-44.66
CID-817	$11.20^{+0.26}_{-0.06}$	$2.53^{+0.28}_{-0.00}$	43.64	45.58	44.49	45.13	45.93
CID-819	$10.40^{+0.31}_{-0.31}$	$1.47^{+0.00}_{-0.25}$	43.35	44.54	43.73	0.00	-44.46
CID-821	$10.97^{+0.16}_{-0.30}$	$2.02^{+0.09}_{-0.06}$	43.55	45.25	44.30	0.00	-44.98
CID-825	$10.79^{+0.22}_{-0.15}$	$1.86^{+0.33}_{-0.02}$	43.66	45.09	44.13	43.86	45.13
CID-828	$11.13^{+0.00}_{-0.00}$	$1.84^{+0.10}_{-0.09}$	42.96	44.80	44.53	43.91	45.09
CID-829	$10.50^{+0.10}_{-0.16}$	$1.07^{+0.16}_{-0.00}$	43.25	44.11	44.10	43.92	44.69
CID-832	$10.37^{+0.32}_{-0.22}$	$2.13^{+0.10}_{-0.00}$	43.47	45.37	43.88	44.26	-44.83
CID-833	$9.71^{+0.36}_{-0.40}$	$0.74^{+0.04}_{-0.28}$	43.17	43.83	43.47	43.60	-44.57
CID-834	$10.62^{+0.45}_{-0.67}$	$2.28^{+0.15}_{-0.00}$	43.54	45.62	44.58	0.00	-44.60
CID-835	$10.38^{+0.28}_{-0.12}$	$1.32^{+0.11}_{-0.36}$	43.56	44.18	44.08	43.62	-44.73
CID-838	$10.33^{+0.23}_{-0.27}$	$1.13^{+0.00}_{-0.16}$	42.81	43.90	43.54	44.01	44.71
CID-839	$11.32^{+0.18}_{-0.24}$	$2.31^{+0.13}_{-0.00}$	44.24	45.59	44.46	43.10	45.37
CID-841	$10.37^{+0.35}_{-0.17}$	$2.26^{+0.06}_{-0.10}$	43.81	45.38	44.50	0.00	-45.37
CID-842	$10.40^{+0.01}_{-0.12}$	$1.14^{+0.09}_{-0.37}$	43.22	44.10	44.18	43.97	-44.64
CID-844	$10.61^{+0.00}_{-0.00}$	$1.19^{+0.15}_{-0.19}$	43.13	44.29	44.20	43.42	-44.42
CID-845	$10.55^{+0.32}_{-0.28}$	$1.58^{+0.06}_{-0.06}$	43.47	44.83	44.02	0.00	-44.30
CID-846	$10.86^{+0.16}_{-0.03}$	$1.42^{+0.12}_{-0.07}$	42.97	44.61	44.16	43.81	-44.61
CID-850	$10.73^{+0.08}_{-0.07}$	$1.16^{+0.07}_{-0.21}$	42.76	44.26	44.25	43.21	-44.23
CID-853	$10.74^{+0.08}_{-0.06}$	$1.44^{+0.09}_{-0.05}$	43.20	44.48	44.21	44.16	44.99
CID-855	$9.80^{+0.58}_{-0.45}$	$1.03^{+0.42}_{-2.60}$	43.82	41.81	42.98	0.00	-44.83
CID-857	$10.51^{+0.24}_{-0.22}$	$1.53^{+0.00}_{-0.63}$	43.91	44.16	44.06	0.00	-45.04

Table B.2 – continued

ID	log $M_{stellar}$ ($M_\odot$)	log SFR^{tot} ($M_\odot$ yr^{-1})	log $L_{2-10\ keV}$ (erg s^{-1})	log L_{2300} (erg s^{-1})	log L_{5100} (erg s^{-1})	log $L_{6\mu m}$ (erg s^{-1})	log L_{IR} (erg s^{-1})
CID-865	$10.49^{+0.11}_{-0.16}$	$1.11^{+0.12}_{-0.16}$	43.20	44.22	44.30	43.73	-44.73
CID-871	$10.74^{+0.20}_{-0.27}$	$2.38^{+0.05}_{-0.10}$	44.38	45.38	44.46	44.94	45.57
CID-872	$10.52^{+0.08}_{-0.16}$	$1.55^{+0.09}_{-0.05}$	43.41	44.79	44.24	0.00	-44.23
CID-875	$10.30^{+0.24}_{-0.26}$	$1.08^{+0.50}_{-0.41}$	43.60	44.04	43.91	0.00	-44.49
CID-876	$10.55^{+0.27}_{-0.25}$	$2.12^{+0.12}_{-0.00}$	43.56	45.39	43.73	44.66	-44.63
CID-877	$10.42^{+0.16}_{-0.11}$	$0.85^{+0.16}_{-0.16}$	43.08	44.00	43.90	42.74	-44.11
CID-880	$10.77^{+0.05}_{-0.08}$	$2.09^{+0.05}_{-0.02}$	43.74	45.20	44.48	45.67	45.05
CID-881	$10.62^{+0.14}_{-0.12}$	$1.13^{+0.10}_{-0.08}$	43.17	44.24	44.14	0.00	-44.28
CID-885	$11.08^{+0.24}_{-0.28}$	$2.21^{+0.03}_{-0.22}$	44.03	45.36	44.44	44.45	-44.99
CID-886	$10.93^{+0.00}_{-0.00}$	$1.44^{+0.10}_{-0.20}$	43.57	44.60	44.59	44.10	-44.70
CID-888	$10.90^{+0.12}_{-0.02}$	$2.15^{+0.08}_{-0.00}$	43.73	45.34	44.56	44.83	45.42
CID-889	$10.21^{+0.30}_{-0.30}$	$1.74^{+0.08}_{-0.25}$	43.12	44.79	43.98	43.73	-44.90
CID-897	$10.51^{+0.10}_{-0.03}$	$1.08^{+0.11}_{-0.06}$	42.64	44.27	44.17	43.18	-44.39
CID-899	$10.72^{+0.14}_{-0.19}$	$1.69^{+0.04}_{-0.05}$	42.94	44.87	43.98	43.60	-44.64
CID-901	$10.87^{+0.15}_{-0.01}$	$1.44^{+0.10}_{-0.05}$	43.20	44.63	44.45	0.00	-44.22
CID-902	$9.92^{+0.17}_{-0.19}$	$1.30^{+0.03}_{-0.31}$	43.55	44.28	43.76	44.03	-44.28
CID-916	$10.44^{+0.25}_{-0.20}$	$1.68^{+0.05}_{-0.11}$	43.80	44.80	44.02	43.91	-44.77
CID-919	$10.70^{+0.19}_{-0.19}$	$2.15^{+0.08}_{-0.03}$	43.04	45.41	43.92	44.42	44.89
CID-921	$10.73^{+0.20}_{-0.25}$	$1.86^{+0.08}_{-0.07}$	43.75	45.08	44.21	44.28	-44.78
CID-924	$10.23^{+0.43}_{-0.34}$	$1.53^{+0.08}_{-0.16}$	43.51	44.51	43.70	44.25	-44.90
CID-928	$11.24^{+0.17}_{-0.04}$	$1.99^{+0.04}_{-0.03}$	43.11	45.02	44.66	44.99	45.28
CID-929	$10.43^{+0.11}_{-0.14}$	$-0.34^{+0.20}_{-0.02}$	42.65	42.94	43.76	0.00	0.00
CID-930	$10.88^{+0.13}_{-0.00}$	$0.79^{+0.14}_{-0.33}$	43.49	43.70	44.51	0.00	-44.23
CID-932	$10.87^{+0.15}_{-0.01}$	$1.51^{+0.02}_{-0.05}$	42.83	44.50	44.50	44.07	44.78
CID-934	$10.54^{+0.15}_{-0.24}$	$0.98^{+0.05}_{-0.26}$	43.52	44.02	44.01	0.00	-44.22
CID-936	$10.55^{+0.31}_{-0.35}$	$1.90^{+0.13}_{-0.05}$	43.35	45.16	43.82	0.00	-44.32
CID-937	$11.04^{+0.28}_{-0.26}$	$2.65^{+0.09}_{-0.00}$	43.68	45.92	44.49	44.80	-45.18
CID-938	$10.27^{+0.12}_{-0.14}$	$0.78^{+0.05}_{-0.10}$	42.75	43.91	43.81	0.00	-43.88
CID-941	$10.69^{+0.28}_{-0.36}$	$0.77^{+0.06}_{-0.73}$	43.34	43.29	43.84	0.00	-44.27
CID-942	$10.65^{+0.23}_{-0.37}$	$1.09^{+0.04}_{-0.12}$	43.12	44.25	43.71	0.00	-44.10
CID-943	$10.84^{+0.14}_{-0.29}$	$1.99^{+0.23}_{-0.05}$	43.31	45.23	44.22	44.00	-44.81
CID-945	$10.73^{+0.20}_{-0.26}$	$1.85^{+0.07}_{-0.55}$	43.68	44.73	44.53	0.00	-45.29
CID-948	$10.40^{+0.41}_{-0.44}$	$0.69^{+0.14}_{-0.89}$	43.51	43.16	43.88	0.00	-44.32
CID-949	$10.77^{+0.19}_{-0.07}$	$1.19^{+0.15}_{-0.00}$	42.94	44.36	44.09	44.05	44.71
CID-952	$9.89^{+0.40}_{-0.27}$	$0.64^{+0.18}_{-0.39}$	43.74	43.60	43.50	0.00	-44.05
CID-956	$10.26^{+0.13}_{-0.14}$	$0.84^{+0.09}_{-0.16}$	42.79	43.92	43.82	0.00	-44.13
CID-957	$11.06^{+0.16}_{-0.02}$	$2.28^{+0.06}_{-0.11}$	43.52	45.45	44.74	44.84	45.16
CID-959	$10.65^{+0.13}_{-0.14}$	$2.28^{+0.16}_{-0.01}$	44.29	45.56	44.60	44.75	-44.74
CID-960	$11.21^{+0.27}_{-0.08}$	$2.06^{+0.07}_{-0.00}$	43.86	44.89	44.62	44.26	45.32
CID-961	$10.66^{+0.26}_{-0.26}$	$1.74^{+0.09}_{-0.13}$	43.54	44.92	44.09	44.43	-44.73

Table B.2 – continued

ID	log $M_{stellar}$ ($M_\odot$)	log SFR^{tot} ($M_\odot$ yr^{-1})	log $L_{2-10\ keV}$ (erg s^{-1})	log L_{2300} (erg s^{-1})	log L_{5100} (erg s^{-1})	log $L_{6\mu m}$ (erg s^{-1})	log L_{IR} (erg s^{-1})
CID-963	$11.10^{+0.12}_{-0.02}$	$1.71^{+0.03}_{-0.10}$	42.94	44.95	44.59	0.00	-44.10
CID-964	$10.79^{+0.26}_{-0.41}$	$1.72^{+0.20}_{-0.49}$	43.97	44.47	44.55	0.00	-45.38
CID-966	$10.54^{+0.20}_{-0.21}$	$1.20^{+0.14}_{-0.30}$	43.59	44.17	44.07	43.54	-44.76
CID-968	$10.65^{+0.14}_{-0.13}$	$0.77^{+0.07}_{-0.70}$	43.26	43.38	44.11	43.29	-44.45
CID-969	$10.22^{+0.52}_{-0.20}$	$1.77^{+0.15}_{-0.07}$	43.72	45.05	44.05	0.00	-44.37
CID-971	$10.64^{+0.28}_{-0.24}$	$1.76^{+0.14}_{-0.27}$	43.70	44.68	44.46	0.00	-45.28
CID-972	$10.59^{+0.33}_{-0.30}$	$1.16^{+0.15}_{-0.18}$	43.44	44.28	43.92	0.00	-44.24
CID-974	$10.23^{+0.14}_{-0.17}$	$1.33^{+0.10}_{-0.09}$	43.20	44.54	43.92	0.00	-44.17
CID-975	$10.89^{+0.13}_{-0.01}$	$1.32^{+0.11}_{-0.03}$	42.93	44.58	44.39	0.00	-43.80
CID-977	$10.75^{+0.08}_{-0.07}$	$1.05^{+0.08}_{-0.26}$	43.28	44.06	44.30	43.62	-44.22
CID-978	$10.15^{+0.32}_{-0.57}$	$1.43^{+0.10}_{-0.08}$	43.22	44.57	43.56	43.96	-44.72
CID-980	$10.16^{+0.25}_{-0.34}$	$1.71^{+0.03}_{-0.45}$	43.82	44.50	43.81	44.24	-45.06
CID-981	$11.27^{+0.00}_{-0.00}$	$1.74^{+0.09}_{-0.03}$	43.35	44.96	44.87	43.85	-44.76
CID-984	$10.57^{+0.04}_{-0.09}$	$0.99^{+0.04}_{-0.03}$	43.96	44.26	44.25	43.70	-44.56
CID-985	$10.71^{+0.21}_{-0.27}$	$1.94^{+0.01}_{-0.19}$	43.46	45.02	44.16	44.07	-44.92
CID-986	$10.50^{+0.41}_{-0.59}$	$2.13^{+0.09}_{-0.06}$	44.46	45.24	43.75	0.00	-45.24
CID-988	$10.80^{+0.15}_{-0.10}$	$0.82^{+0.03}_{-0.05}$	43.28	44.07	44.32	0.00	-42.78
CID-991	$10.71^{+0.00}_{-0.00}$	$0.62^{+0.12}_{-0.46}$	43.35	43.44	44.35	43.25	-44.31
CID-995	$10.84^{+0.27}_{-0.27}$	$2.31^{+0.11}_{-0.03}$	43.54	45.60	44.24	45.36	-45.12
CID-996	$10.77^{+0.00}_{-0.00}$	$0.54^{+0.11}_{-0.31}$	42.63	43.51	44.15	0.00	-43.91
CID-999	$10.50^{+0.23}_{-0.17}$	$1.54^{+0.10}_{-0.08}$	43.29	44.71	44.00	43.49	-44.69
CID-1000	$11.08^{+0.12}_{-0.26}$	$2.07^{+0.05}_{-0.10}$	44.24	44.89	44.53	43.30	45.41
CID-1002	$10.52^{+0.19}_{-0.19}$	$1.48^{+0.15}_{-0.00}$	43.48	44.69	44.24	0.00	-44.60
CID-1003	$10.68^{+0.27}_{-0.19}$	$1.73^{+0.00}_{-0.66}$	44.12	44.35	44.25	44.61	-45.19
CID-1005	$10.61^{+0.34}_{-0.54}$	$2.08^{+0.06}_{-0.15}$	43.95	45.25	43.81	0.00	-45.10
CID-1006	$10.84^{+0.14}_{-0.13}$	$1.48^{+0.32}_{-0.35}$	43.87	44.47	44.54	0.00	-44.80
CID-1007	$10.47^{+0.38}_{-0.41}$	$2.00^{+0.17}_{-0.00}$	43.59	45.27	44.01	44.00	-45.07
CID-1010	$10.83^{+0.15}_{-0.12}$	$1.43^{+0.00}_{-0.35}$	43.62	44.39	43.94	44.02	-44.51
CID-1011	$10.80^{+0.13}_{-0.40}$	$1.99^{+0.13}_{-0.16}$	43.46	45.13	44.18	0.00	-45.22
CID-1013	$10.49^{+0.11}_{-0.14}$	$1.74^{+0.09}_{-0.10}$	43.93	44.93	44.06	44.31	-44.70
CID-1014	$10.32^{+0.46}_{-0.42}$	$1.99^{+0.13}_{-0.08}$	43.88	45.11	43.85	44.44	-45.17
CID-1015	$10.40^{+0.25}_{-0.21}$	$1.70^{+0.04}_{-0.06}$	43.37	44.89	44.01	43.72	-44.77
CID-1016	$10.66^{+0.00}_{-0.00}$	$0.51^{+0.21}_{-0.06}$	43.22	43.39	44.12	43.33	44.29
CID-1017	$10.63^{+0.14}_{-0.22}$	$2.45^{+0.08}_{-0.01}$	43.27	45.67	44.01	44.72	45.46
CID-1019	$10.74^{+0.08}_{-0.06}$	$0.80^{+0.14}_{-0.61}$	42.89	43.50	44.22	43.81	-44.11
CID-1020	$10.90^{+0.12}_{-0.01}$	$2.03^{+0.10}_{-0.00}$	43.26	45.28	44.66	44.12	-44.76
CID-1021	$10.85^{+0.14}_{-0.13}$	$1.67^{+0.09}_{-0.60}$	43.95	44.50	44.68	45.19	-45.16
CID-1025	$10.53^{+0.42}_{-0.65}$	$1.89^{+0.25}_{-0.00}$	43.86	45.12	43.28	0.00	-45.28
CID-1029	$10.50^{+0.24}_{-0.13}$	$2.10^{+0.07}_{-0.04}$	43.67	45.33	44.44	44.17	-44.78
CID-1033	$10.63^{+0.14}_{-0.16}$	$2.09^{+0.00}_{-0.20}$	43.25	45.23	44.40	43.97	-44.90

Table B.2 – continued

ID	log $M_{stellar}$ ($M_\odot$)	log SFR^{tot} ($M_\odot$ yr^{-1})	log $L_{2-10\ keV}$ (erg s^{-1})	log L_{2300} (erg s^{-1})	log L_{5100} (erg s^{-1})	log $L_{6\mu m}$ (erg s^{-1})	log L_{IR} (erg s^{-1})
CID-1036	$11.25^{+0.03}_{-0.16}$	$2.42^{+0.11}_{-0.00}$	44.03	45.72	44.75	44.73	45.49
CID-1037	$10.58^{+0.04}_{-0.10}$	$1.14^{+0.09}_{-0.14}$	43.97	44.29	44.37	0.00	-44.18
CID-1038	$11.30^{+0.12}_{-0.02}$	$1.65^{+0.08}_{-1.18}$	44.14	43.77	44.86	0.00	-45.27
CID-1042	$10.77^{+0.08}_{-0.08}$	$1.28^{+0.05}_{-0.09}$	43.19	44.46	44.27	43.27	-44.56
CID-1043	$10.59^{+0.03}_{-0.10}$	$1.90^{+0.04}_{-0.04}$	43.32	44.97	44.26	44.84	45.17
CID-1046	$10.82^{+0.19}_{-0.06}$	$1.28^{+0.14}_{-0.05}$	43.44	44.51	44.32	0.00	-44.14
CID-1050	$10.73^{+0.08}_{-0.12}$	$0.79^{+0.05}_{-0.57}$	43.16	43.48	44.21	0.00	-44.31
CID-1051	$10.84^{+0.15}_{-0.13}$	$2.16^{+0.07}_{-0.08}$	43.53	45.38	44.15	44.47	-44.78
CID-1055	$10.23^{+0.15}_{-0.12}$	$0.88^{+0.06}_{-0.33}$	43.14	43.87	43.86	0.00	-44.30
CID-1060	$10.99^{+0.23}_{-0.09}$	$2.26^{+0.07}_{-0.06}$	44.23	45.50	44.63	44.95	-45.00
CID-1063	$10.78^{+0.00}_{-0.00}$	$1.27^{+0.06}_{-0.01}$	43.09	44.47	44.38	43.12	-44.49
CID-1068	$10.57^{+0.23}_{-0.21}$	$2.08^{+0.06}_{-0.07}$	43.88	45.28	44.46	0.00	-44.25
CID-1069	$11.57^{+0.22}_{-0.51}$	$1.69^{+0.42}_{-0.49}$	44.14	44.50	43.84	45.39	-45.10
CID-1070	$10.53^{+0.08}_{-0.10}$	$0.93^{+0.10}_{-0.16}$	42.86	44.09	43.99	0.00	-43.99
CID-1071	$11.30^{+0.00}_{-0.00}$	$1.23^{+0.11}_{-0.50}$	43.04	44.04	44.76	44.10	-44.37
CID-1072	$10.66^{+0.31}_{-0.01}$	$1.89^{+0.15}_{-0.06}$	43.74	45.17	44.39	0.00	-44.27
CID-1075	$10.77^{+0.05}_{-0.09}$	$1.49^{+0.14}_{-0.00}$	42.46	44.49	44.04	44.19	45.00
CID-1077	$10.33^{+0.39}_{-0.17}$	$2.05^{+0.16}_{-0.06}$	43.77	45.31	44.10	0.00	-44.62
CID-1078	$10.95^{+0.19}_{-0.17}$	$2.11^{+0.12}_{-0.00}$	43.71	45.25	44.36	45.09	45.44
CID-1080	$11.05^{+0.26}_{-0.20}$	$1.61^{+0.03}_{-0.28}$	43.91	44.67	44.48	43.96	-45.02
CID-1082	$10.75^{+0.06}_{-0.10}$	$2.65^{+0.08}_{-0.05}$	43.70	45.84	44.40	45.35	45.58
CID-1084	$10.29^{+0.63}_{-0.36}$	$2.01^{+0.23}_{-0.47}$	44.49	45.31	43.64	0.00	-45.38
CID-1087	$10.55^{+0.06}_{-0.07}$	$0.55^{+0.19}_{-0.43}$	42.71	43.32	43.96	42.81	-44.12
CID-1088	$10.87^{+0.14}_{-0.01}$	$1.37^{+0.07}_{-0.00}$	43.01	44.60	44.24	44.35	44.58
CID-1091	$11.68^{+0.10}_{-0.22}$	$3.08^{+0.06}_{-0.11}$	44.33	46.15	44.80	45.03	46.18
CID-1094	$9.63^{+0.48}_{-0.70}$	$0.95^{+0.00}_{-0.48}$	43.53	43.72	43.60	0.00	-44.34
CID-1095	$10.72^{+0.08}_{-0.18}$	$1.78^{+0.05}_{-0.15}$	42.85	44.98	44.35	43.72	-44.62
CID-1098	$10.82^{+0.00}_{-0.00}$	$1.38^{+0.05}_{-0.17}$	43.56	44.52	44.51	43.38	-44.48
CID-1100	$10.54^{+0.07}_{-0.06}$	$0.40^{+0.14}_{-0.38}$	43.02	43.30	43.85	43.44	-44.23
CID-1101	$10.60^{+0.25}_{-0.21}$	$1.68^{+0.06}_{-0.17}$	43.20	44.83	44.03	44.10	-44.76
CID-1102	$10.71^{+0.18}_{-0.18}$	$2.44^{+0.09}_{-0.00}$	43.21	45.73	44.47	44.58	45.53
CID-1106	$10.27^{+0.12}_{-0.15}$	$1.14^{+0.07}_{-0.51}$	43.47	43.95	43.94	43.28	-44.56
CID-1107	$11.07^{+0.26}_{-0.22}$	$2.44^{+0.10}_{-0.00}$	44.21	45.55	44.50	43.30	45.69
CID-1112	$10.64^{+0.48}_{-0.39}$	$2.25^{+0.06}_{-0.22}$	44.08	45.51	43.32	0.00	-45.04
CID-1113	$10.80^{+0.24}_{-0.23}$	$1.97^{+0.06}_{-0.07}$	43.61	45.10	44.15	44.65	45.16
CID-1114	$10.46^{+0.12}_{-0.15}$	$0.35^{+0.08}_{-0.50}$	43.18	43.16	43.89	0.00	-43.86
CID-1115	$10.45^{+0.23}_{-0.14}$	$1.62^{+0.08}_{-0.14}$	43.99	44.76	44.04	43.46	-44.77
CID-1116	$10.61^{+0.00}_{-0.00}$	$1.21^{+0.12}_{-0.00}$	42.58	44.31	44.12	42.68	44.49
CID-1117	$10.81^{+0.15}_{-0.11}$	$0.63^{+0.11}_{-0.53}$	42.96	43.42	44.14	0.00	-44.09
CID-1119	$10.93^{+0.12}_{-0.19}$	$1.48^{+0.16}_{-0.00}$	43.48	44.49	44.04	43.98	44.99

Table B.2 – continued

ID	log $M_{stellar}$ ($M_\odot$)	log SFR^{tot} ($M_\odot$ yr^{-1})	log $L_{2-10\ keV}$ (erg s^{-1})	log L_{2300} (erg s^{-1})	log L_{5100} (erg s^{-1})	log $L_{6\mu m}$ (erg s^{-1})	log L_{IR} (erg s^{-1})
CID-1120	$10.85^{+0.17}_{-0.03}$	$1.40^{+0.04}_{-0.12}$	43.51	44.55	44.37	43.65	-44.51
CID-1121	$10.40^{+0.02}_{-0.12}$	$1.08^{+0.06}_{-0.49}$	43.47	43.95	43.94	44.00	-44.65
CID-1123	$9.82^{+0.46}_{-0.57}$	$0.79^{+0.69}_{-0.38}$	43.32	43.59	43.58	0.00	-44.49
CID-1124	$10.41^{+0.21}_{-0.07}$	$1.09^{+0.05}_{-1.21}$	43.47	43.12	44.03	43.71	-44.53
CID-1125	$10.82^{+0.23}_{-0.31}$	$1.28^{+0.12}_{-0.05}$	43.86	44.40	44.12	0.00	-44.30
CID-1126	$10.97^{+0.00}_{-0.00}$	$1.71^{+0.03}_{-0.11}$	43.84	44.58	44.67	44.23	44.99
CID-1127	$11.01^{+0.11}_{-0.32}$	$1.67^{+0.17}_{-0.39}$	44.11	44.54	44.53	44.58	-45.16
CID-1130	$10.59^{+0.03}_{-0.11}$	$1.19^{+0.04}_{-0.13}$	43.01	44.29	44.28	43.16	-44.25
CID-1133	$10.82^{+0.15}_{-0.25}$	$1.67^{+0.00}_{-0.96}$	43.81	44.15	44.26	44.59	-45.13
CID-1135	$11.06^{+0.16}_{-0.02}$	$1.69^{+0.05}_{-0.16}$	44.11	44.83	44.56	44.15	-44.82
CID-1136	$10.89^{+0.22}_{-0.32}$	$2.41^{+0.12}_{-0.01}$	44.21	45.68	44.45	44.78	-45.18
CID-1138	$10.39^{+0.03}_{-0.10}$	$0.96^{+0.08}_{-0.17}$	43.08	44.08	44.07	0.00	-44.08
CID-1139	$10.99^{+0.03}_{-0.10}$	$2.11^{+0.12}_{-0.00}$	43.33	45.33	44.70	44.71	45.39
CID-1144	$10.70^{+0.23}_{-0.28}$	$2.10^{+0.03}_{-0.22}$	44.13	45.20	44.19	44.53	-45.13
CID-1145	$11.18^{+0.05}_{-0.10}$	$1.56^{+0.11}_{-0.20}$	43.74	44.69	44.51	44.32	-44.90
CID-1148	$11.31^{+0.19}_{-0.17}$	$1.74^{+0.09}_{-0.11}$	43.64	44.90	44.54	44.64	-44.88
CID-1149	$11.03^{+0.42}_{-0.24}$	$2.90^{+0.04}_{-0.08}$	43.84	46.05	44.39	43.88	45.52
CID-1150	$10.74^{+0.32}_{-0.46}$	$1.60^{+0.00}_{-0.40}$	43.97	44.41	44.06	0.00	-45.06
CID-1154	$10.28^{+0.28}_{-0.28}$	$1.63^{+0.05}_{-0.37}$	43.94	44.57	44.23	0.00	-44.92
CID-1155	$10.76^{+0.38}_{-0.22}$	$1.81^{+0.12}_{-0.19}$	43.73	44.94	44.80	44.44	-44.99
CID-1156	$10.45^{+0.35}_{-0.37}$	$1.39^{+0.08}_{-1.44}$	43.69	43.28	43.92	0.00	-45.07
CID-1157	$10.54^{+0.08}_{-0.06}$	$1.17^{+0.10}_{-0.00}$	43.44	44.25	44.15	43.83	44.70
CID-1159	$10.34^{+0.35}_{-0.30}$	$1.66^{+0.11}_{-0.65}$	44.24	44.19	44.26	0.00	-45.27
CID-1160	$10.88^{+0.26}_{-0.24}$	$2.30^{+0.04}_{-0.04}$	43.26	45.51	44.22	0.00	-44.93
CID-1162	$11.07^{+0.25}_{-0.30}$	$2.65^{+0.04}_{-0.10}$	43.61	45.82	44.45	43.78	45.45
CID-1166	$10.96^{+0.21}_{-0.18}$	$1.79^{+0.15}_{-0.20}$	44.24	44.96	44.53	44.41	-44.99
CID-1169	$11.04^{+0.00}_{-0.00}$	$1.61^{+0.13}_{-0.10}$	42.79	44.74	44.65	44.27	-44.55
CID-1171	$10.07^{+0.29}_{-0.13}$	$1.59^{+0.05}_{-0.19}$	43.86	44.77	44.26	0.00	-44.30
CID-1172	$11.44^{+0.11}_{-0.14}$	$1.57^{+0.17}_{-1.02}$	44.28	43.85	44.76	0.00	-45.25
CID-1176	$10.71^{+0.11}_{-0.03}$	$0.94^{+0.10}_{-0.64}$	43.06	43.55	44.28	0.00	-44.49
CID-1181	$10.86^{+0.16}_{-0.03}$	$1.31^{+0.03}_{-0.06}$	43.47	44.53	44.35	0.00	-43.74
CID-1183	$11.09^{+0.23}_{-0.22}$	$2.38^{+0.05}_{-0.09}$	43.77	45.49	44.53	44.51	45.71
CID-1185	$10.64^{+0.18}_{-0.04}$	$1.00^{+0.14}_{-0.05}$	43.22	44.26	44.16	44.10	-44.42
CID-1188	$10.64^{+0.15}_{-0.12}$	$1.29^{+0.10}_{-0.23}$	42.90	44.36	44.09	0.00	-44.60
CID-1189	$11.13^{+0.00}_{-0.00}$	$0.82^{+0.11}_{-0.19}$	42.57	43.88	44.52	42.79	-44.19
CID-1190	$10.66^{+0.27}_{-0.27}$	$1.63^{+0.09}_{-0.37}$	43.51	44.62	44.14	44.55	-44.91
CID-1192	$9.44^{+0.47}_{-0.96}$	$1.42^{+0.28}_{-0.47}$	44.40	43.98	43.72	0.00	-45.28
CID-1195	$10.80^{+0.57}_{-0.30}$	$2.60^{+0.03}_{-0.09}$	44.46	45.76	44.98	0.00	-45.36
CID-1199	$10.14^{+0.18}_{-0.20}$	$0.87^{+0.06}_{-0.18}$	42.61	44.03	43.47	0.00	-43.99
CID-1201	$9.22^{+0.56}_{-0.48}$	$1.41^{+0.19}_{-0.88}$	44.07	43.71	43.69	0.00	-45.22

Table B.2 – continued

ID	log $M_{stellar}$ ($M_\odot$)	log SFR^{tot} ($M_\odot$ yr^{-1})	log $L_{2-10\ keV}$ (erg s^{-1})	log L_{2300} (erg s^{-1})	log L_{5100} (erg s^{-1})	log $L_{6\mu m}$ (erg s^{-1})	log L_{IR} (erg s^{-1})
CID-1203	$10.90^{+0.25}_{-0.15}$	$1.95^{+0.08}_{-0.01}$	43.24	45.15	44.08	44.27	45.04
CID-1205	$11.38^{+0.17}_{-0.23}$	$2.39^{+0.11}_{-0.02}$	43.96	45.37	44.82	45.96	45.74
CID-1207	$10.58^{+0.11}_{-0.09}$	$1.89^{+0.04}_{-0.03}$	43.34	45.04	44.26	44.04	45.18
CID-1209	$10.72^{+0.29}_{-0.47}$	$1.84^{+0.00}_{-0.79}$	44.46	44.37	44.28	0.00	-45.29
CID-1211	$10.95^{+0.18}_{-0.30}$	$1.81^{+0.06}_{-0.04}$	43.44	45.04	44.14	44.13	-44.76
CID-1212	$10.43^{+0.19}_{-0.05}$	$0.67^{+0.06}_{-0.84}$	42.87	43.16	44.06	0.00	-44.22
CID-1213	$10.44^{+0.46}_{-0.53}$	$1.50^{+0.17}_{-0.49}$	43.63	44.22	43.81	44.32	-45.07
CID-1214	$10.85^{+0.27}_{-0.23}$	$1.67^{+0.14}_{-0.11}$	44.13	44.87	44.25	0.00	-44.41
CID-1217	$10.86^{+0.13}_{-0.15}$	$1.30^{+0.10}_{-0.26}$	43.05	44.39	44.12	0.00	-44.53
CID-1218	$10.41^{+0.27}_{-0.22}$	$0.88^{+0.33}_{-0.00}$	42.73	44.01	43.74	42.81	44.98
CID-1220	$10.76^{+0.18}_{-0.07}$	$1.84^{+0.09}_{-0.11}$	43.68	45.05	44.43	0.00	-44.38
CID-1223	$11.15^{+0.17}_{-0.31}$	$2.24^{+0.10}_{-0.00}$	44.04	45.51	44.38	44.53	-45.08
CID-1225	$10.60^{+0.17}_{-0.10}$	$1.86^{+0.08}_{-0.16}$	43.62	45.06	44.29	44.12	-44.75
CID-1226	$10.92^{+0.08}_{-0.17}$	$1.24^{+0.10}_{-1.03}$	43.97	43.58	44.22	43.87	-45.04
CID-1228	$10.47^{+0.31}_{-0.02}$	$2.46^{+0.23}_{-0.00}$	44.13	45.73	44.50	44.18	45.46
CID-1229	$10.66^{+0.26}_{-0.16}$	$1.49^{+0.03}_{-0.47}$	43.48	44.40	44.12	43.54	-44.67
CID-1231	$10.78^{+0.03}_{-0.10}$	$0.92^{+0.18}_{-0.00}$	43.00	43.49	44.39	43.98	44.50
CID-1232	$10.72^{+0.10}_{-0.04}$	$1.97^{+0.06}_{-0.08}$	42.65	45.12	44.58	44.36	44.88
CID-1233	$11.31^{+0.10}_{-0.31}$	$2.23^{+0.10}_{-0.16}$	45.21	45.43	44.79	45.02	-45.24
CID-1234	$10.87^{+0.16}_{-0.15}$	$0.87^{+0.62}_{-0.41}$	43.66	43.57	44.29	0.00	-44.50
CID-1237	$10.55^{+0.28}_{-0.18}$	$1.62^{+0.00}_{-0.36}$	42.85	44.59	44.04	0.00	-44.76
CID-1240	$10.72^{+0.08}_{-0.19}$	$0.49^{+0.14}_{-0.47}$	43.50	43.35	43.90	42.71	-44.27
CID-1241	$10.97^{+0.16}_{-0.08}$	$0.62^{+0.11}_{-0.37}$	42.82	43.58	44.22	0.00	-44.06
CID-1242	$10.83^{+0.19}_{-0.05}$	$1.49^{+0.15}_{-0.19}$	43.35	44.61	44.43	44.48	-44.66
CID-1243	$10.40^{+0.22}_{-0.09}$	$0.50^{+0.13}_{-0.57}$	43.19	43.22	44.04	0.00	-44.04
CID-1244	$10.35^{+0.10}_{-0.06}$	$1.47^{+0.06}_{-0.19}$	43.43	44.60	44.06	43.54	-44.59
CID-1245	$10.60^{+0.16}_{-0.10}$	$1.08^{+0.15}_{-0.09}$	43.05	44.26	43.81	43.09	-44.29
CID-1249	$10.99^{+0.31}_{-0.20}$	$2.40^{+0.08}_{-0.04}$	44.03	45.54	44.31	43.67	45.32
CID-1253	$11.27^{+0.25}_{-0.30}$	$2.83^{+0.00}_{-0.07}$	43.73	45.95	44.85	43.87	45.61
CID-1254	$10.58^{+0.16}_{-0.57}$	$2.04^{+0.10}_{-0.00}$	43.00	45.12	44.03	43.48	45.34
CID-1256	$10.70^{+0.00}_{-0.00}$	$1.34^{+0.09}_{-0.14}$	43.14	44.47	44.46	44.10	-44.55
CID-1257	$10.82^{+0.18}_{-0.26}$	$1.64^{+0.00}_{-0.20}$	43.64	44.72	44.51	44.29	-44.89
CID-1259	$10.88^{+0.34}_{-0.53}$	$1.07^{+0.53}_{-0.61}$	44.09	43.71	44.18	0.00	-44.61
CID-1260	$10.91^{+0.00}_{-0.00}$	$1.40^{+0.04}_{-0.09}$	42.62	44.60	44.50	43.13	-44.53
CID-1261	$9.30^{+0.59}_{-0.77}$	$1.48^{+0.01}_{-1.01}$	43.88	43.85	43.60	0.00	-45.09
CID-1267	$10.93^{+0.09}_{-0.05}$	$1.42^{+0.09}_{-0.15}$	43.20	44.56	44.37	0.00	-44.54
CID-1271	$10.44^{+0.40}_{-0.36}$	$1.70^{+0.47}_{-0.00}$	43.98	44.90	43.89	0.00	-44.61
CID-1273	$10.95^{+0.17}_{-0.20}$	$2.49^{+0.05}_{-0.05}$	43.19	45.58	44.07	44.86	45.52
CID-1276	$10.63^{+0.35}_{-0.52}$	$1.66^{+0.11}_{-1.23}$	44.06	43.51	44.23	0.00	-45.29
CID-1279	$10.72^{+0.09}_{-0.04}$	$2.02^{+0.01}_{-0.06}$	43.34	45.07	44.35	44.77	45.21

Table B.2 – continued

ID	log $M_{stellar}$ ($M_\odot$)	log SFR^{tot} ($M_\odot$ yr^{-1})	log $L_{2-10\ keV}$ (erg s^{-1})	log L_{2300} (erg s^{-1})	log L_{5100} (erg s^{-1})	log $L_{6\mu m}$ (erg s^{-1})	log L_{IR} (erg s^{-1})
CID-1280	$11.10^{+0.12}_{-0.02}$	$1.70^{+0.03}_{-0.12}$	43.60	44.71	44.61	44.43	45.20
CID-1283	$10.42^{+0.55}_{-0.60}$	$1.75^{+0.38}_{-0.00}$	43.72	45.08	43.82	0.00	-44.43
CID-1286	$10.78^{+0.34}_{-0.19}$	$1.97^{+0.06}_{-0.03}$	43.72	45.10	44.34	44.68	-45.04
CID-1287	$10.36^{+0.20}_{-0.21}$	$1.95^{+0.00}_{-0.09}$	43.74	45.12	44.05	43.60	45.17
CID-1288	$10.63^{+0.00}_{-0.00}$	$1.23^{+0.10}_{-0.18}$	43.40	44.31	44.21	0.00	-44.44
CID-1290	$10.82^{+0.39}_{-0.47}$	$2.16^{+0.23}_{-0.43}$	43.87	45.17	43.84	0.00	-45.16
CID-1291	$10.48^{+0.00}_{-0.00}$	$0.29^{+0.14}_{-0.34}$	42.95	43.29	44.28	43.43	-44.22
CID-1292	$11.06^{+0.14}_{-0.13}$	$0.43^{+0.10}_{-0.01}$	42.95	43.76	44.40	0.00	0.00
CID-1293	$10.25^{+0.44}_{-0.23}$	$1.26^{+0.51}_{-0.03}$	44.21	44.49	43.94	0.00	-44.58
CID-1294	$10.45^{+0.29}_{-0.18}$	$1.04^{+0.10}_{-0.30}$	43.22	44.10	44.00	0.00	-44.27
CID-1295	$10.82^{+0.00}_{-0.00}$	$1.47^{+0.16}_{-0.00}$	43.26	44.51	44.49	43.83	45.02
CID-1300	$8.85^{+0.37}_{-0.19}$	$0.32^{+0.11}_{-0.99}$	42.80	42.82	42.89	0.00	-43.96
CID-1301	$10.40^{+0.18}_{-0.09}$	$0.22^{+0.12}_{-0.63}$	43.08	42.92	43.83	0.00	-43.83
CID-1306	$10.13^{+0.34}_{-0.18}$	$1.48^{+0.17}_{-0.10}$	43.31	44.77	43.94	0.00	-44.20
CID-1307	$10.89^{+0.25}_{-0.15}$	$1.45^{+0.11}_{-0.18}$	43.38	44.48	44.21	0.00	-44.89
CID-1309	$10.99^{+0.00}_{-0.00}$	$1.49^{+0.05}_{-0.10}$	42.98	44.64	44.45	43.16	-44.27
CID-1310	$11.16^{+0.06}_{-0.08}$	$0.89^{+0.05}_{-0.32}$	42.72	43.89	44.61	0.00	-44.17
CID-1314	$11.08^{+0.10}_{-0.21}$	$1.37^{+0.17}_{-0.21}$	43.55	44.60	44.51	0.00	-44.38
CID-1330	$10.37^{+0.29}_{-0.20}$	$1.09^{+0.31}_{-0.04}$	43.91	44.36	44.05	0.00	-44.19
CID-1335	$10.54^{+0.39}_{-0.17}$	$1.63^{+0.26}_{-0.10}$	43.97	44.84	44.48	0.00	-44.58
CID-1344	$10.35^{+0.20}_{-0.20}$	$1.88^{+0.06}_{-0.01}$	43.83	45.14	43.75	43.96	-44.77
CID-1366	$10.95^{+0.40}_{-0.46}$	$2.00^{+0.23}_{-0.10}$	44.53	45.19	44.34	0.00	-45.28
CID-1401	$10.46^{+0.16}_{-0.02}$	$0.33^{+0.11}_{-0.44}$	42.48	43.23	43.96	0.00	-43.74
CID-1408	$9.68^{+0.35}_{-0.38}$	$0.81^{+0.13}_{-0.09}$	43.36	44.02	43.15	0.00	-43.72
CID-1413	$10.73^{+0.09}_{-0.05}$	$0.68^{+0.06}_{-0.46}$	43.28	43.49	44.30	0.00	-44.18
CID-1414	$10.66^{+0.13}_{-0.14}$	$0.61^{+0.12}_{-0.48}$	42.80	43.38	44.02	43.23	-44.15
CID-1416	$10.76^{+0.19}_{-0.22}$	$1.66^{+0.01}_{-0.24}$	43.72	44.70	44.32	0.00	-44.85
CID-1418	$11.30^{+0.09}_{-0.18}$	$1.74^{+0.06}_{-0.21}$	44.24	44.77	44.94	44.95	-45.11
CID-1419	$10.75^{+0.00}_{-0.00}$	$1.93^{+0.10}_{-0.18}$	43.33	45.12	44.58	43.73	-44.67
CID-1427	$10.43^{+0.13}_{-0.13}$	$0.35^{+0.19}_{-0.56}$	42.82	43.06	43.84	0.00	-43.95
CID-1431	$10.51^{+0.11}_{-0.03}$	$0.12^{+0.22}_{-0.37}$	43.40	42.99	43.99	0.00	-43.74
CID-1433	$10.40^{+0.35}_{-0.16}$	$2.14^{+0.09}_{-0.20}$	43.81	45.28	43.97	44.52	-45.02
CID-1435	$10.70^{+0.09}_{-0.17}$	$1.37^{+0.07}_{-0.02}$	43.00	44.33	43.71	43.35	44.87
CID-1445	$10.29^{+0.25}_{-0.22}$	$1.40^{+0.04}_{-0.03}$	42.94	44.53	43.36	44.30	44.52
CID-1446	$10.50^{+0.13}_{-0.18}$	$1.99^{+0.09}_{-0.02}$	42.91	45.14	44.07	44.35	45.39
CID-1447	$10.85^{+0.18}_{-0.22}$	$2.11^{+0.02}_{-0.33}$	43.92	45.12	44.58	44.80	-45.26
CID-1448	$10.91^{+0.09}_{-0.18}$	$1.37^{+0.06}_{-0.05}$	43.40	44.60	44.42	0.00	-44.20
CID-1450	$10.76^{+0.06}_{-0.08}$	$1.96^{+0.07}_{-0.04}$	43.59	45.18	44.29	43.82	-44.71
CID-1460	$10.16^{+0.33}_{-0.34}$	$1.53^{+0.00}_{-0.14}$	43.28	44.51	43.53	44.36	45.01
CID-1463	$10.58^{+0.16}_{-0.22}$	$0.97^{+0.16}_{-0.10}$	43.94	44.14	44.04	0.00	-44.15

Table B.2 – continued

ID	log $M_{stellar}$ ($M_\odot$)	log SFR^{tot} ($M_\odot$ yr^{-1})	log $L_{2-10\ keV}$ (erg s^{-1})	log L_{2300} (erg s^{-1})	log L_{5100} (erg s^{-1})	log $L_{6\mu m}$ (erg s^{-1})	log L_{IR} (erg s^{-1})
CID-1464	$10.99^{+0.25}_{-0.15}$	$2.92^{+0.11}_{-0.00}$	44.52	46.14	45.36	43.90	45.62
CID-1466	$10.98^{+0.31}_{-0.36}$	$2.12^{+0.00}_{-0.29}$	43.54	45.21	44.10	44.55	-45.04
CID-1467	$10.78^{+0.06}_{-0.20}$	$2.03^{+0.10}_{-0.01}$	42.99	45.06	43.99	42.96	45.12
CID-1468	$10.68^{+0.18}_{-0.15}$	$2.18^{+0.13}_{-0.00}$	43.61	45.40	44.29	44.65	45.79
CID-1472	$10.57^{+0.09}_{-0.08}$	$0.75^{+0.08}_{-0.89}$	42.85	43.18	43.99	0.00	-44.34
CID-1474	$10.63^{+0.26}_{-0.24}$	$1.28^{+0.15}_{-0.53}$	43.50	43.94	44.36	44.52	-44.88
CID-1476	$10.17^{+0.05}_{-0.09}$	$0.96^{+0.07}_{-0.06}$	42.58	43.83	43.82	42.99	44.18
CID-1477	$10.73^{+0.09}_{-0.04}$	$2.01^{+0.12}_{-0.00}$	43.29	45.22	44.44	44.46	44.87
CID-1478	$9.95^{+0.07}_{-0.06}$	$0.07^{+0.16}_{-0.82}$	43.20	42.53	43.61	0.00	-43.65
CID-1480	$10.04^{+0.27}_{-0.37}$	$1.39^{+0.00}_{-0.82}$	43.69	43.69	43.77	0.00	-44.84
CID-1482	$10.68^{+0.16}_{-0.30}$	$1.89^{+0.05}_{-0.35}$	43.97	44.94	44.25	44.40	-45.01
CID-1483	$10.66^{+0.10}_{-0.20}$	$1.27^{+0.16}_{-0.32}$	43.58	44.12	44.06	44.11	-44.79
CID-1488	$10.84^{+0.18}_{-0.04}$	$2.04^{+0.01}_{-0.18}$	43.81	45.22	44.44	43.59	-44.71
CID-1491	$10.56^{+0.06}_{-0.07}$	$0.28^{+0.16}_{-0.29}$	43.13	43.26	43.90	0.00	-43.77
CID-1497	$11.28^{+0.06}_{-0.18}$	$2.29^{+0.04}_{-0.04}$	44.13	45.48	44.76	0.00	-45.27
CID-1499	$10.91^{+0.09}_{-0.18}$	$2.12^{+0.11}_{-0.00}$	43.45	45.35	44.40	44.26	45.63
CID-1503	$11.02^{+0.17}_{-0.10}$	$1.50^{+0.41}_{-0.10}$	44.05	44.60	44.67	0.00	-44.69
CID-1508	$10.87^{+0.15}_{-0.01}$	$1.46^{+0.11}_{-0.00}$	42.53	44.54	44.44	43.98	44.90
CID-1511	$10.83^{+0.00}_{-0.15}$	$1.84^{+0.09}_{-0.00}$	43.28	44.40	44.30	0.00	-45.42
CID-1512	$10.94^{+0.22}_{-0.23}$	$2.07^{+0.20}_{-0.01}$	43.64	43.67	44.22	44.33	45.71
CID-1517	$10.34^{+0.00}_{-0.00}$	$0.31^{+0.12}_{-0.56}$	42.79	43.07	43.97	42.60	-44.13
CID-1518	$10.24^{+0.39}_{-0.23}$	$1.87^{+0.06}_{-0.01}$	43.35	45.17	43.50	0.00	-44.07
CID-1522	$10.34^{+0.09}_{-0.06}$	$1.68^{+0.15}_{-0.00}$	42.88	44.91	44.13	44.35	44.92
CID-1523	$10.23^{+0.31}_{-0.09}$	$1.91^{+0.03}_{-0.13}$	43.29	45.10	44.10	43.59	-44.82
CID-1528	$10.21^{+0.50}_{-0.53}$	$0.91^{+0.65}_{-0.28}$	43.52	43.72	43.83	0.00	-44.43
CID-1531	$10.50^{+0.12}_{-0.02}$	$0.87^{+0.06}_{-1.07}$	42.82	43.03	44.12	43.38	-44.36
CID-1533	$10.61^{+0.31}_{-0.49}$	$2.32^{+0.00}_{-0.15}$	43.81	45.40	43.91	0.00	-45.20
CID-1534	$10.88^{+0.14}_{-0.00}$	$1.66^{+0.07}_{-0.12}$	43.33	44.46	44.54	44.25	45.34
CID-1538	$10.73^{+0.39}_{-0.16}$	$2.78^{+0.38}_{-0.01}$	43.47	45.85	44.72	44.49	45.97
CID-1541	$10.79^{+0.03}_{-0.10}$	$0.70^{+0.04}_{-0.41}$	43.07	43.52	44.25	0.00	-44.07
CID-1546	$10.65^{+0.10}_{-0.36}$	$1.77^{+0.16}_{-0.12}$	43.78	44.98	43.97	44.22	-44.81
CID-1550	$10.45^{+0.14}_{-0.13}$	$0.57^{+0.14}_{-0.70}$	42.99	43.18	43.91	0.00	-44.11
CID-1556	$11.26^{+0.22}_{-0.18}$	$1.49^{+0.31}_{-0.23}$	43.82	44.56	44.50	0.00	-44.69
CID-1559	$10.40^{+0.23}_{-0.23}$	$0.61^{+0.12}_{-0.95}$	43.71	43.04	43.77	0.00	-44.21
CID-1567	$11.01^{+0.16}_{-0.10}$	$1.59^{+0.25}_{-0.38}$	44.10	44.57	44.65	44.82	-45.26
CID-1569	$10.74^{+0.00}_{-0.00}$	$1.23^{+0.10}_{-0.02}$	43.32	44.44	44.43	43.23	-44.62
CID-1572	$10.83^{+0.22}_{-0.16}$	$1.92^{+0.00}_{-0.75}$	44.20	44.51	44.50	0.00	-45.29
CID-1574	$10.95^{+0.05}_{-0.18}$	$1.24^{+0.09}_{-0.06}$	43.69	44.50	44.14	43.87	-44.50
CID-1577	$10.81^{+0.30}_{-0.23}$	$2.67^{+0.40}_{-0.00}$	43.95	45.83	44.65	45.24	45.96
CID-1582	$10.74^{+0.00}_{-0.00}$	$1.28^{+0.16}_{-0.00}$	43.43	44.41	44.67	44.27	44.52

Table B.2 – continued

ID	log $M_{stellar}$ ($M_\odot$)	log SFR^{tot} ($M_\odot$ yr^{-1})	log $L_{2-10\ keV}$ (erg s^{-1})	log L_{2300} (erg s^{-1})	log L_{5100} (erg s^{-1})	log $L_{6\mu m}$ (erg s^{-1})	log L_{IR} (erg s^{-1})
CID-1584	$10.18^{+0.47}_{-0.31}$	$1.47^{+0.11}_{-1.62}$	43.70	43.16	43.97	0.00	-45.19
CID-1586	$10.98^{+0.04}_{-0.10}$	$1.50^{+0.04}_{-0.03}$	44.04	43.73	44.54	44.90	44.62
CID-1589	$10.66^{+0.00}_{-0.00}$	$1.26^{+0.07}_{-0.00}$	43.33	44.35	44.25	43.56	44.54
CID-1591	$11.03^{+0.00}_{-0.00}$	$2.70^{+0.03}_{-0.09}$	44.08	45.88	44.71	45.56	45.73
CID-1598	$10.46^{+0.00}_{-0.00}$	$1.09^{+0.14}_{-0.00}$	42.63	44.14	44.04	43.56	44.37
CID-1606	$10.32^{+0.37}_{-0.31}$	$1.44^{+0.01}_{-0.46}$	44.05	44.31	44.11	0.00	-44.68
CID-1612	$11.06^{+0.10}_{-0.37}$	$1.39^{+0.19}_{-0.29}$	44.08	44.26	44.28	44.40	-45.11
CID-1615	$11.18^{+0.17}_{-0.09}$	$1.81^{+0.03}_{-0.26}$	44.43	44.78	44.51	44.47	-45.12
CID-1618	$10.93^{+0.19}_{-0.28}$	$1.36^{+0.08}_{-0.22}$	43.82	44.47	44.12	0.00	-44.40
CID-1627	$10.94^{+0.08}_{-0.05}$	$2.12^{+0.12}_{-0.01}$	43.61	45.30	44.41	44.46	44.94
CID-1629	$10.38^{+0.19}_{-0.21}$	$1.62^{+0.02}_{-0.17}$	43.86	44.72	44.18	43.51	-44.76
CID-1630	$10.65^{+0.17}_{-0.04}$	$0.58^{+0.14}_{-0.42}$	42.95	43.39	44.21	0.00	-44.04
CID-1633	$10.45^{+0.47}_{-0.53}$	$2.05^{+0.00}_{-0.34}$	43.96	45.01	43.93	0.00	-45.09
CID-1636	$10.69^{+0.20}_{-0.31}$	$1.69^{+0.05}_{-0.10}$	43.69	44.86	44.34	44.30	-44.78
CID-1646	$11.08^{+0.00}_{-0.00}$	$0.75^{+0.08}_{-0.19}$	43.17	43.83	44.55	43.21	-44.24
CID-1651	$10.60^{+0.27}_{-0.45}$	$2.26^{+0.00}_{-0.23}$	43.97	45.29	44.11	0.00	-45.31
CID-1652	$10.65^{+0.00}_{-0.00}$	$0.65^{+0.09}_{-0.55}$	43.12	43.38	44.20	42.92	-44.16
CID-1662	$10.44^{+0.14}_{-0.13}$	$0.61^{+0.12}_{-0.69}$	43.43	43.22	44.12	43.19	-44.52
CID-1664	$10.62^{+0.20}_{-0.06}$	$1.00^{+0.13}_{-0.01}$	43.22	44.29	44.19	43.25	-44.19
CID-1683	$10.62^{+0.17}_{-0.42}$	$1.81^{+0.12}_{-0.12}$	44.32	45.01	44.04	44.73	-44.80
CID-1685	$10.63^{+0.57}_{-0.27}$	$2.01^{+0.36}_{-0.04}$	43.94	45.16	44.28	0.00	-45.24
CID-1687	$10.68^{+0.25}_{-0.24}$	$1.50^{+0.02}_{-0.52}$	44.10	44.38	44.02	44.07	-44.81
CID-1695	$10.58^{+0.20}_{-0.07}$	$1.70^{+0.04}_{-0.03}$	43.49	44.93	44.21	43.88	-44.63
CID-1696	$10.85^{+0.26}_{-0.34}$	$1.93^{+0.60}_{-0.00}$	44.34	45.02	44.77	0.00	44.88
CID-1697	$10.54^{+0.20}_{-0.32}$	$2.07^{+0.00}_{-0.46}$	44.07	45.00	44.35	0.00	-45.26
CID-1701	$10.53^{+0.26}_{-0.16}$	$1.58^{+0.16}_{-0.10}$	42.92	44.79	43.90	43.60	-44.66
CID-1706	$10.42^{+0.00}_{-0.00}$	$1.11^{+0.12}_{-0.28}$	42.74	44.12	44.20	43.42	-44.27
CID-1707	$10.75^{+0.34}_{-0.33}$	$1.72^{+0.18}_{-0.05}$	43.92	44.97	43.89	0.00	-44.38
CID-1711	$10.60^{+0.22}_{-0.09}$	$1.60^{+0.14}_{-0.00}$	43.29	44.23	44.31	44.09	45.35
CID-1735	$9.86^{+0.26}_{-0.28}$	$1.41^{+0.05}_{-0.80}$	43.51	43.88	43.75	44.14	-44.92
CID-1739	$10.08^{+0.23}_{-0.33}$	$1.25^{+0.08}_{-0.16}$	43.32	44.44	43.66	0.00	-44.17
CID-1750	$10.32^{+0.21}_{-0.15}$	$1.76^{+0.08}_{-0.10}$	42.91	44.94	44.06	43.78	-44.55
CID-1752	$10.99^{+0.16}_{-0.23}$	$2.03^{+0.10}_{-0.20}$	43.41	45.20	44.68	44.39	-44.92
CID-1757	$10.35^{+0.06}_{-0.07}$	$1.29^{+0.15}_{-0.08}$	43.55	44.54	43.91	43.55	-44.48
CID-1765	$10.81^{+0.18}_{-0.19}$	$1.80^{+0.22}_{-0.36}$	44.34	44.90	44.53	44.65	-45.30
CID-1769	$10.68^{+0.00}_{-0.00}$	$1.68^{+0.17}_{-0.00}$	43.81	44.40	44.30	44.54	45.29
CID-1771	$10.58^{+0.19}_{-0.08}$	$1.36^{+0.07}_{-0.26}$	43.23	44.35	44.08	43.64	-44.59
CID-1779	$10.57^{+0.00}_{-0.00}$	$0.84^{+0.10}_{-0.87}$	42.76	43.28	44.10	43.18	-44.26
CID-1786	$10.69^{+0.13}_{-0.17}$	$1.82^{+0.11}_{-0.10}$	43.33	45.02	44.33	44.00	-44.80
CID-1790	$11.06^{+0.27}_{-0.20}$	$2.10^{+0.10}_{-0.10}$	43.56	45.32	44.51	44.36	-44.99

Table B.2 – continued

ID	log $M_{stellar}$ ($M_\odot$)	log SFR^{tot} ($M_\odot$ yr^{-1})	log $L_{2-10\ keV}$ (erg s^{-1})	log L_{2300} (erg s^{-1})	log L_{5100} (erg s^{-1})	log $L_{6\mu m}$ (erg s^{-1})	log L_{IR} (erg s^{-1})
CID-1798	$10.74^{+0.25}_{-0.19}$	$1.86^{+0.08}_{-0.05}$	43.38	45.04	44.33	43.68	-44.87
CID-1801	$11.21^{+0.00}_{-0.00}$	$2.39^{+0.04}_{-0.03}$	43.02	45.56	44.85	45.06	45.24
CID-1810	$10.67^{+0.24}_{-0.34}$	$1.17^{+0.24}_{-0.25}$	43.46	44.31	43.95	0.00	-44.49
CID-1831	$10.45^{+0.00}_{-0.00}$	$1.01^{+0.10}_{-0.23}$	42.68	44.16	44.06	0.00	-44.01
CID-1836	$10.58^{+0.04}_{-0.10}$	$1.60^{+0.39}_{-0.00}$	42.89	44.99	44.06	43.02	44.93
CID-1868	$10.82^{+0.46}_{-0.22}$	$2.64^{+0.00}_{-0.07}$	43.81	45.85	44.19	45.14	-44.91
CID-1877	$10.61^{+0.01}_{-0.12}$	$1.31^{+0.12}_{-0.04}$	43.12	44.26	44.16	43.76	44.62
CID-1881	$11.17^{+0.38}_{-0.37}$	$3.09^{+0.00}_{-0.12}$	43.74	46.13	43.94	45.22	45.72
CID-1917	$10.99^{+0.07}_{-0.42}$	$2.86^{+0.00}_{-0.28}$	43.71	45.35	44.47	45.90	46.28
CID-1925	$10.65^{+0.25}_{-0.29}$	$2.30^{+0.13}_{-0.00}$	43.78	45.56	44.42	44.64	-45.26
CID-1932	$10.82^{+0.16}_{-0.11}$	$1.89^{+0.05}_{-0.02}$	43.57	45.12	44.23	44.01	-44.77
CID-1956	$10.98^{+0.18}_{-0.23}$	$1.61^{+0.03}_{-0.72}$	43.69	44.33	44.57	45.18	-45.15
CID-1961	$10.81^{+0.00}_{-0.00}$	$1.32^{+0.11}_{-0.17}$	43.41	44.42	44.41	44.28	-44.29
CID-1972	$11.06^{+0.28}_{-0.18}$	$0.89^{+0.55}_{-0.69}$	43.47	43.57	44.24	0.00	-44.38
CID-1977	$11.25^{+0.29}_{-0.23}$	$1.95^{+0.17}_{-0.08}$	43.68	45.17	44.73	44.80	-45.18
CID-2000	$10.39^{+0.19}_{-0.08}$	$0.94^{+0.10}_{-0.12}$	43.56	44.06	43.97	0.00	-44.10
CID-2002	$10.76^{+0.09}_{-0.07}$	$1.23^{+0.10}_{-0.17}$	42.78	44.34	43.89	43.21	-44.46
CID-2016	$10.99^{+0.03}_{-0.10}$	$1.43^{+0.10}_{-0.08}$	42.81	44.66	44.48	43.21	-44.30
CID-2018	$10.81^{+0.16}_{-0.21}$	$1.48^{+0.07}_{-0.77}$	43.85	44.08	44.28	0.00	-45.08
CID-2027	$10.76^{+0.06}_{-0.08}$	$1.83^{+0.10}_{-0.00}$	43.50	45.10	44.30	0.00	-44.25
CID-2036	$10.96^{+0.06}_{-0.08}$	$1.58^{+0.05}_{-0.02}$	43.15	44.66	44.57	44.19	44.62
CID-2040	$10.62^{+0.25}_{-0.41}$	$2.17^{+0.05}_{-0.28}$	44.30	45.17	44.33	0.00	-45.38
CID-2051	$10.44^{+0.31}_{-0.39}$	$1.68^{+0.06}_{-0.05}$	43.55	44.93	43.74	0.00	-44.09
CID-2057	$10.57^{+0.19}_{-0.20}$	$1.60^{+0.14}_{-0.01}$	43.83	44.85	44.31	43.95	-44.79
CID-2097	$10.70^{+0.00}_{-0.00}$	$1.01^{+0.03}_{-0.04}$	42.94	44.26	44.17	42.99	-44.08
CID-2113	$10.80^{+0.00}_{-0.00}$	$0.68^{+0.05}_{-0.47}$	42.45	43.52	44.34	43.34	-44.26
CID-2125	$10.32^{+0.00}_{-0.00}$	$-0.47^{+0.11}_{-0.03}$	42.73	42.81	43.81	0.00	0.00
CID-2128	$10.28^{+0.17}_{-0.16}$	$0.61^{+0.12}_{-0.93}$	43.87	42.93	43.83	0.00	-44.26
CID-2158	$10.60^{+0.22}_{-0.09}$	$1.11^{+0.12}_{-0.08}$	43.14	44.30	44.20	0.00	-43.98
CID-2177	$11.01^{+0.32}_{-0.39}$	$2.11^{+0.02}_{-0.23}$	44.25	45.11	44.59	0.00	-45.36
CID-2191	$9.97^{+0.28}_{-0.34}$	$1.73^{+0.00}_{-0.66}$	43.99	44.25	44.00	0.00	-45.15
CID-2212	$10.50^{+0.25}_{-0.46}$	$1.93^{+0.04}_{-0.62}$	44.11	44.52	44.39	0.00	-45.38
CID-2223	$10.37^{+0.30}_{-0.37}$	$2.02^{+0.10}_{-0.10}$	43.72	45.16	43.90	44.66	-44.96
CID-2242	$10.64^{+0.14}_{-0.24}$	$1.80^{+0.00}_{-0.98}$	44.13	44.25	44.42	0.00	-45.31
CID-2247	$10.61^{+0.00}_{-0.00}$	$1.13^{+0.11}_{-0.24}$	42.96	44.23	44.14	43.27	-44.26
CID-2309	$10.65^{+0.17}_{-0.14}$	$1.94^{+0.10}_{-0.00}$	43.02	45.20	44.15	43.17	45.17
CID-2310	$10.97^{+0.20}_{-0.09}$	$2.15^{+0.13}_{-0.05}$	43.90	45.34	44.97	44.71	-45.19
CID-2319	$10.31^{+0.22}_{-0.34}$	$1.75^{+0.10}_{-1.03}$	43.94	43.95	44.29	0.00	-45.35
CID-2321	$10.71^{+0.09}_{-0.16}$	$1.15^{+0.09}_{-0.18}$	43.22	44.31	44.21	0.00	-44.12
CID-2323	$10.05^{+0.21}_{-0.24}$	$1.53^{+0.10}_{-0.39}$	43.53	44.33	44.14	0.00	-45.12

Table B.2 – continued

ID	log $M_{stellar}$ ($M_\odot$)	log SFR^{tot} ($M_\odot$ yr^{-1})	log $L_{2-10\ keV}$ (erg s^{-1})	log L_{2300} (erg s^{-1})	log L_{5100} (erg s^{-1})	log $L_{6\mu m}$ (erg s^{-1})	log L_{IR} (erg s^{-1})
CID-2324	$10.72^{+0.10}_{-0.04}$	$1.24^{+0.10}_{-0.09}$	43.01	44.43	44.33	0.00	-44.08
CID-2326	$10.63^{+0.13}_{-0.13}$	$1.73^{+0.10}_{-0.06}$	43.21	44.95	44.33	43.89	-44.73
CID-2327	$11.35^{+0.07}_{-0.07}$	$1.38^{+0.06}_{-0.01}$	43.61	44.10	44.91	44.29	45.07
CID-2356	$10.05^{+0.29}_{-0.28}$	$1.92^{+0.11}_{-0.00}$	42.94	45.11	43.45	42.66	45.25
CID-2413	$10.75^{+0.07}_{-0.07}$	$1.38^{+0.05}_{-0.21}$	43.37	44.50	44.40	43.92	-44.52
CID-2443	$9.61^{+0.24}_{-0.37}$	$1.19^{+0.11}_{-0.67}$	43.25	43.79	43.60	0.00	-44.85
CID-2454	$10.94^{+0.00}_{-0.00}$	$1.41^{+0.12}_{-0.08}$	42.82	44.64	44.46	43.46	-44.29
CID-2460	$11.24^{+0.14}_{-0.13}$	$1.62^{+0.21}_{-0.04}$	43.18	44.87	44.77	0.00	-44.47
CID-2462	$10.60^{+0.30}_{-0.22}$	$1.79^{+0.04}_{-0.19}$	43.69	44.89	44.33	44.28	-44.97
CID-2477	$10.64^{+0.14}_{-0.13}$	$1.28^{+0.05}_{-0.28}$	43.27	44.31	44.13	43.46	-44.51
CID-2482	$10.65^{+0.22}_{-0.28}$	$1.86^{+0.13}_{-0.16}$	44.06	44.85	44.62	0.00	-45.27
CID-2484	$10.59^{+0.26}_{-0.19}$	$1.16^{+0.08}_{-0.33}$	43.89	44.24	44.14	0.00	-44.22
CID-2501	$10.53^{+0.09}_{-0.05}$	$0.25^{+0.19}_{-0.27}$	42.70	43.24	43.88	0.00	-43.74
CID-2504	$10.52^{+0.50}_{-0.22}$	$2.11^{+0.01}_{-0.32}$	43.87	45.12	44.43	0.00	-45.34
CID-2507	$10.66^{+0.22}_{-0.25}$	$1.86^{+0.07}_{-0.00}$	43.44	45.12	44.16	44.02	-44.82
CID-2508	$10.54^{+0.24}_{-0.19}$	$1.73^{+0.00}_{-0.06}$	43.72	44.91	43.96	44.00	-44.69
CID-2512	$10.64^{+0.12}_{-0.14}$	$1.08^{+0.06}_{-0.12}$	42.87	44.17	43.89	43.04	-44.42
CID-2526	$10.50^{+0.32}_{-0.29}$	$1.71^{+0.11}_{-0.46}$	43.76	44.70	44.16	0.00	-45.19
CID-2544	$10.19^{+0.03}_{-0.10}$	$0.50^{+0.14}_{-0.05}$	42.99	43.76	43.66	0.00	-43.19
CID-2574	$10.50^{+0.38}_{-0.15}$	$1.96^{+0.07}_{-0.15}$	43.83	45.12	44.24	44.42	-44.93
CID-2584	$10.84^{+0.14}_{-0.13}$	$1.87^{+0.06}_{-0.01}$	43.23	45.14	44.51	0.00	-44.22
CID-2587	$11.41^{+0.00}_{-0.00}$	$1.91^{+0.12}_{-0.00}$	42.98	44.80	44.99	44.13	45.37
CID-2611	$10.99^{+0.00}_{-0.00}$	$1.50^{+0.13}_{-0.00}$	42.62	44.65	44.47	43.73	44.54
CID-2646	$10.55^{+0.32}_{-0.34}$	$1.57^{+0.13}_{-0.26}$	44.05	44.57	44.06	0.00	-45.13
CID-2655	$10.00^{+0.63}_{-0.17}$	$1.80^{+0.20}_{-0.32}$	44.24	44.96	43.74	0.00	-44.66
CID-2682	$11.14^{+0.08}_{-0.06}$	$1.75^{+0.18}_{-0.28}$	43.86	44.82	44.90	45.02	-45.07
CID-2698	$10.10^{+0.51}_{-0.27}$	$1.82^{+0.17}_{-0.30}$	43.81	44.85	43.89	0.00	-45.27
CID-2704	$10.50^{+0.23}_{-0.16}$	$0.93^{+0.11}_{-0.16}$	43.22	44.06	43.87	0.00	-44.10
CID-2706	$10.33^{+0.09}_{-0.07}$	$1.47^{+0.06}_{-0.06}$	42.98	44.68	43.81	43.78	-44.53
CID-2728	$10.84^{+0.00}_{-0.00}$	$1.51^{+0.02}_{-0.30}$	43.74	44.53	44.78	44.95	-44.82
CID-2738	$10.07^{+0.12}_{-0.16}$	$0.39^{+0.20}_{-0.15}$	42.64	43.52	43.60	42.83	-44.17
CID-2748	$10.20^{+0.37}_{-0.35}$	$1.52^{+0.11}_{-0.20}$	43.52	43.88	43.53	0.00	-45.10
CID-2756	$10.88^{+0.11}_{-0.16}$	$1.39^{+0.14}_{-0.00}$	43.36	44.57	44.39	44.00	44.78
CID-2757	$10.85^{+0.17}_{-0.04}$	$1.46^{+0.08}_{-0.00}$	42.96	44.64	44.54	43.31	-44.51
CID-2761	$10.60^{+0.36}_{-0.46}$	$1.98^{+0.00}_{-1.19}$	43.94	44.04	44.20	0.00	-45.28
CID-2762	$10.65^{+0.09}_{-0.41}$	$1.34^{+0.36}_{-0.51}$	43.65	44.22	44.14	0.00	-44.75
CID-2773	$10.13^{+0.34}_{-0.39}$	$0.98^{+0.16}_{-0.12}$	42.92	44.15	43.51	42.91	-44.43
CID-2819	$10.51^{+0.24}_{-0.28}$	$1.03^{+0.54}_{-0.50}$	43.73	43.90	44.10	0.00	-44.53
CID-2822	$11.05^{+0.00}_{-0.00}$	$0.76^{+0.08}_{-0.20}$	43.32	43.87	44.69	0.00	-43.96
CID-2828	$10.16^{+0.42}_{-0.32}$	$1.29^{+0.11}_{-1.07}$	43.68	43.43	43.92	0.00	-45.00

Table B.2 – continued

ID	log $M_{stellar}$ ($M_\odot$)	log SFR^{tot} ($M_\odot$ yr^{-1})	log $L_{2-10\ keV}$ (erg s^{-1})	log L_{2300} (erg s^{-1})	log L_{5100} (erg s^{-1})	log $L_{6\mu m}$ (erg s^{-1})	log L_{IR} (erg s^{-1})
CID-2835	$10.42^{+0.18}_{-0.09}$	$1.25^{+0.08}_{-0.02}$	42.80	44.22	44.03	43.60	44.89
CID-2844	$10.03^{+0.31}_{-0.41}$	$1.66^{+0.03}_{-0.85}$	43.95	44.01	44.00	0.00	-45.24
CID-2847	$9.74^{+0.64}_{-0.67}$	$0.84^{+0.25}_{-0.81}$	42.94	43.48	42.85	0.00	-44.29
CID-2848	$10.86^{+0.16}_{-0.02}$	$0.95^{+0.08}_{-0.00}$	43.11	43.59	44.23	43.65	44.40
CID-2852	$11.22^{+0.16}_{-0.11}$	$1.64^{+0.10}_{-0.18}$	43.40	44.80	44.62	0.00	-44.51
CID-2856	$10.45^{+0.20}_{-0.41}$	$1.26^{+0.21}_{-0.43}$	43.47	44.11	44.07	44.61	-44.85
CID-2862	$10.79^{+0.22}_{-0.09}$	$0.77^{+0.06}_{-0.00}$	42.99	43.56	44.29	43.36	44.16
CID-2865	$10.82^{+0.15}_{-0.16}$	$0.88^{+0.28}_{-0.73}$	43.92	43.45	44.35	0.00	-44.44
CID-2866	$10.69^{+0.25}_{-0.27}$	$1.76^{+0.06}_{-0.64}$	44.10	44.46	44.38	0.00	-45.29
CID-2891	$10.51^{+0.11}_{-0.03}$	$1.52^{+0.03}_{-0.12}$	42.92	44.32	44.14	43.64	44.81
CID-2919	$10.57^{+0.25}_{-0.37}$	$1.85^{+0.16}_{-0.19}$	43.59	44.99	44.12	44.20	-45.06
CID-2933	$10.37^{+0.26}_{-0.19}$	$0.87^{+0.15}_{-0.24}$	43.31	43.97	43.79	0.00	-44.10
CID-2936	$10.66^{+0.28}_{-0.25}$	$1.72^{+0.13}_{-0.66}$	43.93	44.59	44.50	0.00	-45.28
CID-2939	$10.65^{+0.35}_{-0.23}$	$1.15^{+0.54}_{-0.00}$	44.05	44.40	44.22	0.00	-44.57
CID-2946	$10.77^{+0.21}_{-0.06}$	$2.08^{+0.05}_{-0.12}$	43.06	45.30	44.24	43.64	-44.64
CID-2948	$11.06^{+0.12}_{-0.15}$	$0.49^{+0.93}_{-0.00}$	43.14	43.78	44.42	43.50	-44.55
CID-2956	$10.66^{+0.16}_{-0.03}$	$1.24^{+0.09}_{-0.15}$	43.22	44.39	44.30	0.00	-44.26
CID-2985	$10.84^{+0.24}_{-0.26}$	$1.97^{+0.07}_{-0.01}$	43.63	45.24	43.88	43.80	-44.76
CID-3042	$10.37^{+0.25}_{-0.23}$	$2.28^{+0.00}_{-0.11}$	43.22	45.43	44.21	44.30	-45.09
CID-3051	$11.07^{+0.16}_{-0.16}$	$2.95^{+0.02}_{-0.08}$	44.39	46.12	44.63	44.81	45.47
CID-3060	$10.52^{+0.10}_{-0.04}$	$0.52^{+0.11}_{-0.51}$	43.33	43.24	43.97	0.00	-43.99
CID-3061	$10.86^{+0.15}_{-0.02}$	$1.95^{+0.09}_{-0.09}$	43.08	45.14	44.43	44.17	-44.69
CID-3118	$11.02^{+0.16}_{-0.16}$	$0.65^{+0.08}_{-0.28}$	43.21	43.63	44.01	0.00	-44.06
CID-3122	$11.24^{+0.00}_{-0.00}$	$0.85^{+0.09}_{-0.33}$	43.19	43.90	44.71	43.80	-44.19
CID-3147	$10.84^{+0.14}_{-0.14}$	$1.83^{+0.11}_{-0.00}$	43.71	45.08	44.27	43.84	-44.88
CID-3171	$10.69^{+0.00}_{-0.00}$	$1.19^{+0.15}_{-0.00}$	42.39	44.37	44.36	43.51	44.94
CID-3178	$11.16^{+0.05}_{-0.08}$	$1.67^{+0.06}_{-0.07}$	43.34	44.87	44.69	0.00	-44.28
CID-3189	$10.67^{+0.23}_{-0.40}$	$1.96^{+0.07}_{-0.09}$	43.22	45.17	43.95	43.69	-44.72
CID-3211	$11.14^{+0.07}_{-0.15}$	$2.48^{+0.06}_{-0.01}$	43.49	45.50	44.61	44.09	45.79
CID-3216	$10.98^{+0.16}_{-0.09}$	$1.49^{+0.14}_{-0.00}$	43.32	44.64	44.37	43.91	45.09
CID-3223	$10.75^{+0.31}_{-0.20}$	$2.61^{+0.03}_{-0.28}$	44.25	45.62	44.74	45.46	45.58
CID-3227	$11.30^{+0.14}_{-0.24}$	$1.76^{+0.20}_{-0.23}$	43.83	44.91	44.64	45.07	-45.25
CID-3228	$10.91^{+0.39}_{-0.27}$	$2.07^{+0.16}_{-0.12}$	43.60	45.36	44.29	44.45	-44.94
CID-3234	$11.15^{+0.34}_{-0.16}$	$2.22^{+0.31}_{-0.00}$	43.74	45.50	44.58	43.99	45.80
CID-3244	$10.26^{+0.51}_{-0.26}$	$2.00^{+0.15}_{-0.39}$	44.01	45.09	44.10	44.52	-45.24
CID-3247	$10.71^{+0.11}_{-0.03}$	$0.60^{+0.14}_{-0.38}$	43.49	43.51	44.23	0.00	-44.11
CID-3270	$10.94^{+0.07}_{-0.06}$	$1.11^{+0.13}_{-0.67}$	43.63	43.70	44.78	44.26	-44.84
CID-3282	$10.32^{+0.36}_{-0.32}$	$2.15^{+0.00}_{-0.09}$	43.60	45.29	43.80	43.80	-44.84
CID-3284	$10.99^{+0.21}_{-0.38}$	$2.16^{+0.05}_{-0.14}$	44.10	45.28	44.33	44.62	-45.02
CID-3288	$10.26^{+0.16}_{-0.02}$	$0.40^{+0.04}_{-0.64}$	42.75	43.00	43.90	0.00	-43.92

Table B.2 – continued

ID	log $M_{stellar}$ ($M_\odot$)	log SFR^{tot} ($M_\odot$ yr^{-1})	log $L_{2-10\ keV}$ (erg s^{-1})	log L_{2300} (erg s^{-1})	log L_{5100} (erg s^{-1})	log $L_{6\mu m}$ (erg s^{-1})	log L_{IR} (erg s^{-1})
CID-3294	$10.28^{+0.29}_{-0.45}$	$1.56^{+0.06}_{-0.61}$	43.74	44.27	43.86	43.94	-45.06
CID-3321	$10.52^{+0.09}_{-0.04}$	$1.29^{+0.04}_{-0.22}$	43.34	44.29	44.19	44.17	-44.64
CID-3334	$10.30^{+0.38}_{-0.32}$	$1.88^{+0.02}_{-0.25}$	43.77	44.88	43.80	0.00	-44.62
CID-3339	$10.38^{+0.23}_{-0.55}$	$1.95^{+0.09}_{-0.10}$	43.70	45.06	43.76	44.03	-45.00
CID-3344	$11.14^{+0.00}_{-0.00}$	$0.95^{+0.08}_{-0.38}$	42.68	43.88	44.69	43.47	-44.48
CID-3371	$10.57^{+0.05}_{-0.09}$	$1.16^{+0.07}_{-0.11}$	43.20	44.32	44.22	43.48	-44.42
CID-3384	$9.71^{+0.50}_{-0.43}$	$1.53^{+0.00}_{-1.38}$	44.06	43.44	43.69	0.00	-45.07
CID-3429	$10.39^{+0.26}_{-0.25}$	$2.48^{+0.06}_{-0.11}$	43.62	45.48	44.35	44.73	45.83
CID-3430	$10.61^{+0.21}_{-0.07}$	$1.26^{+0.17}_{-0.00}$	42.98	44.24	44.23	43.79	44.95
CID-3431	$10.71^{+0.38}_{-0.28}$	$2.54^{+0.00}_{-0.17}$	43.83	45.48	44.18	44.17	45.69
CID-3439	$10.56^{+0.05}_{-0.13}$	$0.89^{+0.04}_{-0.03}$	42.61	44.10	43.65	43.13	43.83
CID-3443	$10.28^{+0.44}_{-0.30}$	$2.11^{+0.00}_{-0.27}$	43.85	45.20	44.02	0.00	-45.02
CID-3455	$11.14^{+0.35}_{-0.34}$	$3.00^{+0.00}_{-0.26}$	43.91	46.05	44.75	44.53	45.72
CID-3468	$10.67^{+0.10}_{-0.27}$	$0.62^{+0.11}_{-0.73}$	43.40	43.25	43.98	0.00	-44.22
CID-3495	$11.05^{+0.29}_{-0.16}$	$2.22^{+0.21}_{-0.02}$	44.11	45.39	44.40	44.95	45.69
CID-3512	$11.25^{+0.20}_{-0.12}$	$1.79^{+0.10}_{-0.12}$	43.70	44.89	44.53	0.00	-45.11
CID-3513	$10.74^{+0.00}_{-0.00}$	$1.95^{+0.08}_{-0.04}$	43.44	45.13	44.50	43.59	-44.74
CID-3529	$10.88^{+0.17}_{-0.28}$	$2.08^{+0.00}_{-0.42}$	44.58	45.11	44.31	45.05	-45.25
CID-3545	$10.51^{+0.11}_{-0.02}$	$0.73^{+0.10}_{-0.00}$	43.40	44.04	43.94	43.20	-44.05
CID-3546	$10.39^{+0.54}_{-0.25}$	$2.45^{+0.00}_{-0.27}$	44.00	45.39	44.18	0.00	-45.35
CID-3548	$10.09^{+0.25}_{-0.54}$	$0.95^{+0.08}_{-0.77}$	43.27	43.54	43.62	0.00	-44.43
CID-3549	$10.55^{+0.07}_{-0.06}$	$0.64^{+0.09}_{-0.63}$	43.01	43.27	44.09	0.00	-44.22
CID-3554	$10.68^{+0.00}_{-0.00}$	$1.23^{+0.10}_{-0.18}$	43.30	44.40	44.31	0.00	-44.13
CID-3568	$10.70^{+0.12}_{-0.02}$	$1.29^{+0.14}_{-0.00}$	42.63	44.42	44.32	43.11	44.89
CID-3577	$10.23^{+0.55}_{-0.31}$	$1.88^{+0.00}_{-0.31}$	43.77	44.87	43.65	0.00	-45.00
CID-3583	$10.75^{+0.19}_{-0.17}$	$1.69^{+0.00}_{-0.53}$	43.19	44.43	44.34	0.00	-45.05
CID-3603	$10.91^{+0.19}_{-0.31}$	$1.65^{+0.36}_{-0.18}$	43.67	44.85	44.21	0.00	-44.53
CID-3612	$10.68^{+0.25}_{-0.37}$	$0.94^{+0.53}_{-0.52}$	43.82	43.87	43.92	0.00	-44.49
CID-3629	$10.50^{+0.00}_{-0.00}$	$1.08^{+0.15}_{-0.25}$	43.12	44.14	44.22	43.77	-44.51
CID-3632	$10.80^{+0.18}_{-0.09}$	$1.16^{+0.08}_{-0.12}$	42.85	44.37	44.28	0.00	-44.09
CID-3635	$10.74^{+0.21}_{-0.16}$	$1.87^{+0.07}_{-0.03}$	43.46	45.16	44.38	0.00	-44.31
CID-3642	$10.65^{+0.16}_{-0.03}$	$1.06^{+0.08}_{-0.00}$	43.40	44.37	44.18	43.77	-44.55
CID-3643	$9.73^{+0.18}_{-0.18}$	$1.56^{+0.07}_{-0.00}$	42.85	44.77	43.77	43.56	44.75
CID-3648	$10.68^{+0.11}_{-0.16}$	$0.51^{+0.01}_{-0.54}$	43.19	43.31	43.95	0.00	-43.96
CID-3715	$11.00^{+0.00}_{-0.00}$	$1.68^{+0.06}_{-0.07}$	43.53	44.78	44.68	0.00	44.76
CID-3734	$10.57^{+0.30}_{-0.38}$	$2.21^{+0.10}_{-0.03}$	44.18	45.44	44.21	0.00	-45.22
CID-3760	$10.90^{+0.25}_{-0.20}$	$1.72^{+0.00}_{-0.43}$	44.04	44.52	44.25	44.22	-45.13
CID-3787	$10.21^{+0.34}_{-0.53}$	$1.87^{+0.04}_{-0.56}$	44.03	44.67	44.51	44.58	-45.28
CID-3789	$10.70^{+0.10}_{-0.17}$	$1.31^{+0.11}_{-0.06}$	43.38	44.42	44.23	0.00	-44.56
CID-3806	$9.76^{+0.31}_{-0.27}$	$1.81^{+0.00}_{-1.11}$	44.21	44.14	43.96	0.00	-45.19

Table B.2 – continued

ID	log $M_{stellar}$ ($M_\odot$)	log SFR^{tot} ($M_\odot$ yr^{-1})	log $L_{2-10\ keV}$ (erg s^{-1})	log L_{2300} (erg s^{-1})	log L_{5100} (erg s^{-1})	log $L_{6\mu m}$ (erg s^{-1})	log L_{IR} (erg s^{-1})
CID-3807	$11.44^{+0.00}_{-0.16}$	$1.92^{+0.12}_{-0.24}$	44.26	45.09	45.17	44.95	-45.24
CID-10599	$10.64^{+0.16}_{-0.12}$	$1.72^{+0.18}_{-0.00}$	43.18	45.07	44.47	44.13	-44.56
CID-10972	$11.11^{+0.41}_{-0.13}$	$2.57^{+0.16}_{-0.00}$	43.99	45.84	44.54	45.20	45.77
CID-11178	$10.21^{+0.30}_{-0.16}$	$1.44^{+0.04}_{-0.81}$	43.78	43.94	44.20	0.00	-45.03
CID-11257	$11.05^{+0.00}_{-0.00}$	$0.82^{+0.11}_{-0.00}$	42.82	43.80	44.44	43.95	44.84
CID-11566	$10.71^{+0.22}_{-0.17}$	$1.95^{+0.14}_{-0.09}$	43.12	45.13	44.29	44.05	45.33
CID-12145	$10.43^{+0.23}_{-0.20}$	$0.57^{+0.06}_{-0.70}$	43.08	43.13	43.68	0.00	-44.15
CID-12457	$11.33^{+0.20}_{-0.28}$	$1.88^{+0.14}_{-0.29}$	44.25	44.92	44.92	0.00	-45.00
CID-12500	$10.42^{+0.13}_{-0.16}$	$1.47^{+0.06}_{-0.09}$	43.41	44.70	44.16	43.98	-44.78
CID-12512	$10.38^{+0.42}_{-0.35}$	$1.64^{+0.29}_{-0.08}$	43.55	44.84	43.98	0.00	-44.62
CID-12650	$10.88^{+0.00}_{-0.00}$	$1.75^{+0.09}_{-0.00}$	43.16	44.58	44.48	44.01	45.33
CID-21192	$10.79^{+0.03}_{-0.10}$	$1.43^{+0.11}_{-0.20}$	43.04	44.47	44.38	43.52	-44.46
LID-38	$10.92^{+0.00}_{-0.00}$	$0.75^{+0.15}_{-0.41}$	42.57	43.65	44.29	0.00	-44.08
LID-74	$10.17^{+0.05}_{-0.09}$	$0.67^{+0.07}_{-0.09}$	42.91	43.83	43.82	0.00	-43.76
LID-106	$10.63^{+0.27}_{-0.23}$	$2.12^{+0.01}_{-0.05}$	43.43	45.33	44.17	44.63	-44.74
LID-130	$10.43^{+0.00}_{-0.00}$	$0.67^{+0.11}_{-0.82}$	43.53	43.16	44.07	44.01	-44.07
LID-131	$10.60^{+0.02}_{-0.12}$	$0.78^{+0.14}_{-0.08}$	43.13	44.00	43.80	0.00	-43.68
LID-132	$11.29^{+0.11}_{-0.12}$	$1.82^{+0.12}_{-0.24}$	44.32	44.89	44.71	43.96	-45.08
LID-136	$10.65^{+0.14}_{-0.13}$	$1.06^{+0.08}_{-0.12}$	43.40	44.22	43.87	0.00	-44.24
LID-139	$9.82^{+0.65}_{-0.33}$	$1.60^{+0.14}_{-0.01}$	43.78	44.86	44.29	0.00	-44.09
LID-141	$10.23^{+0.19}_{-0.05}$	$0.77^{+0.07}_{-0.15}$	43.04	43.92	43.91	0.00	-43.83
LID-144	$10.74^{+0.08}_{-0.06}$	$1.36^{+0.08}_{-0.00}$	43.15	44.42	44.33	43.80	45.11
LID-150	$10.87^{+0.26}_{-0.25}$	$2.09^{+0.05}_{-0.34}$	44.39	45.10	44.64	0.00	-45.35
LID-151	$10.98^{+0.04}_{-0.09}$	$1.78^{+0.13}_{-0.25}$	43.90	44.66	44.91	0.00	-45.28
LID-152	$10.90^{+0.12}_{-0.02}$	$1.96^{+0.08}_{-0.03}$	42.42	45.14	44.42	43.70	44.80
LID-155	$9.93^{+0.17}_{-0.20}$	$1.12^{+0.12}_{-0.05}$	42.30	44.35	43.74	0.00	-43.71
LID-156	$10.86^{+0.16}_{-0.02}$	$1.28^{+0.06}_{-0.05}$	42.97	44.51	44.32	0.00	-44.06
LID-157	$10.59^{+0.00}_{-0.00}$	$0.09^{+0.04}_{-0.03}$	42.89	43.33	44.14	42.83	-42.31
LID-176	$10.72^{+0.10}_{-0.03}$	$1.34^{+0.16}_{-0.29}$	42.76	44.37	44.27	43.84	-44.45
LID-179	$10.32^{+0.62}_{-0.29}$	$2.20^{+0.61}_{-0.00}$	43.74	45.23	44.09	0.00	-45.71
LID-180	$10.33^{+0.44}_{-0.31}$	$2.26^{+0.00}_{-0.53}$	44.21	45.15	44.01	0.00	-45.19
LID-184	$10.22^{+0.28}_{-0.20}$	$1.33^{+0.10}_{-0.12}$	43.94	44.53	43.99	0.00	-44.26
LID-185	$11.05^{+0.17}_{-0.13}$	$2.96^{+0.07}_{-0.03}$	43.95	46.10	44.66	45.07	46.29
LID-188	$10.90^{+0.00}_{-0.00}$	$0.56^{+0.09}_{-0.37}$	43.02	43.50	44.58	0.00	-43.99
LID-189	$10.13^{+0.09}_{-0.05}$	$0.94^{+0.09}_{-0.40}$	42.89	43.83	43.82	43.73	-44.52
LID-192	$10.85^{+0.00}_{-0.00}$	$1.39^{+0.05}_{-0.05}$	43.33	44.50	44.49	43.94	44.90
LID-195	$9.87^{+0.25}_{-0.26}$	$0.60^{+0.14}_{-0.06}$	42.88	43.82	43.28	0.00	-43.41
LID-200	$11.13^{+0.00}_{-0.00}$	$1.65^{+0.08}_{-0.00}$	42.97	44.83	44.73	43.96	44.70
LID-228	$10.19^{+0.39}_{-0.44}$	$1.96^{+0.04}_{-0.17}$	43.89	45.09	43.78	0.00	-44.54
LID-229	$10.06^{+0.11}_{-0.16}$	$1.34^{+0.09}_{-0.17}$	42.98	44.47	43.87	43.43	-44.47

Table B.2 – continued

ID	log $M_{stellar}$ ($M_\odot$)	log SFR^{tot} ($M_\odot$ yr^{-1})	log $L_{2-10\ keV}$ (erg s^{-1})	log L_{2300} (erg s^{-1})	log L_{5100} (erg s^{-1})	log $L_{6\mu m}$ (erg s^{-1})	log L_{IR} (erg s^{-1})
LID-234	$10.17^{+0.53}_{-0.53}$	$1.04^{+0.16}_{-0.40}$	43.74	43.95	43.68	0.00	-44.48
LID-239	$9.88^{+0.39}_{-0.35}$	$1.16^{+0.19}_{-0.15}$	43.30	44.24	43.70	0.00	-44.44
LID-240	$11.05^{+0.14}_{-0.13}$	$1.85^{+0.08}_{-0.13}$	42.18	45.06	43.98	44.09	44.29
LID-241	$10.93^{+0.21}_{-0.27}$	$1.24^{+0.10}_{-0.07}$	43.53	44.45	44.18	0.00	-44.25
LID-242	$10.85^{+0.28}_{-0.20}$	$2.11^{+0.06}_{-0.16}$	43.71	45.27	44.49	44.00	-45.10
LID-245	$10.67^{+0.15}_{-0.01}$	$1.21^{+0.12}_{-0.29}$	43.09	44.31	44.38	43.30	-44.36
LID-246	$10.26^{+0.36}_{-0.42}$	$1.41^{+0.43}_{-0.48}$	43.92	44.32	44.12	0.00	-45.26
LID-251	$10.23^{+0.51}_{-0.37}$	$2.11^{+0.00}_{-0.23}$	43.78	45.13	44.00	0.00	-45.29
LID-252	$10.63^{+0.14}_{-0.13}$	$1.17^{+0.06}_{-0.27}$	43.38	44.22	44.12	43.44	-44.47
LID-253	$10.85^{+0.07}_{-0.47}$	$2.19^{+0.14}_{-0.05}$	43.69	44.78	44.43	44.40	45.81
LID-255	$11.03^{+0.16}_{-0.12}$	$1.58^{+0.05}_{-0.09}$	44.12	44.73	44.37	44.11	-44.58
LID-256	$10.74^{+0.08}_{-0.06}$	$1.06^{+0.08}_{-0.04}$	43.20	43.97	44.14	44.06	44.47
LID-258	$10.44^{+0.26}_{-0.41}$	$1.89^{+0.14}_{-0.08}$	43.84	45.17	43.96	43.90	-44.80
LID-260	$9.54^{+0.44}_{-0.31}$	$1.32^{+0.21}_{-0.00}$	42.78	44.48	43.27	0.00	-44.72
LID-261	$10.81^{+0.43}_{-0.30}$	$2.48^{+0.06}_{-0.01}$	43.83	45.75	44.08	44.56	-45.05
LID-262	$10.48^{+0.17}_{-0.15}$	$1.78^{+0.06}_{-0.08}$	43.06	44.99	44.03	43.99	-44.61
LID-265	$10.76^{+0.18}_{-0.31}$	$1.74^{+0.07}_{-0.71}$	43.90	44.39	44.64	0.00	-45.32
LID-267	$11.32^{+0.23}_{-0.18}$	$2.63^{+0.10}_{-0.00}$	43.90	45.86	44.80	44.90	45.58
LID-269	$10.51^{+0.40}_{-0.18}$	$2.36^{+0.08}_{-0.00}$	44.73	45.60	44.46	0.00	-44.95
LID-272	$11.35^{+0.06}_{-0.07}$	$1.65^{+0.00}_{-0.79}$	44.69	44.09	45.17	0.00	-45.16
LID-273	$10.83^{+0.26}_{-0.37}$	$2.00^{+0.03}_{-0.13}$	44.32	45.18	44.34	44.43	-44.88
LID-275	$11.35^{+0.44}_{-0.56}$	$-0.04^{+0.08}_{-0.00}$	43.40	43.25	44.28	0.00	0.00
LID-279	$10.12^{+0.21}_{-0.30}$	$1.55^{+0.08}_{-0.00}$	43.54	44.80	43.98	43.55	-44.47
LID-281	$11.00^{+0.29}_{-0.29}$	$2.75^{+0.00}_{-0.08}$	43.62	45.91	44.91	44.99	-45.10
LID-282	$11.26^{+0.09}_{-0.32}$	$2.52^{+0.04}_{-0.05}$	44.15	45.39	44.52	44.58	45.85
LID-288	$10.78^{+0.25}_{-0.35}$	$2.51^{+0.21}_{-0.05}$	44.44	45.72	45.07	44.78	-45.16
LID-290	$10.78^{+0.10}_{-0.09}$	$1.37^{+0.06}_{-0.17}$	44.17	44.47	44.29	43.92	-44.58
LID-292	$9.82^{+0.32}_{-0.35}$	$0.71^{+0.03}_{-0.81}$	43.03	43.42	43.49	0.00	-44.18
LID-295	$10.74^{+0.20}_{-0.30}$	$1.37^{+0.30}_{-0.62}$	43.59	44.03	44.15	0.00	-45.21
LID-297	$9.96^{+0.44}_{-0.11}$	$1.38^{+0.06}_{-0.25}$	43.93	44.49	44.06	0.00	-44.56
LID-298	$11.08^{+0.25}_{-0.28}$	$2.24^{+0.19}_{-0.03}$	43.84	45.46	44.54	43.93	45.22
LID-299	$10.53^{+0.14}_{-0.04}$	$2.44^{+0.19}_{-0.00}$	43.37	45.74	44.78	44.03	45.42
LID-300	$10.65^{+0.23}_{-0.12}$	$1.71^{+0.03}_{-0.04}$	43.43	44.88	44.43	43.41	44.74
LID-302	$11.40^{+0.35}_{-0.41}$	$2.84^{+0.10}_{-0.00}$	44.69	46.06	44.69	44.22	45.51
LID-303	$10.66^{+0.20}_{-0.24}$	$1.59^{+0.05}_{-0.02}$	43.64	44.47	44.10	44.71	45.03
LID-306	$10.67^{+0.22}_{-0.29}$	$2.13^{+0.10}_{-0.07}$	43.64	45.28	43.77	44.39	45.15
LID-308	$10.56^{+0.18}_{-0.22}$	$1.13^{+0.10}_{-0.09}$	43.15	44.07	43.62	43.04	44.84
LID-310	$10.35^{+0.13}_{-0.06}$	$1.51^{+0.13}_{-0.02}$	43.50	44.78	44.18	44.24	45.04
LID-311	$11.40^{+0.20}_{-0.08}$	$2.04^{+0.20}_{-0.00}$	43.90	45.12	44.85	45.66	45.52
LID-312	$10.92^{+0.09}_{-0.04}$	$2.17^{+0.06}_{-0.01}$	42.64	45.25	44.36	44.33	45.22

Table B.2 – continued

ID	log $M_{stellar}$ ($M_\odot$)	log SFR^{tot} ($M_\odot$ yr^{-1})	log $L_{2-10\ keV}$ (erg s^{-1})	log L_{2300} (erg s^{-1})	log L_{5100} (erg s^{-1})	log $L_{6\mu m}$ (erg s^{-1})	log L_{IR} (erg s^{-1})
LID-313	$10.91^{+0.13}_{-0.18}$	$1.16^{+0.07}_{-0.07}$	43.24	44.39	43.86	43.54	-44.51
LID-315	$10.61^{+0.00}_{-0.13}$	$1.18^{+0.15}_{-0.05}$	43.31	44.38	44.37	43.74	-44.65
LID-317	$10.49^{+0.39}_{-0.29}$	$2.00^{+0.00}_{-0.41}$	43.53	44.95	43.95	0.00	-45.22
LID-318	$10.42^{+0.17}_{-0.26}$	$0.99^{+0.16}_{-0.33}$	42.97	43.99	43.98	0.00	-44.35
LID-319	$11.64^{+0.18}_{-0.04}$	$1.97^{+0.15}_{-0.00}$	43.86	44.46	44.62	45.60	45.71
LID-321	$10.62^{+0.30}_{-0.31}$	$1.46^{+0.07}_{-1.28}$	43.35	43.47	44.19	0.00	-44.98
LID-327	$11.19^{+0.19}_{-0.12}$	$0.94^{+0.19}_{-0.04}$	43.30	44.15	44.23	43.20	-44.18
LID-329	$10.88^{+1.22}_{-0.70}$	$1.09^{+0.04}_{-1.58}$	43.04	42.87	43.90	43.97	-44.66
LID-330	$10.48^{+0.40}_{-0.48}$	$1.49^{+0.46}_{-0.03}$	44.06	44.61	44.09	0.00	-44.76
LID-331	$10.26^{+0.49}_{-0.38}$	$2.04^{+0.00}_{-0.48}$	44.21	44.98	43.88	0.00	-45.24
LID-334	$11.14^{+0.09}_{-0.22}$	$0.70^{+0.23}_{-0.00}$	43.30	43.51	44.19	42.00	44.47
LID-335	$10.71^{+0.00}_{-0.00}$	$1.22^{+0.02}_{-0.09}$	43.15	44.46	44.36	43.70	-44.39
LID-336	$10.55^{+0.28}_{-0.31}$	$1.50^{+0.14}_{-0.05}$	43.67	44.74	44.03	43.87	-44.82
LID-339	$10.43^{+0.43}_{-0.34}$	$2.17^{+0.02}_{-0.34}$	43.92	45.33	44.03	0.00	-45.23
LID-340	$11.02^{+0.53}_{-0.47}$	$2.61^{+0.22}_{-0.00}$	43.72	45.81	44.14	0.00	-45.95
LID-341	$10.65^{+0.38}_{-0.13}$	$2.54^{+0.10}_{-0.07}$	43.99	45.81	44.32	44.56	-44.93
LID-342	$11.18^{+0.19}_{-0.21}$	$1.71^{+0.14}_{-0.08}$	43.56	44.99	44.54	43.97	-44.94
LID-346	$9.79^{+0.45}_{-0.33}$	$0.53^{+0.45}_{-0.34}$	43.18	43.53	43.43	0.00	-44.06
LID-347	$10.86^{+0.28}_{-0.20}$	$1.65^{+0.08}_{-0.00}$	43.78	44.91	44.63	0.00	-44.29
LID-348	$10.68^{+0.25}_{-0.22}$	$0.94^{+0.41}_{-0.61}$	43.42	43.59	43.93	0.00	-44.37
LID-349	$10.68^{+0.14}_{-0.00}$	$1.41^{+0.00}_{-0.35}$	44.04	44.34	44.50	0.00	-44.78
LID-353	$11.06^{+0.20}_{-0.25}$	$1.73^{+0.38}_{-0.32}$	43.79	44.70	44.42	44.69	-44.91
LID-354	$10.84^{+1.05}_{-1.14}$	$0.94^{+0.09}_{-0.00}$	43.16	44.19	43.48	0.00	-43.50
LID-356	$11.13^{+0.25}_{-0.28}$	$1.92^{+0.00}_{-0.29}$	44.25	44.76	44.66	0.00	-45.30
LID-359	$10.18^{+0.29}_{-0.37}$	$1.88^{+0.00}_{-0.63}$	43.88	44.44	44.03	0.00	-45.28
LID-361	$10.79^{+0.21}_{-0.34}$	$1.56^{+0.13}_{-0.43}$	44.08	44.43	44.51	0.00	-44.95
LID-363	$11.39^{+0.43}_{-0.53}$	$2.76^{+0.08}_{-0.12}$	44.91	46.07	44.41	0.00	0.00
LID-364	$10.71^{+0.67}_{-0.61}$	$1.90^{+0.32}_{-0.00}$	43.47	44.80	43.91	0.00	-45.47
LID-366	$10.44^{+0.25}_{-0.44}$	$1.79^{+0.04}_{-0.06}$	42.75	44.97	43.91	42.59	44.97
LID-371	$11.27^{+0.15}_{-0.30}$	$0.67^{+0.16}_{-0.44}$	43.34	43.64	44.45	42.78	-44.03
LID-372	$11.43^{+0.63}_{-0.54}$	$0.06^{+0.41}_{-0.00}$	43.88	43.46	44.19	43.33	-44.28
LID-373	$9.24^{+0.98}_{-0.04}$	$1.67^{+0.00}_{-0.19}$	43.46	44.78	43.81	43.98	-44.67
LID-374	$11.91^{+0.65}_{-1.35}$	$1.09^{+0.01}_{-0.85}$	43.84	43.44	44.25	0.00	-44.69
LID-378	$10.62^{+0.22}_{-0.25}$	$1.35^{+0.02}_{-0.44}$	43.90	44.27	44.17	43.68	-44.80
LID-380	$10.16^{+0.60}_{-0.41}$	$1.27^{+0.11}_{-0.10}$	43.31	44.41	43.98	0.00	-44.54
LID-382	$10.93^{+0.09}_{-0.05}$	$0.70^{+0.03}_{-0.25}$	43.17	43.76	44.57	44.05	-44.34
LID-383	$9.06^{+0.94}_{-1.05}$	$0.78^{+0.16}_{-0.03}$	42.72	44.08	42.85	0.00	-43.03
LID-384	$10.67^{+0.53}_{-0.38}$	$0.78^{+0.15}_{-0.00}$	43.80	44.12	44.11	44.46	-44.41
LID-387	$10.37^{+0.35}_{-0.37}$	$1.31^{+0.12}_{-0.18}$	43.95	44.50	44.51	0.00	-44.34
LID-388	$9.99^{+0.38}_{-0.35}$	$0.66^{+0.16}_{-0.05}$	42.73	43.92	43.70	0.00	-43.39

Table B.2 – continued

ID	log $M_{stellar}$ ($M_\odot$)	log SFR^{tot} ($M_\odot$ yr^{-1})	log $L_{2-10\ keV}$ (erg s^{-1})	log L_{2300} (erg s^{-1})	log L_{5100} (erg s^{-1})	log $L_{6\mu m}$ (erg s^{-1})	log L_{IR} (erg s^{-1})
LID-389	$10.60^{+0.19}_{-0.09}$	$0.84^{+0.10}_{-0.00}$	43.23	44.12	43.94	43.34	-44.23
LID-390	$10.53^{+0.09}_{-0.05}$	$2.00^{+0.03}_{-0.06}$	43.62	45.07	44.47	44.77	45.23
LID-391	$9.49^{+0.35}_{-0.31}$	$1.18^{+0.06}_{-0.08}$	43.15	44.40	42.92	43.60	-42.43
LID-392	$11.24^{+0.00}_{-0.00}$	$1.70^{+0.13}_{-0.05}$	44.17	44.93	44.84	44.02	-44.67
LID-394	$11.46^{+0.16}_{-0.02}$	$1.70^{+0.03}_{-0.92}$	43.73	43.97	44.89	0.00	-45.28
LID-398	$10.85^{+0.13}_{-0.25}$	$1.47^{+0.08}_{-0.19}$	43.47	44.47	44.64	44.09	-44.79
LID-400	$10.51^{+0.23}_{-0.17}$	$0.75^{+0.08}_{-0.05}$	42.64	43.96	43.17	43.80	44.39
LID-402	$10.26^{+0.25}_{-0.42}$	$1.03^{+0.43}_{-0.52}$	43.64	44.02	43.72	0.00	-44.39
LID-403	$11.26^{+0.61}_{-0.55}$	$1.50^{+0.14}_{-0.00}$	43.33	44.60	44.33	42.71	44.99
LID-404	$10.94^{+0.23}_{-0.06}$	$1.66^{+0.08}_{-0.00}$	43.13	44.78	44.44	43.80	44.82
LID-406	$10.19^{+0.31}_{-0.34}$	$1.90^{+0.00}_{-0.69}$	43.75	44.56	44.08	0.00	-45.29
LID-412	$10.54^{+0.27}_{-0.38}$	$2.13^{+0.11}_{-0.08}$	44.25	45.37	44.05	44.37	-45.01
LID-418	$10.96^{+0.78}_{-0.68}$	$0.48^{+0.14}_{-1.54}$	42.97	42.38	43.82	0.00	-44.14
LID-420	$11.80^{+0.46}_{-0.37}$	$0.68^{+0.15}_{-0.76}$	43.34	43.17	44.71	43.05	-44.43
LID-422	$10.81^{+0.31}_{-0.17}$	$2.11^{+0.03}_{-0.22}$	43.97	45.24	44.55	44.56	-45.24
LID-423	$11.10^{+0.10}_{-0.17}$	$0.34^{+0.09}_{-0.06}$	43.41	43.56	44.64	43.05	44.71
LID-424	$11.12^{+0.48}_{-0.40}$	$1.27^{+0.16}_{-0.00}$	43.53	44.60	44.25	0.00	-42.97
LID-427	$10.87^{+0.63}_{-0.38}$	$2.24^{+0.00}_{-0.25}$	44.17	45.16	44.44	0.00	-45.39
LID-428	$10.72^{+0.22}_{-0.34}$	$0.57^{+0.07}_{-0.16}$	42.74	43.79	44.12	43.06	-44.10
LID-431	$11.36^{+0.39}_{-0.56}$	$0.75^{+0.19}_{-0.47}$	42.99	43.42	43.71	0.00	-44.36
LID-433	$10.31^{+0.24}_{-0.17}$	$0.72^{+0.01}_{-0.16}$	42.87	43.91	43.55	43.00	-44.11
LID-434	$10.90^{+0.19}_{-0.34}$	$2.54^{+0.19}_{-0.00}$	43.78	45.87	44.56	45.01	45.39
LID-435	$10.79^{+0.25}_{-0.19}$	$0.94^{+0.09}_{-0.48}$	43.57	43.76	44.09	43.83	-44.27
LID-438	$11.06^{+0.55}_{-0.39}$	$2.63^{+0.12}_{-0.10}$	44.44	45.90	44.23	0.00	-45.31
LID-439	$11.06^{+0.14}_{-0.13}$	$1.81^{+0.13}_{-0.38}$	44.54	44.71	44.96	0.00	-45.35
LID-440	$10.65^{+0.14}_{-0.12}$	$1.43^{+0.10}_{-0.01}$	43.73	44.58	44.24	43.85	44.76
LID-442	$10.48^{+0.12}_{-0.15}$	$0.98^{+0.06}_{-0.25}$	42.78	44.05	43.95	43.09	-44.21
LID-446	$10.41^{+0.21}_{-0.07}$	$0.18^{+0.15}_{-0.37}$	42.56	43.10	43.92	43.01	-42.59
LID-447	$10.27^{+0.28}_{-0.18}$	$0.91^{+0.12}_{-0.30}$	43.32	43.97	43.88	0.00	-44.21
LID-450	$10.62^{+0.41}_{-0.36}$	$2.12^{+0.18}_{-0.13}$	44.08	45.35	44.18	0.00	-45.28
LID-454	$9.96^{+0.63}_{-0.50}$	$1.94^{+0.09}_{-0.02}$	43.36	45.24	43.58	44.04	-44.43
LID-456	$10.81^{+0.49}_{-0.16}$	$2.01^{+0.26}_{-0.00}$	44.63	44.53	44.51	0.00	-45.67
LID-458	$11.32^{+0.33}_{-0.54}$	$1.54^{+0.09}_{-0.01}$	43.56	44.08	44.51	44.14	45.14
LID-459	$10.67^{+0.38}_{-0.40}$	$1.63^{+0.74}_{-0.00}$	44.29	44.70	44.32	0.00	-44.88
LID-465	$11.15^{+0.18}_{-0.18}$	$2.02^{+0.00}_{-0.59}$	44.05	44.77	44.50	0.00	-45.25
LID-466	$10.99^{+0.03}_{-0.11}$	$2.00^{+0.13}_{-0.01}$	43.61	45.25	44.53	44.15	-44.82
LID-467	$10.75^{+0.46}_{-0.38}$	$2.04^{+0.36}_{-0.39}$	44.28	44.99	44.36	0.00	-45.18
LID-468	$10.85^{+0.12}_{-0.15}$	$1.26^{+0.08}_{-0.13}$	43.60	44.37	44.27	44.02	-44.70
LID-469	$10.63^{+0.16}_{-0.12}$	$1.22^{+0.01}_{-0.32}$	43.64	44.24	44.23	44.00	-44.75
LID-470	$10.50^{+0.22}_{-0.35}$	$0.88^{+0.06}_{-0.05}$	43.17	44.12	43.67	43.66	-44.45

Table B.2 – continued

ID	log $M_{stellar}$ ($M_\odot$)	log SFR^{tot} ($M_\odot$ yr^{-1})	log $L_{2-10\ keV}$ (erg s^{-1})	log L_{2300} (erg s^{-1})	log L_{5100} (erg s^{-1})	log $L_{6\mu m}$ (erg s^{-1})	log L_{IR} (erg s^{-1})
LID-474	$10.60^{+0.30}_{-0.34}$	$1.82^{+0.11}_{-0.20}$	43.85	44.96	44.07	44.48	-44.80
LID-475	$10.53^{+0.09}_{-0.05}$	$1.81^{+0.21}_{-0.00}$	43.06	45.04	44.44	44.36	45.26
LID-479	$10.78^{+0.42}_{-0.31}$	$1.89^{+0.10}_{-0.63}$	43.70	44.70	44.35	0.00	-45.26
LID-480	$10.88^{+0.10}_{-0.17}$	$1.43^{+0.11}_{-0.02}$	43.76	44.49	44.31	43.41	44.76
LID-482	$10.39^{+0.55}_{-0.25}$	$2.18^{+0.25}_{-0.05}$	43.67	45.32	43.88	43.06	45.73
LID-486	$10.65^{+0.67}_{-0.47}$	$1.35^{+0.09}_{-0.00}$	43.76	44.59	43.87	44.51	44.92
LID-488	$10.61^{+0.32}_{-0.16}$	$2.26^{+0.08}_{-0.05}$	43.44	45.46	44.27	0.00	-45.15
LID-489	$10.58^{+0.27}_{-0.23}$	$2.05^{+0.18}_{-0.03}$	43.82	45.26	44.44	43.96	44.91
LID-490	$11.41^{+0.15}_{-0.20}$	$1.85^{+0.08}_{-0.19}$	44.22	44.97	44.70	44.62	-45.05
LID-492	$10.65^{+0.17}_{-0.03}$	$1.10^{+0.13}_{-0.12}$	44.20	44.31	44.12	44.41	-44.19
LID-494	$10.51^{+0.22}_{-0.16}$	$1.61^{+0.12}_{-0.00}$	43.23	44.74	44.13	42.91	44.68
LID-498	$11.20^{+0.32}_{-0.16}$	$2.86^{+0.07}_{-0.03}$	44.22	46.08	44.73	45.97	45.85
LID-501	$10.65^{+0.00}_{-0.00}$	$1.16^{+0.08}_{-0.09}$	43.43	44.34	44.60	43.69	-44.42
LID-502	$9.44^{+0.73}_{-0.67}$	$0.68^{+0.18}_{-1.22}$	43.84	42.93	43.31	0.00	-44.19
LID-505	$10.64^{+0.31}_{-0.42}$	$1.20^{+0.53}_{-0.18}$	44.10	44.38	44.12	0.00	-44.48
LID-506	$10.86^{+0.43}_{-0.23}$	$2.61^{+0.13}_{-0.00}$	44.57	45.80	44.58	0.00	-45.83
LID-514	$10.27^{+0.52}_{-0.38}$	$0.96^{+0.45}_{-0.29}$	43.74	44.08	43.80	0.00	-44.40
LID-515	$10.38^{+0.19}_{-0.08}$	$0.20^{+0.22}_{-1.23}$	42.42	42.25	43.78	0.00	-43.88
LID-520	$10.72^{+0.37}_{-0.16}$	$2.57^{+0.13}_{-0.00}$	44.39	45.76	44.62	44.96	-45.36
LID-521	$10.42^{+0.15}_{-0.12}$	$0.93^{+0.01}_{-0.11}$	43.94	44.10	43.83	43.89	-44.41
LID-534	$11.16^{+0.23}_{-0.53}$	$2.63^{+0.02}_{-0.35}$	43.91	45.79	44.35	44.77	45.48
LID-537	$10.48^{+0.11}_{-0.16}$	$0.87^{+0.16}_{-0.05}$	42.86	44.08	43.90	43.19	-44.03
LID-540	$10.80^{+0.18}_{-0.09}$	$1.34^{+0.09}_{-0.05}$	42.62	44.42	44.06	44.07	44.59
LID-541	$10.45^{+0.24}_{-0.42}$	$1.45^{+0.00}_{-0.56}$	43.66	44.19	44.15	43.92	-45.04
LID-550	$10.59^{+0.16}_{-0.09}$	$1.09^{+0.04}_{-0.12}$	43.64	44.26	43.99	43.36	-44.24
LID-553	$11.26^{+0.21}_{-0.28}$	$1.63^{+0.10}_{-0.17}$	44.26	44.62	44.73	0.00	-45.02
LID-554	$11.04^{+0.53}_{-0.46}$	$0.86^{+0.00}_{-0.71}$	43.05	43.37	44.18	43.67	-44.45
LID-555	$10.70^{+0.00}_{-0.00}$	$1.30^{+0.04}_{-0.08}$	43.46	44.35	44.34	43.92	44.97
LID-562	$10.68^{+0.21}_{-0.23}$	$1.30^{+0.10}_{-0.27}$	42.99	44.27	44.08	0.00	-44.77
LID-566	$10.63^{+0.28}_{-0.38}$	$1.26^{+0.42}_{-0.43}$	43.60	44.13	44.33	0.00	-44.63
LID-574	$10.98^{+0.24}_{-0.24}$	$2.63^{+0.10}_{-0.12}$	43.46	45.68	44.52	44.95	45.90
LID-578	$11.49^{+0.20}_{-0.17}$	$1.41^{+0.12}_{-0.55}$	44.63	44.08	45.16	0.00	-44.97
LID-580	$11.79^{+0.75}_{-0.55}$	$1.38^{+0.00}_{-0.82}$	43.58	43.89	44.71	44.29	-44.70
LID-581	$10.92^{+0.24}_{-0.50}$	$2.24^{+0.09}_{-0.00}$	43.91	45.49	44.08	0.00	-45.10
LID-582	$10.76^{+0.40}_{-0.36}$	$1.69^{+0.00}_{-0.79}$	43.49	44.21	44.19	0.00	-45.23
LID-591	$10.91^{+0.20}_{-0.25}$	$1.74^{+0.05}_{-0.44}$	43.92	44.50	44.40	0.00	-45.24
LID-593	$10.60^{+0.21}_{-0.08}$	$1.91^{+0.03}_{-0.14}$	43.03	45.05	44.45	44.44	-44.57
LID-598	$10.39^{+0.14}_{-0.19}$	$1.01^{+0.11}_{-0.04}$	42.56	43.99	43.63	43.21	44.92
LID-600	$10.46^{+0.41}_{-0.39}$	$2.05^{+0.16}_{-0.00}$	43.61	45.34	43.85	0.00	-44.55
LID-611	$10.93^{+0.00}_{-0.00}$	$2.20^{+0.04}_{-0.06}$	42.79	45.32	44.52	44.96	45.12

Table B.2 – continued

ID	log $M_{stellar}$ ($M_\odot$)	log SFR^{tot} ($M_\odot$ yr^{-1})	log $L_{2-10\ keV}$ (erg s^{-1})	log L_{2300} (erg s^{-1})	log L_{5100} (erg s^{-1})	log $L_{6\mu m}$ (erg s^{-1})	log L_{IR} (erg s^{-1})
LID-613	$10.48^{+0.28}_{-0.48}$	$1.80^{+0.08}_{-0.37}$	44.02	44.79	43.95	0.00	-45.23
LID-615	$11.20^{+0.17}_{-0.12}$	$1.81^{+0.20}_{-0.31}$	44.24	44.88	44.69	44.35	-45.12
LID-617	$11.13^{+0.26}_{-0.15}$	$1.68^{+0.15}_{-0.14}$	43.30	44.82	44.38	44.59	-45.01
LID-619	$10.11^{+0.71}_{-0.39}$	$1.81^{+0.15}_{-0.09}$	43.48	45.00	43.69	0.00	-44.63
LID-629	$10.03^{+0.26}_{-0.25}$	$1.32^{+0.00}_{-0.20}$	43.10	44.32	43.63	0.00	-44.46
LID-632	$11.05^{+0.23}_{-0.42}$	$2.75^{+0.00}_{-0.14}$	44.07	45.93	44.44	44.92	-45.14
LID-633	$10.85^{+0.00}_{-0.00}$	$1.13^{+0.10}_{-0.00}$	43.64	43.56	44.47	44.75	44.81
LID-634	$11.05^{+0.25}_{-0.19}$	$1.91^{+0.02}_{-0.07}$	44.08	44.50	44.74	44.79	46.10
LID-637	$11.13^{+0.14}_{-0.21}$	$2.34^{+0.10}_{-0.05}$	44.22	45.39	44.32	45.21	45.60
LID-639	$10.53^{+0.00}_{-0.00}$	$1.02^{+0.11}_{-0.12}$	42.87	44.16	44.24	43.07	-44.22
LID-644	$10.54^{+0.22}_{-0.19}$	$1.37^{+0.07}_{-0.10}$	42.84	44.54	44.16	0.00	-44.30
LID-651	$10.63^{+0.19}_{-0.05}$	$1.87^{+0.06}_{-0.04}$	43.09	45.13	44.44	44.09	-44.58
LID-652	$11.04^{+0.14}_{-0.13}$	$0.42^{+0.11}_{-0.08}$	43.45	43.62	44.26	43.23	-44.40
LID-655	$10.73^{+0.21}_{-0.27}$	$1.79^{+0.05}_{-0.05}$	43.58	45.02	43.89	44.08	-44.63
LID-656	$10.35^{+0.06}_{-0.07}$	$0.88^{+0.06}_{-0.02}$	42.68	44.06	44.13	43.07	44.30
LID-658	$10.24^{+0.38}_{-0.44}$	$1.40^{+0.21}_{-0.26}$	43.92	44.59	43.76	0.00	-44.47
LID-661	$10.61^{+0.20}_{-0.07}$	$0.38^{+0.15}_{-0.37}$	42.75	43.31	44.12	42.57	-44.13
LID-662	$10.91^{+0.00}_{-0.00}$	$2.00^{+0.12}_{-0.01}$	43.44	45.22	44.51	42.74	44.75
LID-665	$10.67^{+0.15}_{-0.15}$	$1.31^{+0.07}_{-0.24}$	43.50	44.35	44.16	0.00	-44.62
LID-667	$9.95^{+0.43}_{-0.39}$	$1.09^{+0.26}_{-0.35}$	43.16	44.13	43.85	0.00	-44.33
LID-672	$10.57^{+0.07}_{-0.08}$	$1.64^{+0.09}_{-0.20}$	43.59	44.81	44.45	44.43	-44.76
LID-673	$10.80^{+0.33}_{-0.22}$	$2.23^{+0.20}_{-0.00}$	43.33	45.56	44.38	45.43	45.31
LID-675	$10.35^{+0.23}_{-0.21}$	$1.95^{+0.09}_{-0.04}$	43.04	45.20	44.15	43.34	44.87
LID-679	$10.87^{+0.00}_{-0.00}$	$1.49^{+0.14}_{-0.27}$	43.99	44.50	44.40	44.28	-44.53
LID-682	$10.67^{+0.13}_{-0.14}$	$1.14^{+0.09}_{-0.00}$	43.30	44.25	44.15	43.89	44.54
LID-683	$10.53^{+0.20}_{-0.24}$	$1.91^{+0.21}_{-0.07}$	44.27	45.06	44.16	44.41	-44.78
LID-684	$10.82^{+0.10}_{-0.12}$	$1.28^{+0.06}_{-0.01}$	43.33	44.31	44.22	44.24	44.73
LID-687	$10.56^{+0.42}_{-0.61}$	$2.29^{+0.00}_{-0.51}$	44.66	45.18	44.15	0.00	-45.29
LID-689	$10.80^{+0.22}_{-0.08}$	$1.22^{+0.11}_{-0.16}$	43.22	44.37	44.27	43.07	-44.12
LID-696	$10.41^{+0.26}_{-0.35}$	$1.54^{+0.09}_{-0.04}$	43.04	44.83	44.13	0.00	-44.22
LID-700	$10.89^{+0.25}_{-0.15}$	$1.54^{+0.05}_{-0.42}$	43.61	44.46	44.37	0.00	-44.96
LID-704	$10.28^{+0.25}_{-0.23}$	$1.10^{+0.14}_{-0.72}$	43.40	43.64	44.06	0.00	-44.71
LID-706	$10.84^{+0.15}_{-0.12}$	$1.18^{+0.05}_{-0.81}$	43.55	43.61	44.51	0.00	-44.75
LID-707	$10.45^{+0.14}_{-0.14}$	$1.02^{+0.11}_{-0.26}$	43.40	44.08	43.90	43.06	-44.30
LID-709	$11.16^{+0.14}_{-0.51}$	$1.77^{+0.12}_{-0.41}$	44.26	44.74	44.56	0.00	-45.27
LID-713	$10.85^{+0.00}_{-0.00}$	$2.01^{+0.13}_{-0.00}$	43.47	45.18	44.55	44.36	45.06
LID-714	$10.67^{+0.14}_{-0.01}$	$1.38^{+0.04}_{-0.10}$	42.97	44.37	44.27	43.98	44.71
LID-715	$11.04^{+0.18}_{-0.05}$	$2.17^{+0.06}_{-0.00}$	43.34	45.40	44.69	44.55	45.35
LID-716	$11.19^{+0.15}_{-0.10}$	$1.48^{+0.05}_{-0.91}$	44.40	43.83	44.46	44.29	-45.08
LID-717	$10.88^{+0.12}_{-0.16}$	$1.69^{+0.12}_{-0.42}$	44.24	44.44	44.43	44.70	-45.21

Table B.2 – continued

ID	log $M_{stellar}$ ($M_\odot$)	log SFR^{tot} ($M_\odot$ yr^{-1})	log $L_{2-10\ keV}$ (erg s^{-1})	log L_{2300} (erg s^{-1})	log L_{5100} (erg s^{-1})	log $L_{6\mu m}$ (erg s^{-1})	log L_{IR} (erg s^{-1})
LID-718	$10.19^{+0.08}_{-0.10}$	$2.11^{+0.03}_{-0.08}$	43.61	45.30	44.39	44.31	-44.49
LID-719	$10.16^{+0.29}_{-0.22}$	$1.84^{+0.09}_{-0.15}$	43.71	45.07	44.27	44.04	-44.73
LID-722	$10.42^{+0.28}_{-0.35}$	$1.64^{+0.20}_{-0.15}$	44.20	44.58	44.20	0.00	-45.29
LID-723	$9.25^{+0.93}_{-0.67}$	$1.60^{+0.06}_{-0.03}$	43.65	44.75	43.26	0.00	-44.26
LID-724	$10.66^{+0.23}_{-0.44}$	$1.51^{+0.27}_{-0.17}$	43.51	44.51	44.33	0.00	-44.61
LID-725	$10.64^{+0.12}_{-0.14}$	$1.21^{+0.09}_{-0.31}$	43.31	44.23	44.22	0.00	-44.41
LID-729	$10.99^{+0.15}_{-0.25}$	$1.74^{+0.10}_{-0.00}$	44.33	45.05	44.42	0.00	-44.06
LID-732	$10.61^{+0.17}_{-0.11}$	$1.71^{+0.02}_{-0.05}$	43.75	44.96	44.25	0.00	-44.08
LID-734	$10.27^{+0.17}_{-0.15}$	$2.19^{+0.05}_{-0.06}$	44.07	45.44	44.67	0.00	-44.38
LID-739	$11.40^{+0.15}_{-0.21}$	$2.26^{+0.08}_{-0.09}$	43.81	45.15	44.79	44.60	45.76
LID-740	$10.40^{+0.32}_{-0.23}$	$2.01^{+0.12}_{-0.05}$	44.23	45.28	44.28	44.17	-45.05
LID-742	$10.63^{+0.22}_{-0.11}$	$1.10^{+0.14}_{-0.15}$	43.33	44.21	43.85	43.99	-44.26
LID-745	$10.67^{+0.44}_{-0.28}$	$2.51^{+0.15}_{-0.00}$	44.05	45.64	43.98	44.64	45.49
LID-746	$11.23^{+0.00}_{-0.00}$	$2.37^{+0.07}_{-0.01}$	43.92	45.57	44.86	44.72	44.99
LID-750	$10.65^{+0.13}_{-0.14}$	$1.72^{+0.11}_{-0.03}$	43.14	44.86	43.76	44.34	44.80
LID-751	$10.92^{+0.19}_{-0.19}$	$2.15^{+0.08}_{-0.08}$	43.82	45.38	44.51	44.65	-45.05
LID-754	$11.34^{+0.00}_{-0.00}$	$1.11^{+0.13}_{-0.31}$	43.29	44.09	44.81	0.00	-44.48
LID-755	$10.92^{+0.35}_{-0.30}$	$2.09^{+0.15}_{-0.09}$	43.99	45.26	44.46	44.86	-45.14
LID-756	$10.55^{+0.44}_{-0.41}$	$1.71^{+0.10}_{-0.64}$	44.17	44.23	44.39	0.00	-45.24
LID-759	$10.65^{+0.13}_{-0.14}$	$0.34^{+0.12}_{-0.37}$	42.53	43.30	44.03	0.00	-43.69
LID-761	$10.21^{+0.29}_{-0.39}$	$0.78^{+0.18}_{-0.00}$	43.52	44.15	43.83	44.39	45.37
LID-771	$11.40^{+0.18}_{-0.11}$	$2.57^{+0.07}_{-0.00}$	44.42	45.78	45.00	0.00	-45.22
LID-772	$10.38^{+0.27}_{-0.35}$	$1.58^{+0.01}_{-0.22}$	43.22	44.61	43.96	0.00	-44.79
LID-773	$10.67^{+0.23}_{-0.31}$	$2.37^{+0.14}_{-0.30}$	44.38	45.51	44.36	0.00	-45.34
LID-774	$10.53^{+0.21}_{-0.27}$	$0.89^{+0.32}_{-0.13}$	43.02	44.05	43.87	0.00	-44.17
LID-779	$10.27^{+0.27}_{-0.12}$	$1.52^{+0.11}_{-0.26}$	43.60	44.62	44.08	44.12	-44.77
LID-783	$10.96^{+0.35}_{-0.34}$	$2.28^{+0.15}_{-0.27}$	43.94	45.59	44.27	44.63	-44.93
LID-785	$10.67^{+0.13}_{-0.13}$	$1.33^{+0.11}_{-0.23}$	44.37	44.34	44.24	43.94	-44.46
LID-787	$11.10^{+0.10}_{-0.17}$	$1.60^{+0.04}_{-0.09}$	43.25	44.74	44.56	0.00	-44.51
LID-800	$10.69^{+0.10}_{-0.17}$	$2.16^{+0.12}_{-0.20}$	43.29	44.86	44.14	0.00	-45.63
LID-943	$9.89^{+0.00}_{-0.00}$	$0.46^{+0.00}_{-1.16}$	42.31	42.62	43.60	43.66	-44.07
LID-946	$11.01^{+0.12}_{-0.40}$	$1.89^{+0.14}_{-0.14}$	44.02	45.08	44.16	44.70	-45.00
LID-949	$10.82^{+0.43}_{-0.31}$	$2.37^{+0.17}_{-0.00}$	44.51	45.67	44.46	0.00	-45.10
LID-950	$11.13^{+0.48}_{-0.29}$	$2.89^{+0.11}_{-0.02}$	43.63	46.12	44.29	44.74	45.57
LID-959	$10.23^{+0.15}_{-0.13}$	$1.40^{+0.13}_{-0.09}$	43.42	44.56	43.69	43.69	-44.40
LID-962	$10.79^{+0.17}_{-0.15}$	$2.02^{+0.01}_{-0.06}$	43.54	45.17	44.30	43.63	45.13
LID-963	$10.50^{+0.09}_{-0.18}$	$1.06^{+0.07}_{-0.29}$	43.05	44.12	44.03	0.00	-44.34
LID-964	$10.39^{+0.43}_{-0.40}$	$1.30^{+0.23}_{-0.19}$	43.46	44.53	43.71	0.00	-44.56
LID-965	$10.80^{+0.19}_{-0.09}$	$1.40^{+0.04}_{-0.24}$	44.13	44.44	44.26	44.07	-44.70
LID-967	$10.19^{+0.03}_{-0.11}$	$1.69^{+0.04}_{-0.02}$	42.34	44.98	44.20	44.18	-44.21

Table B.2 – continued

ID	log $M_{stellar}$ ($M_\odot$)	log SFR^{tot} ($M_\odot$ yr^{-1})	log $L_{2-10\ keV}$ (erg s^{-1})	log L_{2300} (erg s^{-1})	log L_{5100} (erg s^{-1})	log $L_{6\mu m}$ (erg s^{-1})	log L_{IR} (erg s^{-1})
LID-968	$10.92^{+0.09}_{-0.12}$	$2.22^{+0.01}_{-0.05}$	43.73	45.43	44.83	44.61	45.32
LID-969	$10.98^{+0.16}_{-0.21}$	$2.59^{+0.14}_{-0.00}$	44.25	45.82	44.88	44.92	45.65
LID-972	$10.16^{+0.37}_{-0.38}$	$1.95^{+0.00}_{-0.22}$	43.85	45.01	43.53	44.70	-44.97
LID-974	$10.90^{+0.39}_{-0.43}$	$0.45^{+0.08}_{-0.05}$	43.10	43.18	44.00	43.64	44.48
LID-976	$10.76^{+0.29}_{-0.30}$	$1.79^{+0.14}_{-0.00}$	44.22	44.93	44.03	44.72	45.13
LID-978	$10.62^{+0.17}_{-0.10}$	$2.39^{+0.14}_{-0.00}$	44.03	45.66	44.10	45.27	44.81
LID-981	$10.84^{+0.14}_{-0.13}$	$1.55^{+0.06}_{-0.12}$	43.23	44.65	44.46	0.00	-44.67
LID-983	$10.82^{+0.15}_{-0.16}$	$1.31^{+0.03}_{-0.17}$	42.76	44.44	44.26	0.00	-44.29
LID-991	$10.35^{+0.07}_{-0.06}$	$0.63^{+0.10}_{-0.90}$	43.04	43.06	43.88	43.14	-44.42
LID-993	$10.87^{+0.00}_{-0.00}$	$1.57^{+0.17}_{-0.00}$	44.35	44.64	44.81	44.97	45.22
LID-994	$10.51^{+0.00}_{-0.00}$	$0.42^{+0.12}_{-0.46}$	42.48	43.26	44.25	0.00	-43.86
LID-995	$10.73^{+0.21}_{-0.23}$	$1.40^{+0.14}_{-0.17}$	43.47	44.45	44.09	0.00	-44.69
LID-997	$10.97^{+0.04}_{-0.09}$	$1.80^{+0.03}_{-0.04}$	43.28	45.02	44.47	0.00	-44.21
LID-1003	$10.45^{+0.13}_{-0.14}$	$1.54^{+0.09}_{-0.03}$	43.06	44.80	44.29	0.00	-44.13
LID-1008	$10.85^{+0.00}_{-0.00}$	$1.37^{+0.06}_{-0.01}$	42.85	44.49	44.48	44.26	44.47
LID-1009	$10.35^{+0.19}_{-0.17}$	$2.12^{+0.10}_{-0.03}$	43.35	45.36	44.11	44.06	-44.91
LID-1011	$9.81^{+0.49}_{-0.58}$	$1.63^{+0.10}_{-0.10}$	43.29	44.84	43.53	0.00	-44.25
LID-1015	$10.96^{+0.18}_{-0.22}$	$1.97^{+0.06}_{-0.00}$	43.28	45.18	44.12	43.67	45.23
LID-1016	$10.62^{+0.20}_{-0.06}$	$1.20^{+0.03}_{-0.14}$	42.83	44.33	44.32	43.73	-44.58
LID-1024	$11.53^{+0.69}_{-0.70}$	$0.45^{+0.08}_{-1.00}$	43.50	42.75	44.19	0.00	-44.03
LID-1028	$10.11^{+0.57}_{-0.59}$	$0.96^{+0.58}_{-0.39}$	43.67	43.87	43.74	0.00	-44.41
LID-1030	$10.27^{+0.38}_{-0.40}$	$1.04^{+0.36}_{-0.22}$	43.43	44.02	43.84	0.00	-44.40
LID-1038	$11.36^{+0.00}_{-0.00}$	$2.78^{+0.02}_{-0.10}$	43.80	45.74	45.20	43.52	45.60
LID-1039	$11.30^{+0.31}_{-0.41}$	$2.88^{+0.05}_{-0.02}$	44.70	46.15	44.85	0.00	-45.13
LID-1040	$10.47^{+0.29}_{-0.26}$	$0.75^{+0.07}_{-1.45}$	42.77	42.62	43.65	43.39	-43.93
LID-1041	$11.08^{+0.30}_{-0.43}$	$2.67^{+0.16}_{-0.10}$	43.87	45.91	44.08	0.00	-45.56
LID-1047	$11.52^{+1.04}_{-0.90}$	$0.73^{+0.38}_{-0.89}$	43.73	43.29	44.29	0.00	-44.52
LID-1152	$10.13^{+0.71}_{-0.47}$	$1.92^{+0.10}_{-0.07}$	43.49	45.15	43.49	0.00	-44.98
LID-1153	$11.03^{+0.24}_{-0.12}$	$3.07^{+0.00}_{-0.10}$	44.18	46.26	44.60	45.00	45.88
LID-1155	$10.47^{+0.22}_{-0.29}$	$1.59^{+0.14}_{-0.00}$	43.78	44.74	43.94	44.01	45.26
LID-1156	$10.75^{+0.20}_{-0.20}$	$1.16^{+0.07}_{-0.22}$	43.45	44.26	43.73	0.00	-44.35
LID-1159	$10.75^{+0.40}_{-0.41}$	$2.19^{+0.14}_{-0.00}$	44.14	45.49	44.33	44.57	45.35
LID-1160	$11.06^{+0.49}_{-0.31}$	$2.44^{+0.08}_{-0.31}$	43.76	45.69	44.47	44.39	-45.19
LID-1162	$10.05^{+0.17}_{-0.03}$	$0.59^{+0.14}_{-1.30}$	42.94	42.54	43.63	42.93	-44.00
LID-1167	$10.71^{+0.40}_{-0.46}$	$1.89^{+0.10}_{-0.22}$	44.02	44.93	44.22	44.48	-45.27
LID-1169	$10.97^{+0.18}_{-0.19}$	$1.49^{+0.05}_{-0.23}$	43.95	44.55	44.54	44.35	-44.94
LID-1171	$9.87^{+0.75}_{-0.82}$	$1.49^{+0.05}_{-0.11}$	43.46	43.79	43.78	44.51	45.00
LID-1172	$10.23^{+0.51}_{-0.51}$	$1.38^{+0.28}_{-1.09}$	43.83	43.68	43.62	0.00	-45.08
LID-1173	$11.07^{+1.20}_{-0.88}$	$1.28^{+0.11}_{-0.31}$	43.66	44.25	44.16	0.00	-44.78
LID-1174	$11.41^{+0.20}_{-0.07}$	$1.31^{+0.13}_{-0.09}$	42.86	44.59	44.56	43.11	-44.11

Table B.2 – continued

ID	log $M_{stellar}$ ($M_\odot$)	log SFR^{tot} ($M_\odot$ yr^{-1})	log $L_{2-10\ keV}$ (erg s^{-1})	log L_{2300} (erg s^{-1})	log L_{5100} (erg s^{-1})	log $L_{6\mu m}$ (erg s^{-1})	log L_{IR} (erg s^{-1})
LID-1176	$10.42^{+0.29}_{-0.30}$	$1.79^{+0.15}_{-0.08}$	43.55	44.93	44.18	44.49	-45.17
LID-1178	$10.25^{+0.17}_{-0.03}$	$0.76^{+0.08}_{-0.08}$	43.30	43.90	43.98	43.21	-44.24
LID-1180	$10.63^{+0.38}_{-0.50}$	$1.61^{+0.02}_{-0.29}$	43.77	44.64	44.24	44.09	-44.72
LID-1182	$10.55^{+0.30}_{-0.39}$	$2.19^{+0.14}_{-0.04}$	43.83	45.42	43.75	0.00	-45.03
LID-1184	$10.52^{+0.55}_{-0.48}$	$0.74^{+0.09}_{-0.00}$	43.13	44.01	43.38	43.62	44.67
LID-1187	$11.12^{+0.22}_{-0.27}$	$2.25^{+0.09}_{-0.04}$	44.24	45.49	44.54	44.57	-44.84
LID-1188	$10.74^{+0.19}_{-0.21}$	$1.99^{+0.02}_{-0.42}$	44.12	44.97	44.52	0.00	-45.32
LID-1190	$11.27^{+0.28}_{-0.15}$	$2.43^{+0.12}_{-0.00}$	43.82	45.56	44.76	44.19	45.83
LID-1195	$11.63^{+0.58}_{-0.74}$	$1.97^{+0.17}_{-0.00}$	44.08	44.80	44.79	44.51	45.67
LID-1197	$10.59^{+0.52}_{-0.34}$	$1.73^{+0.00}_{-0.57}$	44.11	44.40	44.01	0.00	-45.21
LID-1198	$11.21^{+0.16}_{-0.26}$	$2.49^{+0.24}_{-0.02}$	43.97	45.42	44.35	45.05	45.82
LID-1200	$11.40^{+0.74}_{-0.82}$	$1.03^{+0.00}_{-0.81}$	43.70	43.66	44.47	0.00	-44.35
LID-1201	$10.96^{+0.10}_{-0.35}$	$0.21^{+0.00}_{-0.44}$	42.52	43.09	44.03	0.00	-43.77
LID-1206	$11.02^{+0.29}_{-0.25}$	$2.73^{+0.01}_{-0.07}$	43.88	45.89	44.45	0.00	-45.62
LID-1208	$9.88^{+0.36}_{-0.56}$	$2.22^{+0.08}_{-0.05}$	43.85	44.31	44.18	0.00	-45.77
LID-1211	$10.47^{+0.38}_{-0.43}$	$1.41^{+0.02}_{-0.62}$	43.66	43.96	43.93	0.00	-44.92
LID-1215	$10.71^{+0.24}_{-0.33}$	$0.33^{+0.00}_{-0.55}$	42.94	43.08	43.63	44.14	44.34
LID-1218	$10.78^{+0.04}_{-0.10}$	$2.47^{+0.08}_{-0.01}$	44.06	45.76	44.99	44.98	-44.56
LID-1219	$11.05^{+0.27}_{-0.23}$	$2.77^{+0.00}_{-0.11}$	44.11	45.97	44.90	0.00	0.00
LID-1222	$10.75^{+0.15}_{-0.28}$	$1.82^{+0.12}_{-0.00}$	43.60	45.05	44.36	0.00	-44.47
LID-1223	$10.53^{+0.19}_{-0.19}$	$2.18^{+0.06}_{-0.09}$	42.91	45.37	44.28	43.99	45.16
LID-1227	$10.45^{+0.29}_{-0.45}$	$1.56^{+0.31}_{-0.23}$	44.13	44.77	43.99	0.00	-44.65
LID-1230	$10.51^{+0.38}_{-0.32}$	$2.10^{+0.18}_{-0.00}$	44.16	45.43	43.94	0.00	-44.45
LID-1231	$10.50^{+0.25}_{-0.16}$	$0.37^{+0.08}_{-0.56}$	42.91	43.12	43.76	0.00	-43.87
LID-1235	$10.97^{+0.45}_{-0.54}$	$1.77^{+0.04}_{-0.38}$	43.01	44.29	44.28	0.00	-45.39
LID-1237	$10.32^{+0.65}_{-0.56}$	$1.43^{+0.00}_{-0.36}$	43.90	44.67	43.83	0.00	-44.40
LID-1238	$10.70^{+0.25}_{-0.19}$	$1.36^{+0.00}_{-1.08}$	43.39	43.50	44.49	0.00	-44.93
LID-1239	$11.19^{+0.42}_{-0.48}$	$0.85^{+0.09}_{-0.55}$	42.88	43.52	44.33	43.72	-44.51
LID-1240	$10.83^{+0.83}_{-0.99}$	$1.73^{+0.06}_{-0.09}$	43.35	44.92	44.17	0.00	-44.16
LID-1241	$11.42^{+0.34}_{-0.57}$	$2.85^{+0.10}_{-0.12}$	44.24	46.10	44.26	0.00	-45.30
LID-1242	$11.50^{+0.72}_{-0.74}$	$0.37^{+0.14}_{-0.46}$	43.00	43.35	44.20	0.00	-43.92
LID-1246	$11.20^{+1.24}_{-1.04}$	$0.52^{+0.31}_{-1.13}$	43.13	42.57	43.92	0.00	-44.19
LID-1250	$11.01^{+0.31}_{-0.22}$	$2.65^{+0.00}_{-0.16}$	43.41	45.79	44.62	0.00	-45.38
LID-1253	$11.98^{+0.51}_{-0.82}$	$0.98^{+0.05}_{-0.33}$	44.80	43.97	44.61	44.95	-44.48
LID-1255	$10.23^{+0.35}_{-0.32}$	$2.04^{+0.10}_{-0.19}$	43.97	45.19	44.05	0.00	-45.21
LID-1256	$11.27^{+0.33}_{-0.31}$	$1.28^{+0.12}_{-0.27}$	43.91	44.40	44.55	43.46	44.91
LID-1259	$11.15^{+1.32}_{-1.52}$	$0.31^{+0.86}_{-0.13}$	43.84	43.78	43.60	0.00	-44.09
LID-1260	$11.17^{+0.35}_{-0.10}$	$0.92^{+0.11}_{-0.23}$	43.77	44.00	44.90	0.00	-44.31
LID-1262	$10.62^{+0.49}_{-0.37}$	$1.02^{+0.56}_{-0.85}$	44.02	43.59	44.14	0.00	-44.60
LID-1264	$10.57^{+0.19}_{-0.19}$	$1.27^{+0.16}_{-0.00}$	43.14	44.21	43.85	43.61	44.89

Table B.2 – continued

ID	log $M_{stellar}$ ($M_\odot$)	log SFR^{tot} ($M_\odot$ yr^{-1})	log $L_{2-10\ keV}$ (erg s^{-1})	log L_{2300} (erg s^{-1})	log L_{5100} (erg s^{-1})	log $L_{6\mu m}$ (erg s^{-1})	log L_{IR} (erg s^{-1})
LID-1268	$10.40^{+0.28}_{-0.15}$	$2.03^{+0.00}_{-0.21}$	43.53	45.18	44.23	44.07	-44.91
LID-1269	$10.47^{+0.20}_{-0.30}$	$0.88^{+0.15}_{-0.19}$	43.65	44.01	43.92	0.00	-44.14
LID-1270	$10.04^{+0.41}_{-0.24}$	$1.73^{+0.27}_{-0.00}$	43.50	45.00	43.95	0.00	-44.63
LID-1271	$10.80^{+0.19}_{-0.08}$	$2.80^{+0.00}_{-0.31}$	43.31	45.30	44.70	44.62	46.36
LID-1272	$10.95^{+0.00}_{-0.00}$	$1.39^{+0.15}_{-0.00}$	43.89	44.63	44.26	44.76	44.80
LID-1274	$9.15^{+0.83}_{-0.60}$	$1.02^{+0.11}_{-0.12}$	43.09	44.21	42.72	0.00	-44.14
LID-1275	$10.57^{+0.05}_{-0.09}$	$1.29^{+0.13}_{-0.01}$	42.90	44.28	44.09	43.25	44.71
LID-1276	$10.48^{+0.61}_{-0.58}$	$2.09^{+0.05}_{-0.03}$	44.00	45.33	44.21	0.00	-44.20
LID-1278	$10.75^{+0.18}_{-0.36}$	$2.00^{+0.36}_{-0.27}$	44.28	44.94	44.66	0.00	-45.31
LID-1279	$10.48^{+0.25}_{-0.31}$	$1.58^{+0.49}_{-0.55}$	43.87	44.33	44.18	44.39	-45.03
LID-1280	$10.11^{+0.53}_{-0.58}$	$1.48^{+0.06}_{-0.01}$	42.98	44.70	43.81	43.79	-44.66
LID-1282	$10.67^{+0.12}_{-0.14}$	$2.36^{+0.00}_{-0.15}$	42.63	45.13	44.44	44.42	45.69
LID-1283	$10.87^{+0.15}_{-0.01}$	$-0.01^{+0.06}_{-0.01}$	43.31	42.85	44.29	43.07	44.49
LID-1287	$10.28^{+0.49}_{-0.42}$	$1.24^{+0.39}_{-0.12}$	43.75	44.33	43.71	0.00	-44.38
LID-1288	$11.09^{+0.22}_{-0.26}$	$1.64^{+0.00}_{-0.57}$	43.64	44.37	44.35	0.00	-45.10
LID-1290	$10.73^{+0.21}_{-0.27}$	$1.95^{+0.06}_{-0.16}$	43.48	45.15	44.31	0.00	-44.90
LID-1292	$10.65^{+0.14}_{-0.13}$	$2.07^{+0.17}_{-0.00}$	43.75	45.24	44.37	45.25	45.22
LID-1293	$10.33^{+0.37}_{-0.24}$	$1.51^{+0.13}_{-0.02}$	43.52	44.75	43.95	0.00	-44.24
LID-1294	$11.36^{+0.64}_{-0.61}$	$1.88^{+0.06}_{-0.15}$	44.42	44.74	44.64	44.92	45.25
LID-1296	$11.48^{+0.81}_{-0.92}$	$1.36^{+0.36}_{-0.00}$	43.42	43.88	44.14	43.72	45.12
LID-1297	$10.76^{+0.48}_{-0.32}$	$0.71^{+0.03}_{-0.69}$	42.63	43.27	44.08	43.04	-44.27
LID-1299	$10.86^{+0.20}_{-0.24}$	$1.94^{+0.08}_{-0.08}$	43.19	45.07	44.18	43.09	45.10
LID-1303	$11.48^{+0.69}_{-0.75}$	$-0.49^{+0.14}_{-0.00}$	44.19	42.84	44.11	44.38	-44.46
LID-1309	$11.62^{+0.32}_{-0.13}$	$0.55^{+0.09}_{-0.34}$	42.73	43.26	44.40	0.00	-44.03
LID-1317	$10.59^{+0.37}_{-0.33}$	$0.71^{+0.07}_{-1.08}$	43.67	42.87	43.90	43.35	-44.12
LID-1435	$11.36^{+0.10}_{-0.22}$	$2.59^{+0.05}_{-0.18}$	43.88	45.72	44.59	45.19	45.55
LID-1449	$10.77^{+0.43}_{-0.59}$	$1.60^{+0.80}_{-0.10}$	44.11	44.69	43.36	0.00	-45.17
LID-1453	$10.44^{+0.00}_{-0.00}$	$1.13^{+0.10}_{-1.22}$	43.06	43.19	44.27	44.09	-44.29
LID-1454	$10.19^{+0.40}_{-0.51}$	$1.52^{+0.38}_{-1.53}$	43.59	43.15	43.44	0.00	-45.11
LID-1455	$10.95^{+0.20}_{-0.27}$	$1.66^{+0.01}_{-0.38}$	43.53	44.59	44.23	0.00	-44.99
LID-1457	$10.62^{+0.26}_{-0.40}$	$1.83^{+0.11}_{-0.00}$	43.67	44.51	44.04	44.26	45.36
LID-1459	$10.41^{+0.00}_{-0.00}$	$1.61^{+0.13}_{-0.73}$	43.26	44.17	44.25	44.51	-44.55
LID-1460	$10.02^{+0.38}_{-0.38}$	$1.10^{+0.42}_{-0.20}$	43.59	44.16	43.73	0.00	-44.43
LID-1461	$11.01^{+0.00}_{-0.00}$	$2.16^{+0.07}_{-0.04}$	44.00	45.40	44.77	44.39	-44.80
LID-1462	$11.23^{+0.15}_{-0.13}$	$2.25^{+0.09}_{-0.00}$	44.51	45.51	45.06	45.54	-45.20
LID-1464	$10.43^{+0.14}_{-0.12}$	$1.45^{+0.09}_{-0.03}$	42.70	44.72	43.83	42.92	-44.18
LID-1474	$10.98^{+0.17}_{-0.24}$	$1.86^{+0.04}_{-0.23}$	43.78	44.93	44.47	44.18	-45.02
LID-1475	$10.13^{+0.09}_{-0.04}$	$1.36^{+0.07}_{-0.05}$	43.61	44.62	44.19	44.20	-44.52
LID-1478	$10.78^{+0.04}_{-0.09}$	$1.86^{+0.07}_{-0.00}$	43.83	45.16	44.53	44.43	44.97
LID-1479	$10.42^{+0.20}_{-0.06}$	$1.50^{+0.04}_{-0.09}$	42.83	44.66	44.20	43.38	-44.40

Table B.2 – continued

ID	log $M_{stellar}$ ($M_\odot$)	log SFR^{tot} ($M_\odot$ yr^{-1})	log $L_{2-10\ keV}$ (erg s^{-1})	log L_{2300} (erg s^{-1})	log L_{5100} (erg s^{-1})	log $L_{6\mu m}$ (erg s^{-1})	log L_{IR} (erg s^{-1})
LID-1481	$10.65^{+1.16}_{-1.25}$	$1.32^{+0.06}_{-0.05}$	43.56	44.56	43.43	0.00	0.00
LID-1482	$11.22^{+0.31}_{-0.57}$	$2.55^{+0.00}_{-0.54}$	44.07	44.79	44.53	0.00	-45.77
LID-1485	$10.69^{+0.21}_{-0.43}$	$2.04^{+0.09}_{-0.05}$	43.39	45.32	43.75	43.55	-44.67
LID-1486	$10.54^{+0.27}_{-0.24}$	$1.03^{+0.14}_{-0.13}$	42.65	44.20	43.92	0.00	-44.14
LID-1488	$10.16^{+0.30}_{-0.24}$	$0.62^{+0.25}_{-0.98}$	43.10	42.89	43.70	0.00	-44.24
LID-1490	$10.19^{+0.43}_{-0.40}$	$1.01^{+0.58}_{-1.13}$	43.58	43.14	43.87	0.00	-44.60
LID-1492	$10.68^{+0.30}_{-0.03}$	$2.50^{+0.03}_{-0.17}$	43.81	45.58	44.60	44.63	45.71
LID-1496	$10.65^{+0.36}_{-0.41}$	$1.51^{+0.18}_{-1.16}$	43.72	43.57	44.21	0.00	-45.28
LID-1500	$10.88^{+0.13}_{-0.00}$	$1.46^{+0.08}_{-0.15}$	43.64	44.63	44.35	44.10	-44.54
LID-1501	$10.29^{+0.28}_{-0.26}$	$1.36^{+0.22}_{-0.18}$	43.34	44.62	44.10	0.00	-44.27
LID-1514	$10.57^{+0.32}_{-0.12}$	$2.12^{+0.11}_{-0.03}$	43.69	45.38	43.99	44.07	-44.72
LID-1515	$10.63^{+0.29}_{-0.25}$	$2.18^{+0.12}_{-0.18}$	44.21	45.40	44.37	44.71	-45.02
LID-1518	$10.19^{+0.31}_{-0.32}$	$1.45^{+0.22}_{-0.00}$	43.25	44.76	43.79	0.00	-44.30
LID-1522	$10.31^{+0.32}_{-0.16}$	$1.45^{+0.09}_{-0.00}$	42.85	44.68	44.08	0.00	-44.10
LID-1523	$10.34^{+0.08}_{-0.05}$	$1.10^{+0.03}_{-0.46}$	43.63	43.96	44.30	43.72	-44.48
LID-1524	$10.93^{+0.19}_{-0.32}$	$1.39^{+0.14}_{-0.48}$	43.67	44.19	44.16	44.35	-44.86
LID-1535	$10.45^{+0.26}_{-0.18}$	$1.76^{+0.07}_{-0.11}$	43.21	44.88	44.19	43.81	-44.86
LID-1536	$10.75^{+0.00}_{-0.00}$	$1.98^{+0.06}_{-0.09}$	43.67	45.09	44.64	44.84	45.41
LID-1537	$10.32^{+0.21}_{-0.32}$	$1.44^{+0.37}_{-0.12}$	43.93	44.58	44.26	0.00	-44.72
LID-1539	$10.77^{+0.19}_{-0.07}$	$1.65^{+0.09}_{-0.00}$	43.79	44.29	44.28	44.52	45.20
LID-1540	$10.90^{+0.12}_{-0.02}$	$1.43^{+0.10}_{-0.11}$	43.94	44.59	44.40	43.82	-44.28
LID-1549	$11.06^{+0.18}_{-0.27}$	$1.95^{+0.08}_{-0.14}$	43.81	45.12	44.58	44.66	-45.01
LID-1551	$10.38^{+0.27}_{-0.30}$	$1.30^{+0.14}_{-0.00}$	43.09	44.57	43.65	0.00	-43.62
LID-1553	$10.53^{+0.08}_{-0.05}$	$1.06^{+0.08}_{-0.19}$	42.94	44.12	43.93	43.61	-44.04
LID-1554	$10.74^{+0.34}_{-0.36}$	$1.70^{+0.00}_{-0.81}$	44.22	44.18	44.15	0.00	-45.12
LID-1555	$11.14^{+0.16}_{-0.32}$	$1.59^{+0.05}_{-0.02}$	43.44	44.65	44.64	44.24	45.27
LID-1556	$10.78^{+0.00}_{-0.00}$	$0.95^{+0.08}_{-0.73}$	43.19	43.53	44.43	43.69	-44.27
LID-1559	$10.92^{+0.23}_{-0.33}$	$0.34^{+0.09}_{-0.00}$	43.41	43.66	44.17	43.42	-43.91
LID-1562	$10.69^{+1.08}_{-0.86}$	$0.49^{+0.31}_{-0.17}$	43.66	43.76	43.56	43.71	-44.44
LID-1564	$12.08^{+0.45}_{-0.54}$	$0.93^{+0.20}_{-0.69}$	44.45	43.65	44.73	44.52	-44.61
LID-1565	$11.88^{+0.27}_{-0.11}$	$2.40^{+0.14}_{-0.00}$	44.90	45.50	45.23	45.68	45.80
LID-1567	$10.95^{+0.46}_{-0.32}$	$1.58^{+0.01}_{-1.17}$	44.20	43.81	44.27	0.00	-45.14
LID-1568	$10.54^{+0.82}_{-0.94}$	$1.33^{+0.32}_{-0.38}$	43.62	44.38	43.99	0.00	-44.76
LID-1569	$11.29^{+0.34}_{-0.13}$	$0.68^{+0.25}_{-0.06}$	43.26	43.59	44.28	43.10	44.57
LID-1570	$10.89^{+0.27}_{-0.22}$	$1.40^{+0.13}_{-0.00}$	43.21	44.02	44.35	44.73	45.23
LID-1571	$11.60^{+0.95}_{-0.54}$	$2.30^{+0.03}_{-0.11}$	43.43	44.84	44.56	44.65	46.03
LID-1573	$11.13^{+0.21}_{-0.30}$	$1.60^{+0.05}_{-1.00}$	43.66	43.92	44.64	0.00	-45.22
LID-1578	$11.47^{+1.01}_{-0.86}$	$0.58^{+0.05}_{-0.81}$	43.66	43.15	44.14	0.00	-44.10
LID-1580	$10.87^{+0.17}_{-0.18}$	$1.54^{+0.06}_{-0.24}$	43.92	44.49	44.30	0.00	-44.98
LID-1582	$10.99^{+1.40}_{-1.26}$	$1.70^{+0.00}_{-0.33}$	43.48	44.73	43.93	0.00	-44.72

Table B.2 – continued

ID	log $M_{stellar}$ ($M_\odot$)	log SFR^{tot} ($M_\odot$ yr^{-1})	log $L_{2-10\ keV}$ (erg s^{-1})	log L_{2300} (erg s^{-1})	log L_{5100} (erg s^{-1})	log $L_{6\mu m}$ (erg s^{-1})	log L_{IR} (erg s^{-1})
LID-1585	$11.15^{+0.34}_{-0.20}$	$2.99^{+0.05}_{-0.07}$	44.30	46.23	44.39	45.88	45.48
LID-1586	$10.06^{+0.23}_{-0.25}$	$0.30^{+0.14}_{-0.63}$	42.72	43.01	43.50	0.00	-43.83
LID-1588	$11.15^{+0.00}_{-0.00}$	$1.70^{+0.14}_{-0.11}$	43.34	44.94	44.93	44.08	-44.73
LID-1595	$10.87^{+0.27}_{-0.12}$	$2.71^{+0.23}_{-0.00}$	43.17	46.04	44.37	44.92	46.07
LID-1598	$10.83^{+0.18}_{-0.05}$	$1.96^{+0.07}_{-0.05}$	43.71	45.21	44.93	44.16	-44.91
LID-1599	$10.94^{+0.08}_{-0.06}$	$0.78^{+0.05}_{-0.46}$	43.12	43.61	44.07	43.83	-44.24
LID-1600	$10.83^{+0.19}_{-0.05}$	$0.75^{+0.08}_{-0.45}$	42.78	43.57	44.21	43.59	-44.42
LID-1602	$10.79^{+0.18}_{-0.17}$	$2.18^{+0.06}_{-0.06}$	42.69	45.42	44.56	43.46	44.58
LID-1603	$10.74^{+0.00}_{-0.00}$	$1.43^{+0.10}_{-0.03}$	42.92	43.47	44.46	44.87	45.08
LID-1604	$9.77^{+0.57}_{-0.45}$	$0.67^{+0.22}_{-0.58}$	43.53	43.28	43.57	43.87	-44.79
LID-1606	$10.65^{+0.17}_{-0.03}$	$2.13^{+0.00}_{-0.21}$	43.27	45.26	44.30	44.51	45.18
LID-1608	$10.58^{+0.17}_{-0.30}$	$1.21^{+0.21}_{-0.21}$	43.24	44.25	43.95	0.00	-44.65
LID-1609	$10.04^{+0.28}_{-0.16}$	$0.76^{+0.07}_{-0.35}$	42.99	43.67	43.57	43.51	-44.34
LID-1611	$11.26^{+0.00}_{-0.00}$	$2.33^{+0.10}_{-0.00}$	43.34	45.59	44.79	44.34	45.42
LID-1613	$9.85^{+0.15}_{-0.12}$	$1.02^{+0.17}_{-0.84}$	43.23	43.50	43.76	43.82	-44.24
LID-1615	$11.40^{+0.30}_{-0.23}$	$3.13^{+0.05}_{-0.25}$	44.29	46.39	44.73	45.52	46.17
LID-1616	$9.68^{+0.50}_{-0.44}$	$1.32^{+0.11}_{-0.06}$	43.15	44.59	43.51	0.00	-43.62
LID-1617	$10.52^{+0.36}_{-0.38}$	$1.56^{+0.05}_{-0.34}$	43.67	44.53	43.98	44.07	-45.03
LID-1620	$11.00^{+0.00}_{-0.00}$	$2.27^{+0.17}_{-0.00}$	43.77	45.44	44.81	45.06	45.73
LID-1621	$10.66^{+0.27}_{-0.16}$	$1.90^{+0.04}_{-0.04}$	44.15	44.93	44.38	44.29	45.30
LID-1623	$10.74^{+0.08}_{-0.06}$	$1.17^{+0.07}_{-0.02}$	43.45	44.44	44.34	43.95	-44.55
LID-1624	$10.85^{+0.17}_{-0.03}$	$2.07^{+0.06}_{-0.01}$	44.16	45.29	44.51	44.17	-44.50
LID-1625	$11.57^{+0.18}_{-0.19}$	$2.78^{+0.00}_{-0.18}$	44.37	45.58	44.80	45.72	46.09
LID-1626	$10.31^{+0.25}_{-0.40}$	$1.08^{+0.03}_{-0.48}$	42.94	43.84	43.74	0.00	-44.60
LID-1628	$10.89^{+0.13}_{-0.01}$	$2.27^{+0.06}_{-0.02}$	43.84	45.40	44.74	44.51	45.31
LID-1630	$10.58^{+0.23}_{-0.31}$	$0.85^{+0.17}_{-0.34}$	43.24	43.87	44.02	0.00	-44.16
LID-1634	$10.73^{+0.21}_{-0.19}$	$2.26^{+0.14}_{-0.10}$	43.86	45.53	44.60	44.32	-45.03
LID-1635	$11.46^{+0.14}_{-0.17}$	$2.76^{+0.18}_{-0.00}$	44.85	46.08	45.00	45.71	45.76
LID-1637	$10.48^{+0.35}_{-0.19}$	$1.66^{+0.00}_{-0.20}$	43.82	44.78	43.89	0.00	-44.45
LID-1640	$10.75^{+0.18}_{-0.35}$	$1.54^{+0.10}_{-0.17}$	44.11	44.67	44.04	44.40	-44.69
LID-1642	$10.88^{+0.00}_{-0.00}$	$1.76^{+0.07}_{-0.10}$	43.38	44.58	44.40	44.25	45.29
LID-1643	$10.47^{+0.14}_{-0.14}$	$1.49^{+0.14}_{-0.00}$	43.72	44.80	43.93	44.49	-44.48
LID-1644	$10.44^{+0.18}_{-0.05}$	$0.58^{+0.05}_{-0.57}$	43.44	43.26	43.81	43.44	-44.06
LID-1645	$10.64^{+0.20}_{-0.26}$	$1.86^{+0.07}_{-0.19}$	44.08	45.10	44.17	43.61	-43.99
LID-1646	$12.25^{+0.00}_{-0.00}$	$1.75^{+0.18}_{-0.00}$	45.41	44.40	45.75	45.60	45.56
LID-1650	$10.61^{+0.18}_{-0.08}$	$1.70^{+0.34}_{-0.00}$	43.05	44.91	44.01	44.02	44.80
LID-1651	$10.62^{+0.16}_{-0.11}$	$1.29^{+0.23}_{-0.25}$	43.54	44.29	44.20	43.97	-44.82
LID-1653	$10.61^{+0.01}_{-0.13}$	$1.25^{+0.09}_{-0.28}$	43.55	44.29	44.37	43.41	-44.42
LID-1654	$11.02^{+0.00}_{-0.00}$	$0.84^{+0.09}_{-0.00}$	43.00	43.76	44.40	43.62	44.55
LID-1655	$10.55^{+0.09}_{-0.06}$	$1.34^{+0.09}_{-0.05}$	43.35	44.39	44.11	44.01	44.66

Table B.2 – continued

ID	log $M_{stellar}$ ($M_\odot$)	log SFR^{tot} ($M_\odot$ yr^{-1})	log $L_{2-10\ keV}$ (erg s^{-1})	log L_{2300} (erg s^{-1})	log L_{5100} (erg s^{-1})	log $L_{6\mu m}$ (erg s^{-1})	log L_{IR} (erg s^{-1})
LID-1656	$11.61^{+0.13}_{-0.11}$	$2.05^{+0.09}_{-0.09}$	44.26	45.24	44.88	44.92	-45.03
LID-1657	$10.65^{+0.14}_{-0.13}$	$2.01^{+0.12}_{-0.03}$	43.72	45.28	44.48	43.94	-44.70
LID-1660	$11.12^{+1.30}_{-1.32}$	$1.09^{+0.14}_{-0.86}$	43.72	43.48	44.03	0.00	-44.73
LID-1661	$10.67^{+0.42}_{-0.38}$	$2.05^{+0.08}_{-0.10}$	43.97	45.24	44.01	0.00	-44.97
LID-1662	$10.58^{+0.26}_{-0.23}$	$0.88^{+0.14}_{-0.07}$	42.73	44.04	44.03	43.43	44.27
LID-1664	$11.70^{+0.84}_{-0.70}$	$0.73^{+0.01}_{-0.60}$	43.44	43.54	44.62	0.00	-44.12
LID-1665	$10.24^{+1.25}_{-1.24}$	$1.25^{+0.09}_{-0.07}$	43.40	44.40	43.49	0.00	-44.40
LID-1671	$10.92^{+0.59}_{-0.45}$	$0.33^{+0.10}_{-1.12}$	43.42	42.28	43.69	0.00	-43.85
LID-1675	$10.53^{+0.17}_{-0.24}$	$1.86^{+0.00}_{-0.16}$	43.31	44.97	44.28	43.46	-44.78
LID-1678	$10.24^{+0.26}_{-0.44}$	$1.83^{+0.11}_{-0.09}$	43.46	45.06	43.92	44.04	-44.93
LID-1679	$10.98^{+0.03}_{-0.10}$	$1.25^{+0.08}_{-0.02}$	43.59	43.72	44.36	44.38	44.82
LID-1684	$10.90^{+0.12}_{-0.01}$	$1.48^{+0.05}_{-0.11}$	43.85	44.70	44.60	0.00	-44.13
LID-1685	$10.74^{+0.24}_{-0.24}$	$1.52^{+0.20}_{-0.00}$	44.01	44.16	44.15	43.95	45.17
LID-1686	$11.14^{+0.32}_{-0.27}$	$1.71^{+0.04}_{-0.05}$	43.38	44.80	44.98	44.20	45.48
LID-1688	$10.84^{+0.26}_{-0.27}$	$2.15^{+0.07}_{-0.13}$	43.64	45.24	44.19	44.96	45.25
LID-1689	$11.28^{+0.23}_{-0.31}$	$1.11^{+0.24}_{-0.00}$	43.15	43.58	44.40	43.78	44.56
LID-1690	$11.26^{+1.25}_{-0.93}$	$1.45^{+0.00}_{-0.18}$	43.39	44.38	44.11	0.00	-44.26
LID-1691	$11.10^{+0.30}_{-0.55}$	$2.73^{+0.15}_{-0.06}$	44.46	45.88	44.40	0.00	-45.48
LID-1692	$10.80^{+0.54}_{-0.69}$	$1.34^{+0.27}_{-0.17}$	44.24	44.38	44.12	43.81	-44.65
LID-1693	$11.74^{+0.72}_{-1.74}$	$0.96^{+0.02}_{-0.82}$	43.74	43.43	43.90	0.00	-44.19
LID-1696	$11.00^{+0.33}_{-0.53}$	$2.48^{+0.05}_{-0.05}$	44.36	45.69	44.43	0.00	-45.33
LID-1699	$11.77^{+0.83}_{-0.83}$	$1.18^{+0.05}_{-0.87}$	43.76	43.50	44.58	44.24	-44.79
LID-1702	$10.85^{+0.36}_{-0.40}$	$2.55^{+0.09}_{-0.00}$	44.58	45.75	44.46	0.00	-45.11
LID-1704	$10.79^{+0.22}_{-0.28}$	$1.18^{+0.05}_{-0.10}$	43.53	44.33	43.88	43.64	-44.69
LID-1706	$10.76^{+0.16}_{-0.23}$	$1.81^{+0.01}_{-0.12}$	43.54	44.88	44.42	44.22	-44.93
LID-1708	$10.75^{+0.17}_{-0.28}$	$2.22^{+0.11}_{-0.08}$	44.05	45.49	43.95	44.30	-44.64
LID-1711	$10.50^{+0.38}_{-0.28}$	$1.95^{+0.08}_{-0.21}$	43.54	45.07	43.99	44.50	-44.93
LID-1712	$10.20^{+0.62}_{-0.89}$	$1.50^{+0.13}_{-0.00}$	43.45	44.77	43.33	0.00	-44.15
LID-1715	$10.58^{+0.17}_{-0.08}$	$1.46^{+0.08}_{-0.03}$	43.30	44.26	43.99	44.10	44.91
LID-1716	$10.41^{+0.28}_{-0.40}$	$1.42^{+0.58}_{-0.23}$	43.78	44.46	44.11	0.00	-44.66
LID-1717	$11.37^{+0.62}_{-0.63}$	$1.22^{+0.02}_{-0.05}$	43.94	44.46	44.28	44.16	-44.47
LID-1718	$11.09^{+0.38}_{-0.41}$	$2.21^{+0.02}_{-0.09}$	44.56	45.41	44.52	0.00	-44.95
LID-1719	$12.22^{+0.53}_{-0.78}$	$1.31^{+0.00}_{-0.77}$	43.85	43.38	44.82	44.08	-44.71
LID-1720	$10.73^{+0.18}_{-0.35}$	$2.53^{+0.00}_{-0.25}$	44.15	45.62	44.44	0.00	-45.28
LID-1721	$10.92^{+0.08}_{-0.19}$	$1.39^{+0.12}_{-0.06}$	43.91	44.65	44.69	44.40	-44.53
LID-1726	$10.38^{+0.15}_{-0.08}$	$0.53^{+0.10}_{-0.75}$	42.98	43.12	43.76	43.35	-44.07
LID-1727	$11.27^{+0.13}_{-0.13}$	$1.68^{+0.16}_{-0.14}$	43.67	44.89	44.71	43.89	-44.88
LID-1728	$10.47^{+0.47}_{-0.21}$	$1.82^{+0.26}_{-0.15}$	44.04	44.91	44.34	44.39	-45.20
LID-1731	$11.06^{+0.27}_{-0.22}$	$1.49^{+0.05}_{-0.62}$	43.43	44.22	44.26	0.00	-44.97
LID-1732	$10.70^{+0.23}_{-0.38}$	$1.41^{+0.08}_{-0.74}$	43.54	43.92	44.05	0.00	-45.06

Table B.2 – continued

ID	log $M_{stellar}$ ($M_\odot$)	log SFR^{tot} ($M_\odot$ yr^{-1})	log $L_{2-10\ keV}$ (erg s^{-1})	log L_{2300} (erg s^{-1})	log L_{5100} (erg s^{-1})	log $L_{6\mu m}$ (erg s^{-1})	log L_{IR} (erg s^{-1})
LID-1735	$10.42^{+0.33}_{-0.41}$	$1.62^{+0.02}_{-0.95}$	43.61	44.18	43.88	44.82	-45.06
LID-1736	$10.85^{+0.10}_{-0.16}$	$1.04^{+0.20}_{-0.00}$	42.87	43.48	44.21	43.50	44.74
LID-1740	$11.76^{+0.50}_{-0.41}$	$2.14^{+0.04}_{-0.18}$	42.90	43.57	44.65	0.00	-45.56
LID-1742	$11.49^{+0.44}_{-0.84}$	$1.39^{+0.00}_{-0.37}$	43.51	44.35	44.26	0.00	-44.51
LID-1743	$11.45^{+0.67}_{-0.96}$	$0.46^{+0.05}_{-1.61}$	43.60	42.33	43.90	0.00	-44.11
LID-1744	$10.79^{+0.40}_{-0.36}$	$1.32^{+0.14}_{-0.34}$	43.40	44.10	44.32	0.00	-44.94
LID-1746	$11.77^{+0.75}_{-0.40}$	$0.95^{+0.00}_{-0.47}$	43.51	43.70	44.78	0.00	-44.12
LID-1748	$11.37^{+0.18}_{-0.49}$	$1.32^{+0.01}_{-0.15}$	43.19	44.49	44.48	0.00	-44.23
LID-1750	$9.36^{+0.56}_{-0.73}$	$1.40^{+0.15}_{-0.21}$	44.33	44.51	43.56	0.00	-44.66
LID-1751	$11.07^{+0.13}_{-0.32}$	$0.75^{+0.08}_{-0.38}$	43.21	43.75	44.26	0.00	-44.11
LID-1753	$10.47^{+0.61}_{-0.56}$	$2.07^{+0.17}_{-0.01}$	43.82	45.39	44.74	0.00	-44.17
LID-1757	$8.84^{+0.66}_{-0.45}$	$1.56^{+0.04}_{-1.23}$	43.85	43.46	43.45	0.00	-45.21
LID-1766	$10.69^{+0.11}_{-0.15}$	$1.68^{+0.05}_{-0.07}$	43.14	44.91	44.20	43.49	-44.51
LID-1770	$10.87^{+0.12}_{-0.15}$	$1.20^{+0.13}_{-0.13}$	43.01	44.41	44.22	0.00	-44.17
LID-1776	$10.09^{+0.24}_{-0.17}$	$1.34^{+0.09}_{-0.14}$	43.26	44.50	43.87	43.95	-44.63
LID-1777	$10.82^{+0.22}_{-0.10}$	$2.22^{+0.12}_{-0.00}$	43.66	45.45	44.22	44.36	44.89
LID-1778	$10.97^{+0.22}_{-0.20}$	$1.80^{+0.00}_{-0.22}$	44.20	44.69	44.33	44.33	-44.99
LID-1779	$10.59^{+0.03}_{-0.10}$	$1.01^{+0.02}_{-0.12}$	43.26	43.25	43.97	44.37	44.83
LID-1780	$10.87^{+0.00}_{-0.00}$	$1.52^{+0.12}_{-0.01}$	42.89	44.60	44.50	44.06	44.87
LID-1781	$10.79^{+0.18}_{-0.09}$	$1.20^{+0.14}_{-0.20}$	43.20	44.36	44.09	43.97	-44.56
LID-1789	$10.97^{+0.19}_{-0.08}$	$1.47^{+0.16}_{-0.00}$	43.98	44.61	44.34	44.52	45.40
LID-1790	$10.83^{+0.20}_{-0.10}$	$1.25^{+0.08}_{-0.12}$	43.78	44.37	44.10	43.80	-44.54
LID-1792	$10.95^{+0.00}_{-0.00}$	$1.54^{+0.00}_{-0.08}$	43.81	44.72	44.71	0.00	-44.31
LID-1793	$10.96^{+0.28}_{-0.50}$	$1.71^{+0.00}_{-0.66}$	43.86	44.34	44.23	44.23	-45.15
LID-1795	$10.91^{+0.24}_{-0.22}$	$1.89^{+0.05}_{-0.10}$	44.00	45.06	44.55	0.00	-45.12
LID-1801	$11.00^{+0.35}_{-0.28}$	$1.42^{+0.05}_{-0.09}$	43.57	44.65	44.40	0.00	-44.08
LID-1803	$10.48^{+0.13}_{-0.00}$	$0.92^{+0.12}_{-0.05}$	42.54	44.17	44.07	0.00	-43.71
LID-1805	$10.73^{+0.00}_{-0.00}$	$1.64^{+0.10}_{-0.00}$	43.24	44.44	44.25	42.77	45.17
LID-1806	$10.89^{+0.26}_{-0.29}$	$2.46^{+0.15}_{-0.09}$	43.80	44.97	44.31	44.65	45.91
LID-1810	$10.13^{+0.32}_{-0.49}$	$1.79^{+0.15}_{-0.00}$	43.55	45.05	43.03	0.00	-44.72
LID-1812	$10.64^{+0.18}_{-0.04}$	$0.59^{+0.21}_{-0.38}$	42.43	43.46	44.10	42.90	-44.27
LID-1814	$10.35^{+0.41}_{-0.53}$	$1.96^{+0.07}_{-0.54}$	43.80	44.76	44.12	0.00	-45.31
LID-1817	$10.60^{+0.17}_{-0.10}$	$2.03^{+0.10}_{-0.00}$	43.83	45.28	44.59	44.32	45.48
LID-1818	$10.61^{+0.16}_{-0.11}$	$1.09^{+0.05}_{-0.20}$	43.21	44.23	43.96	0.00	-44.17
LID-1821	$10.79^{+0.13}_{-0.10}$	$2.05^{+0.18}_{-0.00}$	43.48	45.00	44.63	45.46	45.98
LID-1824	$10.60^{+0.56}_{-0.30}$	$1.74^{+0.18}_{-0.07}$	44.19	44.94	44.04	0.00	-44.62
LID-1826	$10.71^{+0.10}_{-0.15}$	$1.98^{+0.05}_{-0.01}$	43.92	45.11	44.66	45.28	45.02
LID-1827	$10.45^{+0.12}_{-0.16}$	$1.14^{+0.00}_{-0.31}$	43.76	44.12	43.93	43.16	-44.56
LID-1830	$11.59^{+0.08}_{-0.24}$	$2.27^{+0.13}_{-0.07}$	43.68	45.50	44.77	45.11	-45.02
LID-1831	$10.79^{+0.19}_{-0.20}$	$2.03^{+0.09}_{-0.17}$	43.96	45.11	44.57	0.00	-45.32

Table B.2 – continued

ID	log $M_{stellar}$ ($M_\odot$)	log SFR^{tot} ($M_\odot$ yr^{-1})	log $L_{2-10\ keV}$ (erg s^{-1})	log L_{2300} (erg s^{-1})	log L_{5100} (erg s^{-1})	log $L_{6\mu m}$ (erg s^{-1})	log L_{IR} (erg s^{-1})
LID-1836	$10.61^{+0.16}_{-0.11}$	$1.75^{+0.09}_{-0.13}$	43.81	44.94	44.14	44.26	-44.65
LID-1837	$10.67^{+0.19}_{-0.16}$	$1.04^{+0.09}_{-0.13}$	42.58	44.22	43.95	0.00	-44.15
LID-1838	$10.67^{+0.24}_{-0.23}$	$2.01^{+0.44}_{-0.00}$	44.43	44.07	44.49	0.00	-45.71
LID-1839	$10.55^{+0.07}_{-0.06}$	$1.05^{+0.00}_{-0.15}$	42.83	44.18	44.18	43.27	-44.09
LID-1840	$10.64^{+0.00}_{-0.00}$	$1.81^{+0.12}_{-0.09}$	43.68	44.37	44.54	45.02	44.89
LID-1841	$11.09^{+0.24}_{-0.25}$	$2.06^{+0.17}_{-0.05}$	43.77	45.32	44.61	44.45	-45.04
LID-1843	$10.21^{+0.60}_{-0.32}$	$1.35^{+0.61}_{-1.70}$	43.65	43.28	43.49	0.00	-45.03
LID-1844	$10.34^{+0.08}_{-0.05}$	$0.56^{+0.17}_{-0.00}$	42.46	42.99	43.81	43.03	44.17
LID-1846	$10.71^{+0.11}_{-0.03}$	$1.44^{+0.10}_{-0.00}$	43.37	44.45	44.27	43.66	44.81
LID-1848	$10.90^{+0.00}_{-0.00}$	$1.68^{+0.00}_{-0.11}$	43.29	44.54	44.53	44.18	45.27
LID-1850	$10.13^{+0.24}_{-0.40}$	$0.71^{+0.03}_{-1.26}$	43.04	42.71	43.61	0.00	-44.31
LID-1856	$10.80^{+0.00}_{-0.00}$	$1.24^{+0.00}_{-0.08}$	44.49	44.47	44.46	44.64	44.50
LID-1858	$10.10^{+0.38}_{-0.78}$	$1.75^{+0.09}_{-0.00}$	44.01	44.96	43.82	0.00	-44.44
LID-1859	$11.10^{+0.00}_{-0.00}$	$2.32^{+0.01}_{-0.08}$	44.29	45.47	45.11	44.76	-45.23
LID-1860	$10.89^{+0.09}_{-0.18}$	$1.80^{+0.00}_{-0.73}$	43.76	44.40	44.57	0.00	-45.26
LID-1861	$10.85^{+0.19}_{-0.27}$	$1.79^{+0.05}_{-0.04}$	43.04	45.04	43.94	43.46	-44.65
LID-1862	$10.62^{+0.20}_{-0.06}$	$1.99^{+0.04}_{-0.03}$	43.34	45.19	44.33	43.72	45.16
LID-1863	$10.78^{+0.13}_{-0.09}$	$1.13^{+0.11}_{-0.00}$	43.49	44.39	44.29	43.58	44.79
LID-1864	$10.55^{+0.26}_{-0.24}$	$1.23^{+0.00}_{-0.38}$	43.39	44.16	43.80	0.00	-44.56
LID-1867	$10.82^{+0.29}_{-0.24}$	$1.83^{+0.16}_{-0.00}$	43.60	45.06	44.26	43.84	45.28
LID-1869	$10.58^{+0.24}_{-0.22}$	$1.89^{+0.04}_{-0.09}$	43.78	45.11	44.29	44.26	-44.68
LID-1871	$11.12^{+0.10}_{-0.04}$	$2.24^{+0.10}_{-0.06}$	44.14	45.49	45.13	44.58	-45.11
LID-1872	$10.84^{+0.00}_{-0.00}$	$1.05^{+0.09}_{-0.00}$	43.58	42.92	44.36	44.97	44.69
LID-1875	$10.59^{+0.30}_{-0.21}$	$1.82^{+0.11}_{-0.04}$	43.91	45.06	44.44	0.00	-44.42
LID-1877	$10.79^{+0.30}_{-0.36}$	$1.80^{+0.00}_{-0.46}$	43.84	44.59	44.12	0.00	-45.22
LID-1880	$10.56^{+0.36}_{-0.46}$	$1.83^{+0.05}_{-0.20}$	43.33	44.85	43.89	0.00	-45.06
LID-1883	$11.09^{+0.23}_{-0.21}$	$1.72^{+0.20}_{-0.29}$	43.89	44.71	44.53	44.97	-45.21
LID-1884	$10.20^{+0.30}_{-0.25}$	$0.88^{+0.05}_{-0.33}$	43.47	43.85	43.67	0.00	-44.23
LID-1885	$10.87^{+0.14}_{-0.01}$	$1.36^{+0.08}_{-0.14}$	43.67	44.56	44.55	43.73	-44.62
LID-1926	$9.43^{+1.30}_{-1.03}$	$0.55^{+0.68}_{-0.52}$	43.37	43.26	43.19	0.00	-44.35
LID-1927	$10.18^{+0.20}_{-0.07}$	$0.06^{+0.25}_{-0.38}$	42.17	42.90	43.36	0.00	-43.49
LID-1964	$10.97^{+0.05}_{-0.08}$	$1.50^{+0.13}_{-0.06}$	43.26	44.70	44.61	43.86	-44.66
LID-1966	$10.94^{+0.19}_{-0.18}$	$2.14^{+0.00}_{-0.24}$	43.37	45.31	44.54	43.95	-44.96
LID-1968	$10.32^{+0.20}_{-0.31}$	$1.15^{+0.60}_{-0.14}$	43.50	44.35	44.18	0.00	-44.60
LID-1971	$10.45^{+0.39}_{-0.37}$	$1.77^{+0.07}_{-0.28}$	43.75	44.78	43.94	44.42	-45.14
LID-1972	$10.53^{+0.41}_{-0.38}$	$0.68^{+0.25}_{-0.52}$	43.41	43.49	43.92	0.00	-44.15
LID-1977	$11.16^{+0.20}_{-0.21}$	$2.29^{+0.15}_{-0.06}$	44.27	45.55	44.59	45.09	-45.05
LID-1978	$10.74^{+0.22}_{-0.18}$	$1.15^{+0.09}_{-0.09}$	43.57	44.35	43.99	0.00	-44.16
LID-1979	$11.10^{+0.24}_{-0.21}$	$2.49^{+0.05}_{-0.07}$	43.72	45.71	44.72	43.42	45.32
LID-1980	$10.82^{+0.17}_{-0.22}$	$1.72^{+0.12}_{-0.35}$	44.17	44.53	44.44	0.00	-45.31

Table B.2 – continued

ID	log $M_{stellar}$ ($M_\odot$)	log SFR^{tot} ($M_\odot$ yr^{-1})	log $L_{2-10\ keV}$ (erg s^{-1})	log L_{2300} (erg s^{-1})	log L_{5100} (erg s^{-1})	log $L_{6\mu m}$ (erg s^{-1})	log L_{IR} (erg s^{-1})
LID-1983	$11.02^{+0.20}_{-0.07}$	$1.52^{+0.01}_{-0.11}$	43.25	44.72	44.54	0.00	-44.17
LID-1987	$11.14^{+0.45}_{-0.63}$	$2.20^{+0.37}_{-0.00}$	43.84	45.48	44.39	0.00	-45.15
LID-1988	$10.60^{+0.17}_{-0.09}$	$0.11^{+0.03}_{-0.15}$	42.44	43.32	43.96	0.00	-42.95
LID-1992	$10.11^{+0.10}_{-0.03}$	$0.64^{+0.09}_{-0.18}$	42.69	43.80	43.79	42.67	-44.09
LID-1994	$10.06^{+0.14}_{-0.12}$	$1.16^{+0.07}_{-0.02}$	42.92	44.42	43.82	0.00	-43.89
LID-1999	$10.54^{+0.20}_{-0.20}$	$0.86^{+0.18}_{-0.06}$	43.09	44.17	43.81	43.28	-44.45
LID-2003	$10.85^{+0.57}_{-0.22}$	$2.45^{+0.29}_{-0.00}$	43.60	45.77	43.98	44.77	45.73
LID-2004	$10.78^{+0.34}_{-0.14}$	$1.59^{+0.00}_{-0.45}$	43.62	44.45	44.02	0.00	-44.94
LID-2007	$10.19^{+0.21}_{-0.22}$	$0.70^{+0.05}_{-0.50}$	43.13	43.48	43.81	0.00	-44.20
LID-2008	$10.14^{+0.35}_{-0.33}$	$1.35^{+0.01}_{-0.80}$	43.27	43.85	43.81	0.00	-44.89
LID-2012	$10.56^{+0.33}_{-0.34}$	$0.98^{+0.39}_{-0.99}$	43.58	43.40	44.21	0.00	-44.49
LID-2017	$10.40^{+0.38}_{-0.53}$	$1.02^{+0.65}_{-0.25}$	43.65	43.99	43.98	0.00	-44.63
LID-2024	$10.86^{+0.27}_{-0.12}$	$1.36^{+0.09}_{-0.09}$	42.98	44.46	44.28	0.00	-44.46
LID-2025	$10.34^{+0.34}_{-0.41}$	$1.22^{+0.21}_{-0.39}$	43.43	44.23	43.70	0.00	-44.39
LID-2027	$11.25^{+0.22}_{-0.34}$	$2.79^{+0.24}_{-0.00}$	43.88	46.10	44.08	43.80	46.08
LID-2028	$11.03^{+0.28}_{-0.15}$	$1.72^{+0.00}_{-0.62}$	43.67	44.40	44.37	0.00	-45.19
LID-2029	$10.64^{+0.13}_{-0.13}$	$1.16^{+0.12}_{-0.17}$	43.66	44.24	44.06	0.00	-44.39
LID-2030	$10.99^{+0.00}_{-0.00}$	$1.55^{+0.09}_{-0.04}$	42.79	44.62	44.61	44.12	44.78
LID-2032	$10.31^{+0.00}_{-0.00}$	$0.43^{+0.10}_{-0.65}$	42.24	43.05	44.04	0.00	-43.97
LID-2037	$11.11^{+0.09}_{-0.16}$	$1.51^{+0.02}_{-0.08}$	43.03	44.74	44.55	0.00	-44.08
LID-2039	$10.40^{+0.27}_{-0.50}$	$0.85^{+0.08}_{-0.94}$	42.99	43.10	43.65	0.00	-44.49
LID-2040	$10.62^{+0.29}_{-0.24}$	$2.00^{+0.22}_{-0.56}$	43.65	44.84	44.56	0.00	-45.30
LID-2047	$10.41^{+0.31}_{-0.22}$	$2.12^{+0.00}_{-0.33}$	43.69	44.97	44.49	0.00	-45.26
LID-2049	$10.08^{+0.19}_{-0.54}$	$1.50^{+0.18}_{-0.10}$	43.61	44.58	43.92	0.00	-44.46
LID-2050	$10.41^{+0.21}_{-0.36}$	$1.14^{+0.34}_{-0.79}$	43.76	43.74	43.89	0.00	-44.48
LID-2056	$11.46^{+0.31}_{-0.69}$	$1.40^{+0.51}_{-0.00}$	43.34	44.53	44.70	43.10	45.07
LID-2058	$10.61^{+0.29}_{-0.19}$	$1.73^{+0.02}_{-0.18}$	43.26	44.84	44.30	0.00	-44.83
LID-2060	$10.61^{+0.23}_{-0.24}$	$1.87^{+0.06}_{-0.01}$	43.50	45.13	44.34	43.67	-44.85
LID-2063	$10.25^{+0.37}_{-0.38}$	$1.64^{+0.00}_{-1.19}$	43.74	43.76	44.00	0.00	-45.23
LID-2064	$10.56^{+0.32}_{-0.35}$	$2.10^{+0.12}_{-0.01}$	43.94	45.36	44.10	0.00	-44.61
LID-2068	$11.00^{+0.40}_{-0.35}$	$2.49^{+0.05}_{-0.15}$	44.17	45.62	44.35	0.00	-45.14
LID-2069	$11.24^{+0.25}_{-0.42}$	$1.87^{+0.07}_{-0.14}$	43.89	44.99	44.34	0.00	-44.98
LID-2071	$11.17^{+0.69}_{-0.72}$	$1.82^{+0.02}_{-0.05}$	43.33	44.97	44.34	44.60	45.45
LID-2072	$11.44^{+0.18}_{-0.05}$	$0.92^{+0.12}_{-0.07}$	42.77	44.17	44.54	43.24	-44.30
LID-2079	$10.31^{+0.19}_{-0.20}$	$1.41^{+0.22}_{-0.00}$	43.53	44.69	44.08	0.00	-44.30
LID-2084	$10.69^{+0.40}_{-0.27}$	$1.75^{+0.00}_{-0.30}$	43.63	44.61	44.62	0.00	-45.08
LID-2086	$10.92^{+0.20}_{-0.34}$	$2.50^{+0.00}_{-0.20}$	44.16	45.58	44.76	0.00	-45.32
LID-2089	$11.22^{+0.28}_{-0.54}$	$0.20^{+0.15}_{-0.52}$	42.69	42.76	43.99	0.00	-43.74
LID-2092	$10.60^{+0.24}_{-0.23}$	$1.82^{+0.08}_{-0.14}$	43.47	45.01	44.17	0.00	-44.44
LID-2093	$12.52^{+0.30}_{-0.87}$	$0.62^{+0.31}_{-0.21}$	43.20	43.79	44.87	0.00	-44.15

Table B.2 – continued

ID	log $M_{stellar}$ ($M_\odot$)	log SFR^{tot} ($M_\odot$ yr^{-1})	log $L_{2-10\ keV}$ (erg s^{-1})	log L_{2300} (erg s^{-1})	log L_{5100} (erg s^{-1})	log $L_{6\mu m}$ (erg s^{-1})	log L_{IR} (erg s^{-1})
LID-2096	$10.63^{+0.74}_{-0.55}$	$0.85^{+0.09}_{-0.03}$	43.04	43.87	43.95	43.19	-44.54
LID-2098	$10.76^{+0.20}_{-0.19}$	$1.31^{+0.17}_{-0.20}$	43.50	44.35	44.16	0.00	-44.32
LID-2099	$10.02^{+0.14}_{-0.27}$	$0.23^{+0.10}_{-1.00}$	42.34	42.53	43.17	0.00	-43.80
LID-2102	$10.48^{+0.45}_{-0.58}$	$0.48^{+0.14}_{-0.51}$	43.07	43.33	43.82	0.00	-43.96
LID-2103	$9.97^{+0.53}_{-0.48}$	$1.87^{+0.17}_{-0.00}$	43.09	45.13	43.69	44.13	44.95
LID-2106	$10.38^{+0.51}_{-0.34}$	$2.23^{+0.00}_{-0.28}$	43.83	45.22	43.90	0.00	-45.25
LID-2109	$11.33^{+0.88}_{-1.36}$	$0.92^{+0.02}_{-0.11}$	43.33	44.19	43.83	0.00	0.00
LID-2111	$11.26^{+0.91}_{-1.01}$	$0.39^{+0.17}_{-1.47}$	43.09	42.23	43.76	0.00	-44.12
LID-2112	$10.12^{+1.47}_{-1.02}$	$0.79^{+0.52}_{-0.70}$	43.31	43.38	43.71	0.00	-44.35
LID-2114	$10.91^{+0.23}_{-0.18}$	$2.67^{+0.07}_{-0.00}$	44.06	45.93	44.62	0.00	-45.08
LID-2115	$12.04^{+0.68}_{-0.67}$	$1.23^{+0.00}_{-1.92}$	43.39	43.27	44.71	0.00	-44.70
LID-2118	$10.68^{+0.20}_{-0.28}$	$2.12^{+0.39}_{-0.00}$	43.33	45.35	44.51	43.96	45.55
LID-2119	$10.51^{+0.38}_{-0.17}$	$1.17^{+0.03}_{-1.18}$	43.42	43.33	43.70	0.00	-44.67
LID-2120	$11.15^{+0.29}_{-0.66}$	$2.40^{+0.13}_{-0.12}$	43.89	45.68	44.06	0.00	-45.22
LID-2122	$9.85^{+0.45}_{-0.37}$	$1.60^{+0.07}_{-0.88}$	43.96	44.03	43.83	0.00	-45.17
LID-2127	$10.56^{+0.06}_{-0.07}$	$1.36^{+0.08}_{-0.12}$	42.93	43.95	44.28	43.88	44.91
LID-2128	$10.17^{+0.49}_{-0.47}$	$0.88^{+0.55}_{-0.45}$	43.59	43.90	43.71	0.00	-44.40
LID-2129	$11.22^{+1.05}_{-0.74}$	$0.46^{+0.15}_{-0.96}$	43.15	42.81	43.96	0.00	-44.13
LID-2132	$10.70^{+0.12}_{-0.02}$	$1.37^{+0.07}_{-0.10}$	42.96	44.38	44.55	43.56	45.04
LID-2142	$10.62^{+0.20}_{-0.06}$	$1.18^{+0.06}_{-0.02}$	42.63	44.33	44.32	44.13	44.48
LID-2143	$10.84^{+0.26}_{-0.17}$	$1.86^{+0.08}_{-0.03}$	43.44	45.08	44.19	44.29	-44.88
LID-2144	$11.51^{+1.04}_{-0.80}$	$0.92^{+0.02}_{-0.95}$	43.33	43.27	44.08	43.96	-44.62
LID-2146	$10.41^{+0.28}_{-0.38}$	$1.50^{+0.13}_{-0.04}$	43.86	44.73	44.08	0.00	-44.28
LID-2153	$10.50^{+0.19}_{-0.17}$	$1.48^{+0.06}_{-0.15}$	43.25	44.62	44.11	43.98	-44.51
LID-2155	$10.03^{+0.00}_{-0.00}$	$1.89^{+0.14}_{-0.02}$	43.33	45.19	44.54	0.00	0.00
LID-2159	$10.34^{+0.19}_{-0.17}$	$1.72^{+0.12}_{-0.07}$	43.47	44.92	44.22	43.73	45.11
LID-2160	$11.11^{+0.30}_{-0.29}$	$2.29^{+0.17}_{-0.00}$	43.82	45.49	44.54	42.19	45.47
LID-2175	$10.40^{+0.45}_{-0.64}$	$1.83^{+0.09}_{-0.17}$	43.75	44.99	43.60	0.00	-44.91
LID-2179	$10.31^{+0.09}_{-0.14}$	$0.83^{+0.11}_{-0.26}$	42.54	43.89	43.79	42.90	-44.08
LID-2180	$10.40^{+0.27}_{-0.20}$	$1.70^{+0.05}_{-0.09}$	43.66	44.85	44.34	43.61	-44.81
LID-2183	$10.40^{+0.60}_{-0.49}$	$1.40^{+0.04}_{-0.26}$	43.52	44.57	43.79	43.37	-44.45
LID-2185	$10.86^{+0.12}_{-0.15}$	$0.66^{+0.17}_{-0.36}$	42.48	43.55	44.19	0.00	-44.21
LID-2193	$10.71^{+0.12}_{-0.03}$	$0.54^{+0.10}_{-0.41}$	42.73	43.38	44.11	0.00	-43.95
LID-2194	$10.56^{+0.19}_{-0.22}$	$1.09^{+0.04}_{-0.26}$	42.76	44.10	43.74	0.00	-44.38
LID-2203	$10.88^{+0.29}_{-0.36}$	$2.26^{+0.24}_{-0.14}$	44.38	45.37	44.32	0.00	-45.30
LID-2209	$10.82^{+0.20}_{-0.07}$	$1.24^{+0.09}_{-0.09}$	42.93	44.45	44.44	43.10	-44.53
LID-2210	$10.44^{+0.17}_{-0.04}$	$1.68^{+0.06}_{-0.01}$	42.93	44.82	44.36	43.96	44.90
LID-2211	$10.89^{+0.13}_{-0.01}$	$0.76^{+0.08}_{-0.37}$	43.08	43.63	44.27	0.00	-44.12
LID-2212	$10.58^{+0.17}_{-0.24}$	$1.10^{+0.04}_{-0.25}$	42.91	44.14	43.78	43.21	-44.41
LID-2214	$10.83^{+0.19}_{-0.05}$	$1.97^{+0.08}_{-0.01}$	42.83	45.18	44.66	44.61	44.98

Table B.2 – continued

ID	log $M_{stellar}$ ($M_\odot$)	log SFR^{tot} ($M_\odot$ yr^{-1})	log $L_{2-10\ keV}$ (erg s^{-1})	log L_{2300} (erg s^{-1})	log L_{5100} (erg s^{-1})	log $L_{6\mu m}$ (erg s^{-1})	log L_{IR} (erg s^{-1})
LID-2215	$10.34^{+0.27}_{-0.25}$	$0.99^{+0.03}_{-0.39}$	43.20	43.99	43.63	0.00	-44.17
LID-2221	$9.97^{+0.56}_{-0.29}$	$1.09^{+0.38}_{-0.46}$	43.37	43.88	43.71	0.00	-44.43
LID-2226	$10.32^{+0.08}_{-0.18}$	$0.91^{+0.12}_{-0.31}$	42.90	43.92	44.08	43.20	-44.50
LID-2231	$10.70^{+0.00}_{-0.00}$	$0.75^{+0.08}_{-0.63}$	42.81	43.44	44.34	43.69	-44.32
LID-2238	$10.78^{+0.33}_{-0.31}$	$1.18^{+0.39}_{-0.39}$	43.47	44.08	44.30	0.00	-44.67
LID-2239	$10.11^{+0.21}_{-0.17}$	$0.91^{+0.00}_{-0.41}$	43.22	43.78	43.76	0.00	-44.35
LID-2240	$10.27^{+0.53}_{-0.50}$	$1.89^{+0.14}_{-0.17}$	43.81	45.10	43.62	0.00	-44.64
LID-2241	$10.85^{+0.24}_{-0.26}$	$2.36^{+0.16}_{-0.07}$	43.73	45.32	44.62	44.42	45.73
LID-2246	$9.86^{+0.54}_{-0.35}$	$1.36^{+0.12}_{-0.43}$	43.32	44.13	43.57	0.00	-44.56
LID-2249	$9.83^{+0.19}_{-0.40}$	$0.76^{+0.08}_{-0.44}$	43.03	43.65	43.54	0.00	-44.15
LID-2251	$10.63^{+0.12}_{-0.18}$	$2.20^{+0.14}_{-0.04}$	43.31	45.46	44.53	44.73	-45.14
LID-2261	$10.57^{+0.31}_{-0.20}$	$2.02^{+0.11}_{-0.00}$	43.49	45.01	44.08	44.53	45.43
LID-2262	$10.70^{+0.46}_{-0.43}$	$1.66^{+0.16}_{-1.17}$	44.15	43.63	44.36	0.00	-45.28
LID-2265	$10.99^{+0.18}_{-0.20}$	$1.38^{+0.05}_{-0.24}$	43.82	44.54	44.27	0.00	-44.28
LID-2268	$11.25^{+0.16}_{-0.03}$	$1.62^{+0.12}_{-0.00}$	42.69	44.89	44.70	44.12	44.80
LID-2272	$11.44^{+0.51}_{-0.34}$	$1.62^{+0.92}_{-0.01}$	43.17	44.90	44.81	0.00	-43.49
LID-2277	$10.73^{+0.23}_{-0.21}$	$1.97^{+0.14}_{-0.00}$	44.08	45.05	44.73	44.73	-45.28
LID-2281	$10.81^{+0.28}_{-0.23}$	$2.33^{+0.02}_{-0.07}$	43.78	45.40	44.30	44.29	45.50
LID-2283	$10.73^{+0.17}_{-0.38}$	$1.43^{+0.00}_{-0.35}$	43.44	44.28	44.10	0.00	-44.75
LID-2284	$10.71^{+0.00}_{-0.00}$	$0.87^{+0.06}_{-0.00}$	42.78	43.42	44.50	43.45	44.84
LID-2293	$10.59^{+0.16}_{-0.31}$	$1.77^{+0.00}_{-0.50}$	43.44	44.57	44.44	0.00	-45.13
LID-2294	$10.83^{+0.25}_{-0.45}$	$2.38^{+0.09}_{-0.06}$	43.96	45.59	44.53	0.00	-45.33
LID-2296	$10.67^{+0.39}_{-0.36}$	$2.33^{+0.10}_{-0.08}$	44.70	45.58	44.49	0.00	-44.73
LID-2297	$11.06^{+0.24}_{-0.25}$	$2.40^{+0.09}_{-0.03}$	43.68	45.57	44.34	0.00	-45.52
LID-2318	$10.88^{+0.00}_{-0.00}$	$1.67^{+0.06}_{-0.16}$	43.04	44.58	44.49	43.95	45.08
LID-2350	$10.43^{+0.15}_{-0.12}$	$1.02^{+0.10}_{-0.21}$	42.85	44.04	44.03	0.00	-44.45
LID-2387	$10.65^{+0.45}_{-0.14}$	$2.72^{+0.02}_{-0.08}$	44.05	45.78	44.29	45.30	45.69
LID-2411	$10.35^{+0.16}_{-0.22}$	$1.40^{+0.03}_{-0.09}$	43.94	44.62	43.93	0.00	-44.13
LID-2414	$11.30^{+0.12}_{-0.02}$	$0.94^{+0.10}_{-0.26}$	43.48	44.04	44.68	43.42	-44.50
LID-2415	$10.50^{+0.12}_{-0.02}$	$0.90^{+0.14}_{-0.01}$	42.91	44.21	44.20	43.22	-44.10
LID-2416	$10.36^{+0.05}_{-0.08}$	$0.19^{+0.14}_{-0.35}$	42.84	43.12	43.85	0.00	-43.61
LID-2423	$10.40^{+0.22}_{-0.09}$	$0.64^{+0.09}_{-0.83}$	43.38	43.14	43.87	0.00	44.21
LID-2424	$10.84^{+0.14}_{-0.13}$	$0.80^{+0.14}_{-0.00}$	42.84	43.59	44.32	43.89	44.63
LID-2425	$10.64^{+0.29}_{-0.24}$	$1.18^{+0.13}_{-0.27}$	43.90	44.12	44.31	0.00	-44.44
LID-2431	$11.13^{+0.00}_{-0.00}$	$2.42^{+0.02}_{-0.05}$	43.69	45.65	45.04	44.73	45.22
LID-2432	$10.48^{+0.11}_{-0.17}$	$0.92^{+0.11}_{-0.00}$	42.80	43.65	43.98	43.05	44.51
LID-2433	$10.07^{+0.50}_{-0.35}$	$2.01^{+0.02}_{-0.06}$	43.21	45.21	43.90	43.99	-44.78
LID-2434	$10.42^{+0.28}_{-0.33}$	$2.01^{+0.01}_{-0.24}$	43.59	45.14	44.23	0.00	-45.02
LID-2437	$10.95^{+0.38}_{-0.52}$	$1.47^{+0.56}_{-0.12}$	44.04	44.39	44.28	0.00	-45.13
LID-2439	$10.44^{+0.22}_{-0.12}$	$1.09^{+0.04}_{-0.21}$	43.69	44.13	44.03	43.69	-44.69

Table B.2 – continued

ID	log $M_{stellar}$ ($M_\odot$)	log SFR^{tot} ($M_\odot$ yr^{-1})	log $L_{2-10\ keV}$ (erg s^{-1})	log L_{2300} (erg s^{-1})	log L_{5100} (erg s^{-1})	log $L_{6\mu m}$ (erg s^{-1})	log L_{IR} (erg s^{-1})
LID-2442	$10.66^{+0.16}_{-0.03}$	$1.21^{+0.03}_{-0.12}$	43.01	44.31	44.31	43.31	-44.42
LID-2444	$10.30^{+0.11}_{-0.02}$	$0.91^{+0.02}_{-0.25}$	42.60	43.92	43.91	42.87	-44.02
LID-2451	$10.61^{+0.00}_{-0.13}$	$1.05^{+0.08}_{-0.11}$	42.65	44.22	44.21	0.00	-44.01
LID-2452	$10.76^{+0.16}_{-0.22}$	$1.88^{+0.00}_{-0.27}$	43.56	44.94	44.46	44.22	-45.09
LID-2453	$10.44^{+0.14}_{-0.14}$	$0.88^{+0.06}_{-0.08}$	42.41	44.06	43.87	43.13	-44.11
LID-2454	$10.21^{+0.84}_{-0.73}$	$1.89^{+0.15}_{-0.10}$	43.43	45.06	43.75	0.00	-44.37
LID-2456	$10.34^{+0.07}_{-0.18}$	$0.94^{+0.09}_{-0.20}$	43.42	43.96	44.21	0.00	-44.25
LID-2458	$10.99^{+0.31}_{-0.34}$	$2.43^{+0.00}_{-0.30}$	44.35	45.35	44.48	43.47	45.94
LID-2459	$11.10^{+0.20}_{-0.30}$	$2.19^{+0.15}_{-0.13}$	44.06	45.42	44.73	44.68	-45.18
LID-2466	$11.02^{+0.00}_{-0.00}$	$1.35^{+0.19}_{-0.00}$	42.74	44.66	45.00	42.70	-44.20
LID-2467	$10.72^{+0.33}_{-0.14}$	$2.82^{+0.08}_{-0.06}$	43.55	45.77	44.16	44.51	46.11
LID-2468	$10.73^{+0.12}_{-0.20}$	$2.15^{+0.00}_{-0.28}$	43.81	45.18	44.60	0.00	-45.28
LID-2472	$11.02^{+0.19}_{-0.06}$	$1.34^{+0.09}_{-0.03}$	42.65	44.63	44.53	0.00	0.00
LID-2496	$10.15^{+0.28}_{-0.19}$	$1.06^{+0.15}_{-0.00}$	42.93	43.72	43.62	42.95	44.89
LID-2498	$10.41^{+0.21}_{-0.07}$	$0.41^{+0.02}_{-0.57}$	42.37	43.15	43.78	0.00	-43.80
LID-2504	$9.86^{+0.20}_{-0.58}$	$0.77^{+0.42}_{-0.32}$	43.11	43.81	43.44	0.00	-44.11
LID-2563	$10.46^{+0.26}_{-0.24}$	$1.82^{+0.02}_{-0.14}$	42.89	44.94	44.28	44.16	-44.95
LID-2569	$10.74^{+0.33}_{-0.46}$	$1.19^{+0.50}_{-1.10}$	43.68	43.45	44.28	0.00	-44.77
LID-2578	$10.56^{+0.47}_{-0.52}$	$1.46^{+0.09}_{-0.74}$	43.54	44.00	43.97	0.00	-45.09
LID-2582	$11.08^{+0.12}_{-0.15}$	$1.46^{+0.07}_{-0.05}$	43.17	44.67	44.57	0.00	-44.29
LID-2588	$10.66^{+0.22}_{-0.28}$	$1.88^{+0.00}_{-0.27}$	43.44	44.96	44.18	43.77	-44.76
LID-2603	$10.87^{+0.16}_{-0.15}$	$2.23^{+0.10}_{-0.00}$	43.56	45.46	44.58	43.98	-44.83
LID-2606	$10.15^{+0.41}_{-0.43}$	$1.99^{+0.00}_{-0.24}$	43.28	45.01	43.69	44.07	-44.89
LID-2609	$10.94^{+0.09}_{-0.29}$	$1.86^{+0.04}_{-0.79}$	43.88	44.44	44.60	0.00	-45.38
LID-2610	$9.48^{+0.37}_{-0.39}$	$0.88^{+0.15}_{-0.13}$	42.45	44.08	43.22	42.89	-44.28
LID-2621	$10.32^{+0.37}_{-0.30}$	$1.94^{+0.09}_{-0.14}$	43.55	45.17	43.95	44.39	-44.90
LID-2624	$10.71^{+0.34}_{-0.25}$	$1.83^{+0.11}_{-0.00}$	43.57	45.09	44.22	42.71	45.56
LID-2625	$10.85^{+0.46}_{-0.29}$	$2.53^{+0.11}_{-0.00}$	43.95	45.78	44.29	44.85	-45.27
LID-2632	$10.61^{+0.37}_{-0.35}$	$1.99^{+0.10}_{-0.14}$	43.61	45.20	43.93	0.00	-44.48
LID-2641	$11.53^{+0.85}_{-0.52}$	$1.50^{+0.00}_{-0.31}$	43.36	44.29	44.46	0.00	-44.74
LID-2642	$10.01^{+0.69}_{-0.98}$	$0.54^{+0.11}_{-0.25}$	43.10	43.54	43.71	0.00	-43.76
LID-2643	$11.26^{+0.09}_{-0.26}$	$1.09^{+0.04}_{-0.13}$	42.80	43.34	44.28	42.13	44.60
LID-2647	$10.81^{+0.19}_{-0.33}$	$1.52^{+0.07}_{-1.08}$	43.87	43.55	44.19	0.00	-45.21
LID-2652	$10.93^{+0.23}_{-0.21}$	$1.36^{+0.08}_{-0.16}$	43.16	44.52	44.16	0.00	-44.25
LID-2653	$11.21^{+0.31}_{-0.56}$	$2.32^{+0.37}_{-0.05}$	44.11	45.45	44.12	0.00	-45.66
LID-2660	$10.82^{+0.16}_{-0.11}$	$0.47^{+0.16}_{-0.89}$	42.92	42.85	44.20	0.00	-44.05
LID-2663	$11.32^{+1.09}_{-1.23}$	$2.05^{+0.08}_{-0.01}$	43.48	45.17	43.94	44.30	45.65
LID-2664	$10.53^{+0.40}_{-0.44}$	$2.09^{+0.12}_{-0.03}$	43.87	45.32	43.84	0.00	-44.61
LID-2665	$10.41^{+0.34}_{-0.38}$	$1.79^{+0.03}_{-0.21}$	43.72	44.72	44.01	0.00	-45.14
LID-2669	$9.80^{+0.36}_{-0.34}$	$1.08^{+0.05}_{-0.40}$	43.17	44.01	43.83	0.00	-44.35

Table B.2 – continued

ID	log $M_{stellar}$ ($M_\odot$)	log SFR^{tot} ($M_\odot$ yr^{-1})	log $L_{2-10\ keV}$ (erg s^{-1})	log L_{2300} (erg s^{-1})	log L_{5100} (erg s^{-1})	log $L_{6\mu m}$ (erg s^{-1})	log L_{IR} (erg s^{-1})
LID-2672	$11.08^{+0.31}_{-0.46}$	$1.91^{+0.36}_{-0.00}$	43.87	45.13	44.39	0.00	-44.99
LID-2680	$10.51^{+0.31}_{-0.47}$	$1.05^{+0.38}_{-0.30}$	43.55	44.06	43.85	0.00	-44.28
LID-2747	$10.73^{+0.07}_{-0.17}$	$1.86^{+0.07}_{-0.19}$	42.89	45.05	44.33	44.22	-44.85
LID-2772	$10.26^{+0.28}_{-0.31}$	$0.77^{+0.64}_{-0.43}$	43.53	43.50	43.98	0.00	-44.45
LID-2774	$10.44^{+0.44}_{-0.21}$	$2.07^{+0.00}_{-0.22}$	43.72	45.17	43.91	44.21	-44.92
LID-2778	$10.15^{+0.06}_{-0.15}$	$0.93^{+0.10}_{-0.00}$	42.91	44.18	44.07	43.52	-44.38
LID-2780	$10.89^{+0.00}_{-0.00}$	$1.45^{+0.08}_{-0.01}$	42.83	44.56	44.47	43.34	44.92
LID-2790	$9.77^{+0.62}_{-0.52}$	$0.14^{+0.61}_{-1.03}$	43.03	42.41	43.06	0.00	-43.74
LID-2793	$10.35^{+0.24}_{-0.26}$	$1.05^{+0.08}_{-0.34}$	43.32	43.96	43.86	0.00	-44.48
LID-2794	$9.98^{+0.57}_{-0.51}$	$1.69^{+0.05}_{-0.22}$	43.53	44.86	43.64	0.00	-44.43
LID-2795	$10.42^{+0.27}_{-0.38}$	$1.77^{+0.14}_{-0.62}$	43.93	44.72	44.18	0.00	-45.29
LID-2796	$10.03^{+0.28}_{-0.22}$	$0.21^{+0.21}_{-0.91}$	42.93	42.64	43.37	0.00	-43.85
LID-2798	$10.01^{+0.20}_{-0.07}$	$0.07^{+0.25}_{-0.59}$	42.80	42.73	43.81	43.93	-44.50
LID-2802	$10.72^{+0.25}_{-0.20}$	$1.82^{+0.03}_{-0.21}$	43.88	44.73	44.27	44.17	-45.15
LID-2803	$11.14^{+0.20}_{-0.28}$	$1.94^{+0.00}_{-0.42}$	43.75	44.70	44.43	0.00	-45.24
LID-2805	$11.08^{+0.14}_{-0.31}$	$1.68^{+0.01}_{-0.30}$	43.36	44.70	44.36	0.00	-44.87
LID-2808	$10.70^{+0.08}_{-0.19}$	$2.52^{+0.12}_{-0.00}$	43.48	45.73	44.29	45.19	45.88
LID-2815	$10.98^{+0.19}_{-0.19}$	$2.08^{+0.05}_{-0.17}$	43.62	44.28	44.48	44.19	45.91
LID-2817	$11.84^{+0.61}_{-0.65}$	$1.48^{+0.15}_{-0.00}$	43.53	44.60	44.59	44.64	-44.70
LID-2818	$11.49^{+0.69}_{-0.60}$	$1.69^{+0.12}_{-0.32}$	43.20	44.47	44.55	44.05	45.31
LID-2821	$11.03^{+0.37}_{-0.28}$	$2.55^{+0.18}_{-0.00}$	44.23	45.93	44.31	0.00	-45.05
LID-2827	$10.93^{+0.09}_{-0.05}$	$1.52^{+0.12}_{-0.05}$	43.12	44.74	44.64	43.98	-44.68
LID-2831	$11.01^{+0.17}_{-0.10}$	$2.13^{+0.10}_{-0.00}$	43.23	45.37	44.66	44.32	45.26
LID-2832	$10.64^{+0.49}_{-0.53}$	$2.19^{+0.03}_{-0.13}$	43.94	45.30	44.04	0.00	-45.28
LID-2836	$10.91^{+0.10}_{-0.03}$	$1.53^{+0.10}_{-0.21}$	43.37	44.67	44.48	43.68	-44.74
LID-2838	$10.92^{+0.31}_{-0.45}$	$1.42^{+0.13}_{-1.00}$	43.62	43.72	44.19	0.00	-45.15
LID-2841	$10.24^{+0.68}_{-0.33}$	$2.07^{+0.11}_{-0.02}$	43.71	45.23	43.91	0.00	-45.22
LID-2843	$10.67^{+0.00}_{-0.00}$	$2.07^{+0.06}_{-0.01}$	42.93	45.16	44.56	44.74	45.57
LID-2844	$10.65^{+0.26}_{-0.28}$	$2.14^{+0.07}_{-0.06}$	43.34	45.36	44.35	0.00	-44.86
LID-2845	$10.30^{+0.00}_{-0.00}$	$0.23^{+0.10}_{-0.46}$	42.46	43.03	43.85	0.00	-43.71
LID-2847	$11.00^{+0.15}_{-0.10}$	$0.74^{+0.09}_{-0.32}$	43.28	43.67	44.04	0.00	-44.09
LID-2853	$9.89^{+0.28}_{-0.41}$	$0.82^{+0.21}_{-0.28}$	42.81	43.85	43.12	43.97	-44.13
LID-2856	$10.46^{+0.36}_{-0.35}$	$1.08^{+0.05}_{-0.08}$	43.20	44.18	43.73	0.00	-44.22
LID-2858	$9.51^{+0.52}_{-0.64}$	$1.22^{+0.01}_{-0.26}$	43.05	44.13	43.25	43.93	-44.69
LID-2871	$10.90^{+0.51}_{-0.57}$	$0.48^{+0.05}_{-0.47}$	42.84	43.29	43.84	0.00	-43.95
LID-2873	$10.84^{+0.17}_{-0.04}$	$1.40^{+0.03}_{-0.13}$	43.11	44.53	44.44	43.33	-44.54
LID-2875	$10.45^{+0.47}_{-0.27}$	$1.45^{+0.25}_{-0.22}$	43.57	44.59	44.21	0.00	-44.38
LID-2876	$10.51^{+0.20}_{-0.33}$	$2.08^{+0.22}_{-0.00}$	43.63	45.01	44.31	44.42	45.69
LID-2880	$11.22^{+0.29}_{-0.34}$	$0.57^{+0.07}_{-0.61}$	42.69	43.27	44.35	42.95	-44.21
LID-2885	$10.39^{+0.54}_{-0.54}$	$1.85^{+0.08}_{-0.06}$	43.61	45.03	43.81	0.00	-44.87

Table B.2 – continued

ID	log $M_{stellar}$ ($M_\odot$)	log SFR^{tot} ($M_\odot$ yr^{-1})	log $L_{2-10\ keV}$ (erg s^{-1})	log L_{2300} (erg s^{-1})	log L_{5100} (erg s^{-1})	log $L_{6\mu m}$ (erg s^{-1})	log L_{IR} (erg s^{-1})
LID-2891	$10.91^{+0.80}_{-0.74}$	$0.97^{+0.06}_{-0.15}$	43.28	44.02	44.10	0.00	-44.13
LID-2893	$9.66^{+0.60}_{-0.77}$	$0.64^{+0.15}_{-0.64}$	43.04	43.35	43.34	0.00	-44.10
LID-2894	$10.64^{+0.18}_{-0.04}$	$0.42^{+0.12}_{-0.36}$	42.51	43.37	44.10	0.00	-43.83
LID-2895	$10.61^{+0.43}_{-0.32}$	$0.42^{+0.11}_{-0.52}$	43.00	43.25	43.76	0.00	-43.95
LID-2896	$9.96^{+0.74}_{-0.60}$	$1.69^{+0.18}_{-0.10}$	43.54	44.93	43.62	0.00	-44.71
LID-2914	$11.22^{+0.30}_{-0.21}$	$2.72^{+0.12}_{-0.07}$	43.99	45.89	44.66	44.13	45.91
LID-2918	$10.14^{+0.11}_{-0.70}$	$1.35^{+0.17}_{-0.56}$	43.79	44.04	43.59	44.01	-44.94
LID-2919	$10.69^{+0.13}_{-0.01}$	$1.28^{+0.06}_{-0.01}$	42.76	44.39	44.30	43.11	44.57
LID-2924	$11.66^{+0.92}_{-1.04}$	$1.97^{+0.06}_{-0.27}$	43.56	44.66	44.30	0.00	-45.48
LID-2927	$10.93^{+0.20}_{-0.19}$	$1.92^{+0.11}_{-0.00}$	43.11	45.23	44.27	44.11	45.18
LID-2930	$10.15^{+0.31}_{-0.17}$	$0.52^{+0.38}_{-0.10}$	42.95	43.71	43.70	0.00	-43.61
LID-2931	$9.95^{+0.64}_{-0.39}$	$1.40^{+0.43}_{-0.46}$	43.23	43.95	42.89	0.00	-44.99
LID-2936	$10.74^{+0.34}_{-0.31}$	$2.75^{+0.00}_{-0.26}$	43.81	45.49	44.33	44.93	45.83
LID-2940	$11.04^{+0.13}_{-0.14}$	$0.75^{+0.08}_{-0.38}$	43.33	43.67	44.31	0.00	-44.10
LID-2941	$10.83^{+0.26}_{-0.38}$	$2.08^{+0.20}_{-0.17}$	44.14	45.16	44.60	44.95	-45.26
LID-2946	$10.60^{+0.14}_{-0.10}$	$1.07^{+0.07}_{-0.00}$	42.69	44.09	44.17	43.22	45.16
LID-2947	$10.54^{+0.34}_{-0.38}$	$1.16^{+0.33}_{-0.17}$	43.65	44.24	44.05	0.00	-44.41
LID-2951	$10.64^{+0.14}_{-0.13}$	$1.29^{+0.04}_{-0.30}$	43.13	44.26	44.16	0.00	-44.55
LID-2952	$11.15^{+0.10}_{-0.29}$	$1.88^{+0.02}_{-0.55}$	44.23	44.70	44.95	0.00	-45.29
LID-2966	$10.43^{+0.00}_{-0.00}$	$0.97^{+0.06}_{-0.21}$	42.73	44.06	44.23	43.63	-44.21
LID-2984	$9.99^{+0.17}_{-0.12}$	$0.25^{+0.08}_{-0.92}$	42.60	42.65	43.47	0.00	-43.85
LID-2986	$10.74^{+0.41}_{-0.32}$	$2.84^{+0.17}_{-0.14}$	44.06	45.59	44.29	0.00	-46.53
LID-2989	$10.76^{+0.35}_{-0.19}$	$2.40^{+0.14}_{-0.00}$	43.64	45.58	44.45	43.34	45.45
LID-3016	$10.00^{+0.38}_{-0.33}$	$1.20^{+0.12}_{-0.16}$	43.04	44.27	43.38	43.21	-44.52
LID-3017	$10.54^{+0.00}_{-0.00}$	$1.10^{+0.04}_{-0.16}$	42.80	44.23	44.31	44.13	-44.17
LID-3018	$10.59^{+0.03}_{-0.10}$	$1.75^{+0.09}_{-0.00}$	42.82	44.95	44.32	43.70	44.65
LID-3021	$10.85^{+0.17}_{-0.04}$	$1.02^{+0.02}_{-0.72}$	43.22	43.58	44.40	43.30	-44.44
LID-3024	$10.44^{+0.40}_{-0.39}$	$2.22^{+0.11}_{-0.08}$	43.36	45.44	44.58	0.00	-45.06
LID-3026	$10.82^{+0.22}_{-0.24}$	$2.09^{+0.13}_{-0.01}$	43.69	45.01	44.38	44.59	45.53
LID-3027	$10.94^{+0.18}_{-0.18}$	$2.06^{+0.07}_{-0.03}$	43.43	45.24	44.53	44.35	-44.83
LID-3034	$10.68^{+0.46}_{-0.63}$	$1.71^{+0.17}_{-0.22}$	43.61	44.81	44.00	0.00	-44.59
LID-3037	$10.93^{+0.08}_{-0.22}$	$1.47^{+0.16}_{-0.31}$	43.59	44.45	44.27	44.18	-44.82
LID-3039	$10.80^{+0.22}_{-0.08}$	$1.65^{+0.08}_{-0.06}$	43.58	44.67	44.57	44.21	45.18
LID-3040	$10.27^{+0.40}_{-0.41}$	$0.89^{+0.40}_{-0.08}$	43.25	43.97	43.61	0.00	-44.29
LID-3041	$10.81^{+0.20}_{-0.07}$	$0.81^{+0.02}_{-0.56}$	42.57	43.57	44.21	43.03	-44.22
LID-3043	$10.41^{+0.17}_{-0.26}$	$1.57^{+0.16}_{-0.12}$	43.78	44.76	43.90	43.70	-44.63
LID-3046	$10.44^{+0.26}_{-0.20}$	$0.99^{+0.18}_{-0.08}$	43.39	44.07	44.08	0.00	-44.25
LID-3048	$10.83^{+0.16}_{-0.12}$	$0.70^{+0.03}_{-0.64}$	43.17	43.45	44.00	0.00	-44.09
LID-3050	$10.26^{+0.00}_{-0.17}$	$0.59^{+0.14}_{-0.86}$	43.23	42.93	43.92	43.16	-44.47
LID-3052	$10.89^{+0.27}_{-0.15}$	$1.97^{+0.00}_{-0.14}$	43.69	44.94	44.40	43.34	45.98

Table B.2 – continued

ID	log $M_{stellar}$ ($M_\odot$)	log SFR^{tot} ($M_\odot$ yr^{-1})	log $L_{2-10\ keV}$ (erg s^{-1})	log L_{2300} (erg s^{-1})	log L_{5100} (erg s^{-1})	log $L_{6\mu m}$ (erg s^{-1})	log L_{IR} (erg s^{-1})
LID-3053	$10.31^{+0.20}_{-0.29}$	$1.23^{+0.10}_{-0.04}$	43.36	44.44	43.56	43.43	-44.48
LID-3055	$11.14^{+0.08}_{-0.05}$	$2.12^{+0.02}_{-0.05}$	43.71	44.78	44.95	45.10	45.58
LID-3056	$11.30^{+0.00}_{-0.00}$	$2.57^{+0.06}_{-0.00}$	43.66	45.66	45.03	45.22	45.76
LID-3058	$10.22^{+0.14}_{-0.12}$	$1.45^{+0.09}_{-0.25}$	42.81	44.55	44.10	43.90	-44.26
LID-3066	$10.38^{+0.40}_{-0.49}$	$1.59^{+0.14}_{-0.00}$	43.45	44.86	43.51	0.00	-44.12
LID-3068	$10.59^{+0.23}_{-0.09}$	$0.61^{+0.03}_{-0.49}$	43.25	43.35	44.17	0.00	-44.05
LID-3071	$10.37^{+0.00}_{-0.00}$	$0.91^{+0.03}_{-0.28}$	42.29	43.94	44.10	0.00	-44.13
LID-3075	$10.34^{+0.35}_{-0.56}$	$1.12^{+0.19}_{-0.28}$	43.68	44.08	43.73	0.00	-44.56
LID-3078	$11.71^{+0.69}_{-0.82}$	$3.16^{+0.00}_{-0.79}$	43.78	46.37	45.24	0.00	-45.06
LID-3079	$10.63^{+0.13}_{-0.13}$	$1.91^{+0.02}_{-0.05}$	43.18	44.98	44.26	45.00	44.95
LID-3083	$10.81^{+0.00}_{-0.00}$	$1.29^{+0.04}_{-0.07}$	43.53	44.51	44.50	43.85	-44.48
LID-3084	$10.51^{+0.34}_{-0.36}$	$2.00^{+0.09}_{-0.03}$	43.52	45.22	43.92	0.00	-44.76
LID-3088	$10.40^{+0.37}_{-0.37}$	$2.13^{+0.01}_{-0.19}$	43.62	45.27	43.95	44.41	-45.02
LID-3089	$10.61^{+0.28}_{-0.40}$	$1.76^{+0.05}_{-0.40}$	43.66	44.74	44.21	0.00	-45.16
LID-3096	$10.84^{+0.18}_{-0.05}$	$1.30^{+0.14}_{-0.06}$	43.22	44.53	44.26	43.64	-44.33
LID-3097	$11.11^{+0.00}_{-0.00}$	$1.68^{+0.06}_{-0.01}$	42.96	44.82	44.46	44.08	44.74
LID-3098	$11.01^{+0.29}_{-0.25}$	$2.87^{+0.06}_{-0.01}$	43.99	46.05	44.56	44.85	45.55
LID-3100	$10.80^{+0.01}_{-0.12}$	$1.36^{+0.08}_{-0.16}$	43.61	44.44	44.25	44.01	-44.79
LID-3101	$10.68^{+0.20}_{-0.27}$	$2.07^{+0.06}_{-0.04}$	43.63	45.22	43.92	44.84	45.66
LID-3105	$10.37^{+0.17}_{-0.22}$	$1.78^{+0.02}_{-0.33}$	43.94	44.66	44.56	0.00	-45.20
LID-3106	$10.85^{+0.16}_{-0.14}$	$2.19^{+0.04}_{-0.03}$	43.45	45.42	44.36	0.00	-44.70
LID-3110	$10.38^{+0.26}_{-0.34}$	$1.63^{+0.00}_{-0.23}$	42.69	44.73	44.04	0.00	-44.59
LID-3112	$10.18^{+0.15}_{-0.22}$	$0.70^{+0.05}_{-0.03}$	42.72	43.99	43.52	0.00	-42.84
LID-3113	$10.96^{+0.06}_{-0.08}$	$2.12^{+0.12}_{-0.00}$	43.40	45.36	44.73	44.50	45.34
LID-3114	$10.44^{+0.41}_{-0.25}$	$2.35^{+0.13}_{-0.07}$	43.86	45.46	44.15	44.63	45.65
LID-3122	$11.20^{+0.46}_{-0.38}$	$1.45^{+0.09}_{-0.11}$	43.40	43.79	44.60	43.59	45.06
LID-3123	$11.18^{+0.19}_{-0.18}$	$1.78^{+0.13}_{-0.14}$	44.23	44.84	44.75	0.00	-45.27
LID-3128	$11.09^{+0.26}_{-0.13}$	$1.87^{+0.00}_{-0.44}$	43.84	44.81	44.53	44.33	-45.19
LID-3130	$10.11^{+0.25}_{-0.32}$	$1.36^{+0.17}_{-0.00}$	43.36	44.62	44.05	0.00	-44.28
LID-3132	$10.72^{+0.09}_{-0.04}$	$1.38^{+0.05}_{-0.18}$	42.82	44.50	44.40	43.07	-44.50
LID-3133	$11.07^{+0.56}_{-0.68}$	$1.01^{+0.12}_{-0.05}$	43.06	43.09	44.03	43.50	44.48
LID-3135	$10.58^{+0.14}_{-0.09}$	$0.96^{+0.08}_{-0.04}$	43.37	44.22	43.86	44.31	-44.42
LID-3141	$10.84^{+0.15}_{-0.13}$	$1.16^{+0.07}_{-0.07}$	42.94	44.36	44.08	0.00	-44.09
LID-3143	$10.83^{+0.00}_{-0.00}$	$1.55^{+0.08}_{-0.00}$	42.92	44.58	44.40	44.03	45.19
LID-3146	$11.36^{+0.18}_{-0.58}$	$2.11^{+0.13}_{-0.00}$	43.89	45.16	44.87	0.00	-45.45
LID-3150	$11.06^{+1.27}_{-1.10}$	$0.93^{+0.10}_{-0.28}$	43.91	43.92	43.91	0.00	-44.28
LID-3154	$11.34^{+0.20}_{-0.20}$	$2.34^{+0.10}_{-0.00}$	43.69	45.64	44.78	44.84	-44.87
LID-3155	$11.03^{+0.83}_{-0.44}$	$0.19^{+0.14}_{-1.44}$	43.06	42.01	43.49	0.00	-43.82
LID-3156	$10.68^{+0.38}_{-0.38}$	$1.90^{+0.08}_{-0.14}$	43.55	45.08	43.95	0.00	-44.86
LID-3160	$10.94^{+0.47}_{-0.47}$	$2.47^{+0.16}_{-0.03}$	44.36	45.74	44.07	0.00	-45.25

Table B.2 – continued

ID	log $M_{stellar}$ ($M_\odot$)	log SFR^{tot} ($M_\odot$ yr^{-1})	log $L_{2-10\ keV}$ (erg s^{-1})	log L_{2300} (erg s^{-1})	log L_{5100} (erg s^{-1})	log $L_{6\mu m}$ (erg s^{-1})	log L_{IR} (erg s^{-1})
LID-3166	$9.61^{+0.51}_{-0.44}$	$1.52^{+0.12}_{-0.05}$	43.51	44.75	43.88	0.00	-44.21
LID-3171	$10.40^{+0.39}_{-0.38}$	$1.75^{+0.04}_{-0.52}$	43.84	44.71	44.17	44.06	-45.14
LID-3176	$10.64^{+0.14}_{-0.13}$	$1.03^{+0.10}_{-0.00}$	42.64	44.19	43.74	43.38	44.20
LID-3178	$11.25^{+0.28}_{-0.19}$	$2.35^{+0.00}_{-0.10}$	44.29	45.51	44.71	44.44	-45.07
LID-3179	$10.40^{+0.14}_{-0.23}$	$0.45^{+0.16}_{-0.81}$	42.99	42.97	43.78	0.00	-44.00
LID-3180	$10.45^{+0.32}_{-0.37}$	$1.55^{+0.35}_{-0.17}$	43.97	44.69	44.40	0.00	-44.84
LID-3181	$11.61^{+1.00}_{-0.74}$	$0.63^{+0.10}_{-0.41}$	42.94	43.54	44.35	0.00	-44.09
LID-3191	$10.09^{+0.41}_{-0.41}$	$0.92^{+0.44}_{-0.59}$	43.41	43.81	43.71	0.00	-44.35
LID-3194	$10.12^{+0.37}_{-0.38}$	$0.94^{+0.56}_{-0.24}$	43.84	44.01	43.83	0.00	-44.49
LID-3195	$10.57^{+0.20}_{-0.10}$	$1.13^{+0.10}_{-0.17}$	43.17	44.24	43.97	0.00	-44.32
LID-3199	$11.40^{+0.41}_{-0.40}$	$0.96^{+0.08}_{-0.00}$	43.42	43.01	44.07	44.02	44.77
LID-3206	$11.09^{+0.00}_{-0.00}$	$1.75^{+0.08}_{-0.04}$	43.57	44.77	44.59	43.09	44.98
LID-3208	$10.85^{+0.30}_{-0.30}$	$2.38^{+0.15}_{-0.03}$	44.04	45.65	44.56	45.23	-45.01
LID-3219	$10.41^{+0.28}_{-0.28}$	$1.01^{+0.02}_{-0.24}$	42.83	43.99	43.63	0.00	-44.34
LID-3220	$10.87^{+0.21}_{-0.25}$	$1.57^{+0.00}_{-0.27}$	43.45	44.49	44.31	0.00	-44.83
LID-3221	$10.82^{+0.24}_{-0.44}$	$0.93^{+0.02}_{-0.68}$	43.52	43.51	43.97	0.00	-44.42
LID-3223	$11.28^{+1.13}_{-1.31}$	$0.56^{+0.34}_{-1.22}$	43.47	42.71	43.95	0.00	-44.18
LID-3224	$11.28^{+0.59}_{-0.57}$	$1.15^{+0.18}_{-0.00}$	43.21	43.74	43.85	43.89	44.92
LID-3230	$9.68^{+0.50}_{-0.41}$	$1.71^{+0.03}_{-0.28}$	43.37	44.69	43.47	44.17	-44.89
LID-3233	$10.55^{+0.19}_{-0.20}$	$1.36^{+0.05}_{-0.34}$	43.48	44.24	44.06	43.49	-44.63
LID-3241	$10.93^{+0.21}_{-0.26}$	$2.31^{+0.01}_{-0.12}$	43.58	45.24	44.59	0.00	-45.54
LID-3243	$10.42^{+0.34}_{-0.39}$	$2.06^{+0.37}_{-0.00}$	43.92	45.20	43.98	0.00	-45.43
LID-3245	$10.41^{+0.17}_{-0.10}$	$1.17^{+0.06}_{-0.03}$	42.57	44.38	43.57	43.09	-44.18
LID-3246	$10.00^{+0.27}_{-0.46}$	$1.78^{+0.00}_{-1.04}$	43.80	43.79	43.88	0.00	-45.22
LID-3247	$10.67^{+0.00}_{-0.00}$	$1.51^{+0.03}_{-0.15}$	42.94	44.42	44.24	44.00	44.92
LID-3250	$10.59^{+0.16}_{-0.34}$	$1.02^{+0.64}_{-0.39}$	43.81	43.84	44.13	0.00	-44.63
LID-3251	$10.61^{+0.18}_{-0.09}$	$0.80^{+0.03}_{-0.86}$	43.13	43.29	43.94	0.00	-44.34
LID-3253	$10.97^{+0.05}_{-0.09}$	$1.69^{+0.15}_{-0.00}$	42.94	44.71	44.44	44.67	45.12
LID-3258	$10.23^{+0.21}_{-0.11}$	$1.49^{+0.14}_{-0.09}$	43.19	44.73	44.07	0.00	-44.23
LID-3263	$10.89^{+0.25}_{-0.26}$	$1.52^{+0.01}_{-0.47}$	43.91	44.28	44.40	44.39	-45.15
LID-3264	$10.39^{+0.19}_{-0.08}$	$0.98^{+0.06}_{-0.25}$	43.27	44.05	44.13	0.00	-44.10
LID-3273	$10.51^{+0.21}_{-0.28}$	$1.79^{+0.15}_{-0.11}$	43.25	45.00	43.91	44.20	-44.80
LID-3275	$9.79^{+1.11}_{-0.97}$	$1.74^{+0.10}_{-0.00}$	43.39	44.98	43.66	44.16	-44.73
LID-3276	$10.29^{+0.32}_{-0.24}$	$1.61^{+0.00}_{-0.26}$	43.65	44.69	44.00	0.00	-44.70
LID-3278	$11.77^{+0.76}_{-1.08}$	$2.22^{+0.14}_{-0.00}$	43.37	45.51	44.29	42.74	44.97
LID-3279	$10.76^{+0.61}_{-0.30}$	$2.55^{+0.19}_{-0.00}$	44.16	45.68	44.02	44.99	45.83
LID-3280	$10.24^{+0.14}_{-0.13}$	$0.15^{+0.07}_{-0.81}$	42.78	42.67	43.58	0.00	-43.70
LID-3283	$9.86^{+0.41}_{-0.16}$	$1.70^{+0.14}_{-0.09}$	43.67	44.92	43.87	43.51	-44.67
LID-3285	$10.15^{+0.34}_{-0.23}$	$1.18^{+0.05}_{-0.15}$	43.17	44.36	43.44	43.75	-44.55
LID-3289	$11.11^{+0.22}_{-0.17}$	$2.41^{+0.12}_{-0.00}$	43.90	45.64	44.83	44.99	45.38

Table B.2 – continued

ID	log $M_{stellar}$ ($M_\odot$)	log SFR^{tot} ($M_\odot$ yr^{-1})	log $L_{2-10\ keV}$ (erg s^{-1})	log L_{2300} (erg s^{-1})	log L_{5100} (erg s^{-1})	log $L_{6\mu m}$ (erg s^{-1})	log L_{IR} (erg s^{-1})
LID-3291	$10.41^{+0.44}_{-0.31}$	$1.62^{+0.51}_{-0.07}$	43.61	44.78	43.71	0.00	-44.46
LID-3295	$10.49^{+0.15}_{-0.17}$	$0.58^{+0.05}_{-0.69}$	43.38	43.14	43.87	0.00	-44.12
LID-3296	$10.48^{+0.24}_{-0.30}$	$2.19^{+0.00}_{-0.28}$	44.12	45.21	44.49	0.00	-45.28
LID-3303	$10.53^{+0.09}_{-0.05}$	$1.21^{+0.08}_{-0.16}$	43.05	44.28	44.19	0.00	-44.45
LID-3307	$10.66^{+0.13}_{-0.14}$	$1.80^{+0.04}_{-0.10}$	43.16	44.96	44.06	43.50	-44.64
LID-3308	$10.65^{+0.12}_{-0.17}$	$1.18^{+0.05}_{-0.05}$	42.99	44.23	43.96	42.98	45.24
LID-3309	$10.74^{+0.20}_{-0.32}$	$1.45^{+0.06}_{-0.71}$	43.67	43.90	43.95	44.01	-45.00
LID-3312	$10.46^{+0.29}_{-0.27}$	$2.30^{+0.03}_{-0.10}$	43.49	45.28	44.20	44.39	45.25
LID-3313	$10.54^{+0.19}_{-0.32}$	$1.86^{+0.09}_{-0.33}$	44.05	44.82	44.40	0.00	-45.30
LID-3320	$10.61^{+0.31}_{-0.28}$	$1.94^{+0.02}_{-0.41}$	43.92	44.80	44.52	0.00	-45.30
LID-3324	$10.75^{+0.19}_{-0.28}$	$0.81^{+0.13}_{-0.71}$	44.11	43.39	44.20	0.00	-44.36
LID-3329	$11.06^{+0.13}_{-0.14}$	$1.79^{+0.00}_{-0.75}$	44.08	44.36	44.78	0.00	-45.28
LID-3335	$10.71^{+0.00}_{-0.00}$	$1.40^{+0.03}_{-0.03}$	43.22	44.41	44.05	43.75	44.65
LID-3336	$10.67^{+0.10}_{-0.17}$	$1.32^{+0.01}_{-0.10}$	42.86	44.19	44.01	43.58	44.65
LID-3343	$10.26^{+0.28}_{-0.25}$	$1.24^{+0.10}_{-0.05}$	42.85	44.45	43.74	0.00	-44.19
LID-3347	$10.95^{+0.17}_{-0.06}$	$2.09^{+0.05}_{-0.03}$	43.71	45.34	44.21	0.00	-44.33
LID-3356	$10.48^{+0.11}_{-0.16}$	$0.82^{+0.02}_{-0.96}$	42.39	43.17	43.89	43.25	-44.31
LID-3357	$11.01^{+0.28}_{-0.38}$	$2.07^{+0.10}_{-0.14}$	44.22	45.19	44.56	0.00	-45.28
LID-3360	$10.94^{+0.08}_{-0.06}$	$1.96^{+0.08}_{-0.04}$	43.72	44.64	44.81	0.00	-45.44
LID-3364	$11.24^{+0.25}_{-0.28}$	$2.68^{+0.15}_{-0.00}$	44.44	45.80	44.65	0.00	-45.87
LID-3365	$10.76^{+0.19}_{-0.18}$	$1.84^{+0.10}_{-0.09}$	43.04	45.04	44.32	43.65	-44.65
LID-3367	$10.35^{+0.34}_{-0.35}$	$2.00^{+0.13}_{-0.09}$	43.64	45.27	43.95	0.00	-44.49
LID-3369	$11.16^{+0.63}_{-0.59}$	$0.65^{+0.18}_{-0.93}$	44.00	43.06	44.15	0.00	-44.30
LID-3404	$10.87^{+0.25}_{-0.24}$	$2.02^{+0.01}_{-0.15}$	43.63	45.22	44.30	0.00	-44.33
LID-3405	$10.18^{+0.14}_{-0.37}$	$1.20^{+0.18}_{-0.00}$	42.72	44.36	43.61	43.41	45.04
LID-3427	$10.94^{+0.49}_{-0.28}$	$2.72^{+0.01}_{-0.29}$	43.38	45.88	44.09	43.72	45.57
LID-3450	$11.26^{+0.11}_{-0.27}$	$2.14^{+0.20}_{-0.00}$	44.01	44.96	44.78	44.82	45.84
LID-3452	$10.68^{+0.14}_{-0.00}$	$0.19^{+0.04}_{-0.68}$	42.44	42.81	44.17	0.00	-43.73
LID-3453	$10.99^{+0.31}_{-0.35}$	$2.02^{+0.17}_{-0.30}$	43.88	45.15	44.42	44.68	-45.24
LID-3463	$10.86^{+0.48}_{-0.41}$	$2.23^{+0.28}_{-0.00}$	44.05	45.61	44.35	0.00	-45.26
LID-3464	$10.45^{+0.00}_{-0.00}$	$0.52^{+0.12}_{-0.61}$	43.06	43.20	44.10	43.65	-43.84
LID-3470	$10.56^{+0.00}_{-0.00}$	$1.16^{+0.07}_{-0.17}$	43.26	44.25	43.97	43.83	-43.92
LID-3476	$10.91^{+0.23}_{-0.23}$	$1.72^{+0.06}_{-0.25}$	43.29	44.76	44.54	44.13	-45.00
LID-3480	$10.65^{+0.20}_{-0.27}$	$1.18^{+0.05}_{-0.16}$	43.26	44.29	43.93	43.83	-44.63
LID-3482	$10.35^{+0.43}_{-0.43}$	$1.51^{+0.14}_{-0.14}$	43.68	44.70	43.78	0.00	-44.26
LID-3483	$10.74^{+0.00}_{-0.00}$	$1.40^{+0.14}_{-0.01}$	43.26	44.35	44.34	43.89	44.92
LID-3486	$11.16^{+0.16}_{-0.07}$	$1.79^{+0.14}_{-0.16}$	44.04	44.77	44.85	45.25	-45.28
LID-3487	$10.19^{+0.22}_{-0.09}$	$1.02^{+0.00}_{-1.30}$	43.19	42.95	44.03	43.25	-44.31
LID-3489	$10.27^{+0.20}_{-0.43}$	$1.78^{+0.00}_{-0.59}$	43.94	44.44	43.99	44.20	-45.17
LID-3493	$10.26^{+0.21}_{-0.28}$	$1.50^{+0.03}_{-0.13}$	43.29	44.66	44.08	43.90	-44.79

Table B.2 – continued

ID	log $M_{stellar}$ ($M_\odot$)	log SFR^{tot} ($M_\odot$ yr^{-1})	log $L_{2-10\ keV}$ (erg s^{-1})	log L_{2300} (erg s^{-1})	log L_{5100} (erg s^{-1})	log $L_{6\mu m}$ (erg s^{-1})	log L_{IR} (erg s^{-1})
LID-3494	$11.32^{+0.19}_{-0.21}$	$2.84^{+0.09}_{-0.19}$	43.99	46.06	45.02	45.21	45.73
LID-3495	$10.42^{+0.15}_{-0.12}$	$0.97^{+0.08}_{-0.17}$	43.35	44.08	43.81	43.19	-44.20
LID-3500	$10.78^{+0.19}_{-0.08}$	$1.28^{+0.05}_{-0.13}$	43.11	44.48	44.21	0.00	-44.12
LID-3501	$10.66^{+0.23}_{-0.26}$	$1.82^{+0.11}_{-0.08}$	43.21	45.03	44.34	43.65	-44.90
LID-3502	$10.38^{+0.18}_{-0.08}$	$0.04^{+0.09}_{-0.11}$	42.54	43.10	43.66	42.97	43.94
LID-3503	$10.95^{+0.53}_{-0.52}$	$2.62^{+0.17}_{-0.00}$	43.76	45.87	44.21	0.00	-45.66
LID-3509	$10.21^{+0.30}_{-0.28}$	$0.79^{+0.04}_{-0.44}$	43.06	43.70	43.59	0.00	-44.14
LID-3510	$10.35^{+0.49}_{-0.65}$	$1.43^{+0.14}_{-2.46}$	43.62	42.39	43.92	0.00	-45.19
LID-3512	$10.61^{+0.54}_{-0.36}$	$2.05^{+0.11}_{-0.01}$	43.81	45.31	43.69	0.00	-44.99
LID-3515	$11.59^{+0.37}_{-0.27}$	$1.50^{+0.03}_{-0.04}$	43.75	43.75	44.60	43.41	45.00
LID-3516	$10.62^{+0.14}_{-0.34}$	$1.64^{+0.06}_{-0.53}$	44.15	44.42	44.34	44.76	-45.24
LID-3517	$10.45^{+0.45}_{-0.44}$	$1.95^{+0.48}_{-0.00}$	43.95	45.15	43.93	0.00	-44.97
LID-3524	$10.25^{+0.17}_{-0.03}$	$0.70^{+0.11}_{-0.08}$	42.67	43.95	43.85	43.31	-44.13
LID-3559	$10.31^{+0.39}_{-0.30}$	$1.10^{+0.81}_{-0.00}$	43.87	44.40	43.90	0.00	-44.39
LID-3563	$10.73^{+0.09}_{-0.04}$	$0.52^{+0.12}_{-0.35}$	43.01	43.45	44.09	0.00	-43.95
LID-3564	$10.89^{+0.25}_{-0.15}$	$1.58^{+0.00}_{-0.30}$	43.51	44.52	44.25	43.70	-44.93
LID-3565	$10.37^{+0.33}_{-0.35}$	$1.62^{+0.02}_{-0.38}$	43.66	44.44	44.19	45.23	-45.14
LID-3567	$10.66^{+0.12}_{-0.15}$	$0.68^{+0.05}_{-0.58}$	43.13	43.41	44.13	0.00	-44.17
LID-3570	$10.74^{+0.17}_{-0.23}$	$2.52^{+0.11}_{-0.00}$	43.82	45.81	44.49	44.97	-44.69
LID-3572	$10.98^{+0.04}_{-0.09}$	$1.56^{+0.07}_{-0.00}$	42.95	44.73	44.46	43.86	44.45
LID-3576	$10.49^{+0.22}_{-0.41}$	$1.53^{+0.07}_{-0.77}$	43.49	44.13	43.94	44.77	-44.96
LID-3578	$10.68^{+0.26}_{-0.19}$	$1.66^{+0.03}_{-0.52}$	43.66	44.38	44.28	0.00	-45.16
LID-3582	$10.96^{+0.45}_{-0.45}$	$-0.27^{+0.01}_{-0.14}$	42.99	42.98	43.89	0.00	0.00
LID-3583	$10.85^{+0.41}_{-0.41}$	$2.41^{+0.13}_{-0.00}$	44.19	45.73	44.24	44.98	-45.05
LID-3585	$10.35^{+0.40}_{-0.31}$	$1.09^{+0.39}_{-0.44}$	43.78	43.86	43.93	0.00	-44.48
LID-3587	$10.74^{+0.17}_{-0.23}$	$2.25^{+0.08}_{-0.08}$	43.89	45.25	44.20	45.56	45.47
LID-3592	$11.82^{+0.63}_{-0.88}$	$1.25^{+0.00}_{-0.94}$	43.33	43.63	44.36	43.49	-44.64
LID-3593	$10.86^{+0.23}_{-0.50}$	$1.36^{+0.14}_{-0.07}$	43.19	43.99	44.32	42.66	44.80
LID-3595	$10.13^{+0.36}_{-0.32}$	$1.47^{+0.04}_{-0.91}$	43.59	43.91	43.91	0.00	-45.09
LID-3603	$10.87^{+0.40}_{-0.33}$	$0.98^{+0.05}_{-0.12}$	43.36	44.24	44.06	43.97	-44.31
LID-3606	$10.85^{+0.35}_{-0.18}$	$1.96^{+0.17}_{-0.00}$	43.42	44.36	44.08	0.00	-45.59
LID-3609	$10.93^{+0.98}_{-1.14}$	$1.27^{+0.00}_{-0.87}$	43.03	43.68	44.17	43.50	-44.77
LID-3611	$11.66^{+0.74}_{-0.83}$	$0.87^{+0.06}_{-0.26}$	43.06	43.76	44.10	0.00	-44.26
LID-3612	$10.97^{+0.17}_{-0.18}$	$2.13^{+0.06}_{-0.07}$	43.66	45.24	44.44	43.00	45.22
LID-3613	$10.95^{+0.19}_{-0.21}$	$0.41^{+0.12}_{-0.62}$	42.95	43.10	44.19	43.46	-43.90
LID-3618	$11.08^{+0.79}_{-0.72}$	$-0.31^{+0.15}_{-0.00}$	42.73	43.01	43.79	0.00	0.00
LID-3620	$10.91^{+1.41}_{-1.26}$	$0.64^{+0.20}_{-1.33}$	43.49	42.98	43.79	0.00	-44.26
LID-3625	$11.10^{+0.23}_{-0.20}$	$2.19^{+0.24}_{-0.00}$	43.58	45.50	44.54	44.14	45.59
LID-3635	$10.99^{+0.00}_{-0.00}$	$1.40^{+0.14}_{-0.00}$	43.18	43.79	44.60	44.68	45.05
LID-3636	$10.79^{+0.34}_{-0.20}$	$2.09^{+0.04}_{-0.15}$	43.87	45.19	44.52	44.78	-45.21

Table B.2 – continued

ID	log $M_{stellar}$ ($M_\odot$)	log SFR^{tot} ($M_\odot$ yr^{-1})	log $L_{2-10\ keV}$ (erg s^{-1})	log L_{2300} (erg s^{-1})	log L_{5100} (erg s^{-1})	log $L_{6\mu m}$ (erg s^{-1})	log L_{IR} (erg s^{-1})
LID-3637	$10.81^{+0.15}_{-0.24}$	$1.48^{+0.04}_{-0.39}$	43.35	44.41	44.22	0.00	-44.84
LID-3644	$11.09^{+0.23}_{-0.31}$	$2.37^{+0.16}_{-0.00}$	44.64	45.35	44.54	0.00	-45.79
LID-3647	$10.79^{+0.31}_{-0.34}$	$1.74^{+0.10}_{-0.31}$	43.48	44.91	44.22	44.28	-44.79
LID-3648	$10.71^{+0.23}_{-0.16}$	$0.38^{+0.25}_{-0.57}$	42.79	43.10	44.18	43.33	-43.93
LID-3649	$10.16^{+0.95}_{-0.34}$	$0.15^{+0.18}_{-0.59}$	42.85	42.92	43.29	0.00	-43.64
LID-3664	$10.65^{+0.14}_{-0.14}$	$1.47^{+0.15}_{-0.06}$	42.91	44.34	44.06	44.02	45.17
LID-3665	$12.19^{+0.61}_{-0.47}$	$1.48^{+0.26}_{-0.00}$	43.70	44.06	45.05	43.59	45.12
LID-3670	$10.45^{+0.29}_{-0.12}$	$1.36^{+0.07}_{-0.64}$	43.43	44.06	44.31	44.15	-45.14
LID-3699	$10.65^{+0.00}_{-0.00}$	$1.29^{+0.04}_{-0.15}$	43.30	44.43	44.68	44.01	-44.77
LID-3701	$10.55^{+0.21}_{-0.24}$	$0.75^{+0.09}_{-0.82}$	43.00	43.21	43.76	43.91	-44.83
LID-3702	$11.00^{+0.16}_{-0.10}$	$1.48^{+0.25}_{-0.61}$	43.57	44.26	44.50	45.26	-45.10
LID-3703	$10.76^{+0.19}_{-0.23}$	$1.49^{+0.09}_{-0.32}$	43.66	44.40	44.21	44.28	-45.02
LID-3715	$10.31^{+0.46}_{-0.28}$	$1.80^{+0.12}_{-0.03}$	43.65	44.79	43.60	44.35	45.41
LID-3728	$10.68^{+0.23}_{-0.27}$	$1.76^{+0.07}_{-0.10}$	43.23	44.88	43.97	44.07	-44.59
LID-3740	$10.80^{+0.14}_{-0.23}$	$1.83^{+0.18}_{-0.00}$	43.39	45.10	44.21	43.66	45.18
LID-3743	$10.07^{+0.23}_{-0.14}$	$0.06^{+0.16}_{-0.66}$	43.28	42.72	43.63	0.00	-43.55
LID-3745	$10.88^{+0.00}_{-0.00}$	$1.56^{+0.17}_{-0.00}$	43.50	44.61	44.42	44.34	45.05
LID-3747	$10.89^{+0.26}_{-0.20}$	$1.86^{+0.05}_{-0.18}$	43.87	44.01	44.24	44.13	45.35
LID-3749	$10.63^{+0.13}_{-0.13}$	$1.09^{+0.15}_{-0.18}$	42.74	44.24	43.97	43.15	-44.44
LID-3751	$10.85^{+0.27}_{-0.19}$	$1.56^{+0.08}_{-0.08}$	43.71	44.52	44.42	44.37	-44.99
LID-3752	$11.12^{+0.12}_{-0.04}$	$2.35^{+0.00}_{-0.37}$	44.02	44.44	44.85	44.18	45.66
LID-3753	$10.73^{+0.00}_{-0.00}$	$1.46^{+0.09}_{-0.00}$	42.67	44.36	44.26	43.98	44.94
LID-3755	$10.89^{+0.13}_{-0.00}$	$0.80^{+0.14}_{-0.56}$	42.98	43.56	44.29	43.05	-44.08
LID-3759	$10.90^{+0.12}_{-0.04}$	$2.02^{+0.11}_{-0.00}$	43.38	45.18	44.29	45.35	45.34
LID-3760	$10.81^{+0.76}_{-0.55}$	$1.11^{+0.03}_{-0.17}$	42.95	44.08	44.25	0.00	-44.29
LID-3762	$10.45^{+0.23}_{-0.35}$	$0.94^{+0.00}_{-0.23}$	42.96	43.97	43.96	0.00	-44.11
LID-3763	$9.52^{+0.92}_{-1.10}$	$1.31^{+0.00}_{-0.41}$	43.29	44.19	43.14	0.00	-44.72
LID-3766	$10.68^{+0.14}_{-0.01}$	$1.11^{+0.12}_{-0.16}$	42.69	44.24	44.32	0.00	-44.23
LID-3767	$10.68^{+0.14}_{-0.00}$	$0.58^{+0.11}_{-0.40}$	43.18	43.42	44.15	0.00	-44.05
LID-3769	$11.01^{+0.21}_{-0.08}$	$1.72^{+0.01}_{-0.09}$	43.37	44.66	44.47	44.66	45.26
LID-3773	$11.03^{+0.00}_{-0.00}$	$0.73^{+0.10}_{-0.19}$	42.90	43.83	44.73	0.00	-43.95
LID-3774	$10.70^{+0.24}_{-0.22}$	$1.62^{+0.01}_{-0.47}$	43.42	44.39	44.29	0.00	-45.09
LID-3777	$10.64^{+0.18}_{-0.05}$	$1.11^{+0.03}_{-0.15}$	43.13	44.26	44.16	43.08	-44.14
LID-3778	$10.77^{+0.18}_{-0.29}$	$1.59^{+0.01}_{-0.80}$	43.45	44.08	44.28	0.00	-45.18
LID-3779	$10.84^{+0.15}_{-0.13}$	$1.38^{+0.05}_{-0.19}$	43.02	44.41	44.14	0.00	-44.67
LID-3780	$10.43^{+0.15}_{-0.12}$	$0.83^{+0.08}_{-0.12}$	42.66	44.01	43.92	0.00	-43.54
LID-3781	$10.79^{+0.03}_{-0.14}$	$1.45^{+0.11}_{-0.00}$	42.96	44.42	44.23	44.64	45.32
LID-3788	$10.95^{+0.07}_{-0.07}$	$0.37^{+0.17}_{-0.00}$	42.93	43.67	44.40	42.85	-44.32
LID-3789	$10.48^{+0.61}_{-0.47}$	$0.91^{+0.25}_{-0.33}$	42.81	43.94	43.79	0.00	-44.23
LID-3790	$10.14^{+0.33}_{-0.32}$	$1.55^{+0.15}_{-0.82}$	43.74	44.03	44.12	0.00	-45.26

Table B.2 – continued

ID	log $M_{stellar}$ ($M_\odot$)	log SFR^{tot} ($M_\odot$ yr^{-1})	log $L_{2-10\ keV}$ (erg s^{-1})	log L_{2300} (erg s^{-1})	log L_{5100} (erg s^{-1})	log $L_{6\mu m}$ (erg s^{-1})	log L_{IR} (erg s^{-1})
LID-3791	$10.82^{+0.00}_{-0.00}$	$0.86^{+0.08}_{-0.48}$	43.08	43.64	44.45	0.00	-44.34
LID-3793	$10.75^{+0.06}_{-0.09}$	$2.04^{+0.10}_{-0.12}$	43.46	45.26	44.03	44.15	-44.62
LID-3796	$11.08^{+0.23}_{-0.30}$	$1.52^{+0.27}_{-0.03}$	43.62	44.73	44.72	0.00	-44.77
LID-3797	$10.78^{+0.46}_{-0.19}$	$2.64^{+0.09}_{-0.14}$	44.44	45.77	44.29	0.00	-45.60
LID-3801	$11.01^{+0.66}_{-0.48}$	$-0.64^{+0.53}_{-0.28}$	43.18	42.32	43.76	42.85	-44.16
LID-3803	$11.22^{+0.10}_{-0.34}$	$2.54^{+0.10}_{-0.01}$	43.73	45.68	44.32	43.95	45.68
LID-3805	$10.88^{+0.42}_{-0.43}$	$1.54^{+0.03}_{-1.16}$	43.50	43.62	44.26	0.00	-45.16
LID-3806	$11.33^{+0.79}_{-0.79}$	$1.31^{+0.00}_{-0.36}$	42.89	44.10	44.09	43.47	-44.61
LID-3807	$11.11^{+0.09}_{-0.17}$	$2.24^{+0.00}_{-0.13}$	42.67	45.38	44.28	44.26	45.44
LID-3810	$10.63^{+0.27}_{-0.40}$	$1.87^{+0.08}_{-0.42}$	43.64	45.03	44.08	0.00	-45.18
LID-3811	$11.29^{+0.25}_{-0.14}$	$2.64^{+0.19}_{-0.00}$	44.02	45.94	44.93	43.85	45.54
LID-3813	$11.01^{+1.25}_{-0.85}$	$1.46^{+0.34}_{-0.35}$	43.45	44.40	44.20	43.49	-44.73
LID-3816	$11.35^{+0.32}_{-0.30}$	$0.02^{+0.01}_{-0.42}$	43.19	42.92	44.49	43.88	-44.17
LID-3818	$10.64^{+0.07}_{-0.14}$	$1.72^{+0.12}_{-0.10}$	43.06	44.87	44.15	43.48	44.97
LID-3819	$10.69^{+0.25}_{-0.20}$	$1.84^{+0.17}_{-0.08}$	43.54	45.04	44.41	0.00	-45.21
LID-3821	$10.43^{+0.33}_{-0.14}$	$1.69^{+0.16}_{-0.02}$	43.13	44.65	43.93	43.95	45.09
LID-3826	$10.55^{+0.07}_{-0.07}$	$1.73^{+0.00}_{-0.07}$	42.44	44.93	44.30	43.11	-44.21
LID-3828	$10.87^{+0.10}_{-0.32}$	$2.11^{+0.03}_{-0.10}$	43.65	44.80	44.42	44.52	45.60
LID-3829	$10.52^{+0.18}_{-0.19}$	$1.06^{+0.07}_{-0.34}$	43.07	44.06	43.78	43.25	-44.56
LID-3833	$10.98^{+0.19}_{-0.16}$	$1.88^{+0.25}_{-0.08}$	43.63	44.48	44.72	44.80	45.84
LID-3834	$10.47^{+0.42}_{-0.26}$	$1.76^{+0.00}_{-0.28}$	43.72	44.69	44.26	44.69	-45.10
LID-3835	$10.94^{+0.24}_{-0.41}$	$2.39^{+0.14}_{-0.13}$	43.92	45.32	44.31	0.00	-45.63
LID-3837	$10.40^{+0.29}_{-0.38}$	$1.83^{+0.00}_{-0.25}$	43.47	44.85	43.62	43.80	-44.86
LID-3838	$10.51^{+0.27}_{-0.40}$	$1.04^{+0.09}_{-0.28}$	43.71	44.10	44.00	0.00	-44.28
LID-3839	$10.01^{+0.27}_{-0.24}$	$1.10^{+0.13}_{-0.06}$	42.50	44.33	43.47	42.70	-44.23
LID-3842	$10.32^{+0.40}_{-0.38}$	$1.51^{+0.39}_{-0.18}$	43.62	44.66	44.12	0.00	-44.72
LID-3845	$10.37^{+0.56}_{-0.45}$	$2.60^{+0.08}_{-0.31}$	44.18	45.20	43.71	0.00	-45.85
LID-3846	$10.76^{+0.06}_{-0.08}$	$1.47^{+0.06}_{-0.41}$	43.24	44.43	44.33	43.63	-44.32
LID-3848	$10.97^{+0.17}_{-0.35}$	$1.68^{+0.13}_{-0.11}$	43.85	44.81	44.40	0.00	-45.11
LID-3849	$10.91^{+0.11}_{-0.03}$	$2.10^{+0.04}_{-0.05}$	43.48	45.32	44.69	43.96	-44.75
LID-3853	$11.31^{+0.18}_{-0.24}$	$1.80^{+0.20}_{-0.22}$	43.44	44.92	44.91	0.00	-44.87
LID-3855	$10.42^{+0.30}_{-0.37}$	$2.23^{+0.10}_{-0.01}$	43.37	45.51	44.02	44.85	-44.68
LID-3857	$10.31^{+0.37}_{-0.41}$	$1.60^{+0.00}_{-0.18}$	43.08	44.18	44.08	0.00	-44.95
LID-3863	$11.00^{+0.12}_{-0.31}$	$2.18^{+0.05}_{-0.02}$	43.34	45.43	44.20	44.35	45.18
LID-3864	$11.43^{+0.38}_{-0.31}$	$1.00^{+0.03}_{-0.04}$	43.42	43.76	44.31	44.24	44.44
LID-3867	$10.59^{+0.16}_{-0.18}$	$1.80^{+0.24}_{-0.00}$	42.98	44.93	44.30	43.17	45.24
LID-3868	$10.50^{+0.50}_{-0.17}$	$2.50^{+0.04}_{-0.07}$	43.71	45.67	44.35	44.90	-44.96
LID-3869	$10.58^{+0.13}_{-0.50}$	$1.93^{+0.00}_{-0.06}$	43.18	45.10	43.88	43.90	45.36
LID-3870	$10.44^{+0.49}_{-0.65}$	$0.89^{+0.55}_{-1.51}$	43.65	42.62	43.70	0.00	-44.48
LID-3871	$10.54^{+0.08}_{-0.06}$	$1.18^{+0.05}_{-0.15}$	43.50	44.31	44.21	43.27	-44.53

Table B.2 – continued

ID	log $M_{stellar}$ ($M_\odot$)	log SFR^{tot} ($M_\odot$ yr^{-1})	log $L_{2-10\ keV}$ (erg s^{-1})	log L_{2300} (erg s^{-1})	log L_{5100} (erg s^{-1})	log $L_{6\mu m}$ (erg s^{-1})	log L_{IR} (erg s^{-1})
LID-3872	$10.48^{+0.14}_{-0.00}$	$1.62^{+0.12}_{-0.00}$	42.68	44.72	44.18	44.26	44.78
LID-3877	$10.15^{+0.49}_{-0.58}$	$1.98^{+0.12}_{-0.05}$	44.20	45.20	44.06	0.00	-44.48
LID-3878	$10.83^{+0.66}_{-0.79}$	$0.13^{+0.26}_{-0.69}$	43.42	42.62	43.40	0.00	-43.67
LID-3880	$10.12^{+0.39}_{-0.43}$	$1.51^{+0.12}_{-0.97}$	43.51	43.87	43.88	44.14	-45.00
LID-3881	$11.31^{+0.34}_{-0.55}$	$1.60^{+0.13}_{-0.00}$	43.03	44.55	44.63	43.71	45.24
LID-3883	$11.19^{+1.22}_{-1.12}$	$1.26^{+1.54}_{-0.90}$	43.14	43.59	44.31	44.63	-44.86
LID-3885	$10.71^{+0.22}_{-0.37}$	$0.97^{+0.42}_{-0.77}$	44.06	43.69	44.03	0.00	-44.39
LID-3886	$11.01^{+0.14}_{-0.38}$	$2.01^{+0.31}_{-0.00}$	43.84	44.88	44.40	44.57	45.71
LID-3887	$10.44^{+0.28}_{-0.11}$	$0.58^{+0.05}_{-0.79}$	42.93	43.09	43.73	0.00	-44.13
LID-3888	$10.61^{+0.32}_{-0.39}$	$1.72^{+0.08}_{-0.67}$	43.53	44.06	44.39	0.00	-45.33
LID-3890	$9.55^{+1.46}_{-1.15}$	$1.48^{+0.05}_{-0.19}$	43.45	44.64	43.08	0.00	-44.09
LID-3891	$10.68^{+0.22}_{-0.47}$	$1.64^{+0.16}_{-0.51}$	44.01	44.59	44.23	0.00	-45.16
LID-3892	$10.49^{+0.69}_{-0.55}$	$0.47^{+0.18}_{-0.00}$	43.63	43.79	43.96	0.00	-43.05
LID-3898	$11.27^{+0.00}_{-0.00}$	$1.11^{+0.13}_{-0.00}$	43.08	43.92	44.73	43.78	44.75
LID-3901	$10.42^{+0.20}_{-0.06}$	$0.83^{+0.00}_{-0.97}$	42.93	43.17	43.98	43.42	-44.45
LID-3902	$10.40^{+0.14}_{-0.25}$	$1.47^{+0.10}_{-0.00}$	43.31	44.53	43.90	43.44	44.80
LID-3903	$10.86^{+0.16}_{-0.14}$	$0.96^{+0.09}_{-0.76}$	43.87	43.46	44.27	44.10	-44.97
LID-3908	$11.36^{+0.17}_{-0.30}$	$1.92^{+0.10}_{-0.47}$	44.07	44.96	44.95	44.87	-45.09
LID-3921	$10.32^{+0.00}_{-0.00}$	$0.85^{+0.19}_{-0.12}$	43.13	44.00	44.08	43.51	-44.45
LID-3922	$9.83^{+0.46}_{-0.17}$	$1.51^{+0.02}_{-0.22}$	43.35	44.40	43.65	44.44	46.18
LID-3923	$10.95^{+0.06}_{-0.08}$	$1.60^{+0.14}_{-0.00}$	43.50	44.57	45.00	44.37	45.44
LID-3928	$10.49^{+0.39}_{-0.28}$	$1.83^{+0.21}_{-0.00}$	43.29	45.18	43.91	0.00	-44.35
LID-3929	$11.24^{+0.18}_{-0.05}$	$1.75^{+0.08}_{-0.08}$	43.54	44.97	44.52	43.75	-44.53
LID-3931	$11.30^{+0.22}_{-0.24}$	$2.73^{+0.10}_{-0.03}$	43.55	45.89	44.64	45.62	45.94
LID-3932	$10.96^{+0.20}_{-0.20}$	$1.49^{+0.14}_{-0.11}$	42.94	44.71	44.53	0.00	-44.39
LID-3940	$10.53^{+0.12}_{-0.04}$	$1.58^{+0.00}_{-0.17}$	43.02	44.19	44.19	43.73	45.06
LID-3942	$10.54^{+0.08}_{-0.05}$	$1.15^{+0.08}_{-0.00}$	42.77	44.20	44.28	43.49	44.54
LID-3944	$10.63^{+0.19}_{-0.11}$	$1.18^{+0.06}_{-0.06}$	43.70	44.19	43.91	44.09	44.61
LID-3945	$10.02^{+0.28}_{-0.32}$	$1.02^{+0.11}_{-0.00}$	42.67	44.28	43.50	0.00	-43.64
LID-3950	$10.85^{+0.12}_{-0.15}$	$1.32^{+0.11}_{-0.11}$	43.06	44.54	44.19	43.49	-44.38
LID-3951	$11.10^{+0.00}_{-0.00}$	$1.50^{+0.13}_{-0.05}$	43.26	44.75	44.65	43.20	-44.53
LID-3953	$9.89^{+0.83}_{-0.62}$	$0.73^{+0.10}_{-1.24}$	43.35	42.82	43.46	0.00	-44.37
LID-3955	$10.17^{+0.44}_{-0.42}$	$1.15^{+0.29}_{-0.52}$	44.18	43.99	44.00	44.33	-45.05
LID-3958	$11.03^{+0.23}_{-0.18}$	$2.64^{+0.21}_{-0.00}$	44.13	45.89	44.54	44.82	45.64
LID-3959	$10.19^{+0.31}_{-0.22}$	$0.78^{+0.05}_{-0.57}$	42.75	43.57	43.54	43.00	-44.35
LID-3960	$10.58^{+0.16}_{-0.24}$	$0.66^{+0.08}_{-0.81}$	43.56	43.12	43.76	43.14	-44.58
LID-3961	$10.49^{+0.24}_{-0.15}$	$1.62^{+0.02}_{-0.23}$	43.93	44.75	44.03	44.00	-44.71
LID-3963	$10.82^{+0.16}_{-0.19}$	$2.66^{+0.31}_{-0.00}$	43.95	45.97	44.74	45.00	45.72
LID-4030	$11.17^{+0.17}_{-0.25}$	$1.55^{+0.09}_{-0.01}$	43.28	44.80	44.26	0.00	-44.21
LID-4039	$10.88^{+0.13}_{-0.25}$	$1.65^{+0.15}_{-0.36}$	44.04	44.47	44.46	0.00	-45.28

Table B.2 – continued

ID	log $M_{stellar}$ ($M_\odot$)	log SFR^{tot} ($M_\odot$ yr^{-1})	log $L_{2-10\ keV}$ (erg s^{-1})	log L_{2300} (erg s^{-1})	log L_{5100} (erg s^{-1})	log $L_{6\mu m}$ (erg s^{-1})	log L_{IR} (erg s^{-1})
LID-4077	$10.15^{+0.23}_{-0.30}$	$1.02^{+0.11}_{-0.00}$	42.78	44.29	43.19	0.00	-43.38
LID-4078	$10.64^{+0.27}_{-0.26}$	$1.86^{+0.08}_{-0.16}$	43.55	44.98	44.36	0.00	-44.84
LID-4086	$9.76^{+0.89}_{-1.11}$	$1.51^{+0.12}_{-0.09}$	43.63	44.70	43.48	43.93	-44.64
LID-4090	$11.03^{+0.35}_{-0.35}$	$1.75^{+0.07}_{-0.25}$	43.99	44.80	44.35	0.00	-45.00
LID-4103	$10.83^{+0.15}_{-0.12}$	$1.79^{+0.05}_{-0.08}$	43.08	45.01	44.29	44.09	-44.61
LID-4129	$10.10^{+0.50}_{-0.27}$	$2.00^{+0.10}_{-0.12}$	44.16	45.10	44.05	0.00	-45.28
LID-4141	$10.84^{+1.39}_{-1.24}$	$1.90^{+0.04}_{-0.10}$	43.66	45.08	43.91	0.00	-44.17
LID-4148	$10.68^{+0.21}_{-0.38}$	$1.78^{+0.05}_{-0.06}$	43.86	45.03	44.40	0.00	-44.35
LID-4150	$10.41^{+0.26}_{-0.25}$	$2.14^{+0.07}_{-0.07}$	43.96	45.31	44.26	0.00	-45.27
LID-4170	$10.46^{+0.32}_{-0.33}$	$0.64^{+0.10}_{-0.81}$	43.17	43.19	43.57	0.00	-44.18
LID-4182	$11.69^{+0.76}_{-0.90}$	$0.67^{+0.37}_{-0.39}$	43.31	43.46	44.54	43.72	-44.72
LID-4213	$10.77^{+0.34}_{-0.17}$	$1.64^{+0.10}_{-0.01}$	43.45	44.87	44.31	0.00	-44.27
LID-4235	$11.11^{+0.22}_{-0.29}$	$2.26^{+0.00}_{-0.10}$	43.74	45.37	44.80	43.57	45.17
LID-4240	$11.00^{+0.12}_{-0.24}$	$1.70^{+0.13}_{-0.18}$	43.15	44.80	44.16	44.33	45.02
LID-4272	$11.37^{+0.16}_{-0.08}$	$2.48^{+0.25}_{-0.00}$	43.83	45.74	45.10	43.96	45.78
LID-4320	$10.76^{+0.60}_{-0.43}$	$2.39^{+0.15}_{-0.11}$	43.60	45.22	43.87	0.00	-45.88
LID-4325	$10.81^{+0.20}_{-0.07}$	$2.04^{+0.18}_{-0.00}$	43.20	45.20	44.49	44.30	45.39
LID-4329	$10.32^{+0.23}_{-0.16}$	$0.56^{+0.07}_{-0.10}$	42.87	43.05	43.52	43.48	44.59
LID-4339	$10.86^{+0.27}_{-0.26}$	$1.97^{+0.13}_{-0.12}$	43.93	45.12	44.49	0.00	-45.26
LID-4343	$10.30^{+0.23}_{-0.13}$	$1.04^{+0.10}_{-0.23}$	43.15	44.01	44.00	43.42	-44.62
LID-4345	$10.91^{+0.12}_{-0.19}$	$2.10^{+0.11}_{-0.09}$	43.58	45.13	44.50	43.41	45.51
LID-4351	$11.01^{+0.31}_{-0.23}$	$2.58^{+0.27}_{-0.00}$	43.76	45.92	44.30	0.00	-45.43
LID-4354	$10.80^{+0.41}_{-0.21}$	$2.60^{+0.00}_{-0.27}$	43.81	45.51	44.03	43.23	45.86
LID-4356	$10.53^{+0.19}_{-0.33}$	$1.27^{+0.25}_{-0.07}$	43.91	44.51	44.14	0.00	-44.25
LID-4363	$10.94^{+0.08}_{-0.06}$	$1.74^{+0.10}_{-0.05}$	43.20	44.67	44.48	43.54	45.50
LID-4369	$10.72^{+0.43}_{-0.32}$	$2.34^{+0.19}_{-0.03}$	43.71	45.65	43.99	44.66	-45.00
LID-4377	$11.05^{+0.14}_{-0.13}$	$2.00^{+0.14}_{-0.07}$	43.80	45.23	44.43	44.64	-44.70
LID-4393	$10.67^{+0.25}_{-0.18}$	$2.16^{+0.00}_{-0.15}$	43.56	45.02	44.13	0.00	-45.46
LID-4398	$10.33^{+0.46}_{-0.68}$	$1.17^{+0.60}_{-0.25}$	43.90	44.35	43.53	0.00	-44.40
LID-4456	$10.90^{+0.12}_{-0.02}$	$1.40^{+0.13}_{-0.07}$	43.13	44.67	44.48	0.00	-44.12
LID-4501	$10.49^{+0.40}_{-0.28}$	$1.59^{+0.13}_{-0.69}$	43.97	44.11	44.26	0.00	-45.27
LID-4505	$10.46^{+0.27}_{-0.19}$	$0.56^{+0.44}_{-0.57}$	44.16	43.18	43.99	0.00	-44.07
LID-4511	$10.31^{+0.22}_{-0.26}$	$0.43^{+0.08}_{-0.77}$	43.02	42.94	43.32	42.72	-44.11
LID-4550	$10.38^{+0.22}_{-0.22}$	$1.44^{+0.20}_{-0.00}$	43.46	44.73	44.04	44.10	45.28
LID-4567	$9.63^{+0.76}_{-0.55}$	$0.85^{+0.08}_{-0.44}$	43.32	43.82	43.28	0.00	-44.17
LID-4582	$10.08^{+0.38}_{-0.40}$	$0.26^{+0.17}_{-0.29}$	43.27	43.30	43.38	0.00	-43.66
LID-4603	$10.49^{+0.48}_{-0.27}$	$2.18^{+0.13}_{-0.04}$	43.97	45.37	44.20	0.00	-45.37
LID-4655	$11.39^{+0.28}_{-0.39}$	$2.96^{+0.08}_{-0.00}$	44.27	46.26	44.42	45.33	45.86
LID-4665	$10.10^{+0.26}_{-0.19}$	$1.12^{+0.10}_{-0.33}$	43.50	44.02	43.96	43.63	-44.72
LID-4697	$11.23^{+0.91}_{-0.88}$	$1.14^{+0.08}_{-0.27}$	43.18	44.08	44.07	0.00	-44.37

Table B.2 – continued

ID	log $M_{stellar}$ ($M_\odot$)	log SFR^{tot} ($M_\odot$ yr^{-1})	log $L_{2-10\ keV}$ (erg s^{-1})	log L_{2300} (erg s^{-1})	log L_{5100} (erg s^{-1})	log $L_{6\mu m}$ (erg s^{-1})	log L_{IR} (erg s^{-1})
LID-4714	$9.94^{+0.41}_{-0.48}$	$1.14^{+0.41}_{-0.24}$	43.51	44.25	43.56	0.00	-44.44
LID-4730	$9.72^{+0.73}_{-0.64}$	$1.40^{+0.27}_{-0.10}$	43.66	44.64	43.43	0.00	-44.41
LID-4848	$11.20^{+0.48}_{-0.36}$	$1.77^{+0.10}_{-0.37}$	44.24	44.60	44.58	0.00	-45.28
LID-4856	$10.54^{+0.08}_{-0.06}$	$1.11^{+0.03}_{-0.22}$	42.61	44.17	44.08	43.70	-44.12
LID-4883	$11.21^{+0.15}_{-0.24}$	$2.18^{+0.06}_{-0.05}$	44.06	45.34	44.79	44.69	-45.30
LID-4886	$10.69^{+0.24}_{-0.27}$	$1.68^{+0.12}_{-0.13}$	43.21	44.88	44.08	0.00	-44.33
LID-4888	$10.30^{+0.09}_{-0.18}$	$0.99^{+0.13}_{-0.33}$	43.04	43.96	43.95	43.07	-44.50
LID-4889	$10.93^{+0.00}_{-0.00}$	$1.52^{+0.11}_{-0.17}$	43.03	44.69	44.24	43.84	-44.42
LID-4911	$10.50^{+0.37}_{-0.31}$	$2.16^{+0.17}_{-0.00}$	43.48	45.32	44.32	43.82	45.54
LID-4918	$10.53^{+0.09}_{-0.05}$	$1.09^{+0.05}_{-0.20}$	42.92	44.18	44.26	43.70	-44.41
LID-4930	$10.85^{+0.60}_{-0.51}$	$2.21^{+0.22}_{-0.00}$	44.03	45.34	44.29	0.00	-45.32
LID-4939	$10.65^{+0.23}_{-0.20}$	$1.88^{+0.05}_{-0.17}$	43.33	45.07	44.12	0.00	-44.69
LID-4967	$11.03^{+1.02}_{-1.26}$	$0.60^{+0.13}_{-0.59}$	43.30	43.37	43.65	0.00	-44.17
LID-5012	$10.40^{+0.31}_{-0.16}$	$0.86^{+0.32}_{-0.15}$	43.30	44.01	43.92	0.00	-44.11
LID-5014	$11.17^{+0.05}_{-0.09}$	$2.52^{+0.12}_{-0.00}$	43.42	45.77	45.08	45.18	45.25
LID-5022	$10.80^{+0.00}_{-0.00}$	$1.00^{+0.13}_{-0.00}$	42.75	43.55	44.28	43.38	44.61
LID-5027	$9.16^{+0.67}_{-0.67}$	$0.23^{+0.28}_{-0.26}$	43.30	43.23	43.09	0.00	-43.55
LID-5051	$10.06^{+0.48}_{-0.52}$	$1.47^{+0.00}_{-0.95}$	43.68	43.82	43.65	0.00	-44.99
LID-5125	$10.66^{+0.24}_{-0.31}$	$1.37^{+0.03}_{-0.34}$	43.35	44.31	44.04	0.00	-44.77
LID-5134	$9.73^{+0.35}_{-0.36}$	$0.75^{+0.50}_{-0.82}$	43.14	43.27	43.60	0.00	-44.31
LID-5139	$10.79^{+0.61}_{-0.63}$	$1.04^{+0.07}_{-0.39}$	43.57	43.97	44.21	0.00	-44.46
LID-5415	$10.86^{+0.25}_{-0.28}$	$2.04^{+0.28}_{-0.00}$	43.71	45.14	44.27	43.77	45.64
LID-5568	$11.07^{+0.00}_{-0.00}$	$0.65^{+0.09}_{-0.15}$	42.27	43.76	44.49	0.00	-43.83
LID-5583	$10.01^{+0.39}_{-0.37}$	$1.65^{+0.00}_{-0.93}$	43.34	44.14	43.79	0.00	-45.15
LID-5714	$11.09^{+0.13}_{-0.01}$	$2.20^{+0.13}_{-0.00}$	43.08	45.42	44.90	45.10	45.24
LID-5970	$9.88^{+0.24}_{-0.15}$	$1.01^{+0.12}_{-0.04}$	42.77	44.28	43.59	0.00	-43.33
LID-6057	$10.63^{+0.15}_{-0.12}$	$1.07^{+0.06}_{-0.07}$	43.19	43.33	44.32	43.95	44.71
LID-6208	$11.15^{+0.21}_{-0.18}$	$1.65^{+0.13}_{-0.08}$	43.47	44.72	44.35	0.00	-45.08
LID-10003	$10.72^{+0.38}_{-0.28}$	$2.21^{+0.02}_{-0.17}$	44.03	45.38	44.25	0.00	-44.31
LID-10004	$10.74^{+0.27}_{-0.61}$	$0.71^{+0.12}_{-1.12}$	44.03	42.90	43.76	0.00	-44.34
LID-10008	$10.94^{+0.21}_{-0.28}$	$2.31^{+0.12}_{-0.00}$	42.97	45.60	44.48	43.80	-44.54

NOTE: Parameters derived from the SED fitting. The columns are (1) *Chandra* source ID from Civano et al. (2016); (2) host galaxy stellar mass; (3) host galaxy SFR; (4) absorption-corrected X-ray luminosity in 2–10 keV band; (5) rest-frame UV luminosity at 2300Åof the host galaxy component; (6) rest-frame luminosity at 5100Åof the host galaxy component; (7) rest-frame 6μm luminosity of the AGN component; and (8) IR luminosity,

$L_{8-1000\mu m}$, of the starburst component. Negative values represent the maximum IR luminosity of the *Herschel*-undetected sources.

Appendix C
Spectroscopic Observations

In Table C.1, I present the identified spectroscopic redshifts from the Keck/DEIMOS and Subaru/FMOS observations. The ID is from the X-ray catalog of COSMOS (Marchesi et al. 2016), and UDS (Kocevski et al. submitted). I assign a quality flag that gives the confidence in the redshift measurement. Flag 2 indicates a reliable redshift due to high S/N spectra and multiple spectral features. Flag 1 indicates that a redshift is not securely identified, due to either low S/N or the presence of only a single emission line with no additional features. All the Flag 1 spectroscopic identifications are consistent with the photometric redshifts of the same sources.

Table C.1: Spectroscopic Redshift Identification

ID	R.A.	decl.	Redshift	Quality	Spectral Features
CID-12	149.681	2.268	0.902	2	OII,Hb
CID-20	150.170	2.219	1.156	2	OII
CID-25	150.231	2.255	2.174	1	MgII
CID-36	150.158	2.139	1.826	2	MgII
CID-45	150.194	2.107	2.909	2	CIII,CII
CID-46	150.196	2.119	2.164	1	CIII
CID-54	150.312	2.036	0.697	2	OII,Hb
CID-55	150.318	2.055	1.808	2	MgII
CID-56	150.324	2.100	1.080	2	OII
CID-58	150.327	2.094	2.594	1	CIII
CID-61	150.358	2.025	1.478	2	MgII,OII
CID-64	150.365	2.144	3.328	2	CIV,CIII
CID-66	150.378	2.196	1.512	2	NeV,MgII
CID-69	150.422	2.175	0.979	2	MgII,NeV,OII,Hb
CID-70	150.405	2.270	1.638	2	MgII
CID-77	150.150	2.475	0.688	2	OII,Hb
CID-78	150.158	2.415	0.900	2	OII,Hb
CID-85	150.096	2.293	0.360	2	Hb,Ha
CID-87	150.133	2.303	1.607	1	MgII,OII
CID-92	150.289	2.382	1.581	2	OII
CID-97	150.321	2.333	2.179	1	CIII,MgII
CID-98	150.329	2.381	1.520	1	MgII,OII
CID-101	150.342	2.393	1.210	2	OII
CID-102	150.348	2.391	1.847	2	MgII
CID-103	150.290	2.455	1.432	2	MgII
CID-107	150.051	2.494	1.315	2	OII
CID-112	150.103	2.530	1.320	2	MgII,OII
CID-115	150.062	2.660	0.437	2	Hb,Ha
CID-117	150.189	2.606	1.021	2	OII
CID-118	150.199	2.598	0.901	2	OII,Hb
CID-121	150.192	2.544	2.725	1	CIV,CIII
CID-125	150.215	2.583	5.310	1	Lya
CID-127	150.227	2.538	1.801	1	CIII,CII
CID-134	150.241	2.538	1.849	1	MgII,CIII
CID-142	150.054	2.590	0.698	2	Hb
CID-146	150.095	2.634	1.183	1	OII
CID-152	150.163	2.622	1.188	2	OII
CID-157	149.675	1.983	1.333	2	MgII,OII
CID-162	149.736	2.028	2.454	2	CIII,MgII
CID-164	149.738	1.979	0.526	1	Hb
CID-165	149.743	1.952	1.187	1	OII
CID-175	149.574	2.085	1.627	2	MgII

Table C.1 – continued

ID	R.A.	decl.	Redshift	Quality	Spectral Features
CID-179	149.587	2.037	1.850	2	CIII,MgII
CID-183	149.605	2.052	2.813	2	CIV,CIII
CID-187	149.639	2.003	2.622	1	CIV,CIII
CID-189	149.652	2.059	1.177	2	OII
CID-190	149.656	2.076	0.223	2	Ha
CID-201	149.906	1.917	0.677	2	OII,Hb
CID-207	149.848	1.921	0.714	1	Hb
CID-215	149.874	2.031	1.230	2	OII
CID-256	150.112	1.904	0.971	2	OII
CID-261	150.021	1.791	1.165	2	OII,NeIII
CID-263	150.043	1.779	0.348	2	OII,Hb,Ha
CID-264	150.044	1.757	0.735	2	OII,Hb
CID-269	150.106	1.750	1.673	1	NeV,OII
CID-271	150.109	1.725	1.303	2	OII
CID-301	150.360	1.720	1.444	2	OII
CID-307	149.823	2.090	2.051	2	MgII
CID-319	149.822	2.152	1.050	1	OII
CID-330	149.956	2.028	1.754	1	MgII
CID-331	149.855	2.132	0.955	2	OII
CID-333	149.859	2.108	1.485	1	OII
CID-334	149.864	2.059	1.225	2	OII
CID-340	149.895	2.047	2.187	2	MgII
CID-346	149.931	2.119	2.213	2	CIII,MgII
CID-350	150.010	2.053	1.446	2	OII
CID-352	150.059	2.015	2.498	2	CIII
CID-358	150.105	1.981	0.372	2	Hb,Ha
CID-369	150.253	1.997	1.171	2	MgII,OII
CID-372	150.265	2.008	0.850	2	OII,Hb
CID-375	150.309	1.891	1.574	2	OII
CID-379	150.339	1.928	1.608	1	MgII
CID-380	150.352	1.932	1.373	1	MgII,OII
CID-384	150.366	1.925	0.447	2	Hg
CID-393	150.408	1.868	0.394	1	Ha
CID-394	150.416	1.968	1.221	1	OII
CID-395	150.421	1.945	0.209	2	Hb,Ha
CID-399	150.431	1.935	2.177	2	CIII,MgII
CID-421	149.665	2.310	2.150	1	MgII
CID-422	149.667	2.286	1.028	2	MgII,OII,Hb
CID-424	149.678	2.349	2.017	1	CIV,CIII,MgII
CID-427	149.693	2.267	0.905	2	OII,Hb
CID-431	149.714	2.355	1.085	1	H+K
CID-433	149.715	2.299	1.195	2	OII
CID-437	149.737	2.264	1.243	2	OII

Table C.1 – continued

ID	R.A.	decl.	Redshift	Quality	Spectral Features
CID-438	149.739	2.366	1.662	1	CIII,MgII
CID-452	150.004	2.237	1.407	2	MgII,OII
CID-453	149.929	2.298	1.626	1	OII
CID-454	149.868	2.331	1.486	2	MgII
CID-456	149.884	2.338	1.022	2	OII,Hb
CID-464	150.100	2.200	1.260	1	OII
CID-467	150.102	2.105	2.285	2	MgII
CID-469	150.109	2.132	1.253	2	OII
CID-473	149.979	2.309	1.456	2	OII
CID-481	150.423	2.014	2.283	2	CIII,MgII
CID-485	150.431	1.988	0.976	2	OII,Hb
CID-489	150.449	2.093	0.329	2	Ha
CID-490	150.458	2.062	2.324	2	CIII,MgII
CID-495	150.506	2.058	2.015	2	CIII,MgII
CID-498	149.978	2.398	1.457	2	OII
CID-506	149.850	2.398	1.190	2	OII
CID-510	149.917	2.385	1.128	2	MgII,OII,Hb
CID-513	149.706	2.420	1.122	2	MgII,OII
CID-514	149.726	2.419	0.125	2	Hb
CID-517	149.738	2.434	2.097	2	CIII,MgII
CID-521	149.762	2.435	3.297	1	CIV,CIII
CID-525	149.790	2.432	1.548	1	MgII,NeV
CID-526	149.809	2.480	1.583	2	OII
CID-531	150.004	2.389	1.846	2	MgII
CID-538	150.435	2.143	0.967	2	OII
CID-543	150.452	2.145	1.298	2	CII,MgII,OII
CID-547	150.473	2.198	0.404	2	OII,Ha
CID-548	150.484	2.162	1.642	2	MgII
CID-549	150.488	2.150	0.876	2	OII,Hb
CID-550	150.510	2.103	1.141	1	OII
CID-553	150.532	2.189	0.829	2	MgII,Hb
CID-554	150.540	2.168	0.879	2	OII
CID-555	150.559	2.177	0.868	2	OII
CID-556	149.860	2.545	1.596	2	MgII
CID-559	149.886	2.511	1.003	2	OII
CID-560	149.892	2.579	1.320	2	OII
CID-566	149.956	2.502	1.459	2	MgII,OII
CID-567	149.959	2.553	1.318	2	OII
CID-569	149.778	2.567	0.727	2	OII,Hb
CID-576	149.810	2.576	0.971	2	OII,Hb
CID-577	149.811	2.558	2.152	1	CIII,MgII
CID-591	150.443	2.323	1.371	2	OII
CID-592	150.461	2.359	1.020	2	OII

Table C.1 – continued

ID	R.A.	decl.	Redshift	Quality	Spectral Features
CID-594	150.501	2.354	0.237	2	Ha
CID-595	150.506	2.246	0.999	2	OII,Hb
CID-596	150.519	2.321	1.836	2	CIII,MgII
CID-599	150.536	2.273	1.081	2	MgII,OII
CID-602	150.558	2.261	1.455	1	CIII,CII
CID-604	150.582	2.288	1.340	2	MgII,OII
CID-611	149.953	2.660	0.892	2	OII
CID-612	149.975	2.679	0.538	2	Hb
CID-614	149.991	2.590	0.887	1	OII
CID-617	150.007	2.670	2.510	2	CIII
CID-618	150.008	2.705	0.580	2	Hb
CID-619	150.009	2.627	1.002	2	OII
CID-620	150.015	2.666	1.174	2	OII
CID-631	150.374	2.460	1.281	2	OII
CID-636	150.438	2.416	2.025	2	CIII
CID-642	150.496	2.413	1.368	2	MgII,OII
CID-645	150.520	2.425	2.245	1	CIII
CID-648	150.235	2.216	1.368	2	OII
CID-649	150.262	2.277	1.368	2	OII
CID-660	150.223	2.501	0.992	2	OII
CID-673	150.199	1.731	2.556	1	CIV
CID-689	150.415	1.934	1.175	1	OII
CID-690	150.447	1.883	0.691	1	OII,Hb
CID-697	149.985	2.236	1.641	2	OII
CID-703	149.762	2.468	0.976	1	OII
CID-704	149.778	2.459	1.320	1	OII
CID-705	149.782	2.471	3.326	2	CIV,CIII
CID-710	150.538	2.188	0.925	2	OII,Hb
CID-711	149.840	2.538	1.396	1	MgII
CID-725	150.271	2.365	2.969	1	CIII
CID-726	150.129	2.624	0.700	2	Hb
CID-729	149.555	1.989	1.482	1	MgII,OII
CID-732	149.980	1.960	1.169	1	OII
CID-737	150.232	1.628	0.404	1	OII,Hb,Ha
CID-745	150.412	1.859	1.240	1	OII
CID-764	150.305	2.053	1.178	2	OII
CID-776	150.203	2.380	1.258	2	OII
CID-788	150.133	2.379	2.031	1	MgII
CID-793	150.041	2.563	1.443	2	OII
CID-800	149.813	1.968	0.907	1	OII
CID-804	149.645	1.968	0.880	2	OII,Hb
CID-807	150.025	1.878	1.796	2	MgII
CID-811	149.948	1.932	0.342	2	Hb,Ha

Table C.1 – continued

ID	R.A.	decl.	Redshift	Quality	Spectral Features
CID-815	150.009	1.853	0.850	2	OII,Hb
CID-828	149.862	2.173	0.884	2	OII,Hb
CID-833	149.928	2.062	0.946	2	OII
CID-834	149.918	2.154	1.919	1	MgII
CID-841	150.026	2.004	0.923	1	OII
CID-864	149.882	2.318	1.617	1	MgII,OII
CID-865	149.884	2.212	1.155	2	OII
CID-876	150.157	2.089	1.129	2	OII
CID-881	149.849	2.384	1.314	2	OII
CID-888	150.052	2.306	0.749	2	OII,Hb
CID-901	150.412	2.207	1.269	2	OII
CID-917	150.193	2.220	3.090	2	CIV,CIII
CID-919	150.166	2.134	0.838	2	OII,Hb
CID-923	150.353	2.133	1.297	2	OII
CID-925	150.303	2.161	1.817	2	MgII
CID-931	150.360	2.074	0.928	2	OII
CID-943	150.416	2.175	1.388	1	OII
CID-948	150.371	2.073	1.165	2	OII
CID-956	150.213	2.477	0.911	2	OII,Hb
CID-958	150.069	2.231	1.869	2	MgII
CID-965	150.152	2.308	3.177	2	CIV,CIII
CID-966	150.171	2.337	1.260	2	OII
CID-975	150.212	2.402	0.906	2	OII,Hb
CID-996	150.122	2.526	0.606	2	Hb
CID-1002	149.717	2.008	1.623	1	OII
CID-1010	149.672	1.941	0.937	1	OII
CID-1013	149.818	2.053	1.231	2	OII
CID-1015	149.865	2.016	1.377	2	OII
CID-1017	149.889	1.920	1.479	2	OII
CID-1025	149.904	1.867	1.511	2	OII
CID-1031	150.108	1.862	1.359	2	MgII,OII
CID-1051	150.253	1.871	1.374	2	OII
CID-1055	149.737	2.090	0.379	2	Hb,Ha
CID-1057	149.812	2.111	0.979	2	OII
CID-1063	149.702	2.122	0.891	2	OII,Hb
CID-1064	149.706	2.132	1.972	2	MgII
CID-1072	149.850	2.132	1.481	2	OII
CID-1075	149.878	2.032	0.678	2	Hb
CID-1078	149.940	2.140	1.478	2	OII
CID-1081	150.043	2.104	0.998	2	OII,Hb
CID-1086	150.111	1.973	2.233	2	MgII
CID-1092	150.099	2.018	0.360	2	Hb,Ha
CID-1104	150.231	1.999	2.218	2	CIII,CII,MgII

Table C.1 – continued

ID	R.A.	decl.	Redshift	Quality	Spectral Features
CID-1109	150.345	1.993	1.827	1	MgII
CID-1124	149.833	2.134	1.020	2	OII
CID-1148	150.019	2.219	1.563	2	OII
CID-1163	150.164	2.179	3.154	1	CIII
CID-1164	150.057	2.209	0.186	2	Ha
CID-1167	150.202	2.068	1.856	2	CII,MgII
CID-1170	150.109	2.157	1.821	2	MgII
CID-1197	149.894	2.433	3.380	2	CIV
CID-1204	149.962	2.320	0.933	2	OII
CID-1218	150.048	2.374	0.938	2	OII,Hb
CID-1220	150.080	2.266	1.405	2	OII
CID-1222	150.096	2.231	1.759	1	MgII
CID-1225	150.436	2.161	1.300	2	OII
CID-1229	150.373	2.203	1.172	2	OII
CID-1231	149.928	2.535	0.668	2	OII,Hb
CID-1236	149.846	2.482	3.360	2	CIV
CID-1237	149.868	2.455	1.313	2	OII
CID-1242	149.978	2.504	1.171	2	OII
CID-1243	150.002	2.461	0.733	2	OII,Hb
CID-1244	149.957	2.479	1.028	2	OII,Hb
CID-1251	150.441	2.303	0.756	1	MgI
CID-1265	150.464	2.328	2.152	1	CIV,CIII
CID-1279	150.406	2.518	0.877	2	OII,Hb
CID-1280	150.412	2.474	1.265	1	H+K
CID-1281	150.416	2.526	1.444	2	MgII,OII
CID-1284	150.474	2.392	2.598	1	CIV,CII
CID-1295	149.921	2.250	0.881	2	OII,Hb
CID-1305	150.045	2.218	2.177	2	MgII
CID-1306	150.524	2.094	1.269	2	OII
CID-1314	149.948	2.594	1.752	1	MgII
CID-1330	150.077	2.511	1.244	2	OII
CID-1368	150.332	1.921	0.098	2	Hb,Ha
CID-1388	150.285	2.019	0.309	2	Hb,Ha
CID-1392	150.455	1.967	3.471	2	CIV,CIII
CID-1408	150.358	2.264	0.775	2	OII,Hb
CID-1427	150.100	2.457	0.722	2	OII,Hb
CID-1447	150.392	2.183	2.957	2	CIV,CIII
CID-1448	150.362	2.196	1.272	2	OII
CID-1463	150.111	2.330	1.254	1	OII
CID-1467	149.837	1.972	1.020	2	OII
CID-1472	150.006	1.897	0.793	2	OII
CID-1474	149.924	1.889	1.551	2	OII
CID-1476	149.936	1.933	0.599	2	OII,Hb

Table C.1 – continued

ID	R.A.	decl.	Redshift	Quality	Spectral Features
CID-1479	150.167	1.858	0.335	2	Hb,Ha
CID-1482	150.153	1.880	1.624	2	OII
CID-1489	149.754	2.126	1.952	2	MgII
CID-1498	149.774	2.142	0.354	2	Hb,Ha
CID-1499	150.009	2.026	1.193	2	OII
CID-1548	150.006	2.295	0.223	2	Ha
CID-1551	149.902	2.327	1.948	1	MgII
CID-1563	150.555	2.369	1.634	1	CIII,MgII
CID-1569	150.596	2.365	1.082	2	OII
CID-1574	150.605	2.437	1.003	1	OII
CID-1583	150.634	2.383	0.372	2	OII,Ha
CID-1630	149.909	2.706	0.888	2	OII,Hb
CID-1634	150.576	2.181	0.555	2	OII,Hb
CID-1636	150.527	2.038	1.370	1	OII
CID-1656	150.272	1.614	3.512	2	Lya,CIII
CID-1662	150.310	1.686	0.980	2	OII
CID-1664	150.317	1.658	0.684	2	OII,Hb
CID-1671	150.336	1.601	0.228	2	Hb,Ha
CID-1683	149.820	1.762	1.440	2	OII
CID-1739	150.496	2.380	1.275	2	OII
CID-1750	150.525	2.422	1.061	2	OII
CID-1759	150.561	2.346	1.834	1	MgII
CID-1769	150.596	2.336	1.090	1	OII
CID-1771	150.609	2.343	1.063	1	OII
CID-1831	150.455	2.431	0.986	2	OII
CID-1877	150.284	2.494	0.910	2	OII,Hb
CID-1913	149.977	2.487	2.089	2	MgII
CID-1975	149.951	2.695	1.456	1	MgII
CID-1976	149.952	2.651	3.080	2	CIII,CII
CID-1995	150.424	2.292	0.813	2	OII,Hb
CID-2000	150.434	2.225	1.181	2	OII
CID-2002	150.443	2.230	0.865	2	OII
CID-2057	150.295	2.275	1.355	2	OII
CID-2062	150.321	2.285	1.267	2	OII
CID-2128	150.092	2.322	1.259	1	OII
CID-2212	149.742	2.535	2.919	2	Lya,CIII
CID-2229	149.800	2.470	1.901	1	MgII
CID-2252	149.877	2.444	1.964	2	MgII
CID-2258	149.886	2.446	1.233	1	OII
CID-2321	150.489	2.152	1.110	2	OII
CID-2323	150.491	2.118	1.173	1	OII
CID-2324	150.493	2.116	0.845	2	OII,Hb
CID-2356	150.136	2.225	1.024	2	OII

Table C.1 – continued

ID	R.A.	decl.	Redshift	Quality	Spectral Features
CID-2443	150.127	2.175	1.408	2	OII
CID-2462	149.879	2.315	1.549	2	OII
CID-2470	149.913	2.357	2.975	1	CIV,CIII
CID-2477	149.937	2.300	0.934	2	OII,Hb
CID-2484	149.970	2.279	1.374	2	OII
CID-2508	149.721	2.360	1.193	2	NeV,OII
CID-2512	149.731	2.368	0.834	2	OII,Hb
CID-2564	150.307	2.054	2.011	2	MgII
CID-2584	150.387	1.952	1.373	2	OII
CID-2682	150.037	2.110	2.431	1	CIII
CID-2704	150.112	2.125	0.958	1	OII
CID-2728	150.238	2.056	1.506	2	MgII,OII
CID-2738	149.950	2.092	0.633	2	Hb
CID-2797	149.799	2.169	0.262	2	Ha
CID-2822	149.883	2.172	1.001	1	OII
CID-2902	149.847	2.147	0.470	2	Hb,Ha
CID-2933	150.330	1.908	0.982	2	OII
CID-2936	150.340	1.887	1.198	1	OII
CID-2938	150.341	1.761	2.957	2	CIV,CIII
CID-2946	150.391	1.916	1.133	2	OII
CID-2949	150.403	1.879	3.571	2	CIV,CIII
CID-2956	150.423	1.871	1.411	2	OII
CID-3020	150.289	1.910	0.219	2	Ha
CID-3021	150.306	1.875	1.755	2	MgII
CID-3061	150.113	2.009	1.182	2	OII
CID-3118	149.952	2.014	1.103	1	OII
CID-3178	149.851	2.083	1.355	2	OII
CID-3242	149.711	2.145	1.530	2	MgII,OII
CID-3270	150.202	1.724	1.309	2	MgII
CID-3282	150.255	1.692	1.391	1	OII
CID-3293	150.306	1.762	3.310	2	Lya
CID-3321	150.086	1.674	1.116	1	MgII
CID-3371	149.938	1.739	0.862	2	OII,Hb
CID-3385	150.031	1.858	1.819	2	MgII
CID-3562	149.626	1.981	3.963	2	Lya,CIII
CID-3570	149.641	2.108	1.244	2	OII
CID-3583	149.664	1.962	1.671	1	OII
CID-3665	150.233	2.476	0.374	2	Hb,Ha
CID-3714	150.240	2.353	1.266	2	OII
CID-11566	150.405	2.278	1.352	1	OII
CID-11725	150.463	2.121	0.424	2	OII,Ha
CID-12145	150.454	1.857	1.248	1	OII
CID-12390	150.198	1.672	0.216	2	OII,Hb,Ha

Table C.1 – continued

ID	R.A.	decl.	Redshift	Quality	Spectral Features
LID-74	150.334	2.457	0.876	2	OII
LID-132	150.518	2.525	1.818	1	MgII
LID-155	150.426	2.552	0.673	2	OII,Ha,Hb
LID-233	149.931	2.724	3.084	2	CIII
LID-260	150.615	2.515	0.684	2	OII,Hb
LID-264	150.674	2.532	2.556	1	CIV,CIII
LID-285	150.458	2.718	1.534	2	MgII
LID-286	150.477	2.710	1.206	2	MgII,OII
LID-287	150.480	2.677	1.566	1	OII
LID-288	150.483	2.715	2.666	1	CIV,CIII
LID-291	150.497	2.660	0.851	2	MgII,Hb
LID-299	150.318	2.737	1.790	2	MgII
LID-315	150.401	2.729	1.126	2	OII
LID-324	150.192	2.829	1.519	1	MgII
LID-334	150.254	2.832	0.501	2	OII,Hb,Ha
LID-336	150.260	2.769	1.308	1	OII
LID-337	150.266	2.759	1.258	2	OII
LID-338	150.271	2.820	1.209	2	MgII,OII
LID-373	149.921	2.886	3.976	2	CIV
LID-374	149.922	2.875	1.252	2	OII
LID-375	149.958	2.797	0.080	2	Hb,Ha
LID-392	150.447	2.750	1.165	2	OII
LID-397	150.475	2.886	0.190	2	Hb,Ha
LID-401	150.479	2.798	1.996	1	MgII
LID-403	150.484	2.829	0.950	2	OII
LID-405	150.491	2.775	1.433	2	MgII,OII
LID-410	150.514	2.810	2.623	2	CVI,CIII
LID-414	150.577	2.768	1.381	2	MgII,OII
LID-437	150.447	2.899	1.260	2	MgII,OII
LID-463	150.508	2.697	1.091	1	MgII
LID-468	150.537	2.684	1.213	1	OII
LID-469	150.538	2.715	1.288	1	OII
LID-471	150.588	2.773	1.999	1	CIII
LID-473	150.598	2.781	0.431	1	OII
LID-479	150.640	2.811	2.680	1	CIV
LID-485	150.665	2.757	2.034	2	CIII,MgII
LID-512	150.538	2.784	2.899	2	CIV
LID-515	150.547	2.811	0.765	1	OII
LID-525	149.961	2.884	2.428	2	CIII,MgII
LID-536	149.893	2.823	1.257	1	OII
LID-559	149.829	2.908	1.414	1	OII
LID-578	149.889	2.844	1.396	1	OII
LID-579	149.895	2.876	2.079	2	CIII,MgII

Table C.1 – continued

ID	R.A.	decl.	Redshift	Quality	Spectral Features
LID-580	149.906	2.875	1.236	2	OII
LID-581	149.922	2.825	2.091	1	CIII
LID-589	149.749	2.732	3.171	2	Lya,CIV
LID-592	149.786	2.907	1.561	2	MgII
LID-611	149.848	2.569	0.913	2	OII
LID-623	149.667	2.381	2.765	1	CIV,CIII
LID-629	149.725	2.457	1.043	1	OII
LID-633	149.572	2.263	0.706	2	OII,Hb
LID-636	149.607	2.342	2.393	2	CIII,MgII
LID-637	149.612	2.354	1.376	1	NeV,OII
LID-638	149.613	2.264	1.421	2	MgII
LID-644	149.658	2.323	1.008	2	OII
LID-651	149.725	2.268	1.029	2	OII
LID-657	149.506	2.185	3.225	2	CIV,CIII
LID-660	149.530	2.222	2.361	2	CIII,MgII
LID-662	149.539	2.183	0.951	1	MgII,OIII
LID-665	149.559	2.181	1.176	2	OII
LID-673	149.621	2.080	1.452	2	MgII,OII
LID-683	149.492	2.075	1.379	2	MgII,OII
LID-684	149.494	2.040	0.979	2	OII
LID-685	149.498	2.077	2.030	2	CIII,MgII
LID-722	149.552	2.384	2.322	1	CIV
LID-725	149.571	2.403	1.167	1	OII
LID-727	149.613	2.272	2.464	2	CIV
LID-731	149.381	2.362	0.772	2	OII
LID-732	149.392	2.342	1.127	2	OII
LID-735	149.402	2.297	1.175	2	MgII,OII
LID-736	149.408	2.326	1.264	2	MgII,OII
LID-737	149.411	2.282	2.522	2	CIII
LID-738	149.417	2.319	1.477	2	MgII,CIII
LID-740	149.434	2.274	1.697	1	MgII
LID-744	149.441	2.288	0.476	2	OII,Hb,Ha
LID-763	149.643	2.349	2.665	1	MgII,OII
LID-957	149.496	1.968	3.261	2	Lya,CIV
LID-1008	149.867	1.748	0.562	2	OII,Hb
LID-1009	149.892	1.728	1.437	1	OII
LID-1015	149.996	1.751	1.097	1	OII
LID-1016	150.032	1.688	1.006	1	OII
LID-1024	150.118	1.586	0.840	2	OII,Hb
LID-1026	150.137	1.620	2.003	1	CIII
LID-1228	149.990	1.573	1.638	2	CIII,MgII,OII
LID-1229	149.990	1.602	2.214	1	CIII
LID-1239	150.001	1.541	0.893	2	OII

Table C.1 – continued

ID	R.A.	decl.	Redshift	Quality	Spectral Features
LID-1245	150.023	1.534	3.098	2	Lya,CIV,CIII
LID-1247	150.026	1.523	1.042	1	OII
LID-1290	149.815	1.635	1.475	1	OII
LID-1293	149.834	1.620	1.760	1	CIII
LID-1295	149.849	1.633	2.486	1	CIV,CIII,MgII
LID-1296	149.849	1.595	1.316	2	OII
LID-1305	150.275	1.576	1.247	2	MgII,OII
LID-1306	150.276	1.594	2.906	2	CIV,CIII
LID-1460	150.433	1.666	1.620	1	MgII
LID-1461	150.448	1.686	1.405	1	MgII,OII
LID-1462	150.470	1.725	2.829	2	CIV,CIII
LID-1476	150.490	1.868	1.263	2	MgII,OIII
LID-1492	150.483	1.915	2.062	1	MgII
LID-1497	150.520	1.926	1.734	1	NeV
LID-1502	150.575	1.977	1.539	2	CIII,MgII
LID-1509	150.514	2.040	0.425	2	OII,Ha
LID-1519	150.585	2.081	3.326	2	Lya,CIV,CIII
LID-1522	150.589	2.097	1.160	2	OII
LID-1535	150.587	2.199	1.425	2	OII
LID-1536	150.591	2.176	1.263	2	OII
LID-1539	150.631	2.255	1.430	2	OII
LID-1552	150.660	2.265	0.455	1	MgI
LID-1557	150.492	1.699	1.066	2	OII,Hg
LID-1578	150.526	1.829	1.127	2	OII
LID-1595	150.564	1.901	1.395	2	OII
LID-1599	150.607	1.935	0.680	1	Hb
LID-1613	150.598	2.014	0.796	2	OII,Hb
LID-1616	150.628	2.032	0.936	2	OII
LID-1618	150.632	2.003	1.826	1	CIII,MgII
LID-1620	150.637	2.008	1.269	1	OII
LID-1623	150.655	1.996	0.978	2	OII,Hb
LID-1691	150.712	1.588	1.757	1	MgII
LID-1710	150.717	1.930	3.567	1	CIII
LID-1770	150.607	2.372	0.982	1	K,H
LID-1776	150.644	2.351	1.092	1	OII
LID-1777	150.646	2.350	1.090	1	OII
LID-1779	150.661	2.349	0.731	1	K,H,Hb
LID-1780	150.667	2.347	0.982	2	OII,Hb
LID-1802	149.672	2.625	2.084	2	CIII,MgII
LID-1807	149.695	2.653	0.317	2	OII,Hb,Ha
LID-1808	149.696	2.603	3.303	1	Lya,CIII
LID-1812	149.721	2.665	0.741	1	Hb,MgI
LID-1832	149.598	2.685	2.402	2	CIV,CIII

Table C.1 – continued

ID	R.A.	decl.	Redshift	Quality	Spectral Features
LID-1833	149.609	2.690	2.059	1	CIII,MgII
LID-1846	149.573	2.711	0.867	2	OII,Hb
LID-1850	149.599	2.589	0.947	1	OII
LID-1853	149.621	2.613	3.563	1	Lya,CIII
LID-1855	149.635	2.599	2.536	2	CIV,CIII
LID-1964	150.593	2.539	1.138	2	OIII
LID-2011	150.744	2.456	0.366	2	Hb
LID-2038	150.410	2.693	2.792	1	CIII
LID-2056	150.245	2.844	1.258	2	OII
LID-2071	150.150	2.864	1.329	2	OII
LID-2081	149.974	2.810	1.560	1	CII,MgII
LID-2092	150.456	2.814	1.380	1	OII
LID-2093	150.472	2.849	1.202	1	OII
LID-2095	150.482	2.834	1.260	2	OII
LID-2102	150.513	2.875	0.887	2	OII,Hb
LID-2111	150.424	2.862	1.183	1	OII
LID-2112	150.429	2.852	1.256	2	OII
LID-2115	150.474	2.832	1.259	2	OII
LID-2121	150.574	2.552	3.128	2	Lya,CIV
LID-2184	149.773	2.886	3.173	1	CIII
LID-2189	149.850	2.865	3.686	1	Lya
LID-2200	149.736	2.758	2.861	2	CIV,CIII
LID-2201	149.745	2.891	0.347	2	OII,Hb,Ha
LID-2209	149.758	2.579	0.955	2	OII,Hb
LID-2215	149.683	2.384	0.959	2	OII
LID-2229	149.641	2.355	0.831	1	Hb
LID-2231	149.651	2.290	0.757	2	OII
LID-2239	149.548	2.078	0.959	1	OII,Hb
LID-2245	149.619	2.108	0.255	2	OII,Hb,Ha
LID-2273	149.383	2.374	3.374	2	Lya,CIV
LID-2278	149.445	2.360	0.340	2	Hb,Ha
LID-2279	149.451	2.296	3.101	1	CIII
LID-2286	149.387	2.743	0.737	1	OII,Hb
LID-2346	149.733	2.335	1.581	1	MgII,OII
LID-2473	150.073	1.756	3.045	1	Lya,CIV,CIII
LID-2494	150.283	1.583	4.182	1	Lya,CIV
LID-2623	149.892	1.619	0.032	2	Hb,Ha
LID-2669	150.295	1.684	1.259	2	OII
LID-2673	150.318	1.605	0.212	2	Ha
LID-2728	150.499	2.149	0.175	1	Ha
LID-2776	150.464	1.845	2.710	1	CIV
LID-2782	150.470	2.020	0.425	2	OII,Hb,Ha
LID-2793	150.561	2.037	1.579	1	OII

Table C.1 – continued

ID	R.A.	decl.	Redshift	Quality	Spectral Features
LID-2796	150.591	2.128	0.723	1	OII
LID-2798	150.579	2.252	0.886	1	OII
LID-2826	150.473	1.890	0.671	2	OII,Hb
LID-2834	150.574	1.853	0.062	2	Ha
LID-2843	150.581	2.023	0.532	2	OII,Hb
LID-2844	150.616	2.079	1.424	1	OII
LID-3016	150.472	2.489	0.926	1	OII
LID-3021	150.520	2.424	0.881	2	OII,Hb
LID-3023	150.563	2.542	0.465	1	OIII,Ha
LID-3033	150.480	2.496	2.952	1	CIV
LID-3044	150.293	2.524	1.363	2	OII
LID-3072	150.687	2.547	1.670	1	OII
LID-3097	150.459	2.733	0.795	1	OIII
LID-3110	150.382	2.753	1.148	2	OII
LID-3124	150.271	2.784	0.495	2	OII,Hb,Ha
LID-3133	150.095	2.889	0.814	2	OII,Hb
LID-3154	149.976	2.849	1.557	2	OII
LID-3219	150.621	2.785	0.834	2	OII,Hb
LID-3220	150.646	2.791	1.407	1	OII
LID-3239	150.530	2.795	0.315	2	OII,Hb,Ha
LID-3242	150.560	2.810	0.488	2	OII,Hb,Ha
LID-3245	150.601	2.633	0.631	1	OII,Hb
LID-3258	149.771	2.729	1.236	2	OII
LID-3280	149.723	2.729	0.581	1	OII,Hb
LID-3296	149.663	2.337	2.558	1	CIV,CIII
LID-3297	149.724	2.370	2.390	1	CIV,CIII
LID-3305	149.656	2.311	0.311	2	OII,Hb,Ha
LID-3313	149.553	2.151	2.675	1	CIV,CIII
LID-3314	149.561	2.137	2.411	1	CIII
LID-3329	149.527	2.092	2.423	1	CIII
LID-3335	149.564	2.030	0.724	2	OII,Hb
LID-3336	149.583	2.046	0.819	2	OII,Hb
LID-3337	149.591	2.036	0.382	1	Hb,MgI
LID-3349	149.412	2.410	1.063	1	OII
LID-3353	149.480	2.207	0.282	2	OII,Hb,Ha
LID-3452	149.518	1.986	0.678	2	OII,Hb
LID-3456	149.660	1.974	2.146	2	CIII,MgII
LID-3509	150.089	1.659	0.975	1	OII
LID-3515	150.231	1.571	0.828	2	OII,Hb
LID-3516	150.240	1.631	2.265	1	CIII
LID-3587	149.931	1.735	1.427	1	OII
LID-3603	149.926	1.596	0.773	2	OII,Hb
LID-3605	149.931	1.596	0.221	2	Ha

Table C.1 – continued

ID	R.A.	decl.	Redshift	Quality	Spectral Features
LID-3609	149.960	1.608	1.274	2	OII
LID-3611	149.980	1.542	1.180	2	OII
LID-3625	149.984	1.686	1.496	1	OII
LID-3649	149.813	1.615	0.843	1	OII
LID-3699	150.402	2.077	1.333	1	MgII,OII
LID-3701	150.428	2.169	1.316	1	OII
LID-3740	150.393	1.677	1.235	2	OII
LID-3745	150.419	1.719	0.998	2	OII,Hb,OIII
LID-3760	150.514	1.875	1.245	2	OII
LID-3762	150.422	1.931	1.175	2	OII
LID-3766	150.510	1.963	0.880	2	OII,Hb
LID-3767	150.515	1.999	0.842	2	OII,OIII
LID-3774	150.506	2.126	1.750	1	CIII,MgII
LID-3779	150.580	2.092	1.237	2	OII
LID-3780	150.609	2.074	0.615	2	OII,Hb
LID-3796	150.420	1.611	1.873	1	MgII
LID-3797	150.439	1.593	1.982	1	CIII
LID-3813	150.545	1.822	1.209	1	OII
LID-3826	150.534	1.979	0.670	2	Hb
LID-3827	150.553	1.874	1.299	1	OIII
LID-3901	150.582	2.440	0.881	2	OII,Hb
LID-3931	149.562	2.696	1.887	2	CIII,MgII
LID-4027	150.523	2.526	0.430	2	Hb,Ha
LID-4112	150.394	2.718	3.484	2	Lya,CIII
LID-4150	150.431	2.816	2.858	2	Lya,CIV
LID-4188	150.502	2.841	1.258	2	OII
LID-4264	149.878	2.846	0.354	2	OII,Hb,Ha
LID-4345	149.565	2.158	1.589	1	OII
LID-4356	149.496	2.066	1.449	2	OII
LID-4509	149.513	1.957	2.452	2	CIV,CIII
LID-4551	149.849	1.749	0.667	2	OII,Hb
LID-4567	150.158	1.708	0.808	1	MgII
LID-4582	150.366	1.607	0.614	1	OII
LID-4603	150.115	1.717	2.870	1	CIV,CIII
LID-4841	150.355	1.591	1.166	2	MgII,OII
LID-5014	150.659	2.318	1.149	2	OII
LID-5585	150.486	1.872	4.446	2	Lya,CIV
LID-5970	149.645	2.171	0.945	1	OII
XUDS-004	34.402	-5.366	1.035	2	MgII,OIId
XUDS-009	34.507	-5.330	1.952	1	CIII,MgII
XUDS-013	34.371	-5.314	0.493	2	OII,H+K,G,OIIId,NaI,Ha,NIId
XUDS-016	34.542	-5.312	2.122	1	MgII
XUDS-019	34.357	-5.301	1.421	2	NeV,OII

Table C.1 – continued

ID	R.A.	decl.	Redshift	Quality	Spectral Features
XUDS-040	34.290	-5.270	4.398	1	Lya
XUDS-041	34.389	-5.264	0.603	2	OII,H+K,G,OIIId,MgI
XUDS-044	34.552	-5.259	0.694	2	OII,Hb,OIIId
XUDS-054	34.370	-5.247	0.920	2	OII,H+K,G,Hb,OIII
XUDS-058	34.287	-5.238	1.275	2	OII,H+K
XUDS-073	34.385	-5.214	3.212	2	Lya,SiIV,CIIICIV,
XUDS-081	34.212	-5.195	0.250	2	Hg,Hb,OIII,Ha,NII
XUDS-084	34.219	-5.192	1.441	2	OIId
XUDS-098	34.323	-5.171	3.940	2	Lya,NV,SiIV,CIV,HeII,CIII
XUDS-112	34.398	-5.145	1.558	1	NeV
XUDS-122	34.519	-5.128	0.549	2	OII,H+K,OIIId
XUDS-124	34.341	-5.124	0.649	2	OII,Hb,OIIId
XUDS-136	34.216	-5.103	0.629	2	OII,H+K,Hb,OIIId
XUDS-151	34.254	-5.086	0.000	2	Star
XUDS-169	34.179	-5.056	3.109	1	CIII
XUDS-179	34.183	-5.042	2.947	2	Lya,CIV,CIII
XUDS-188	34.665	-5.026	1.357	1	OII
XUDS-197	34.176	-4.985	0.627	2	OII,Hb,OIIId
XUDS-200	34.228	-4.962	1.103	2	MgII,NeV,H+K,Hg
XUDS-203	34.510	-5.371	1.485	2	CIII,MgII
XUDS-217	34.395	-5.288	1.720	1	MgII,OIId
XUDS-219	34.345	-5.276	2.765	2	CIV,CIII
XUDS-236	34.272	-5.232	0.629	2	OII,H+K,OIII
XUDS-246	34.386	-5.205	1.379	2	OIId,H+K
XUDS-251	34.343	-5.194	1.670	2	CIII,MgII
XUDS-257	34.409	-5.182	1.421	2	FeIabs,OII,H
XUDS-258	34.551	-5.179	2.735	2	CIV,HeII,CIII
XUDS-274	34.369	-5.142	0.044	2	OIII,Ha,NIId,SIId
XUDS-306	34.170	-5.046	3.859	2	Lya,CIV?
XUDS-308	34.212	-5.037	0.423	2	OII
XUDS-329	34.338	-5.370	0.633	2	OII,K,G,Hb,OIIId
XUDS-337	34.400	-5.343	2.560	2	CIV,CIII,MgII
XUDS-345	34.380	-5.306	0.309	2	Hb,OIII,MgI,NaI,Ha,NIId,SIId
XUDS-354	34.293	-5.286	0.053	2	Hb,OIIId,MgI,NaI,Ha,NIId,SIId
XUDS-402	34.679	-5.077	0.961	2	OIId,H+K,G,HB,OIIId
XUDS-433	34.264	-4.926	0.571	2	H+K,G,OIIId
XUDS-461	34.366	-5.186	0.572	1	H+K,G
XUDS-466	34.709	-5.165	2.090	2	CIII,MgII
XUDS-473	34.378	-5.133	0.141	2	Hb,OIIId,Ha,NIId,SIId
XUDS-491	34.657	-4.981	1.407	2	OIId,NeIII
XUDS-515	34.235	-5.120	0.936	1	OII
XUDS-540	34.354	-5.166	1.091	2	OII,H+K,Hg
XUDS-547	34.689	-5.020	2.330	2	SiII?,CIV,CIII,MgII

Table C.1 – continued

ID	R.A.	decl.	Redshift	Quality	Spectral Features
XUDS-566	34.514	-5.291	0.646	2	H+K,G,MgI
XUDS-570	34.335	-5.244	0.921	2	OII,H+K,G
XUDS-601	34.526	-5.213	1.043	2	NeV,OII,NeIII,Hg
XUDS-617	34.530	-5.381	0.451	2	OII,H+K,G,Hb,OIIId,MgI,NaI
XUDS-620	34.312	-5.332	0.644	2	OII,H+K,G,MgI
XUDS-628	34.522	-5.298	2.158	2	CIV,CIII,MgII
XUDS-631	34.549	-5.264	0.644	2	H+K,G,Hbabs
XUDS-643	34.503	-5.242	1.043	2	H+K,Hgabs
XUDS-651	34.537	-5.218	1.812	1	MgII
XUDS-653	34.558	-5.206	0.429	2	OII,H+K,G,MgI,NaI
XUDS-674	34.182	-5.126	0.668	2	OIII,NeIII,H+K,G,Hb,OIIId
XUDS-679	34.298	-5.106	0.565	2	OII,OIII
XUDS-779	34.191	-5.076	1.482	2	NeV,OIId
XUDS-814	34.574	-5.316	0.370	2	MgI,NaI,Hb,Ha,NIId,SIId
XUDS-825	34.513	-5.232	0.603	2	OII,H+K,Hgabs,HBabs,OIII
XUDS-1014	34.346	-5.250	0.572	2	OIId
XUDS-001	34.454	-5.385	0.990	2	Ha,NII,SII
XUDS-008	34.304	-5.331	0.812	2	Ha,NII,SII
XUDS-012	34.431	-5.318	1.621	2	Hb,OIIId,Ha,NII
XUDS-015	34.515	-5.314	1.713	1	Ha
XUDS-016	34.542	-5.312	2.526	2	Hb,OIIId
XUDS-026	34.513	-5.292	1.626	2	Ha,NII,SII
XUDS-027b	34.363	-5.291	2.335	1	OIII
XUDS-029	34.199	-5.287	1.027	2	Ha
XUDS-043	34.469	-5.260	0.949	2	Ha,SII
XUDS-045	34.276	-5.259	1.741	1	Ha,NII
XUDS-068	34.448	-5.223	1.668	2	Ha,NIId
XUDS-070	34.446	-5.218	1.665	1	Ha
XUDS-089	34.572	-5.185	1.650	2	Ha,NII
XUDS-106	34.431	-5.158	1.609	2	Ha,NII
XUDS-107	34.197	-5.156	1.654	2	Hb,OIIId,Ha,NII
XUDS-113	34.300	-5.140	1.656	2	Hb,OIIId,Ha,NII,SII
XUDS-119	34.177	-5.135	2.487	1	OIII
XUDS-120	34.587	-5.133	1.434	1	Hb
XUDS-125	34.143	-5.124	1.724	1	Ha
XUDS-132	34.340	-5.108	0.984	2	Ha,NII,SIId
XUDS-133	34.326	-5.108	1.608	2	Ha,NII
XUDS-139	34.260	-5.099	1.610	1	Ha,NII
XUDS-141	34.382	-5.092	3.736	1	OII
XUDS-142	34.380	-5.092	1.036	1	Ha
XUDS-159	34.529	-5.071	0.723	1	Ha
XUDS-173	34.463	-5.051	0.873	2	Ha,NII,SII
XUDS-175	34.589	-5.047	1.485	2	Ha,NIId,SII

Table C.1 – continued

ID	R.A.	decl.	Redshift	Quality	Spectral Features
XUDS-178	34.160	-5.042	1.655	2	Ha
XUDS-182	34.516	-5.035	2.338	2	Hb,OIII
XUDS-198	34.534	-4.979	0.715	2	Ha,SIII
XUDS-205	34.468	-5.354	2.267	1	OIII
XUDS-206	34.244	-5.331	2.253	1	OII
XUDS-213	34.653	-5.293	1.533	2	Ha,NIId,SII
XUDS-217	34.395	-5.288	1.709	2	OIII,Ha
XUDS-218	34.503	-5.281	1.692	1	Ha
XUDS-231	34.596	-5.237	2.412	2	Hb,OIII
XUDS-238	34.394	-5.230	1.624	2	Ha,NII,SII
XUDS-239	34.568	-5.229	1.544	2	Ha,NII
XUDS-240	34.242	-5.227	1.478	2	Ha,SII
XUDS-261	34.425	-5.176	1.473	1	Ha
XUDS-264	34.544	-5.175	1.633	2	OIII,OIII,NII
XUDS-265	34.599	-5.174	1.624	2	OIII,Ha,NIId,SII
XUDS-272a	34.356	-5.150	1.592	1	Ha
XUDS-276	34.315	-5.135	1.505	2	Ha,NII,SII
XUDS-281	34.119	-5.128	1.598	2	Ha,SII
XUDS-291	34.483	-5.082	1.611	1	Hb
XUDS-300	34.148	-5.056	1.609	1	Ha
XUDS-302	34.123	-5.053	2.337	2	Hb,OIIId
XUDS-311	34.439	-5.031	1.536	2	Hb,Ha,NIId
XUDS-314	34.397	-5.025	2.516	2	Hb,OIIId
XUDS-315	34.302	-5.024	1.625	1	Ha
XUDS-316	34.570	-5.015	1.498	1	Ha
XUDS-325	34.474	-4.963	1.402	2	Hb,OIIId,SII
XUDS-326	34.318	-4.935	1.541	2	Ha,NII,SII
XUDS-335	34.272	-5.348	1.625	1	Ha,SII
XUDS-336	34.468	-5.347	0.864	1	SIII
XUDS-341	34.690	-5.317	1.649	1	Ha
XUDS-347	34.143	-5.304	1.602	1	Ha,NII
XUDS-379	34.593	-5.180	1.472	1	Ha,NII
XUDS-382	34.178	-5.177	1.722	1	Ha
XUDS-383	34.354	-5.165	1.578	2	OIII,Hb
XUDS-384	34.409	-5.163	2.521	1	OIII
XUDS-389	34.441	-5.152	1.584	2	Ha,NII
XUDS-440	34.581	-5.359	2.464	1	OIId
XUDS-444	34.446	-5.345	1.534	1	Ha
XUDS-445	34.220	-5.338	1.659	1	Ha
XUDS-457	34.619	-5.207	1.650	1	Ha
XUDS-497	34.343	-5.390	1.459	2	OIII,Ha,Ha,NII
XUDS-519	34.169	-5.085	2.526	1	OIII
XUDS-530	34.482	-4.926	1.590	2	Ha,NII

Table C.1 – continued

ID	R.A.	decl.	Redshift	Quality	Spectral Features
XUDS-547	34.689	-5.020	2.335	1	OIII
XUDS-561	34.349	-5.380	1.603	1	Ha
XUDS-583	34.494	-5.049	0.841	1	SiII
XUDS-590	34.463	-5.273	1.483	1	Ha,NII,SII
XUDS-597	34.534	-5.243	1.628	2	Ha,SII
XUDS-614	34.429	-5.060	0.879	2	Ha,NII
XUDS-632	34.304	-5.264	1.527	1	Ha,NII
XUDS-637	34.181	-5.253	1.046	1	Ha
XUDS-667	34.316	-5.151	1.648	1	Ha
XUDS-682	34.547	-5.103	1.008	1	Ha
XUDS-716	34.357	-5.332	1.544	2	Ha,SII
XUDS-737	34.600	-5.259	1.627	2	Hb,OIIId,Ha
XUDS-740	34.591	-5.249	1.634	1	Ha,NII
XUDS-849	34.139	-5.085	1.566	2	Ha,NII
XUDS-863	34.552	-5.034	1.454	2	Ha,NII,SIId
XUDS-870	34.625	-4.992	1.507	2	Ha,NII
XUDS-887	34.682	-5.290	1.602	1	Ha,NII,SII
XUDS-948	34.295	-4.958	1.697	1	Ha,NII
XUDS-984	34.345	-5.119	1.491	1	Ha